# Flare Stars
# In The Solar Vicinity
## A Search For Young Stars

Dissertation
der Fakultät für Physik
der Ludwig-Maximilians-Universität
München

vorgelegt am 08.09.2003
von Brigitte König
aus Starnberg

# Contents

# List of Figures

# Kurzzusammenfassung

Junge Sterne in Sonnennähe (innerhalb von 100 pc) sind in vieler Hinsicht eine interessante Stichprobe: Sie sind relativ hell und durch ihre räumliche Nähe kann mit adaptiver Optik an 8 bis 10 m Teleskopen (z.B. VLT oder Keck) eine hohe räumliche Auflösung erreicht werden. Im K-Band liegt diese bei etwa 50 mas, also 5 AE bei Sternen näher als 100 pc; 5 AE ist etwa der Abstand von Jupiter und Sonne. Diese Möglichkeit kann dazu genutzt werden, umgebendes Material wie Scheiben aus Staub und Gas, sowie enge stellare und substellare Begleiter zu studieren.

Eine Stichprobe bestehend aus jungen Sternen in Sonnennähe im Entwicklungstadium zwischen klassischen T Tauri Sternen mit Scheibe und der Nullalterhauptreihe kann der Katalog der sogenannten Flaresterne - zusammengestellt von Gershberg et al. (1999) - sein, denn junge Sterne sind häufig variabel und zeigen Ausbrüche (Flares). Um zunächst zu verifizieren, daß diese Sterne tatsächlich jung sind und nicht nur deshalb oberhalb der Hauptreihe in einem Hertzsprung-Russell Diagramm zu liegen kamen, weil sie alt oder nicht aufgelöste Doppel- oder Mehrfachsterne sind, haben wir die 223 oberhalb der Hauptreihe liegenden Sterne der 463 Sterne des Katalogs spektroskopiert; die Entfernung der Sterne wurde meist durch Hipparcos gemessen und liegt bei wenigen bis 100 pc. Ziel war es, die Lithiumabsorptionslinie bei 6708 Å zu detektieren, die alle jungen Sterne zeigen. Zusätzlich dazu sollten weitere spektroskopische Signaturen, wie die Auffüllung oder Emission der H$\alpha$-, Magnesium Ib- und Kalziumlinien identifiziert werden. Die G- und K-Sterne der nördlichen Hemisphere wurden außerdem mit hoher spektraler Auflösung sowie hohem Signal-zu-Rauschverhältnis aufgenommen, um die Sterne mit Methoden der Spektralsynthese zu untersuchen und um deren physikalische Parameter wie Oberflächengravitation, chemische Zusammensetzung und Temperatur zu bestimmen. Die Altersbestimmung der 223 Sterne ergab, daß ihr Alter zwischen 10 Ma und der Nullalterhauptreihe liegt und 17 eindeutig Vorhauptreihensterne sind. Es ist zu bemerken, daß wir im Laufe dieser Arbeit den nächsten Vorhauptreihenstern entdeckt haben (HIP 108405 A, mit 10±10 Ma in 16.1 pc Entfernung), jünger als GJ 182 (27 pc, 20±10 Ma), der bisherige Rekordhalter. Ein Planet mit einer Masse von 5 $M_{Jup}$ um einen für diese Stichprobe typischen M-Stern hätte in einer Entfernung von 16 pc eine scheinbare Helligkeit im K-Band von 14.5 bis 17.5 mag, also einen Magnitudenunterschied im K-Band $\Delta$K zwischen Stern und Begleiter von 8 bis 11 mag und wäre somit in einem Abstand von 1" entsprechend einem projiziertem Abstand von 16 AE vom Stern entfernt, mit 8 bis 10 m Teleskopen detektierbar.

Alle neuentdeckten jungen Flaresterne wurden in den letzten Monaten mit NAOS/CONICA beobachtet, um deren Umgebung nach entfernten Begleitern abzusuchen. Je nach Eigenbewegung der Sterne müssen diese ein oder mehrere Jahre später ein zweites Mal aufgenommen werden, um mitbewegende Begleiter von stillstehenden Hintergrundobjekten zu unterscheiden.

Wir haben in dieser Arbeit erstmals Radialgeschwindigkeitsmessungen bei jungen Sternen mit dem Échellespektrograph der Thüringer Landessternwarte durchgeführt. Anhand exemplarischer Messungen kann man deutlich die Probleme einer solchen Messung sehen, wie Variabilität aufgrund von stellarer Aktivität und Sternflecken. Man kann aber auch sehen, daß es prinzipiell möglich ist Planeten um aktive junge Sterne zu detektieren. Zur Bestätigung der Ergebnisse und um längere Umlaufperioden zu messen, müssen die Sterne noch eine weitere Saison beobachtet werden.

# Abstract

Young stars close to the sun (within 100 pc) yield an interesting sample in many respects: They are relatively bright and because of their close distance we can resolve the surroundings of these stars by using adaptive optics on 8 to 10 m class telescopes (e.g. VLT or Keck). In the K-band the achievable angular resolution is about 50 mas which corresponds to 5 AU at a star closer than 100 pc; 5 AU is about the distance between the Sun and Jupiter. This possibility can be used to study surrounding material such as disks made up of gas and dust as well as stellar and substellar companions.

A sample consisting of young stars in the solar vicinity and in an evolutionary stage between the classical T Tauri phase with a disk and the zero-age main sequence can be provided by the catalog of flare stars and related objects compiled by Gershberg et al. (1999) because young stars are often variable and exhibit large eruptions (flares). In a first step we need to verify that these stars are indeed young and did not come to lie above the main sequence in a Hertzsprung-Russell diagram because they are old or unresolved binaries or multiples. Therefore, we have taken spectra of 223 stars lying above the main sequence (of the 463 stars of the sample). The distances to these stars were measured (in most cases by Hipparcos) and they are located at a few to 100 pc. The goal was to detect lithium absorption at 6708 Å which all young stars have in common. In addition to the detection of lithium, we want to identify other age indicators such as filling in or emission of the H$\alpha$-, the magnesium Ib- and the calcium lines. The G- and K-type stars of the northern hemisphere were also observed with high resolution, and high signal-to-noise ratio spectroscopy to study these objects with methods of spectral synthesis analysis to determine the surface gravity, the chemical composition, and the temperature. The age determination of these 223 stars lead to a value between 10 Myr and the zero-age main sequence, they are indeed nearby and 17 stars are clearly pre-main sequence. In the course of this work, we discovered the closest pre-main sequence star (HIP 108405 A, 10±10 Myrs at a distance of 16.1 pc). The star is younger than GJ 182 (27 pc, 20±10 Myr) which held the record up to now. A planet with a mass of 5 $M_{Jup}$ in orbit of a (for this sample) typical M-star, would have an apparent magnitude in the K-band of 14.5 to 17.5 mag at a distance of 16 pc. This would lead to a magnitude difference $\Delta$K of 8 to 11 mag between the star and the companion, which could be detected with 8 to 10 m class telescopes at a separation of 1" or a projected separation of 16 AU.

All newly discovered young flare stars were imaged using NAOS/CONICA to search for distant companions. Depending on the space motion of the stars, they have to be reobserved in one or more years to distinguish comoving companions from stagnant background stars.

In this work we have measured radial velocity variations of young stars for the first time using the échelle spectrograph of the Thüringer Landessternwarte. In these measurements one can see the problems of such an investigation, such as variability caused by activity and stellar spots. But one can also see that it is in principle possible to detect planets around active young stars. To verify the results and to measure longer rotation periods, we have to observe these stars for another season.

# Chapter 1

# Introduction

As an introduction to young stars we will first summarize the star formation process from the cloud to single stars, binaries, or multiple systems. We emphasize here that this is an incomplete view which concentrates mainly on the principles and to place the flare stars, which are discussed in the following chapters, into the general picture.

## 1.1 The model developed in the 1960's

In the 1940's it became clear that star formation is an ongoing process (Joy & van Biesbroeck, 1944; Joy, 1945). The question that arose and which is still not solved in complete detail is: How does a gas and dust cloud form a star and what phases of this formation process can we observe?

### 1.1.1 From a gas and dust cloud to a protostar

If the self gravitation of the cloud becomes higher than the gas pressure for any reason the cloud starts to contract. A usual initial cloud like this has a particle density of $\rho = 10^{-19} \frac{\text{g}}{\text{cm}^3}$ and a temperature of $10\,\text{K}$. The cloud is transparent in infrared light with wavelength $\lambda > 10\,\mu\text{m}$ and opaque for visible light.

The initial contraction of the cloud takes place at almost constant temperature and the energy which is set free is used to increase the kinetic energy of the infalling particles. Energy which is set free by collision of particles is radiated away at infrared wavelength where the cloud is still transparent.

When the density of the cloud reaches a critical density ($\rho \sim 10^{-14} \frac{\text{g}}{\text{cm}^3}$) and a temperature higher than $15\,\text{K}$ the cloud becomes opaque at infrared wavelengths. The infrared radiation is reabsorbed by the gas particles. The probability that an infrared quantum will be absorbed is proportional to the density $\rho$ of the gas times the radius $R$ of the cloud and the density $\rho \sim \frac{M}{R^3}$ where $M$ is the mass of the cloud. The cloud becomes more opaque as the density increases. The gas cloud still contracts but now the energy which is released by the contraction is used to heat the gas.

The collapse stops when the gravitation force and the force by the gas pressure are in equilibrium. This is first reached at the center of the cloud while the outside is still contracting. The center now has a temperature of $T \simeq 2100\,\text{K}$ and a density $\rho \simeq 2 \cdot 10^{-8} \frac{\text{g}}{\text{cm}^3}$. On the border of the infalling gas to the core, the kinetic energy of the gas is converted to heat.

At a temperature of $\sim 2000\,\text{K}$, the molecules begin to be destroyed, especially the $H_2$ molecules are dissipated. At higher temperatures atoms are ionized. Further release of kinetic energy triggers the process of destroying molecules and ionizing atoms. During this process the temperature of the core stays constant.

Due to ongoing accretion to the core the mass of the core grows and the hydrostatic equilibrium becomes unstable. The core contracts again. When most of the molecules are reduced to atoms, the temperature of the core rises again and the core reaches hydrostatic equilibrium. On the border of the core, gas is falling in, so that the accretion process is ongoing and the core grows until it becomes unstable again. This process repeats until the gas reservoir is exhausted.

In the surrounding region of the protostar all molecules are destroyed and the gas is dissipated. When the protostar has reached its final hydrostatic equilibrium the object enters the 'Hayashi'-phase. A $1\,M_\odot$ star has a radius of $R \sim 50 R_\odot$ in this model at this age.

### 1.1.2 What can we observe at this phase?

The initial gas cloud has a temperature of $10\,K$. We can observe thermal emission of the dust at wavelength $\lambda > 10\,\mu m$. When the cloud becomes opaque, the emission maximum is shifted to a shorter wavelength. In the phase of isothermal contraction the luminosity of the object rises fast. When the gravitational potential of the hydrostatic core grows, the luminosity of the protostar reaches $\sim 300 L_\odot$ and heats the outer surrounding material up to $\sim 3000\,K$. The protostar is visible in red light. Its spectral energy distribution looks like a normal cool star.

### 1.1.3 The phase of slow contraction

The next evolutionary phase is the phase of slow contraction. Because the protostar is indistinguishable from a normal star, we will now call it a 'young star'. Protostars with masses below $3\,M_\odot$ are fully convective when they reach the phase of slow contraction. Young stars with masses below $0.3\,M_\odot$ stay fully convective their complete life time.

Hayashi has shown in 1961 that for slowly contracting, fully convective stars the following two statements hold: the luminosity of the star must decrease as the radius decreases, and the surface temperature does not depend on the mass of the object and depends only slightly on its luminosity.

The young star with a mass $M > 0.3\,M_\odot$ contracts further and in its center the convection stops and energy is transported by radiation. The temperature of the core has reached $T = 3 \cdot 10^6\,K$ and thermonuclear reactions start. In the beginning the thermonuclear reaction replaces the energy lost by radiation. The compression continues with rising temperature in the core and which again triggers the thermonuclear reaction. The compression ends when the radiative pressure is high enough. For a $1\,M_\odot$-star this is the case when its effective temperature $T_{\text{eff}}$ has reached $5800\,K$ and its luminosity $L \sim 0.7\,L_\odot$. The star reaches the 'main sequence'. Only stars with masses below $\sim 0.07\,M_\odot$ never reach this phase. These low mass objects do not reach high enough temperature in their core to start a stable thermonuclear reaction.

The thermonuclear reaction of young stars with masses $M > 0.07\,M_\odot$ starts sequentially. At a relative low temperature beryllium and lithium burn and form helium. The energy released is relatively small. At higher temperatures deuterium and hydrogen are burned to form helium by proton capture reactions.

The higher the mass of the star, the shorter is the time it needs to reach the main sequence phase. It is possible that young low mass stars are frequent on the solar vicinity because of their contraction time scales.

This rather simple picture was developed in the 1960's mainly by Hayashi and Nakano. It does not include rotation or magnetic fields.

### 1.1.4 Collapse under selfgravitation

How the condensation of a cloud core out of low density gas regions happens is not clear. A collapse of a cloud under self gravitation caused by gravitational instabilities can be estimated. The critical mass for this effect is called *Jeans mass* and the scales on which this happens *Jeans length*. The argument is the following (Binney & Tremaine, 1987): The gas of a cloud with mass $M$, and density $\rho_0$ is initially distributed uniformly and it behaves isothermal with sound speed $c_s$. In this state the cloud is stable and there is no net pressure or gravitational force.

Now we imagine a spherical region with radius $r$ in the center of this cloud where the gas is slightly compressed. The density is higher by a factor $\chi\rho_0$ here. The outward pressure force arising from this is:

$$F_P \sim \frac{\nabla P}{\rho} \sim \chi \frac{c_s^2}{r} \tag{1.1}$$

and the higher density causes an inward directed gravitational force of:

$$F_G \sim \frac{GM\chi}{r^2} \sim G\rho_0\chi r. \tag{1.2}$$

The gravity wins on large scales: $r^2 \geq c_s^2/G\rho_0$. A thorough analysis leads to a Jeans length of:

$$\lambda_J = \sqrt{\left(\frac{\pi c_s^2}{G\rho_0}\right)} \tag{1.3}$$

and a Jeans mass of

$$M_J = \lambda_J^3 \rho_0 = \frac{1}{\sqrt{\rho_0}} \left(\frac{\pi c_s^2}{G}\right)^{\frac{3}{2}} \tag{1.4}$$

According to the analysis clouds with higher density cores with masses grater than the Jeans mass will collapse under selfgravitation. Note that if the density gets higher the mass necessary to collapse the cloud caused by selfgravitation is smaller.

## 1.2 Improved models

Observations have made it necessary to develop models which are improved in several respects. Protostars rotate, they usually are born in multiple systems, the gas cloud is not homogeneous and spherical, and we observe magnetic fields in young stars.

### 1.2.1 Centrally concentrated clouds

The so called Bonnor-Ebert sphere is one special solution and popular solution of the differential equation of hydrostatic equilibrium under the boundary conditions that the density drops to zero on the borders of the cloud. The central density is about 5.8 times the mean density of the gas and the density drops almost isothermally with increasing radius.

### 1.2.2 Inhomogeneous gas clouds

The density distribution in a cool cloud is not homogeneous. Because the needed time for contraction increases with increasing density of the cloud, the inhomogeneity must grow in the stadium of isothermal contraction. Shortly after the begin of the contraction the inhomogeneity of the density increases rapidly: The central density grows more rapid than in the

model of Hayashi & Nakano. As in their model shock waves arise at the border to the opaque hydrostatic core and the free falling isothermally contracting surrounding material.

The slow compression of the core continues and at a temperature of $\sim 2000\,\mathrm{K}$ the molecules are destroyed and the atoms are ionized. This process requires a lot of energy and the equilibrium in the core becomes unstable. The core starts to contract fast and a new equilibrium is formed with a core formed of plasma and a temperature of $T \approx 20,000\,\mathrm{K}$, a core mass of $M_{\mathrm{core}} = 1.5 \cdot 10^{-3}\,\mathrm{M_\odot}$, and a core radius of $R_{\mathrm{core}} = 1.3\,\mathrm{R_\odot}$.

The core is more compact than in the model of Hayashi & Nakano. The speed of the infalling material is higher. The kinetic energy released in the instreaming amount of material is higher. At the moment the compact core is formed, the envelope material still has the initial parameters of the cloud. The reason for that is that the huge decrease of density from the center to the envelope causes the pressure to drop fast which again slows down the contraction. The resulting protostar behaves different: A hot and compact core which radiates in the optical and on which material is accreted from the thin envelope over a long time span. In an observation the object would appear extremely cool and only visible in infrared light. When the envelope has fallen onto the protostar, it has reached the Hayashi-track and is optically visible. A $1\,\mathrm{M_\odot}$-star has a radius of $R = 2 \cdot \mathrm{R_\odot}$ in this stage of evolution in this model.

### 1.2.3   Rotation of the cloud

The rotation of a cloud around a rotation axis causes the collapse not to be spherical symmetric. The centrifugal force at a point located further from the rotation axis is higher than it would be at a point close to the axis. Also it is higher if the angular velocity is higher. We therefore expect the contraction to be faster in the direction of the axis than perpendicular to it. The cloud shape changes from spherical to a 'disk'-like shape.

Because the angular moment is conserved the contraction of the cloud must lead to an increasing angular velocity of its rotation. The cloud can fragment into two or more smaller clouds which rotate around their common center of mass. This is the principle idea of how double and multiple systems form. Most of the angular momentum of the initial cloud is now converted into angular momentum of the cloud fragments rotation their common center of mass. The angular momentum of each fragment rotating around itself is relatively small.

If the separation of the fragments is big enough each fragment can now perform its collapse like a single cloud with small angular momentum. The material at the center of mass of the fragment forms an opaque core and the material further away will form a disk which will grow in this phase. The friction between the different layers in the disk cause the exchange of angular momentum and the inner part of it are accreted to the core. The contraction of the cloud envelope continues and the material close to the rotation axis falls directly onto the protostar while the material with higher angular momentum falls onto the disk. When the cloud disappears the protostar will turn into a young star with a disk.

The questions which are not solved with this model today are:

- Which mechanisms redistribute the angular momentum and how effective are they?

- At which evolutionary stage do the double or multiple systems begin to be formed? Are they formed during the isothermal collapse or later as a result of the fragmentation of an opaque disk-like envelope?

- The observations show that the protostars loose mass through jets at the same time as they accrete mass from the disk. This leads to the explanation that angular momentum might be transported along the rotation axis through jets. The mechanisms that drive these jets are still unclear.

### 1.2.4   Magnetic field in protostars and young stars

It is observed that magnetic fields play a role in the collapse of a cloud. As a estimate of the critical mass we can use the so called *magnetic Jeans mass* where

$$M_{\mathrm{J,mag}} \sim \frac{\Phi}{\sqrt{G}} \tag{1.5}$$

and which depends only on the magnetic flux $\Phi$, and $G$ is the gravitation constant.

We observe jets and outflows, as well as a circumstellar disk. It is believed that the magnetic field plays a key role in regulating the collapse by transferring disk orbital motion to collimated outflows. The coupling of the magnetic field with neutral material is believed to happen in a small fraction of ionized material ($N_{\mathrm{ion}}/N_{\mathrm{neutr}} = 10^{-8}$). The ionisation is caused by low energy cosmic rays.

Observations of keV-radiation and MeV-particles in young stellar objects as well as in T Tauri stars are common. Thermal X-ray emission is generated by hot gas at a temperature of about $T \simeq 10^7$ K. The heating nergy is believed to be produced by violent reconnection events of the magnetic field lines. The strong magnetic field on T Tauri stars can be observed by Zeemann splitting of spectral lines. Also large stellar spots and plage regions can be observed by optical photometry. The young stars also have powerful non-thermal radio-continuum flares.

It is believed that the magnetic field is generated in a rotation and convection driven dynamo analog to the solar dynamo models. But also some unusual field configurations can be possible: star-disk, star-envelope, and disk-disk fields. These configurations cannot be observed directly.

The theory of the coupling of a disk with a protostar or a young star was developed out of the theory to describe X-ray binaries and accreting neutron stars from Ghosh & Lamb (1978, 1979). The disk material in a thin layer of the inner disk which is corotating with the star is coupled to the magnetic field lines of the protostar or young star. The material moves along the magnetic field lines to the surface of the star. The material of the disk which is outside the corotation radius and the material inside exchange angular momentum. The total angular momentum is zero. In this way it is possible that no angular momentum is transported onto the star. This model does not explain why classical T Tauri stars which are known to accrete through a disk do not start to rotate faster and faster but are fairly slow rotators.

In the more recent model from Shu et al. (1994, 1997) the star disk configuration is the following: Because of a constant accretion rate the disk is forced to corotate within a certain radius. Material is accreted along the magnetic field lines inside this radius, and also angular momentum is transported from the disk to the star. Outside the corotation radius material is blown away in the so called X-wind. Also angular momentum is transported away from the disk in this wind. The model is able to describe the fairly slow rotation of the classical T Tauri stars but is not able to explain the unsteady accretion rate which is observed in theses young stars.

## 1.3   Observed evolution stages

We have described the principle ideas of star formation. Now what kind of objects can we observe in nature. A classification schema was developed by Lada (1987), and Andre & Montmerle (1994) based on the observed infrared emission of the young objects. The spectral energy distribution (SED) is converted into an index $s$. To derive $s$ the flux $F$ is measured
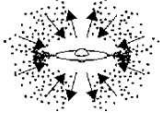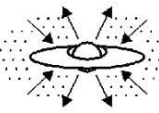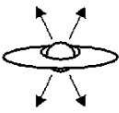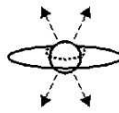
| PROPERTIES | Infalling Protostar | Evolved Protostar | Classical T Tauri Star | Weak-lined T Tauri Star | Main Sequence Star |
|---|---|---|---|---|---|
| SKETCH | | | | | |
| AGE (YEARS) | $10^4$ | $10^5$ | $10^6$ - $10^7$ | $10^6$ - $10^7$ | $> 10^7$ |
| mm/INFRARED CLASS | Class 0 | Class I | Class II | Class III | (Class III) |
| DISK | Yes | Thick | Thick | Thin or Non-existent | Possible Planetary System |
| X-RAY | ? | Yes | Strong | Strong | Weak |
| THERMAL RADIO | Yes | Yes | Yes | No | No |
| NON-THERMAL RADIO | No | Yes | No ? | Yes | Yes |

**Figure 1.1:** Classification scheme of young stellar objects according to their infrared emission. Taken from Feigelson & Montmerle (1999).

typically between $\lambda \sim 2\,\mu$m and $\lambda \sim 50 - 100\,\mu$m. The flux is converted to the index via:

$$\nu F_\nu = \lambda F_\lambda \sim \lambda^s. \tag{1.6}$$

**Class 0 - Bok globules**

These sources are very red objects which emit a large amount of light in the infrared and millimeter range compared to their total luminosity. Their radiation is dominated by the massive cold envelopes which are consisting of gas and dust at a temperature of $30\,$K. In the central region the collapse is ongoing and we observe collimated outflows on the poles. In the envelope a disk rapidly forms with a size of $10^3$ to $10^4\,$AU. The age of these objects is about $10^4\,$yr.

Observers call these objects Bok globules which are opaque clouds and which are believed to be the site of star formation (Bok & Reilly, 1947). They have masses of a few times the solar mass and radii of a few tenth of a parsec (Clemens & Barvainis, 1988). Many have young stars inside (Yun & Clemens, 1990) and some are undergoing a collapse (Wang et al., 1995).

**Class I - YLW 15**

Objects with $s > 0$. Their spectral energy distribution rises towards longer wavelength. These objects are about $10^5\,$yr old. Most of the material from the envelope is accreted to the

protostar or the disk. The disk size is a few hundred AU. The opening angle of the outflow is larger than in the class 0 sources.

YLW 15 is an example for such an object. Besides the characteristic infrared emission it shows quasi periodic X-ray flares which can be explained by a disk which is linked to the star by a magnetic field (Tsuboi et al., 2000).

### Class II - Classical T Tauri stars

Objects which fulfill $-\frac{4}{3} \leq s \leq 0$. Class II sources show the infrared designation of classical T Tauri stars. Most observed phenomena can be explained by a star interacting with a disk. Young members of this class drive outflows and all drive strong winds with mass loss rates of $\simeq 10^{-7}\,\mathrm{M_\odot/yr}$ and velocities of $\simeq 200\,\mathrm{km/s}$. Accretion takes place though a magnetosphere which extends to the corotation radius of the disk. The age of these objects lies between 0.5 to $3 \cdot 10^{6}\,\mathrm{yr}$.

Thorough studies of stars in the stage of class II, the so called classical T Tauri stars were performed by several groups. These stars are all located in or near molecular clouds but they are also visible at optical wavelength. Their optical spectra shows emission lines which are explained by surrounding envelope and disk material, as well as lithium absorption. Veiling due to accretion from the surrounding disk can be observed in these stars. The stars still show infrared excess caused by the disk which is heated by the star. The disk can of course also be observed at submillimeter wavelength.

### Class III - Weak-line T Tauri stars

The spectral index $s \sim -3$. The overall energy distribution is according to black body radiation. There is no accretion disk observed. In the Hertzsprung-Russell diagram the occupy the region of the classical T Tauri stars to the zero-age main sequence. The loss of the disk from class II to class III phase is accompanied by planet formation. About 1/3 of the classical T Tauri stars have disk massive enough to form primitive solar nebula. At an age of 20 to 30 Myr all indicators of circumstellar disk around these stars have disappeared they enter the post T Tauri phase.

Weak-line T Tauri stars can be distinguished from classical T Tauri stars by the Balmer emission lines in the optical spectrum. As the star evolves the disk is accreted to the star or has started to form planetesimals so that it becomes optical thin. The infrared excess weakens and also the accretion rate and the Balmer emission lines became weaker. Veiling is not observed anymore. But lithium absorption at 6707 Å is also strong. X-ray emission is still observed in these stars.

### Post T Tauri stars - UV Cet type flare stars

In the optical spectrum H$\alpha$, calcium, and magnesium are now seen in absorption. The core of these lines are filled in. Some of these stars show lithium absorption but it is not characteristic for these stars. The spectral energy distribution is like a main sequence star so that it cannot be distinguished from them by simple photometric indices.

## 1.4   Stars on the main sequence

When the central hydrogen fusion starts the stars have a homogeneous chemical composition. In the Hertzsprung-Russell diagram all stars are aligned on a line where higher mass stars are more luminous than stars with a lower mass. The line is called zero-age main sequence (ZAMS).

The stars stay on the main sequence until they have burned most of their hydrogen in the core. During that stage they do not change their spectral signatures much (e.g. lithium disappears). Small flare events can be observed but usually the stars do not exhibit frequent flares. For a $1\,M_\odot$-star the time passed on the main sequence is about $7 \cdot 10^9$ yr. For a B0V-star the time is much shorter ($2 \cdot 10^6$ yr), and for an M5V-star much longer ($1.5 \cdot 10^{11}$ yr).

## 1.5  Post-main sequence stars

At the time most of the core hydrogen is used up a new phase in the lifetime of the star begins. For stars with masses $M \leq 2.5\,M_\odot$ the helium fusion ignites explosive. The star undergoes a helium flash. In the beginning of this the star becomes more luminous. In the core helium is accumulated. The pressure in the center is so high that the electron gas is Fermi-Dirac degenerated before the ignition of the helium. When more than $M_{\mathrm{He}} \simeq 0.45\,M_\odot$ is accumulated and a temperature of $T \simeq 8 \cdot 10^7$ K is reached the helium fusion starts explosively.

Because the electron gas is degenerated the pressure does not depend on the temperature so that the energy released in the helium flash does not lead to an expansion and cooling. Instead the helium core collapses in free-fall time. This stops when a temperature is reached which is so high that the electron gas degeneration is not possible anymore.

The explosion shock is absorbed by the massive shell. The star survives the helium flash. It reaches a new equilibrium situation at a smaller luminosity. In its center it a hydrostatic helium fusion and in its shell a hydrogen fusion is established.

## 1.6  What do we know about local young stars

Star formation plays a key role in the understanding of not only of 'how the sun and the planets were formed', but also of how our galaxy - the milky way - and other far away galaxies have formed. Star formation is not well understood locally but in close by galaxies, star formation can be observed seeing bright blue distinct regions and even at higher red shift, galaxies appear blue if star formation is ongoing. Or as Dr. Lee Hartmann, CfA would put it: 'Star formation scales with red shift $z$: $R_{\mathrm{SF}} \sim z$, where $R_{\mathrm{SF}}$ denotes the star formation rate'[†] . So at red shifts of $z \geq 1$ star formation appears quite well understood, but at $z \sim 0.1$ (e.g. Andromeda), we resolve structure and thus the theory runs into some difficulties, while local star formation ($z = 10^{-4}$), we are just at beginning of understanding, and a lot of open questions still arise. Though in the further text we are dealing with fairly evolved young stars they are still in the pre-main sequence phase. We hope to shed light on the origin of local young stars.

Recently previously unknown associations of young stars were discovered in the solar vicinity (at about 50 to 70 pc from the sun) which came to an absolute surprise to the community. Theories predicted young stars only in star forming clouds such as Taurus-Auriga at 140 pc, Chameleon at 160 pc or Orion at 340 pc, in which stars are still produced. The questions which rise immediately are the following: How old are these groups and how did they evolve? If a young star is found to be indeed isolated, how and when did it get there? Are there even more young nearby groups of stars within 100 pc? Can we give reliable criteria so that we can identify such groups of individual isolated stars? These questions will be addressed by several approaches in this thesis. But not all the questions can be answered for each individual star of the sample. The techniques and approaches for an answer to these questions will be developed and discussed.

The newly discovered association TW Hydrae (TWA) at a distance of about 60 pc, and the Horologium - Tucana Association at a distance of $\sim 50$ pc each have about 20 confirmed

---

[†] Discussion at the meeting in Ouro Preto, Brazil, April 05 - 10, 2003: Open Issues in star formation

comoving members. All of them show signatures of youth but remnants of cold gas in their vicinity is not observed. For example, the central star of TWA, TW Hydra itself, is classified as a classical T Tauri star. All the stars in the region of TW Hydra show a strong lithium absorption line in their spectra, and also the H$\alpha$-line is seen in emission or is at least filled in. Both features are signatures of youth in the spectrum of low mass stars and stars with spectral types up to G. Around these stars searches for disk material as well as direct imaging for planets is ongoing (see Jayawardhana et al., 1999; Neuhäuser et al., 2000; Telesco et al., 2000; Marengo et al., 2000; Jayawardhana et al., 2001; Brandeker et al., 2001; Jayawardhana et al., 2002; McCabe et al., 2002). Additionally we know some translucent clouds like MBM-12 (Hearty et al., 2000). The age or distance of the stellar members of this cloud is still under discussion, it could be as young as $\sim 1\,$Myrs and it is located in a distance range of 60 to 240 pc (Luhman, 2001).

On the other hand there are some groups of stars in the solar vicinity, which are older than 10 Myr but still pre-main sequence or zero-age main sequence such as the member stars of the local association, the Ursa Major association, the Pleiades super cluster, including the Pleiades Group and Field stars, the Hyades Cluster, and the $\beta$ Pictoris moving group. For a summary on these associations see Eggen (1998) and Jayawardhana & Greene (2001). These groups, associations and clusters were identified mainly by kinematic data, but the membership can also be investigated spectroscopically as they show a common elemental abundance, such as for the elements iron or lithium. They have spectroscopic signatures indicating the activity level and which are strongly depending on the age of the star: the filling in of the H$\alpha$-line, the calcium H & K lines, as well as the magnesium Ib line, or for younger stars emission in the core of these lines or for T Tauri stars, the H$\alpha$-line can be completely in emission. Investigating these features in great detail could reveal the star formation history of the association as well as the true membership to each cluster. Large associations and clusters could have formed sequentially and thus have member stars of different ages. As an example of the identification by using only space motion, one could mistake Pleiades stars with TW Hydra association members which have a very similar space motion. A lot of stars are identified as local association members, but they could truly belong to other associations with similar space motion. The true membership can be identified by the chemistry of the stars (Fuhrmann, 2004) or by youth indicators in their spectrum (Montes et al., 2001). The kinematics of the local association is very similar to other associations, e.g. the $\beta$ Pictoris group. Sometimes the Pleiades are believed to be part of the local association. On the other hand a big association could have a star formation history. The Ursa Major association has a canonical age of 300 Myrs (Soderblom & Mayor, 1993), but recent work has shown that it could also have an age of 500 Myrs (King et al., 2003) or as we suggest 200 Myrs (this work, Chap. 4.1.1). All of the authors could be right and the UMa could have had ongoing star formation for 300 Myrs and the age spread could then easily be understood. For a discussion, see Chap. 4.1.1.

Young stars with intermediate ages between T Tauri stars and main sequence stars are difficult to identify because of the lack of significant features such as strong emission lines as seen in the spectrum of T Tauri stars. There were many attempts to find these stars, such as studying the ROSAT all sky survey for X-ray luminous stars, double stars which consist of two stars whit a high mass ratio where one star is an O-, B- or A-star on the main sequence and the secondary is a pre-main sequence G-, K-, or M-star. They are called Lindroos binaries. The idea here is to use the fact that the higher mass star evolves on a much faster time scale than the low mass companion. If the high mass companion is on the main sequence or even post-main sequence, the low mass companion could still be pre-main sequence. For a detailed study of such objects see the PhD thesis of Huélamo (2002).

A second approach is to look for low mass stars with a high level of activity. Red dwarf

flare stars are thought to be the missing link between the T Tauri phase and the main sequence phase of a star. The stars are in a quiescence phase similar to normal main sequence stars but in the flare phase they show signatures of young stars, e.g. core emission in H$\alpha$- and calcium-, X-ray emission and IR-excess. Relying on these signatures, the stars are at least as young as the Pleiades, which means the F-, G- and K-stars in a flare star sample should still show the lithium absorption at 6707 Å as a prominent feature. For the lower mass stars such as late K to M, the lithium could already be destroyed though the star is young.

Though lithium is not a very reliable quantitative age indicator, since it can be destroyed in close binaries faster than in single stars of the same spectral type, we can use it as a qualitative signature which is easy to identify. On the other hand lithium can also be produced in stellar flares, which would lead to a high lithium abundance or even an overabundance. The stars of our survey are known to exhibit flares, so we will use the lithium absorption only as a hint and not as a unique criterion for the youth of the star. In using the lithium criterion, we must always be aware that an active star can have lithium but still be old. In each detection of lithium we will be very critical about the conclusions we draw.

As a consequence of identifying young stars close to the sun (within 100 pc), we obtain an optimal sample in our search for planets by direct imaging techniques. The stars are fairly young and therefore the planets around them are also young. Theories for giant planet formation agree that the planets form out of the disk surrounding the star after the star formation process is quite advanced. The young planet contracts and therefore has its own energy source. The contraction heats up the planet atmosphere and the planet emits light in the infrared. The planet to star luminosity ratio is predicted to be smallest (i.e. best using the currently available infrared detectors, adaptive optics systems, and telescopes) in the infrared K-band.

The direct detection of a planet or a low mass object would enable us to calculate dynamical masses as well as to study the atmospheres of these young gaseous hot Jupiter-like planets. The main advantage would be that the time scales as well as the theories for migration of giant planets to nearby orbits or the in situ formation of giant planets could be tested.

The young stars of the northern hemisphere are additional targets to search for planets using the Tautenburg échelle spectrograph of the Thüringer Landessternwarte by measuring the radial velocity shift of the spectral lines of the star. The so called 'radial velocity planets' are found by periodic Doppler shift of the stellar spectral lines which occur because the companion and the star move around their common center of mass of the star and the planet which is in case of a planet close to the center of mass of the high mass star. This makes the star periodically approach and move away from us. The measurement of radial velocity variations only yield a lower mass limit $m \sin i$ for the companion which depends on the inclination $i$ of the orbit to the line of sight. The observation of radial velocity variations of younger stars is more challenging than around older stars because of the stellar activity. Young stars are variable and have spots or exhibit large and smaller flares. If these variations occur during a radial velocity measurement, they might mimic radial velocity variations of a companion and/or the period of the star itself could be mistaken as the orbital motion of a companion. Despite this challenge, the detection of planets or substellar companions around young stars can hold information on the time scales of planet formation and on the formation and evolution process of binary stars with a substellar or low mass companion.

## 1.7 Details of flare stars

Flare stars (FSs) were discovered in the late 1940s in the solar vicinity and were named UV Cet-type variables (classical FSs). The study of these FSs especially in the solar vicinity but also in star clusters and associations has fundamental significance for the study of the

evolutionary process and the physics of red dwarf stars. Because of the lack of significant features, it is still difficult to identify stars which are more evolved than T Tauri stars (TTS, low mass pre-main sequence stars), but not yet on the main sequence. In the following we will give the definition of the IAU and the working definition which we use according to Gershberg et al. (1999). We will also give the definition for other types of flare stars.

## 1.7.1   Definition of flare stars

In the recent years great progress was made in the understanding of stellar evolution from the collapse of a cloud or cloud segment through the T Tauri phase to the main sequence. By now observations have shown that about half the stars are binaries and among the young stars maybe more than 2/3 of the stars are binaries or multiple stars. On the other hand, theories which predict binary stars and calculations of the birth of binary stars are in contradiction to the observations that these stars are the common case, not well established. Much work in this field is in progress (Zinnecker & Mathieu, 2001).

As pointed out above, the observations of stars at different evolutionary stages is not yet satisfying, astronomers have started to define which criteria stars have to fulfill to be a good candidate for being in an intermediate evolutionary stage between the T Tauri phase and the main sequence. Binary stars could always spoil the sample as binaries in close orbits could produce flare activity. The same is true for more evolved stars which have swallowed a formerly orbiting planet or a low mass companion and which could mimic features of young stars. RS CVn stars, for example can show strong lithium absorption in their spectrum though they are evolved.

**Definition by Xth IAU General Assembly**

Red dwarf flare stars are defined by the International Astronomical Union (IAU) General Assembly as follows:

> Dwarf stars of spectral classes dM3e to dM6e characterized by rare very short flares with amplitudes from 1 mag to 6 mag. Maximum brightness (usually sharp) is attained in a few, or several tens of seconds after commencement of the flare, total duration of the flare being equal to about ten to fifty minutes.

**Definition by Gershberg et al. (1999)**

Gershberg et al. (1999) give the following definition for UV Cet-type variables:

> UV Cet-type variables are stars on the lower part of the main sequence which show phenomena inherent to the solar activity. The main manifestations of the solar activity are detected on such stars: sporadic flares, dark spots, X-ray and UV bursts.

The Gershberg catalog contains also the so called related objects. These are not low mass M-stars as the IAU definition demands, but they can also be higher mass stars like K- and G-type stars.

In the following Chapters if we simply refer to flare stars, we will always mean variable stars according to the definition given by Gershberg et al. (1999). If it must be stated more clearly which subgroup of variable stars we are addressing, we will use the correct designation.

**Discussion of the Definitions**

The definition of the IAU General Assembly is very strict and makes the stars difficult to detect, since for a completed sample one has to survey the entire sky with a long time baseline and with different filters to include only stars of spectral type dM3e-dM6e. A combined spectroscopic and photometric survey would be preferred with the same time baseline to detect the changing spectroscopic features as the stars show flares. The theoretical understanding of M-star atmospheres is now making great progress. But spectral synthesis analysis of M-stars is still difficult to perform. Yet, the opacity distribution functions of the two and three atom molecules are not reliable. Dust and cloud formation as well as the settling of dust in the atmosphere are challenging problems of recent theoretical astrophysics. These stars do not show a relative continuum in their spectrum which is dominated by molecular absorption bands. Also the convection layer is known to be very deep and can reach into the center (fully convective stars). Combined with the fast rotation and the magnetic field, the M-stars are expected to exhibit flares.

The flare mechanism can be explained by an $\alpha$-$\Omega$-dynamo, a combination of convective motion, and differential rotation which power the magnetic field. The magnetic field is linked to the plasma of the star. It also reaches out to large distances from the star. At these distances the plasma becomes thin and there is evidence that the magnetic field is no longer linked to it. The still connected foot points of the magnetic field on the surface get dragged along and therefore the magnetic field gets twisted up. If the magnetic field becomes stronger, the magnetic field lines recombine and relief energy, a flare occurs. The $\alpha$-$\Omega$ dynamo is the most successful model to explain flare activity in stars, yet it cannot explain all flare phenomena in stars.

The definition by Gershberg et al. (1999) allows a much wider range of stars to be included, e.g. the so called related objects (G- and K-stars). The discovery of UV Cet-type FSs is much easier because different long term surveys, such as the ROSAT all sky survey, or different combinations of optical surveys can be investigated in several wavelength ranges. In addition to M-dwarfs the criterion of Gershberg et al. (1999) also includes F-, G-, and K-type stars in which the atmospheres are well understood when they have arrived on the main sequence, and this knowledge can be used to investigate the pre-main sequence nature of the FSs. This experience will enable us establish spectroscopic criteria and to distinguish the FSs stars from the old post-main sequence RS CVn stars. The later also show flare like activity and often were and still are sometimes confused with the young flare stars. On the other hand the definition by Gershberg allows a wide range of objects to enter the sample and in the end we might use a much stricter criterion to rule out objects which do not belong to the sample because they are not pre-main sequence. It could also be possible that there are different types of flare stars which have a common nature and hence are somewhat the same type of object just seen from a different perspective, or with a not fully complete observational data set.

According to the recent definition given by Gershberg et al. (1999), red dwarf flare stars are on the lower part of the main sequence and show activity similar to the sun (sporadic flares, dark spots, variable emission from the chromosphere and the corona, radio, X-ray and UV outbursts). One of the most challenging problems in present astrophysics is the understanding of the mechanisms that drive stellar flares. Flares occur on magnetically active stars where the differential rotation as well as a convective layer are believed to drive the $\alpha$-$\Omega$-dynamo. The younger the star, the faster it rotates, when it is no longer coupled to the surrounding disk material for any reason. This can be observed in weak-line T Tauri stars in Taurus as well as in other star forming regions. Later on, as the star evolves it looses angular momentum and again slows down. The way this can be observed is the activity level of the star: the

younger the star the higher the activity level. But life is not that simple and it is known that also evolved stars on the main sequence and post-main sequence stars can show outbursts.

Ambartsumian (1954) noted that classical flare stars are similar to normal red dwarf stars at minimum light and during flares show some peculiarities in the line emission like TTS (H$\alpha$-core emission, calcium H&K and magnesium core emission or filling in). FSs of higher luminosity were also discovered in the Orion association (Haro & Morgan, 1953) which supports the theory that FSs and TTS have a common nature. The existence of UV Cet-type FSs in young T associations also stresses the indications for a connection between FSs and TTS. In the solar vicinity at a distance closer than 100 pc a total number of 463 FSs are known at present and listed in the Gershberg et al. (1999) published catalog, in the further text referred to as the Gershberg catalog or the flare star catalog.

As Haro (1957) already pointed out, the flare state of red dwarf stars is an evolutionary state which follows the classical TTS stage. Later Ambartsumian et al. (1970) suggested that this is the only possible path of evolution for red dwarf stars. This can be deduced from estimations of the total number of flare stars in open clusters and associations, i.e. from the number and space density of observed flare stars detected down to a limiting magnitude (mass). This number is comparable to the total number of known members of stellar cluster (or association) down to a limiting magnitude (e.g. for the Pleiades 12 mag). This means all late type stars go through a flare stage during their early evolution.

The UV Cet-type stars are believed to be relatively young (possibly zero-age or pre-main sequence stars) with ages $\sim$ 100 Myrs or younger. They may be former members of recently dispersed T or OB associations or may be ejected stars from associations after three body encounters (like run-away TTS). Local dispersed associations as the hosts of these stars do not appear unlikely: The translucent high latitude cloud MBM 12 with ongoing star formation (Hearty et al., 2000; Luhman, 2001), the TW Hydra association at $\sim$ 60 pc, which has dispersed its gas and dust (Webb et al., 1999), the Horologium association (Torres et al., 2000) and the Tucana association (Zuckerman & Webb, 2000) are already known. It is still under discussion if the Horologium and the Tucana associations are two distinct associations or if they are only one (Zuckerman et al., 2001b). They are located next to each other in the sky and the age indicators of the stars could support a common age. But there are still some uncertainties in the age because the distance to these associations is yet not well known. Most of the bona fide members and member candidates were too faint, so that they were not observed with the Hipparcos satellite. GAIA and DIVA will be capable to perform accurate astrometry for these fainter stars. Also crowding and binaries are not such a big problem for these two satellites as it was for the Hipparcos mission.

Hence, there are indeed young T associations within $\sim$ 100 pc. A few isolated young nearby stars were known before the ROSAT and the HIPPARCOS mission, e.g. GJ 182 at a distance of 27 pc and with an age of 20 Myrs. Note that GJ 182 is a member of the flare star catalog.

## 1.7.2 The nature of other types of flare stars

The detection of flares in stars is not unusual and can be related to different physical reasons. Young pre-main sequence stars, main sequence stars as well as very old cataclysmic variables can show huge light variations. Even on the sun we can experience flare activity which can influence the daily life on earth, e.g. we can observe polar lights sometimes even far away from the poles as it could be seen in Munich in the winter 2000. These rare events take place if the activity level on the sun is extremely high. But also in recent time, we occasionally experience a disturbed radio or TV signal that can be due to outbursts on the sun.

In the literature there are several types of flare or variable stars. Above we have defined

the flare stars as we want to use it for our further work or more precisely the red dwarf or UV Cet-type flare stars. For completeness we give the definitions of related objects such as BY Dra type variables and T Tauri stars. The red dwarf flare stars are frequently wrongly classified as post-main sequence RS CVn type variables. A definition of those will also be given.

An improved system of variability classification is used in the fourth edition of the General Catalog of variable stars (GCVS), based on recent developments in classification principles and taking into account the suggestions of a number of specialists. Variability types are grouped according to the major astrophysical reasons for variability:

- eruptive variables: FU, GCAS, I, IA, IB, IN, INA, INB, INT, IT, IN(YY), IS, ISA, ISB, RCB, RS, SDOR, UV, UVN, WR

- pulsating variables: ACYG, BCEP, BCEPS, CEP, CEP(B), CW, CWA, CWB, DCEP, DCEPS, DSCT, DSCTC, L, LB, LC, M, PVTEL, RR, RR(B), RRAB, RRC, RV, RVA, RVB, SR, SRA, SRB, SRC, SRD, SXPHE, ZZ, ZZA, ZZB

- rotating variables: ACV, ACVO, BY, ELL, FKCOM, PSR, SXARI

- cataclysmic (explosive and novalike) variables: N, NA, NB, NC, NL, NR, SN, SNI, SNII, UG, UGSS, UGSU, UGZ, ZAND

- eclipsing binary systems: E, EA, EB, EW, GS, PN, RS, WD, WR, AR, D, DM, DS, DW, K, KE, KW, SD

- intense variable X-ray sources: X, XB, XF, XI, XJ, XND, XNG, XP, XPR, XPRM, XM

- other symbols: BLLAC, CST, GAL, L:, QSO, S, *, +

In the following the definitions are given only for the variable star types we will use in the following paragraphs.

**RS CVn type variables**

> Eruptive variables of the RS Canum Venaticorum (RS CVn) type. This type is ascribed to close binary systems with spectra showing Ca II H and K in emission, their components having enhanced chromospherically activity that causes quasi-periodic light variability. The period of variation is close to the orbital one, and the variability amplitude is usually as great as 0.2 mag in V (UX Ari). They are X-ray sources and rotating variables. RS CVn itself is also an eclipsing system.

The RS CVn binary stars are a well established class of chromospheric active stars. Peculiar changes in amplitude, shape, mean light level and phase of minimum light of these stars have been long standing puzzling problems for astronomers. Though the problem of these unusual photometric behavior of the RS CVn stars could be explained in terms of extinction of the light by circumstellar material, or by pulsation of one of the components with same period as that of the orbital period. But the explanation in terms of the surface activity, in the form of dark stellar spots on the surface is widely accepted. In terms of the stellar spot model, the short term photometric variations (Period = $P_{\text{orb}}$) seen in these object have been attributed to the rotational modulation of the star light by the cool dark spot analogous to sunspot present on the active component of the system and may cover 10% to 50% of the visual hemisphere. Star spot models can also account for the long term variations in light curves and are the effect of changes in size, location and distribution of the spots on the

stellar surface. The explanation of light variation of these stars is not simply hypothetical; however, coordinated optical, spectroscopic observations, and Doppler imaging techniques strongly support this model.

### FU Ori type variables

Orion variables of the FU Orionis type. These variables are characterized by gradual increases in brightness by about 6 mag in several months, followed by either almost complete constancy at maximum light that is sustained for long periods of time or slow decline by 1-2 mag. Spectral types at maximum light are in the range Ae($\alpha$) - Gpe($\alpha$). After an outburst, a gradual development of an emission spectrum is observed and the spectral type becomes later. These variables probably mark one of the evolutionary stages of T Tauri-type Orion variables (INT, see below), as evidenced by an outburst of one member, V1057 Cyg, but its decline (2.5 mag in 11 years) commenced immediately after maximum brightness was attained. All presently known FU Ori variables are coupled with reflecting cometary nebulae.

### INA and INB Orion variables

INA Orion variables of early spectral types (B-A or Ae). They are often characterized by occasional abrupt Algol-like fading (T Ori).

INB Orion variables of intermediate and late spectral types, F-M or Fe-Me (BH Cep, AH Ori). F-type stars may show Algol-like fadings similar to those of many INA stars; K-M stars may produce flares along with irregular light variations.

### INT, IT Orion variables

INT, IT Orion variables of the T Tauri type. Stars are assigned to this type on the basis of the following (purely spectroscopic) criteria: spectral types are in the range Fe-Me. The spectra of most typical stars resemble the spectrum of the solar chromosphere. The feature specific to the type is the presence of the fluorescent emission lines Fe II 4046, 4132 Å(anomalously intense in the spectra of these stars), emission lines [Si II] and [O I], as well as the absorption line Li I 6707 Å. These variables are usually observed only in diffuse nebulae. If it is not apparent that the star is associated with a nebula, the letter "N" in the symbol for the type may be omitted, e.g., IT (RW AUR).

### BY Dra type variables

BY Draconis-type variables, which are emission line dwarfs of dKe to dMe spectral type showing quasiperiodic light changes with periods from a fraction of a day to 120 days and amplitudes from several hundredth to 0.5 mag in V. The light variability is caused by axial rotation of a star with a variable degree of non uniformity of the surface brightness (spots) and chromospheric activity. Some of these stars also show flares similar to those of UV Cet stars, and in those cases they also belong to the latter type and are simultaneously considered eruptive variables.

It is under discussion whether UV Cet variables and BY Dra variables are of a common nature.

**UVN Flaring Orion variables**

UVN Flaring Orion variables of spectral types Ke-Me. These are phenomenologically almost identical to UV Cet variables observed in the solar neighborhood. In addition to being related to nebulae, they are normally characterized by being of earlier spectral type and greater luminosity, with slower development of flares (V389 Ori). They are possibly a specific subgroup of INB variables with irregular variations superimposed by flares.

**Cataclysmic (Explosive and Nova-like) Variables**

These are variable stars showing outbursts caused by thermonuclear burst processes in their surface layers (novae) or deep in their interiors (supernovae). We use the term "nova-like" for variables that show nova-like outbursts caused by a rapid energy release to the surrounding space and also for objects not displaying outbursts but resembling explosive variables at minimum light by their spectral (or other) characteristics. The majority of explosive and nova-like variables are close binary systems, their components having strong mutual influence on the evolution of each star. It is often observed that the hot dwarf component of the system is surrounded by an accretion disk formed by matter lost by the other, cooler, and more extended star.

All descriptions of variable star types are taken from the GCVS.

**T Tauri stars**

They are named after the prototype T Tau discovered in the constellation of Taurus. T Tauri stars represent an early stage in the evolution of stars that are similar to the Sun. The nearest occur in the Taurus molecular cloud and the rho Ophiuchus Cloud, both about 460 light years (140 pc) away.

Many T Tauri stars emit large amounts of infrared radiation indicating that they are surrounded by dusty clouds that have become warm by absorbing starlight and re-emitting it in the infrared part of the spectrum. T Tauri stars also vary erratically in brightness, as if they are being intermittently obscured. One way to interpret these and other observations is that the stars are encircled by a rotating disk of gas and dust which may one day give rise to families of planets. According to an estimate, about 60% of T Tauri stars younger than 3 million years may possess dusty disks, compared with only 10% of stars that are 10 million years old. The implication is that the disappearance of disks in older stars is linked to the appearance of planets.

# Chapter 2

# The sample

The sample of flare stars and related objects was compiled by Gershberg et al. (1999) from a much older list of flare stars. The main criterion is the flare activity of the stars in different wavelength ranges. Since the data was composed out of several sources which in some cases could not be checked, several tests were performed before starting the survey. Also the data was revised for some objects. For multiple objects reliable photometry of the components is especially important. For some stars high angular resolution photometry was performed to search for possible planets and stellar companions.

## 2.1  Revising the catalogs

A first step in understanding the Gershberg sample was to examine the input catalogs and to review the photometry and the spectral classification of all the stars. The data was then used to choose the most interesting, meaning the youngest stars to begin the survey. Therefore, the Hipparcos, the HD-, the BD-, and the GJ-number were used to compare directly the original data of the Hipparcos, the Tycho, the catalog of nearby stars (Gliese & Jahreiss, 1995) and the publication of Hawley et al. (1997) with the data in the Gershberg catalog. Also the references cited in Gershberg et al. (1999) were compared. The first thing to arouse ones suspicious was that some Hipparcos parallaxes have not been adapted correctly. In a second glance at the data, some stars have entered the Gershberg sample, because the apparent magnitude was confused with the absolute magnitude, and therefore these stars appeared to have emitted a huge flare. At this point it cannot be excluded that the stars with this error in the Gershberg catalog might conceivably be flare stars and the reference list in the Gershberg catalog was not complete. A simple comparison of the Gershberg catalog stars with the SIMBAD database has shown that for example some subgiants and giants are among the Gershberg sample stars. These stars are definitely not classical flare stars but can still be members of the so called related objects. Giant and subgiant stars can still be young stars. We have compared all the input stars with the following catalogs: Hawley et al. (1997), the Hipparcos and Tycho catalog, the online version of the Catalog of Nearby Stars (CNS4) available at `http://www.ari.uni-heidelberg.de/aricns/`, and with several other publications and catalogs listed in Gershberg et al. (1999). The main reference for the photometry is the Tycho mission. The data set for this mission is the most homogeneous.

A second step was to revise the parallaxes listed in the Gershberg catalog because some stars are even located below the main sequence in a region of the Hertzsprung-Russell diagram (H-R diagram), where there are no stars expected. The main source of error could only be the distance to those stars, because we do not expect white dwarfs to have entered the Gershberg sample. Yet, we have identified a detached white dwarf binary (GJ 459.1), a low mass X-ray

binary (V801 Aql) and a cataclysmic variable (AM Her) among the sample stars. Double checking the parallaxes listed in the Gershberg catalog with the original catalogs showed that for some stars the parallax has not been taken from any referenced catalog and did not correspond to any parallax given either by Hipparcos, Hawley et al. (1997), or the CNS4. In cases where no parallaxes are given in the Gershberg catalog or we could not confirm the source of parallaxes given, we adopt the values given in the catalogs listed above with preference to Hipparcos values.

To revise the photometry we correlated again the Gershberg catalog with the above mentioned catalogs and added the Tycho catalog. For many stars the photometry data was far off, but the origin of the data in the Gershberg catalog again could only be cleared for a small number of stars. For the further work, we use the V- and B-band photometry published in the Tycho catalog if possible. In cases where no data from the Tycho survey was available, we used the SIMBAD data base. The luminosity was computed using the revised V-band magnitudes, the revised distances, the bolometric corrections (B.C.) according to the revised spectral type and transformed with the tables given by Kenyon & Hartmann (1995), and assuming no extinction since the sources that are closer than 100 pc, which is in all cases consistent with the Tycho B-V color and the spectral energy distribution.

## 2.2 The flare stars in the H-R diagram

A first test was to plot the stars in a Hertzsprung-Russell diagram. For this the spectral type given in the Gershberg catalog was converted to a temperature using Kenyon & Hartmann (1995) for the G-, K-, and early M-type stars, and for the M7-, M8-, and M9-stars using Luhman (1999) (see Fig. 2.2). To guide the eye we underlayed theoretical tracks and isochrones from D'Antona & Mazzitelli (1994). These are not state of the art, but are used for a general point of reference in the diagram. In the latter, when we need a more sophisticated view of the special stars, we use the Baraffe et al. (1998) models, but as shall be seen in Chapter 4.1.1, we must take care about which set of model parameters we use.

In general one can see that most stars lie close or above the main sequence. The reason for this can be explained as follows: Most of the stars are pre-main sequence, like GJ 182 which is included in the Gershberg sample, some are unresolved binaries, and some are on the giant branch (see the individual discussion of those stars).

After correcting for known double stars using Hawley et al. (1997), we replotted the H-R diagram. This results in a plot where all the stars are on the lower part of the main sequence. Many stars appear to be above the main sequence, i.e. are pre-main sequence stars. But this is only one indication for youth which could still be wrong because of unidentified double stars, wrong distances, etc. One to three stars could also be post-main sequence stars from their position in the H-R diagram, lying on the giant branch. At a first glance the Gershberg sample looks rather homogeneous except for a few objects. Hence, we need additional confirmation such as lithium absorption, H$\alpha$-emission, and other activity indicators as calcium H & K and magnesium Ib line core emission.

In the following chapters the more detailed analysis of the flare stars observed for this work will be described. The basic ideas is that we wanted to perform spectroscopy of all stars at least once with low resolving power of about $\Delta\lambda/\lambda$ of 6,000 or with high resolving power of about $\Delta\lambda/\lambda$ of 60,000. The spectra are used to identify signatures of youth as described above. The high resolution spectra of the F-, G- and K-type stars are also analyzed using spectral syntheses methods described in Chapter 3. The goal is to obtain spectroscopy of all the stars and to confirm or reject their preliminary candidates from the Hertzsprung-Russell diagram that may or may not be pre-main sequence by youth indicators.
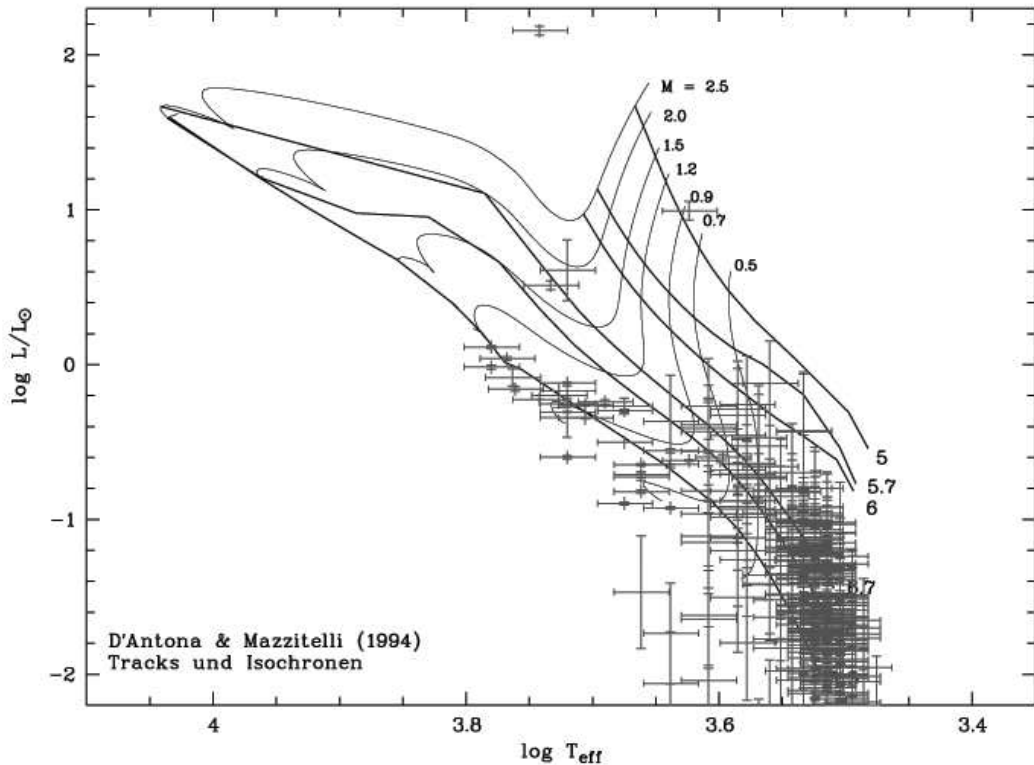
**Figure 2.1:** D'Antona & Mazzitelli (1994) tracks and isochrones underlaying the sample stars. The sample stars are plotted using the revised input data and the spectral type with temperature conversion taken from Kenyon & Hartmann (1995) and Luhman (1999). The corrections for binary stars and the distance show that the stars are quite homogeneously spread on the lower part of the main sequence. Only the stars with an available distance are shown with a distance from 2.5 pc to 100 pc. Masses are in units of a solar mass and ages are given as $\log t/\mathrm{yr}$.

In the following chapters, we will again see Hertzsprung-Russell diagrams but with underlying tracks and isochrones matching the nature of the stars shown (pre-main sequence, post-main sequence). In some cases, we will use the models from different authors to be confident with the results we achieve. We will use the resolved astrometric and spectroscopic binary $\chi^1$ Orionis A & B to test pre-main sequence evolution modeling, and will explain why we prefer a certain model parameter set.

All in all the sample seems to yield promising candidates for young, nearby stars for the surveys carried out and described in the following chapters.

## 2.3 Space velocity of the sample stars

We have constructed a Bottlinger diagram to investigate the space motion of the sample. In the UV-plane the space motion of some stars can be identified with known young associations in the solar vicinity. In the sequel, we will discuss the membership of these flare stars with the associations and discuss the spectroscopic criteria which are sufficient to find young stars. The associations we consider are the following: Ursa Major Association (UMa), TW Hydra Association (TWA), Horologium-Tucana Association (HorA - Tuc), $\beta$ Pictoris Association ($\beta$ Pic), the translucent cloud MBM 12, IC 2391 and Coma Ber. All the asso-
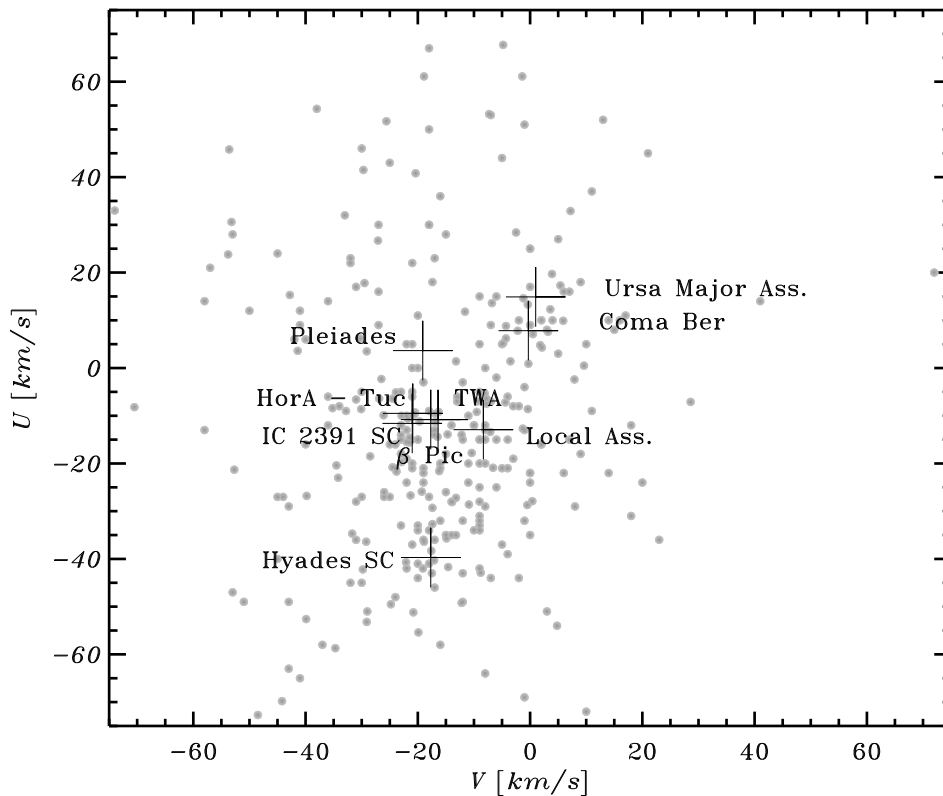
**Figure 2.2:** Space velocities in the UV-plane of the sample stars compared to the mean space velocity of known local young associations of stars. The flare stars of the Gershberg sample are marked with gray dots and the big black crosses mark the mean space velocity of the young associations.

ciations lie within 100 pc from the sun. The space velocity for $\beta$ Pictoris, IC 2391, and the Pleiades was taken from Robichon et al. (1999). The data for Horologium-Tucana Association from Torres et al. (2000), for the Ursa Major Association from Montes et al. (2001). For MBM 12 the space motion was not measured. The space motion of the flare stars was compiled the using newer version of the Gliese & Jahreiss (1995) catalog available on the Internet (`http://www.ari.uni-heidelberg.de/aricns/`).

## 2.4   Observation and Data Reduction

For a log-file of the observations, see Appendix 6.3. This table gives a complete list of the optical spectroscopy that was obtained for the stars and the equivalent with of the lithium absorption line at 6707 Å. Some stars were observed more than once, because they seemed particularly interesting, or because we could use them to compare low resolution to high resolution spectra as well as to compare the performance of DFOSC to CAFOS. Additionally, visual companions were observed. These companions were either known to be comoving from the Digitized Sky Survey 1 and 2 (DSS1 & DSS2), and from Hipparcos data, or they were suspected to be related. The DSS1 & DSS2 can be accessed via Internet with

`http://archive.eso.org/dss/dss`.

## 2.4.1 Low resolution spectroscopy

Some low resolution spectroscopic data of the northern FSs were observed in 2000 at Calar Alto, Spain using the focal reductor instrument CAFOS (Calar Alto Faint Object Spectrograph) mounted on the 2.2 m telescope. The resolving power of the instrument using the 'green' grism was $\Delta\lambda/\lambda \sim 6,000$ in the region of H$\alpha$ and the wavelength coverage is $5,600 - 6,800$ Å.

The low resolution spectroscopic data of the southern flare stars were obtained mostly in 2001, using the 1.54 m Danish telescope operated by ESO, La Silla, Chile. The instrument used was DFOSC (Danish Faint Object Spectrograph and Camera). DFOSC is a multipurpose focal reductor instrument which can be used in short slit low resolution échelle mode with a resolving power of $\Delta\lambda/\lambda \sim 6,000$ in the region of H$\alpha$. The complete optical wavelength range is covered and the instrument's performance is comparable to CAFOS though the telescope is smaller. The resolving power of about $6,000$ in the red wavelength range is sufficient to resolve lithium at 6707 Å from calcium at 6718 Å, but there is a contribution from nearby iron lines to the lithium line which cannot be resolved and which can lead to an overestimation of the equivalent width of the lithium absorption line.

### Data reduction of the DFOSC and CAFOS data

The data reduction and analysis of the DFOSC and CAFOS data were performed using the astronomical software package Image Reduction and Analysis Facility (IRAF) provided by the National Optical Astronomy Observatories (NOAO) in Tucson, Arizona. For the CAFOS data the long slit package was used and for the DFOSC data the échelle package.

For both spectrographs at the beginning of the night dedicated flat field and bias images were obtained. The flat field images were taken using both the external flat field screen mounted in the dome and the internal flat field lamp of the instruments. From those individual flat field images a mean master flat field was created removing the hot pixels (pixels that have detected a cosmic ray and are therefore saturated) by comparing the consecutive images and removing pixels which are saturated and replacing them from the other image which were scaled to the same count rate, assuming the detector has a linear behavior.

A mean bias image was created averaging all bias images from each night. The bias images was subtracted from all the science images. The spectra from the science images were extracted using individual apertures for each star and in each order of the spectrum. With the same aperture the flat field region was extracted and a normalized flat field for the individual science image was computed which was not corrected for the blaze angle of the grating respectively grism. This enables us to at least qualitatively remove the influence of the blaze angle on the science data assuming the lamp is perfectly white. Each science image is now divided by its dedicated flat field. In two cases the telescope was pointed in an extreme direction so that the instrument flexure of DFOSC caused the stellar spectrum to come to lie on a position on the CCD which was not exposed with the white light flat field lamp. In these two cases we extracted the complete area of each order which was exposed by they white light lamp, and summed up the CCD rows after removing the curvature of the spectrum. We did the same with the stellar spectrum. We divided the summed stellar spectrum by the summed white light spectrum. The two stars were not particularly interesting so we did not try to repeat the observations with a correct flat field.

After the division by the flat field image, the spectrum is extracted by considering the previously determined aperture. A wavelength calibration for each spectrum was applied using the internal reference lamps for each instrument. For CAFOS these lamps are located

inside the instrument and the light is projected directly onto the slit by a mirror which can be flipped into the path of light. For DFOSC the helium argon lamp is located in the skybaffle and an internal thorium argon lamp is located in the instrument and can be projected onto the entrance slit with a mirror similar to CAFOS. The light of the helium argon lamp is reflected into the slit by closing the cover of the skybaffle. During the night the helium argon lamp is used since it is more time efficient and for a spectrograph with a resolving power of $\Delta\lambda/\lambda = 6,000$ there are enough helium and neon emission lines in the red wavelength regime to guaranty a good wavelength calibration. Immediately after each science target and before moving the telescope, the wavelength calibration image (arc image) was taken. These arc images are extracted using the individual aperture of the associated stellar spectrum and then identifying the reference wavelength of the emission lines of the lamp. The wavelength reference is assigned to the science targets. For DFOSC this is important because the instrument flexure can be very high as we have already mentioned when describing the flat field procedure.

### 2.4.2 High resolution spectroscopy

For the collection of spectroscopic data of the sample, we performed high resolution spectroscopy using the 2.2 m telescope at Calar Alto, Spain equipped with the fiber coupled échelle spectrograph FOCES (Fiber Optics Cassegrain Échelle Spectrograph). The performance of the spectrograph allows a resolving power of $\Delta\lambda/\lambda = 60,000$. This and the well defined continuum throughout the orders (Korn, 2002) enables us to perform spectral synthesis analysis of the F-, G-, and late K-stars of the sample. Especially the continuum can be extrapolated from one order to the other. We also know the position and the curvature of the continuum at lines which span more than one order like the Balmer-, magnesium-, or calcium lines. To know the exact shape of the continuum at these lines is required to measure e.g. the effective temperature using the H$\alpha$- and H$\beta$-line profiles, or to confirm the surface gravity using the magnesium Ib line profiles.

Additionally, M-stars of the Gershberg FSs sample which could not be observed at Calar Alto because of bad weather and technical problems, high resolution échelle spectroscopy was performed using the Tautenburg 2 m multipurpose Schmidt-telescope equipped with a short slit échelle spectrograph. The resolving power of the instrument is $\Delta\lambda/\lambda = 67,000$, but the continuum is not as well defined as for the FOCES spectrograph. This is mainly due to the way flat field images are taken. Anyway, for the M-stars the spectral synthesis analysis cannot be performed, because the input of opacities for molecules and the atmospheric LTE model might not be sufficient.

**FOCES observation and data reduction**

The FOCES data were reduced using a dedicated software package implemented in IDL (Interactive data language) which was developed by the construction team of the FOCES spectrograph and provided by Thomas Gehren and Klaus Fuhrmann, but it is also available at the Calar Alto Observatory. Each afternoon bias, flat field and thorium argon images were taken. For the flat field images the internal flat field lamp was used which is located close above the fiber entrance and the light is projected onto the entrance diaphragm by moving a mirror into the light path. A series of three flats were taken, where the first image was well exposed in the red wavelength regime, the second image was well exposed in the green wavelength regime and the red wavelength regime was overexposed and in the third flat field image, the blue wavelength regime was well exposed while the red part of the spectrum was overexposed. After these three images the telescope was moved to another position in the dome simulating the movement of the telescope as during the observations in the night. This

procedure was repeated ten times each afternoon. During all the calibration and science exposures the so called 'fiber shaker' was active, which shakes the fiber close to the entrance of the spectrograph. This reduces the noise which is introduced onto the spectrum by the fiber, as was shown by empirical test. An idea why this 'fiber noise' is introduced if the fiber is not moved is the following: The fiber is connected at the upper and lower end to a fiber head which is mounted to the telescope and the spectrograph, respectively. This coupling squeezes the fiber. When the fiber lies in a certain position, some wavelengths are transmitted through the fiber well and others are absorbed or scattered in the fiber. These specific wavelengths which are not transmitted through the fiber but scattered depend on the curvature of the fiber. Shaking it only slightly will remove this effect because the curvature of the fiber is changed permanently. Additionally, the movement of the telescope during the acquisition of the flat field images simulates the position of the fiber during observations. Also the position of the fiber while the telescope is moved changes the performance, because the great overall curvature of the fiber is changed. The points of the fiber which are squeezed have a different diffraction index than the free fiber. The fiber cladding and the core are deformed at these two positions which can introduce scattering of light through the cladding.

The bias and thorium-argon images (arcs) were taken at the beginning and the end of the night. Wavelength calibration during the night is not necessary because the instrument is mechanically decoupled from the telescope by the fiber and therefore mechanically very stable, meaning the spectrograph does not move when the telescope is pointed. It is located in a dedicated room below the telescope. The temperature in this room does not change appreciably during the night, even though it is not especially temperature stabilized. For the spectral synthesis analysis, we do not need a subpixel precision for the wavelength calibration. We are not measuring high precision radial velocity variations which can be caused by the presence of planets or (sub)stellar companions. For this kind of observation a long time baseline is required in any case. For our purpose the precision is sufficient and we did not want to lose observing time, because each thorium argon image takes about five minutes including the movement of the lamps and mirrors as well as the warming up of the lamp.

The bias of each science and flat field image was subtracted using a mean bias image created of all acquired bias images in the observing run. As a next step the spectra, the flat field, and the arc image were extracted and the corresponding rows of the CCD of each order were coadded after applying a weight to each row of the extracted order depending on the count rate. After that each coadded order of the flat field image is normalized to one and the coadded orders of each science image are divided by the corresponding flat field order. This is necessary, because the fiber illuminates the central rows of each order much stronger than the rows on the edge. Dividing the rows on the edge which have a pixelcount close to zero by a flat field, that also has a pixelcount close to zero, will result in an unreliable pixelcount number. For a description of the implemented method, see Horne (1986).

After the flat fielding the wavelength calibration is assigned. To check if major shifts of the wavelength have occurred we compare the different thorium argon images acquired in the beginning and at the end of each observing night first. In case of shifts, the wavelength calibration is done using the thorium argon image which was taken closest to the observing date.

**Reduction of the Tautenburg data**

For the Tautenburg data the situation is slightly different. The spectrograph is located in the Cassegrain focus of the multipurpose Schmidt telescope, which means that the lightpath leads across a mirror which is inserted instead of the Schmidt camera and which reflects the light through the axis of the telescope onto the entrance slit of the spectrograph. This mirror has

a curvature the way that the short focal length of the Schmidt telescope is prolonged, so that spectroscopy in the Cassegrain focus is possible. This configuration of a Schmidt Telescope is not very typical. [†]

This setup means the spectrograph is mechanically decoupled from the telescope as FOCES and indeed it is also located in a climate controlled room at a stable temperature. The light is projected directly onto the entrance slit of the spectrograph, so that the star can move along the slit during the night. Each star, therefore, has an individual aperture. The light of the lamp used for flat fielding is projected directly onto the slit by a mirror so the illumination of the slit is different for the flat field images and the science targets. This results in a very unreliable flat field correction as the light paths of the lamps and the stars are different. The data cannot be used for spectral synthesis analysis, yet. Attempts are made to change the flat fielding procedure and to use a flat field screen mounted inside the dome. First tests performed with this setup by Matthias Ammler show that the flat field correction has improved and that now the spectra look promising for the spectral synthesis analysis. In the future the Tautenburg staff plans to equip the spectrograph with an optical fiber.

The data reduction and calibration of the science targets was performed similar to the procedure described for DFOSC (see Section 2.4.1).

The spectrograph is temperature stabilized and therefore does not change its instrument characteristics during the night. Additionally, it is equipped with an iodine cell which can be used as a stable wavelength reference for radial velocity planet or companion star search down to a radial velocity signal of $3\,\mathrm{m/s}$. In Chapter 5 we will describe the radial velocity measurements with this equipment which are currently still ongoing for the most promising young stars of the flare star sample.

---

[†] This design was chosen because of the special conditions in Tautenburg. The original design was made following the construction plans of the Palomar survey telescope with a closed metal tube to block the stray light. But in Tautenburg they desired to be able to perform spectroscopy in bright time when the moon is up. So they designed the Schmidt Telescope with a Cassegrain focus. The Schmidt camera is removed and a mirror is inserted instead.

Also it is remarkable how the location was chosen: At the time when the telescope was built, the scientists were convinced that the best seeing conditions could be found on a small hill located in a forest. Bearing this in mind, Tautenburg is perfect.

The third remarkable feature of the Tautenburg telescope is the dome heating. To avoid having fog settle on the cooler mirrors, one has two possibilities: One cools the telescope during daytime or night fall with an air condition or a big fan to the temperature which is present in the night. Or you heat up the dome and telescope. For Tautenburg, the second possibility was chosen. (Dr. Eike Guenther, private communications)

# Chapter 3

# Stellar atmospheres models

The stellar light observed on earth or from space is emitted from the outer regions of the star, the atmosphere. The atmosphere can be divided into the photosphere and the chromosphere. The inner section of the star where the energy is produced, cannot be observed directly because photons which are generated in the center of the star interact with material of the lower sections and the atmosphere. The atmosphere of the star is the region where the energy coming from the center of the star is absorbed and reemitted, and finally escapes the star. We will formulate the mathematical equations to describe the physics of the observed phenomena. In this chapter we will give the basic ideas of the model atmospheres of late F-, G-, and early K-type stars. After this it will be explained how to calculate model spectral lines and compare with observed lines in order to derive the physical parameters of the stars.

The easiest case would be that the star emits as a black body. But as very early spectroscopic observations of stars have shown, this is not true. Already in 1814 Fraunhofer observed absorption lines in the spectrum of the sun and later on around 1823 in other stars as well. He already knew that the overall emission does not follow a simple black body curve. The development of 'real physics' began with Kirchhoff and Bunsen (1859) in Heidelberg. During that time the beginning of spectral analysis was set with the interpretation of the Fraunhofer lines. 1860 Kirchhoff formulated Kirchhoff's law, which gives the relation between emission and absorption of radiation in thermodynamical equilibrium.

## 3.1 Assumptions

When observing stars from the earth, we perceive all stars except the sun to be point sources. So in principal we do not observe a spatially resolved object but only the integrated light from the surface pointed towards us. Surface features like stellar spots, plage regions, convection and granulation are not resolved.

Assuming that the height of the atmosphere is small compared to the radius of the star, we can describe the atmosphere to be plane-parallel. This simplifies the equations a lot. Observations of the sun show that the atmosphere is about 400 km deep whereas the radius of the sun is 700,000 km. The assumption that the atmosphere is small holds for the sun and we can assume that it is the same for stars which are comparable to the sun.

For young stars or M-, L-, or T-type stars, the convection layer might be deeper or even reach to the center. For these stars Ludwig et al. (2002) have simulated the convection with their three dimensional hydrodynamical computer model of the atmosphere (Allard et al., 2001). The chemical composition of these stars also plays a major role, because the atmospheres are cool so that two and three atomic molecules are stable and can be observed. The chemistry of these cool stars poses a huge problem since opacity functions are not yet well
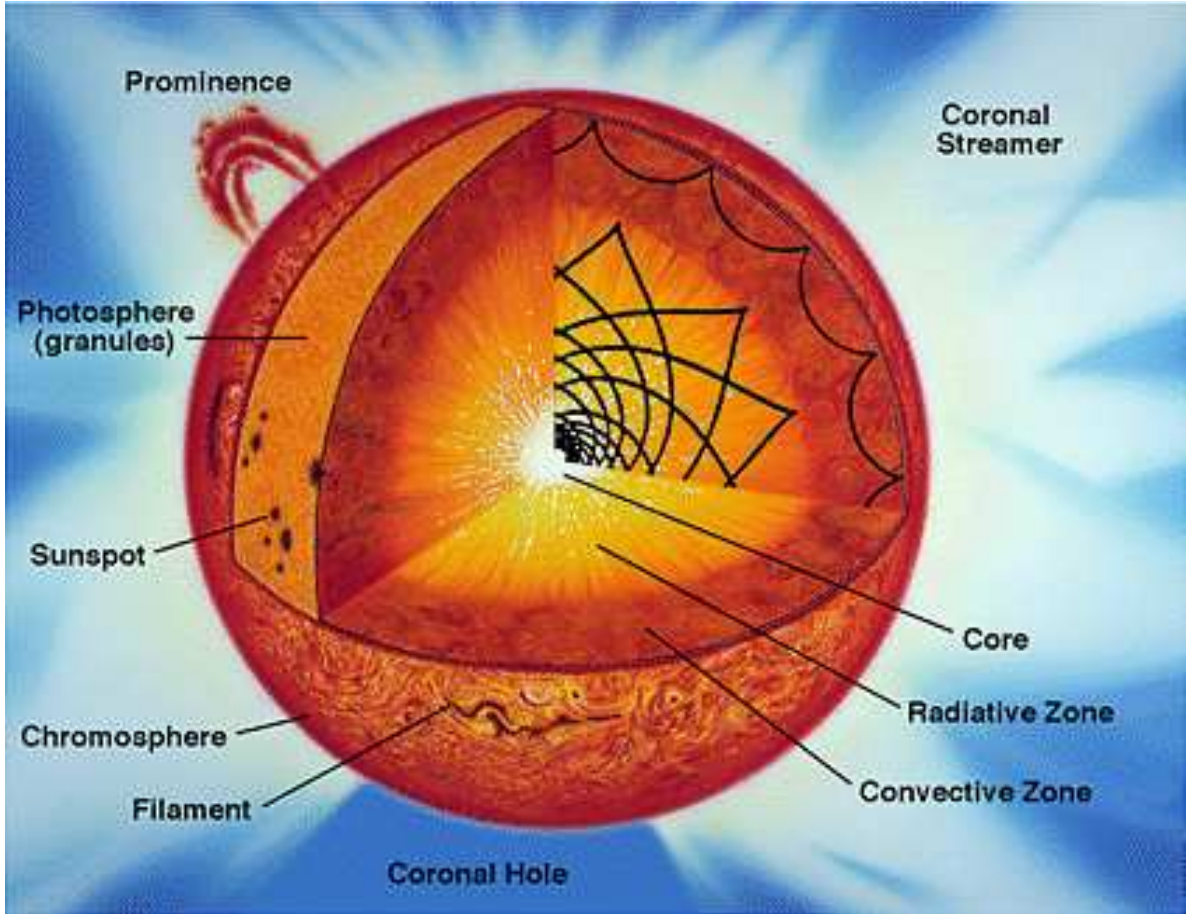
**Figure 3.1:** A schematic view of the different layer in the sun. For the modeling of the star only the atmosphere is important. The atmosphere includes the photosphere and the chromosphere.

calculated. Measurements in the laboratory of the emission and absorption of these molecules must be determined at these temperatures and pressure conditions of a star. Having this in mind, we will not try to model these cool objects with our model atmosphere code.

The next assumption would be that the star is in thermal equilibrium (TE). In this case the star is a closed system and isothermal object, not losing energy or material to the surrounding medium, especially not radiating. The energy of the system in TE is distributed equally among the different degrees of freedom. Of course we describe the gas of the atmosphere as an ideal gas. The intensity distribution of the spectrum of such a system is a Planck distribution:

$$B_\nu(T) = \frac{2h\nu^3}{c^2} \frac{1}{\exp\left(\frac{h\nu}{kT}\right) - 1} \tag{3.1}$$

where $h$ is Planck's constant ($h = 6.62618 \times 10^{34}$Js), $k$ Boltzmann's constant ($k = 1.38066 \times 10^{-23}$JK$^{-1}$ = $8.61733 \times 10^{-5}$eV), $c$ is the speed of light ($c = 2.99792458 \times 10^8$ms$^{-1}$), $T$ is the effective temperature of the star, and $\nu$ denotes the frequency of the emitted light. It is clear that a real star is not in thermodynamic equilibrium. The ratio of particles with a velocity $v_r$ to the total number of particles follows a Maxwell distribution

$$\frac{dN(v_r)}{N_{\text{tot}}} = \left(\frac{m}{2\pi kT}\right)^{\frac{3}{2}} \exp\left(\frac{-mv_r^2}{2kT}\right) dv_r. \tag{3.2}$$

The effective temperature $T$ is equal to the radiative temperature $T_{\rm rad}$ and the kinetic temperature $T_{\rm kin}$ which describes the distribution of the particle velocities. $m$ denotes the mass of the particles.

Thermodynamic equilibrium is not in agreement with observations, but to simplify the model we can assume local thermodynamic equilibrium (LTE). This means locally a blob of gas in a certain layer is in thermodynamic equilibrium but from one layer of the star to the next higher layer, the temperature changes. The temperature depends on the depth in the atmosphere. In LTE we assume that the kinetic temperature of the plasma is almost equal to its radiative temperature. This can be done since the amount of energy lost on the surface of the star is small compared to energy content of the star.

## 3.2   Energy transport

Next we have to explain how energy transport through the stellar atmosphere takes place. We assume that no energy is produced in the atmosphere but only in the central part of the star. The atmosphere depends strongly on the amount of energy produced in the center, how it is transported, and how the photons interact with the material of the atmosphere. For energy transport, convection as well as radiative transport can occur. The interaction can be absorption and emission of photons by the chemical elements contained in the atmosphere, collisions between electrons, electrons and atoms, and atoms as well as with molecules.

We assume hydrostatic equilibrium between the gravitational force that contracts the star and the pressure of the gas, and the radiation that expands the star. The energy in our model is generated in the interior of the star. The interior of the star is assumed to be uniform. Energy transport from the core to the outer layers of the atmosphere not only takes place by convective motion, but also by radiation.

In the atmosphere energy is absorbed by the atoms and reemitted at another wavelength range. The effect was accounted for by introducing line opacities of the chemical atomic and molecular species contained in the star. The radiation (energy) which is escaping the star can be observed and this is the only way to learn more about the stellar interior. We assume that the total amount of energy emitted is produced in the central not observable region of the star and transported to the outside. In G-stars the energy is transported by radiation rather than by convection. The problem to be solved is the description of how the physical parameters of the material making up the star couples to the spectrum.

### 3.2.1   Radiative energy transport

We set up the coordinate system of our plane-parallel atmosphere the way that the atmosphere is aligned perpendicular to the $x$ coordinate. Energy is transported by radiation in the direction $x$. The change of the specific intensity $I_\nu$ over an increment of path length $\mathrm{d}x$ is the sum of losses and gains over that path length,

$$\mathrm{d}I_\nu = -\kappa_\nu \rho I_\nu \mathrm{d}x + j_\nu \rho \mathrm{d}x. \tag{3.3}$$

$\kappa_\nu$ and $j_\nu$ are the absorption and emission coefficients at a frequency $\nu$, respectively, $\rho$ denotes the density of the gas.

### 3.2.2   Convective energy transport

Convective energy transport takes place in most stars. Especially in cool stars, the convection zone is deep and in the outer part of the atmosphere the energy transport is dominated by convection. Convection is a hydrodynamical process and resolving the hydrodynamical equations

numerically takes a lot of computation power. We therefore introduce a phenomenological description of the problem.

On the surface of the star we assume that convection takes place as observed on the sun. This motion is described by the path an average gas cell takes on its way through the atmosphere. On the sun we observe large convective cells and also smaller convective motions which is called granulation and can be divided into super granulation and micro granulation. On the surface of an unresolved star these smaller and larger convection regions cannot be resolved. The overall dynamic motion is therefore described by the mixing length theory and it can be observed in Doppler broadening of spectral lines.

Convection only takes place if a rising gas cell is not able to dissipate its energy fast enough by radiative energy transport. If this happens the rising cell must have a sufficiently high opacity to prevent complete energy loss by radiation. It ends when the rising gas volume has disposed its energy completely to the surrounding medium or else it stops on the boundary of the atmosphere. In our model we do not account for convective overshooting. The flux $\Phi$ that is transported through the layers can be expressed by the physical parameters of the cell: $\Delta T$ is the temperature excess of the cell above the surrounding medium, $\rho$ is the gas density in the cell, $C_p$ the specific heat at constant pressure and $v$ the cells upward velocity:

$$\Phi = C_p v \rho \Delta T. \tag{3.4}$$

Convection is favored if the opacity of the gas is high.

**The mixing length formulation**

A simplified way to think of convection is to describe the length of the path an average gas cell takes on its way through the atmosphere (often referred to as the mixing length theory).

$$\Lambda = \alpha H_p \tag{3.5}$$

where $\Lambda$ denotes the mixing length. From observations of the solar atmosphere, convection is standing in a linear relation to the the pressure scale height, $H_p$. The pressure scale height is proportional to the height in which in the pressure drops by a factor $1/e$. To put the pressures scale height into a relation with the mixing length, we introduce the factor $\alpha$, the mixing length parameter. The main problem arises when scaling the mixing length parameter. The parameter mixing length $\Lambda$ cannot even be observed directly on the surface of the sun. We have to make sure that the energy transport is not only performed by convection but also by radiation. For a discussion on the problems of scaling the mixing length parameter, $\alpha$, see the PhD thesis of Jan Bernkopf (2001).

**Conditions for convection - The Schwarzschild criterion**

The convective cell as it rises through the atmosphere is buoyed additionally at each level as it continues to rise. Since the density in the outer layers drops and the cell is expected to stay in pressure equilibrium, it must expand. To figure out if the cell will continue to rise or if it will start to sink, we calculate the density change in the cell.

Assuming the convective cell behaves adiabatically, meaning no energy leakage occurs from the rising cell, we obtain the Schwarzschild criterion (1906):

$$P\rho^{-\beta} = const. \tag{3.6}$$

where P is the total pressure, $\rho$ the density in the cell and $\beta$ the ratio of specific heats. In

other words:

$$\frac{d \log \rho}{d \log P} = \frac{1}{\beta}. \tag{3.7}$$

We now have to compare $\left.\frac{d \log \rho}{d \log P}\right|_{\text{cell}}$ to $\left.\frac{d \log \rho}{d \log P}\right|_{\text{photosphere}}$. In order to have convection, the density in the cell must decrease at least as rapidly as the average photosphere density. Using the gas law in the following formulation: $P = (\rho/\mu)kT$, where $\mu$ is the mean molecular weight, $\rho$ the density and $k$ the Boltzmann constant, this leads to:

$$\left.\frac{d \log \rho}{d \log P}\right|_{photosphere} = 1 + \frac{d \log \mu}{d \log P} - \frac{d \log T}{d \log P} \tag{3.8}$$

So the criterion for convection can be written in the following way:

$$\left.\frac{d \log T}{d \log P}\right|_{photosphere} > 1 - \frac{1}{\beta} + \frac{d \log \mu}{d \log P} \tag{3.9}$$

If Equation 3.9 is fulfilled, meaning the gradient on the left side is high, energy is also transported by convection. This is the case if the opacity of the gas in the cell is high. The energy transport by radiation always takes place.

### 3.2.3 Heat transport

Heat transport in the atmosphere and the inner part of the star can be ignored since the average distance the electrons interact is very small and therefore it is very inefficient. It is an important process in compact stars such as the neutron stars or white dwarfs as well as in the corona of normal stars. In any case, heat transport can be calculated as a diffusion process but in the sequel we will not include it in the model.

## 3.3 Interaction between radiation and material

Radiation interacts with the material of the stars. There are several effects which can take place. A specific energy level can be absorbed by the electron of a specific element of the atmospheric material. The amount of energy depends on the electron configuration of the chemical elements. On the other hand chemical elements can emit or reemit energy depending on their electron configuration.

### 3.3.1 Atomic excitation and ionisation in TE

The excitation $\chi_n$ denotes the energy of an electron in the level $n$ above the ground level. The energy between the ground level and the continuum is called the ionisation potential, $I$. The population of each level depends on the mechanism for populating and depopulating. In some cases collisional interaction dominates and in others radiative interaction. When collision dominates, we can calculate the population from the following equations.

**Boltzmann equation - Excitation**

The number of atoms per unit volume in a level $n$ can be expressed in terms of a fraction of all atoms of the same species and is

$$\frac{N_n}{N} = \frac{g_n \exp \chi_n/kT}{g_1 + g_2 \exp -\chi_2/kT + g_3 \exp -\chi_3/kT + ...} = \frac{g_n}{u(T)} \exp -\frac{\chi_n}{kT} \tag{3.10}$$

where the denominator is written as $u(T) = \sum g_i \exp{-\chi_i/kT}$ and is called the partition function. Tabulated partition functions for several elements of interest can be found in the literature. The $g_i$ are the statistical weights for the $i$th energy level.

**Saha equation - Ionisation in a collision dominated gas**

The ionisation in a collision dominated gas can be calculated as follows

$$\frac{N_1}{N_0} P_e = \frac{(2\pi m)^{3/2}(kT)^{5/2}}{h^3} \frac{2u_1(T)}{u_0(T)} \exp\left(-\frac{I}{kT}\right), \tag{3.11}$$

where $N_1/N_0$ is the ratio of ions to neutral particles, $u_1/u_0$ the ratio of ionic to neutral partition functions, $h$ the Planck constant, $k$ the Boltzmann constant, $m$ the electron mass, $T$ the temperature, and $I$ the ionisation potential. Numerically, this transforms to

$$\frac{N_1}{N_0} = \frac{\Phi(T)}{P_e} = \frac{1}{P_e} 0.665 \frac{u_1}{u_0} T^{5/2} 10^{-5040 \cdot I/kT}. \tag{3.12}$$

The ratio of double ionized to single ionized particles is calculated in the same way.

### 3.3.2 Radiative interaction

Photons interact with the gas material. These absorption and emission processes are frequency dependent. Assuming LTE simplifies this enormously because the gas conditions such as temperature and density are locally independent. One can use the equations for the ideal gas as the equation of state. The interaction among the local layers takes place only through energy transport. For the energy transport we only need the frequency $\nu$ dependent absorption coefficients, $\kappa_\nu$, of the matter.

**Line absorption or bound-bound transitions**

A bound electron on a lower energy level absorbs a photon with a specific energy (frequency $\nu$) and moves to a higher energy level in the atom. The physical description is done by an electric dipole which absorbs energy from the surrounding radiation. The opacity $\kappa_\nu$ at a given frequency $\nu$ is described in the following equation:

$$\kappa_\nu = \frac{1}{4\pi\epsilon_0} \frac{\pi e^2}{m_e c} \cdot f \cdot \Psi(\nu) \cdot N_m \cdot E(\nu, T). \tag{3.13}$$

$\epsilon_0$ the dielectric constant, $e$ is the electron charge, $m_e$ the mass of an electron, $c$ the speed of light, $f$ the oscillation strength, $\Psi(\nu)$ the profile function of the absorption line, $N_m$ the occupation number of the lower atom level, and $E(\nu, T)$ a correction term for stimulated emission.

The profile function and the correction term of the stimulated emission are calculated by quantummechanical calculations. The occupation number of the lower level in LTE can be calculated simply by using Boltzmann statistics:

$$\frac{N_n}{N_m} = \frac{g_n}{g_m} \exp\left(-\frac{h\nu_{nm}}{kT}\right). \tag{3.14}$$

In the stellar atmosphere, especially at temperatures corresponding to the spectral type G (the effective temperature of the sun, a G2V-star, is 5740 K), the atoms of the gas can be ionized. The kinetic energy must therefore be also distributed to the ionized atoms. To

describe this fact, we need to use Saha-Boltzmann statistics:

$$\frac{N_{m,0}}{N_{m+1,0}} = N_e \frac{1}{2} \left( \frac{h^2}{2\pi m_e kT} \right)^{\frac{2}{3}} \frac{g_{m,0}}{g_{m+1,0}} \exp\left( \frac{\chi_m}{kT} \right). \tag{3.15}$$

$g_{i,0}$ are the statistical weights of the energy levels $m$ and $m+1$.

### Ionisation - recombinations or bound-free transitions

The energy needed to ionize an atom must be higher than the minimal energy required. For the recombination any amount of energy above the minimum energy level can be emitted. The ionisation and recombination are a continuous process. It can be described using an equation like Equation 3.13 by replacing the profile function by a continuous term.

### Scattering or free-free transitions

Free-free transitions are a continuous process. Electrons are in the Coulomb potential of the ions. They enhance their kinetic energy by absorbing photons. To compute these opacities, one has to know the ion and the electron density. These can be derived using the ideal gas laws.

## 3.4 Hydrostatic equilibrium

The hydrostatic equilibrium establishes a relation between pressure and optical depth. In the following we formulate the equation for a plane-parallel atmosphere. We consider a small volume in the atmosphere. The increment in the pressure over a distance $dx$ is:

$$dP = \frac{dF}{dA} = \frac{\rho dA g dx}{dA} = \rho g dx \tag{3.16}$$

where $dAdx$ is the small volume element at a certain level in the atmosphere, $g$ refers to the gravitation and $\rho$ denotes the density. Moving inward with increasing $x$, the pressure increases. Using the relation $d\tau = \kappa_\nu \rho dx$, we derive the hydrostatic equation we need:

$$\frac{dP}{d\tau_\nu} = \frac{g}{\kappa_\nu} \tag{3.17}$$

The pressure in the equation is the total pressure needed to support the small volume $dxdA$ at a certain level in the atmosphere. In cool stars this is the main source of pressure contributing to the total pressure. In hot stars radiative pressure could become the main source of pressure, also turbulent pressure or magnetic pressure could be significant in these stars.

## 3.5 Sources of opacities

To compute the radiations field of a star at each point of its atmosphere correctly, one has to include all continuous and line opacity sources.

### 3.5.1 Continuous opacity sources

The continuous opacity usually varies only slightly with the wavelength. Big variations are the absorption edges of metals and hydrogen which are important below 5,000 Å. The background opacity is dominated in the range of 5,000 to 16,000 Å by bound free transitions of H and

He, bound-free and free-free transitions of H$^-$, and free-free transitions of H$_2^-$-molecules and absorption caused by H$_2^-$-molecules, bound-free transitions by He I, free-free transition by He$^-$, bound-free transitions of neutral metals such as C I, N I, O I, Si I, Fe I, Mg I, Ca I, and Al I, and free-free transitions of positively charged ions.

### 3.5.2   Line opacities
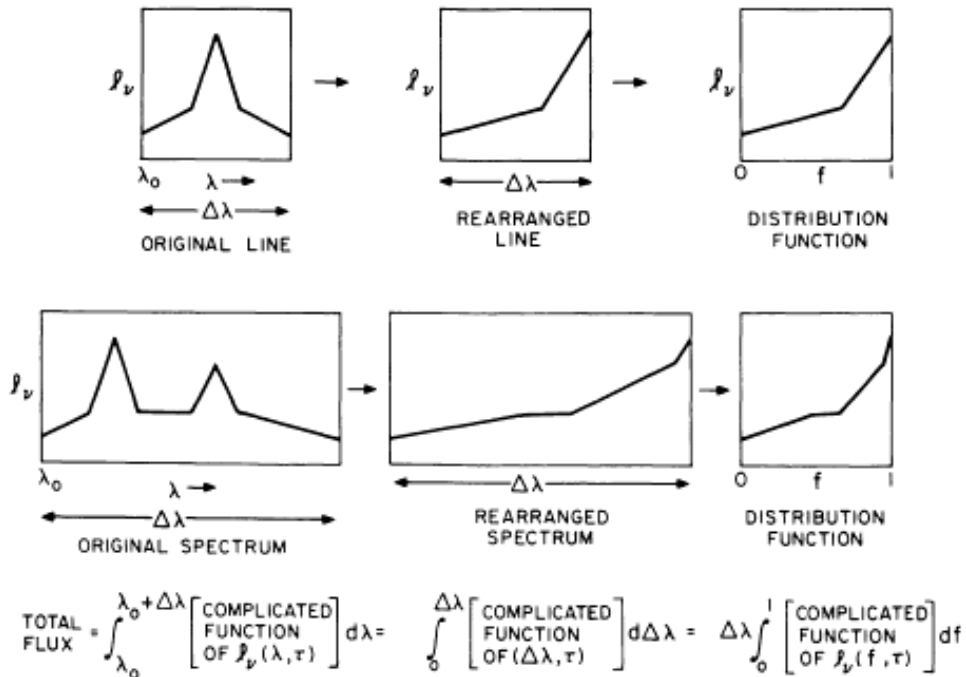


**Figure 3.2:** Schematic representation of the redistribution of real spectral absorption lines to derive the distribution function. Taken from Kurucz (1979). In the figure Kurucz has denoted $l_\nu$ as the absorption coefficient.

In a solar like star discontinuous sources of opacities are also important. These arise because of line transition of atoms, ions and molecules. To compute the line opacities in a stellar atmosphere directly for all elements would take a great amount of computing power. Just to compute the line opacities one would need to compute several million line transitions. Kurucz (1979) has developed a different approach: He rearranged a 10 Å range of spectral lines to one "superline" as shown in Fig. 3.2. On the left top segment in this sketch, we see the original interval of length $\Delta\lambda$ which is rearranged to a function rising on the right side. The second sketch shows the same for two lines. Normalizing the wavelength interval results in the distribution function. In the calculation, the spectrum is divided into a number of wavelength intervals and the distribution function is tabulated for a range of gas pressure, abundance, and microturbulent velocity.

At this point we have lost the information of the position of the absorption lines. For the computation of the atmosphere this is sufficient because we only need the integrated opacities, For calculating concrete spectral lines on the other had we need to know the correct wavelength position.

## 3.6  Computed spectral lines

Spectral lines are computed with the same atmosphere code as described above, only now the line absorption of each line is treated independently and not by opacity distribution functions as before. For this reason the atmosphere model is run with an input of the atomic data instead. This input can be adjusted, since moving to cooler stars, molecules become important. If changing the temperature too much, one must consider running the initial atmosphere models with the appropriate opacity distribution function.

The immediate output is the surface flux of the star at the given temperature which in the last step is normalized to one, to compare with the observed normalized spectra. This enables us not to be fooled by continuous absorption due to the atmosphere of the earth and response of the spectrograph and CCD camera, where at least the instrumental response should be removed by the reduction process (flat field division).

### 3.6.1  Dependence on the element abundance

Intuitively, it is clear that the line depths are strongly dependent on the chemical contents of the star, especially with an increase in the abundance of the element measured. But the change of the line depth as well as the line width are not simply linearly proportional.

In weak-lines the Doppler core dominates. The width of the line is set by $\Delta\lambda_D$. The depth of all points in the line profile grows proportionally to the abundance $A$ and the width is proportional to $A$.

The line saturates when the center of the line approaches the maximum value. The minimum residual flux is fixed by the boundary temperature $T_0$ at $B_\nu(T_0)$ at LTE. The saturation increases asymptotically towards a constant value.

When the optical depth in the line wings becomes significant compared to $\kappa_\nu$, the abundance at which this begins is strongly dependent on the size of the damping constant $\gamma$. If $\gamma$ were constant for a line, the equivalent width would be proportional to $A^{\frac{1}{2}}$. But $\gamma$ is dependent on the temperature and pressure which means that it is dependent on the depth.

### 3.6.2  Dependency on other stellar parameters

The spectral output is generally dependent on the temperature of the star since this is the source of the radiation in the optical wavelength range and therefore directly related to the spectral output of the star observed in that wavelength range.

Certain spectral lines or line ratios depend mainly directly or indirectly on only one parameter such as surface gravity, iron abundance, $\alpha$-enhancement, presence of a magnetic field (though this is only true for the iron I line at 6173 Å in the optical part of the spectrum). This dependence can directly be used to measure these values in the stellar atmosphere. In the following, we will describe these lines and the physical effect that causes them.

**Temperature dependence**

The Balmer lines of F-, G- and early K-stars have been shown to be strongly dependent on the temperature but less dependent on other stellar parameters such as surface gravity and metallicity. For the cooler stars the Balmer lines became weak, so that they cannot be used for a sensitive measurement.

To calculate the Balmer line profiles we use the set of precalculated model atmospheres, meaning we have a grid of model parameters, e.g. temperature and pressure layers, partial pressures, partition functions, etc. The line absorption coefficient $\kappa_\lambda$ at a given wavelength $\lambda$

can be written as follows:

$$\kappa_\lambda = \frac{1}{\rho} \frac{\pi e^2}{m_e c} \cdot \frac{P_{r_{r,m}}}{kT} \cdot \frac{g_{n,r,m} e^{-\chi_n/kT}}{U_{r,m}} \cdot \frac{\lambda^2}{c} \cdot f \cdot \Phi(\lambda) \cdot E(\lambda, T) \qquad (3.18)$$

We have to calculate the profile of the line $\Phi$ which is broadened by several mechanisms. The broadening mechanism are the following: linear Stark-effect which is due to an interaction between the ions and the electrons, the resonant broadening due to an interaction with neutral hydrogen atoms, as well as radiation damping and the Doppler effect. For a detailed discussion of the broadening mechanisms and the calculation of the Balmer lines see the PhD-thesis of Fuhrmann (1993).

**Pressure and surface gravity dependence**

The pressure dependence in F-, G-, and K-stars is seen in three different effects: The first effect is the change of the ratio of line absorber to continuous opacities (ionisation equilibrium), the second effect is the pressure sensitivity of $\gamma$ on strong lines and the third is the pressure dependence of the Stark broadening in strong lines. For cool stars the gas pressure is related to the electron pressure approximately by $P_g = P_e^2/constant$. On the other hand the gas pressure is controlled by the surface gravity $P_g = constant \cdot g^{\frac{2}{3}}$. The electron pressure is also influenced by the surface gravity: $P_e = constant \cdot g^{\frac{1}{3}}$. Therefore, in cool stars the surface gravity dependence can be translated into an electron or gas pressure dependence.

There are three principal reasons why an absorption line reacts on surface gravity. One reason is the dependence of the continuous emission from the $H^-$-ions on the electron pressure which is directly dependent on the surface gravity:

**Lines formed by any atom or ion where most of the element is in the next higher ionisation stage:** If one knows a pair of lines where almost all of the atoms are in the next higher ionisation stage and just a small fraction is in the lower ionisation stage, the gravity dependence of the continuum has an influence on the depth in which the absorption line arises for the ions in the next higher ionisation stage; while for the atoms or ions in the lower ionisation stage the optical depth in which the line arises is always the same. For the lines of the atom in the two ionisation stages $r, r+1$, the following approximation holds:

$$\frac{N_{r+1}}{N_r} = \frac{\Phi(T)}{P_e}, \qquad (3.19)$$

where $\Phi(T)$ contains all the gravity independent terms of the Boltzmann equation, $P_e = constant \cdot g^{\frac{1}{3}}$ is the electron pressure and $N_{r+1}/N_r$ the ratio of the number of ions in the higher ionisation stage to the number of ions or atoms in the lower ionisation stage. Since almost all atoms are singly ionized, $N_{r+1}$ is constant and almost equal to the number of all atoms of that species. This means $N_r \sim const \cdot P_e$ and $j_\nu \sim constant$. In a cool star $H^-$ dominates $\kappa_\nu \sim P_e$. In the ratio $j_\nu/\kappa_\nu$ the electron pressure dependence cancels out and thus the line absorption is independent of the surface gravity.

**Lines formed by any atom or ion where most of the element is in one ionisation stage:** Almost all atoms of this element is in the ionisation stage $r$, meaning $N_r = N_{\text{total}} = constant$. For theses absorption lines exactly the opposite happens: $N_r \sim P_e$ and therefore $\kappa_\nu \sim P_e$. In the ratio $j_\nu/\kappa_\nu$, the surface gravity dependence remains. The continuous emission changes as the electron pressure $P_e$ changes with gravity. So the surface gravity dependence of e.g. iron II is actually due to the surface gravity dependence of the electron pressure,

which influences the continuous emission. The photosphere deepens in geometrical depth. The number of line absorbers in the line of sight rises.

**The iron I/II ionisation equilibrium:**   As described above, the relation of the iron I/iron II line depth is strongly dependent on the temperature and the surface gravity. At a given temperature only one value for the gravity will yield a consistent iron abundance. The simultaneous fit of equivalent width of all unblended iron I and II lines leads to a surface gravity value for a given temperature. This dependence is not primarily based on the line dependence of these lines but on the line-to-continuum ratio. In other words, the fact that most iron lines are ionized once (iron II) the surface gravity dependence of the continuous emission term, which is mainly continuous emission from $H^-$, is electron pressure dependent, which is related to surface gravity.

In the case of iron I the electron pressure dependence of the absorption term cancels the electron pressure dependence of the continues emission, while for iron II the contrary is the case. In other words the emission from the continuum weakens and therefore the depth at which the iron II absorption occurs, the line gets weaker as the surface gravity increases.

**Saturated lines:**   Wing of strong lines can be dependent on the surface gravity. Ryan (1998) gives an overview of the approximations one has to make to compute the elastic collision, the dominant broadening mechanism for strong lines. In cool stars where the continuous emission is dominated by $H^-$ ($\kappa_\nu \sim Pe$), the wings of a strong line for a neutral atom where most of the element is ionized are surface gravity dependent. The following approximation holds for these lines:

$$\frac{j_\nu}{\kappa_\nu} \approx constant \cdot \gamma, \tag{3.20}$$

where the emission coefficient is proportional to the damping constant ($j_\nu \sim \gamma$). The damping constant $\gamma$ consists of van der Waals broadening $\gamma_6$ and Stark broadening $\gamma_4$ and a gravity independent term $\gamma_{nat}$. For the van der Waals broadening we have the following dependence:

$$\gamma_6 = \Phi_6(T) \cdot P_g, \tag{3.21}$$

where $\gamma_6 = 17 \cdot C_6^{2/5} v^{3/5} n_{pertuber}$ is the damping constant and $v$ is the relative velocity between atoms and perturbing particles, $n_{pertuber}$ is the number of perturbing particles.

For the quadratic Stark broadening we, use

$$\gamma_4 = \Phi_4(T) \cdot P_e. \tag{3.22}$$

In the equations above, $\Phi_4(T)$ and $\Phi_6(T)$ are the pressure independent terms. In a star where $\kappa_\nu$ is dominated by negative hydrogen (cool stars), $\kappa_\nu$ is proportional to the electron pressure $P_e$.

The wings of a strong line for a neutral atom where most atoms are ionized ($j_\nu$ is proportional to $P_e$) are proportional to

$$\frac{j_\nu}{\kappa_\nu} \approx constant \cdot \gamma = constant \cdot [\Phi_6(T) \cdot P_g + \Phi_4(T) \cdot P_e + \gamma_{nat}]. \tag{3.23}$$

Depending on the relative size of the damping constant, there may be no gravity dependence ($\gamma_{nat}$ dominant), or a maximum gravity dependence ($g^{\frac{2}{3}}$, van der Waals dominant).

For the ionic lines of an element, which is mostly in the upper excitation state, we find

$$\frac{j_\nu}{\kappa_\nu} \approx constant \cdot \frac{\gamma}{P_e} = \tag{3.24}$$
$$= constant \cdot \left[ \Phi_6(T)\frac{P_g}{P_e} + \Phi_4(T) + \frac{\gamma_{nat}}{P_e} \right] \approx$$
$$\approx constant \cdot g^{\frac{1}{3}} + constant + constant \cdot g^{-\frac{1}{3}}$$

Again, all gravity dependences are possible. The calibration of the Stark and van der Waals effect is done relative to the sun. Therefore, we rely on the effects as long as the effective temperature of the investigated star is comparable to the sun. A double check of the measured gravity must be performed e.g. using the Hipparcos measurements (see Section 4.14).

**Surface gravity dependence of Mg Ib:**   magnesium Ib lines are strongly broadened by the Stark effect. This effect dominates in deeper layers of the stellar atmosphere. As we have seen above this can induce a sensitivity to surface gravity. In additional to that, the magnesium Ib lines are also strongly sensitive to the electron pressure. For a review of this matter, see Gray (1976).

## 3.7   How to derive abundances

Abundances of an element are derived from the curve of growth for each spectral line. The abundance is read from the curve of growth by entering the observed equivalent width of the spectral line. This process must include a handling of the micro turbulent velocity, as well as the instrument profile, the rotational velocity, and other broadening mechanisms for the observed spectral lines.

A large number of lines of the same element species must be measured and from each line the abundance $A$ is determined. Under the assumption that the atmosphere is chemically homogeneous only the right choice of the desaturating mechanisms give the same abundance for all the lines.

To avoid problems with uncertainties in $gf$ values, we perform our analysis relative to the sun. We then derive an abundance ratio, $A/A_r$, relative to the reference star $r$, in our case the sun. Usually the following notation $[A/H] = \log \frac{A}{A_\odot}$ in common. For example for the iron abundance, $[Fe/H] = \log \frac{A(Fe)}{A(Fe)_\odot}$.

The method of synthesis analysis involves the computation of complete spectral intervals in which all observed lines should be included. The method works best when all lines involved have known atomic parameters. In our further work we try to use only unblended lines to avoid blend calculations where one could easily miss weak lines.

# Chapter 4

# Flare stars in stellar associations

Flare stars are young stars which have not yet reach the main sequence during their life time. So in principle it should not be a surprise to observe flare stars in nearby young stellar associations like the TW Hydrae-, the Horologium-, or Tucana Association, all three of which lie within 100 pc. We are confident in identifying new member stars of these associations because there are known flare stars associated with the Taurus Auriga and the Orion starforming region. Our sample of flare stars contain stars which are located close to and in the line of sight of those regions. Space motion is the way to preselect stars belonging to an association.

**Table 4.1:** Space motions of young stellar associations with stars within 100 pc.

| Association | U [km/s] | V [km/s] | W [km/s] | Reference |
|---|---|---|---|---|
| Ursa Major Ass. | $+14.15 \pm 0.68$ | $+2.83 \pm 1.31$ | $-8.73 \pm 1.87$ | King et al. (2003) |
| Hyades SC | $+40.4$ | $-18.3$ | $-1.9$ | Eggen (1992) |
| IC 2391 SC | $+20.8$ | $-15.9$ | $-8.3$ | Eggen (1992) |
| Local Ass. | contains the | | | |
| Pleiades SC | $+11.5$ | $-21.0$ | $-10.5$ | Eggen (1992) |
| TWA | $-12.1 \pm 0.7$ | $-17.1 \pm 0.8$ | $-5.5 \pm 0.9$ | Torres et al. (2003) |
| HorA | $-9.5 \pm 1.0$ | $-20.9 \pm 1.1$ | $-2.1 \pm 1.9$ | Torres et al. (2000) |
| TucA | $-10.5 \pm 2.3$ | $-20.8 \pm 2.4$ | $+0.3 \pm 3.0$ | Zuckerman & Webb (2000) |
| $\beta$ Pic Ass. | $-9.5 \pm 1.2$ | $-16.4 \pm 1.1$ | $-9.4 \pm 0.9$ | Torres et al. (2003) |
| AnA | $-7.1 \pm 0.8$ | $-28.0 \pm 1.1$ | $-12.4 \pm 1.2$ | Torres et al. (2003) |
| LSR | $10.00 \pm 0.36$ | $5.25 \pm 0.62$ | $7.17 \pm 0.38$ | Dehnen & Binney (1998) |

## 4.1 The Ursa Major association

The Ursa Major association is interesting to study because its age lies between the age of the Pleiades and the Hyades and is on the time scale which is needed to dissolve a cluster of 200 Myr (Wielen, 1971). A discussion of the cluster age can be found in Sec. 4.1.1. It has a tangible nucleus which is located in the stellar constellation, Ursa Major. Its 3-dimensional space motion is well measured because most of its members lie within 25 pc and are therefore bright. Spectroscopic criteria such as chromospheric emission allow independent classification from the space motion of candidate stars. The space motion is different enough from the local

standard of rest and from other clusters.

### 4.1.1   $\chi^1$ Orionis B
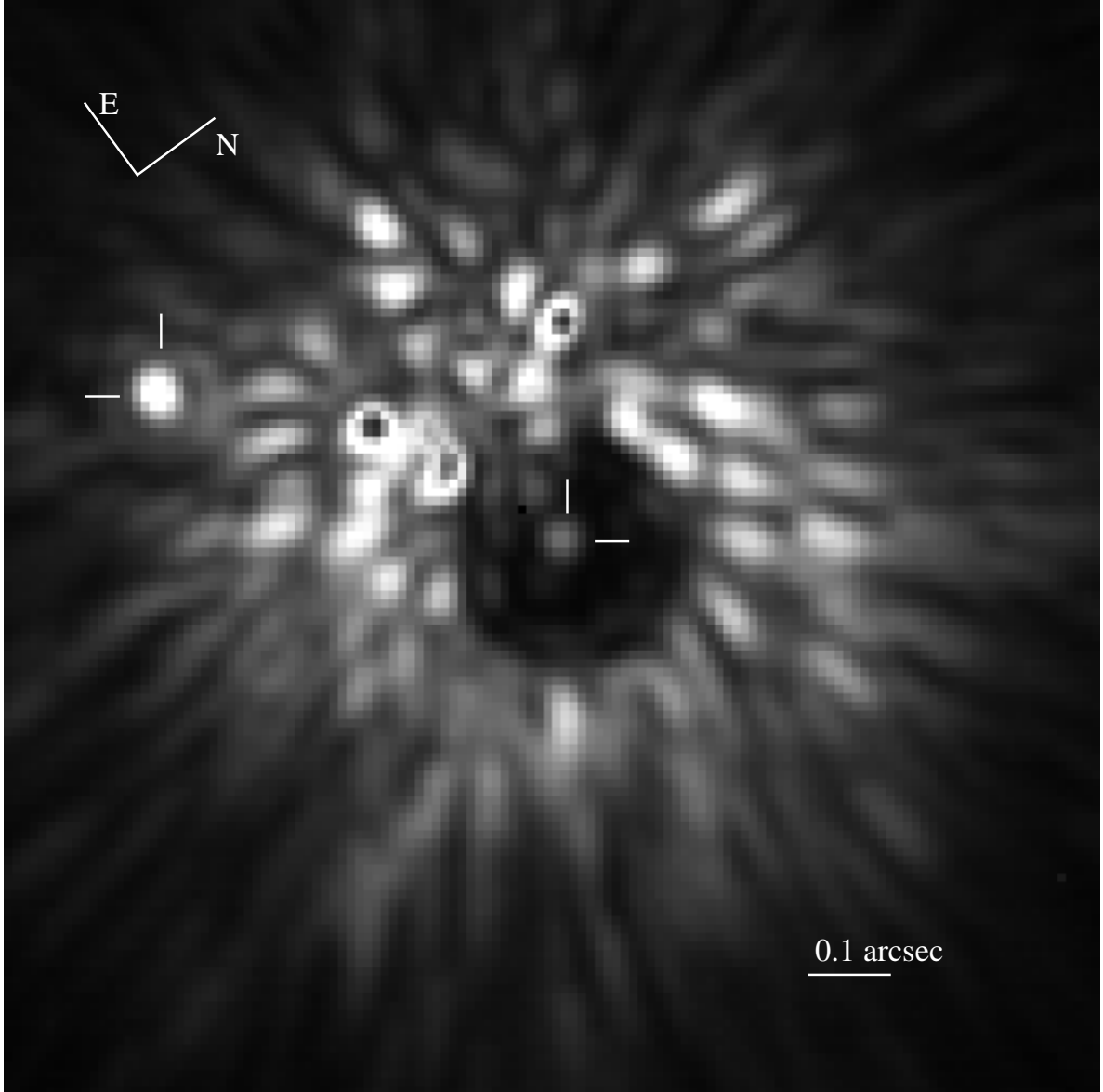


**Figure 4.1:** The H-band image of $\chi^1$ Ori behind the coronograph in the center and the companion to the left. Note the diffraction ring around the companion.

The star $\chi^1$-Orionis is well known to the stellar community. It is visible by eye and it is regarded as a young solar twin, though it is a bit hotter than the sun at a spectral classification of G0V. Up to now many studies of this object have been performed, especially since it was noticed that the star is a spectroscopic and astrometric binary. For the further work, these thorough studies will play a major role.

König et al. (2002) have shown that $\chi^1$ Orionis is a member of the Ursa Major Association, an association of stars in the solar vicinity with distinct space motion and spectral signatures. In particular the stars of the UMa show lithium absorption , H$\alpha$- and calcium H & K line core filling in, a signature for fairly young stars. For several years it has been known that

the star is a binary, only the direct detection of the low mass companion is lacking up to this date.

In the following, we present an H-band image of the companion of $\chi^1$ Orionis taken with the Keck adaptive optic system and NIRC 2 camera equipped with a 300 mas-diameter coronographic mask. The direct detection of this companion star enables us to calculate dynamical masses using only Kepler's laws ($M_A = 1.01 \pm 0.13\,M_\odot$, $M_B = 0.15 \pm 0.02\,M_\odot$), and to study stellar evolutionary models for a wide spread of masses. The application of Baraffe et al. (1998) pre-main sequence models implies an age of 70-130 Myrs. This is in conflict with the age of the primary, a confirmed member of the Ursa Major Cluster with a canonical age of 300 Myrs. As a consequence, either the models at low masses underestimate the age or the Ursa Major Cluster is considerably younger than previously assumed. In the following we will discuss how to determine the absolute masses of the two companions and the tests of pre-main sequence models we performed.

### Introduction

$\chi^1$ Ori is a G0V-star and is known to be a single lined spectroscopic and astrometric binary. The orbital parameters were first derived by Lippincott & Worth (1978). Since then Irwin et al. (1992) published precise radial velocity measurements of the orbit. Gatewood (1994) published an astrometric parallax of the orbit of $\chi^1$ Ori. Recently, Han & Gatewood (2002) using their new astrometric data and the radial velocity data from Marcy & Butler (1992, 1998) presented a period of P = 5156.7±2.5 days and a mass ratio $q = M_B/M_A = 0.15 \pm 0.005$.

McCarthy (1986) claimed to have detected the companion directly by speckle imaging techniques, but this has not yet been confirmed. They derive $M_V = 6.1$ mag, which would place the companion star to $\chi^1$ Ori about 4 mag above the main sequence (Henry et al., 1999). Han & Gatewood (2002) claim that McCarthy (1986) and subsequent attempts by speckle observations have not been able to detect the companion directly due to instrument limitations.

The G-type star $\chi^1$ Ori and its companion form a binary with a very small mass ratio. A direct detection of the secondary would be significant, as it would allow the masses to be determined without astrophysical assumptions. The derived mass and observed luminosity allow the age to be inferred from comparison to pre-main sequence evolutionary tracks, which in turn enables a calibration of other alternate estimators.

### Data reduction and analysis

We observed $\chi^1$ Ori on Feb. 28, 2002, using the Keck 2 telescope equipped with the NIRC2 camera and the adaptive optic system (Wizinowich et al., 2000), an H-band filter and a 300 mas diameter coronograph. The coronograph is semi transparent with a throughput slightly below half a percent as determined by us (different from what is given in the manual, but confirmed by the Keck staff), so the position of the star behind it can be measured precisely. The total integration time was 0.18 s. The FWHM of the companion is 50 mas.

We performed the data reduction, using the reduction software MIDAS (Warmels, 1992) provided by ESO. We divided the image by a normalized master sky flat. We subtracted the background of $\chi^1$ Ori B depending on the distance from $\chi^1$ Ori A: $\chi^1$ Ori B is located in the PSF wing of the component A which causes the main contribution to the background emission. To obtain a background subtracted instrumental magnitude of B we subtract an azimuthal averaged background (a one pixel wide annulus around A excluding B) for each pixel used.

We determined the magnitude of the companion as well as that of two stars used as photometric standards: the UKIRT faint standard FS 11, H = 11.276±0.003 mag (Hawarden

et al., 2001) and TWA-5B, H $= 12.14 \pm 0.06$ mag (Lowrance et al., 1999). The standards were observed in the same night, and analyzed with the same procedure. We used 121 different aperture sizes starting with the brightest central pixel and calculating a background subtracted peak-to-peak flux ratio and then consecutively adding the next brightest pixel until we end up with a $121 = 11 \times 11$ pixel aperture box. For aperture sizes from 1 to 50 pixels, the resulting instrumental magnitude did not change significantly, so we use this value. By comparing the background subtracted instrumental magnitude of the companion to the background subtracted instrumental magnitudes obtained for TWA-5 B and FS 11, we measure the apparent H-band magnitude for the $\chi^1$ Ori companion of $7.70 \pm 0.15$ mag, taking into account also the slightly different FWHM and Strehl ratios. With the Hipparcos parallax for $\chi^1$ Ori of $115.43 \pm 1.08$ mas, we obtain $M_H = 8.01 \pm 0.15$ mag for the B-component.

**Dynamical masses of $\chi^1$ Orionis A & B**
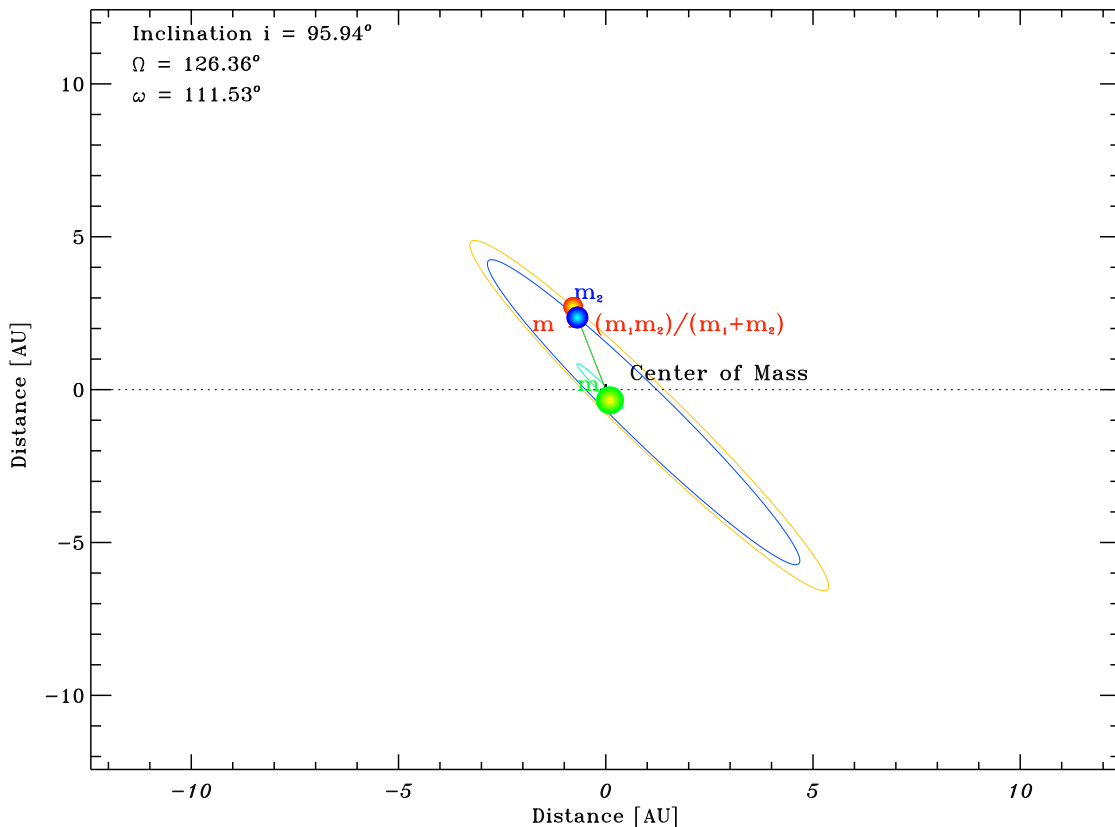


**Figure 4.2:** Schematic view of the projection of the orbit on the sky of $\chi^1$ Ori A & B. In this sketch the positions of both stars with masses $m_1$ and $m_2$, as well as the position of the reduced mass, an analytical simplification made to calculate the orbit, at the date of observation is shown.

In Fig. 4.2 we can see a schematic sketch of the configuration of the system at the date of observation. The orbit is now projected to the face on view and the classical Keplerian orbit of the two stars can be seen (Fig. 4.1.1). Using the orbital elements for $\chi^1$ Ori published by Han & Gatewood (2002) ($i = 95.937 \pm 0.790$ deg, $\omega = (111.527 \pm 0.230)°$, $\Omega = (126.360 \pm 0.583)°$, $T_0(\mathrm{JD}) = 2,451,468.2 \pm 3.083$, $P = 5156.291 \pm 1.508$ days, $e = 0.452 \pm 0.002$), we can calculate the absolute masses of $\chi^1$ Ori A and B directly using Kepler's laws. The measured apparent

separation between the components A and B is $\rho = 0.4976 \pm 0.0036$ arcsec using a pixel-scale of $0.009942 \pm 0.000500$ arcsec/pixel as determined by the NIRC 2 team (Campbell, priv. comm.). The physical separation is $r = 4.33 \pm 0.08$ AU.
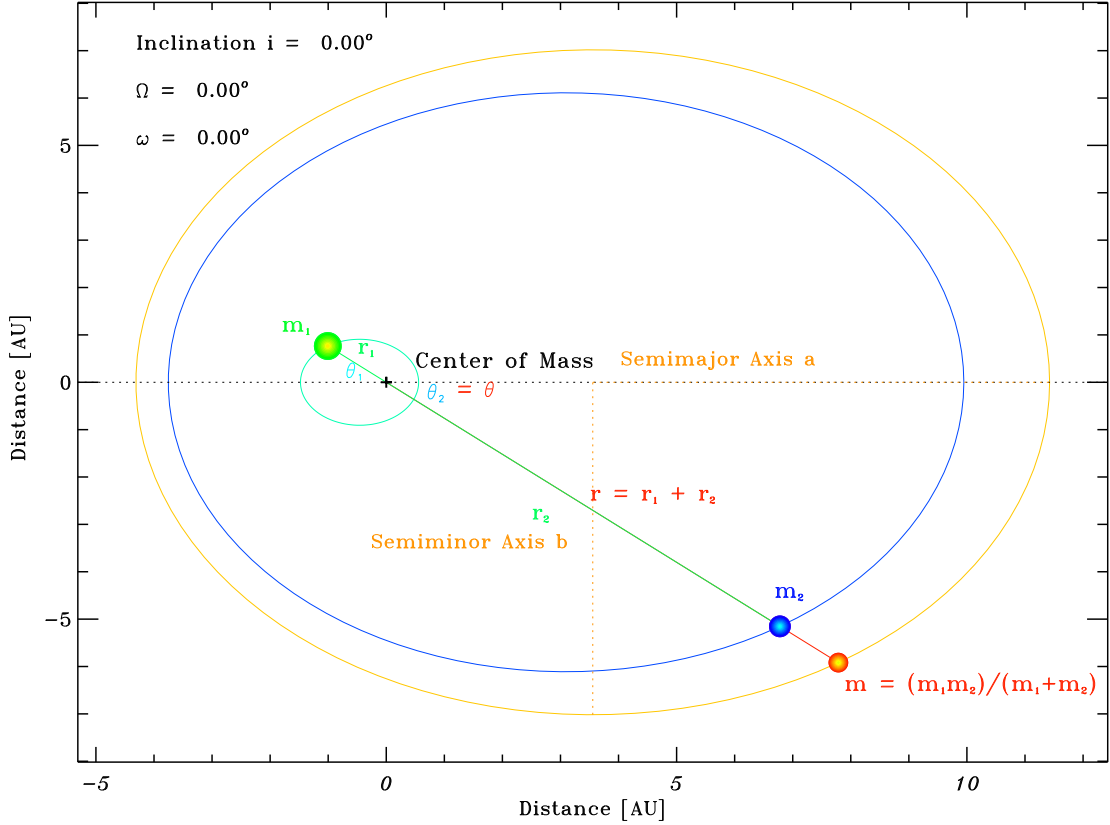


**Figure 4.3:** The schematic orbit projected to be seen face on. We have also shown the orbit of the socalled reduced mass which is actually used to calculate the orbit of the two stars.

**Equations to solve:** As indicated in Fig. 4.1.1, we have measured the apparent projected separation $\rho$ at a certain time $\Delta T_{obs}$ from the periastron passage $T_0$. The projected separation $\rho$ can be transformed into a real separation $r$ because the inclination $i$ of the system is known. We do not now calculate the orbit of the two stars but we calculate the orbit of the reduced mass around the center of mass. There is an analytical way to prove that the two problems are similar and this simplifies the equations. The left side of Eq. 4.1 calculates the area the vector $r$ swept out since its periastron-passage. The right side uses Kepler's third law, which states that the area swept out by the vector $r$ is similar to the fraction of the swept out time, $\Delta T_{obs}/P$ of the orbit. The following integral can be integrated analytically and solved for $\Phi$, the angle at the current measurement of the position:

$$\int_0^\Phi \frac{a(1-e)}{1+e\cos\varphi}d\varphi = \frac{\Delta T_{obs}}{P}\int_0^{2\pi}\frac{a(1-e)}{1+e\cos\varphi}d\varphi \tag{4.1}$$

Knowing the angle $\Phi$ at the date of observation, we can calculate the semi major axis $a$:

$$a = \frac{r(1+e\cos\Phi)}{1-e} \tag{4.2}$$

Once the semi major axis $a$ is know the total mass of the system can be calculated using:

$$M = m_1 + m_2 = \frac{4\pi^2 a^3}{GP^2} \tag{4.3}$$

And knowing from Han & Gatewood (2002) that

$$M = m_1 + 0.15m_1 \tag{4.4}$$

we can now calculate the individual masses of the stars.

Solving these equations, we find a mass for the primary of $M_A = 1.01 \pm 0.13\,M_\odot$ and for the secondary of $M_B = 0.15 \pm 0.02\,M_\odot$. Using the parallax determined by Han & Gatewood (2002) of $\chi^1$ Ori of $115.69 \pm 0.74$ mas, we would find the masses to be $M_A = 1.02 \pm 0.08\,M_\odot$ and $M_B = 0.15 \pm 0.01\,M_\odot$. The error bars are fairly large but further direct measurements will improve the orbital solution, in particular the separation and the position of the orbit in the sky. The position angle between $\chi^1$ Ori A and B on the observing date (MJD = 52334.33952) is $(123.22 \pm 0.12)°$. The observed position and position angle is only 13 mas and 2.8° away from the predicted values by Han & Gatewood (2002).

**Spectral synthesis analysis of $\chi^1$ Orionis**
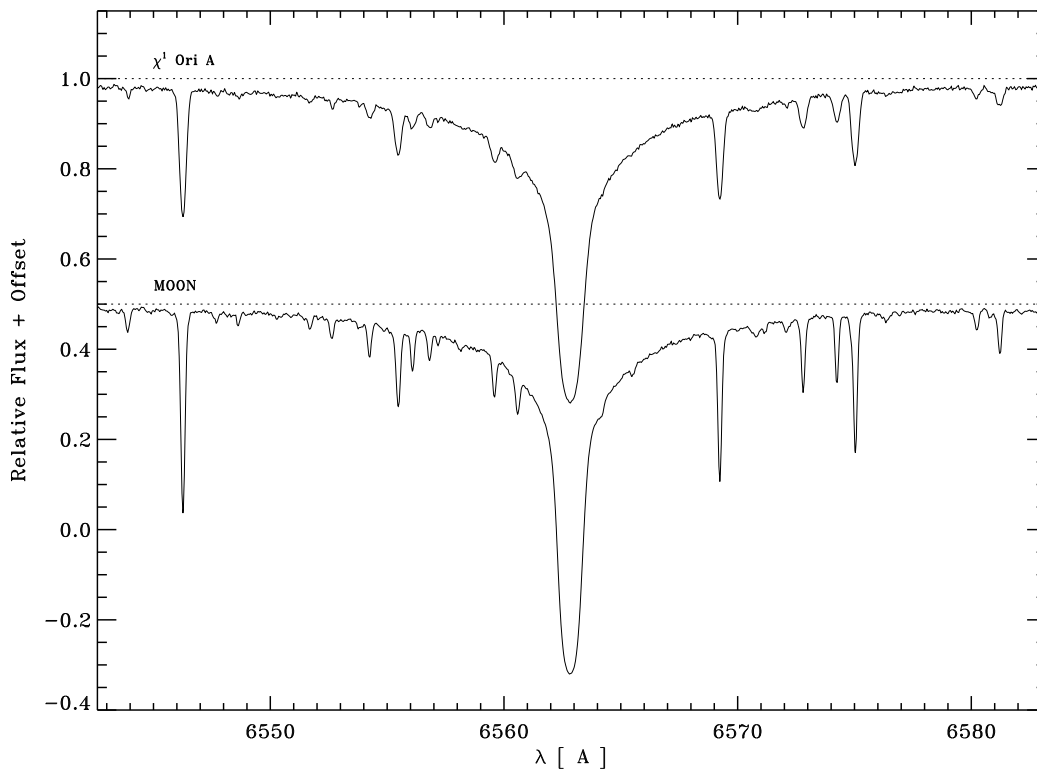


**Figure 4.4:** A spectrum of $\chi^1$ Ori A compared to the moon (= reflected sun light) in the range of H$\alpha$ at 6563 Å. Note the large rotational velocity of $\chi^1$ Ori A, $v \sin i = 8.7$ km/s, and the slightly filled in line core of H$\alpha$.

The basic stellar parameters of $\chi^1$ Ori A are derived from a model atmosphere analysis of

high resolution, high S/N échelle spectra (Fig. 4.4 and 4.5) obtained in January 2000 at the Calar Alto Observatory, Spain, 2.2 m telescope with FOCES (Pfeiffer et al., 1998). The fairly high projected rotational velocity, $v \sin i = 8.7 \pm 0.8$ km s$^{-1}$, the strong lithium feature at $\lambda 6707$ (Fig. 4.5), the "dipper star like" kinematics ($U/V/W = 24/7/0$ km s$^{-1}$), and the filled in line cores of H$\alpha$ (Fig. 4.4) and the Ca II infrared triplet all consistently confirm that $\chi^1$ Ori must belong to the Ursa Major Cluster. As in Fuhrmann et al. (1997), we deduce the effective temperature of the primary, $T_{\mathrm{eff}} = 5920 \pm 70$ K, from the Balmer line wings and the surface gravity, $\log g = 4.39 \pm 0.10$, from the iron ionisation equilibrium and the wings of the Mg Ib lines. We find the metallicity to be slightly below the solar value ([Fe/H]$= -0.07 \pm 0.07$), again very typical for the mean abundance of Ursa Major Cluster stars of $\langle$[Fe/H]$\rangle = -0.09$ (Boesgaard & Friel, 1990). With a bolometric magnitude $\mathrm{M}_{\mathrm{bol}} = 4.60 \pm 0.05$, and $T_{\mathrm{eff}}$ and
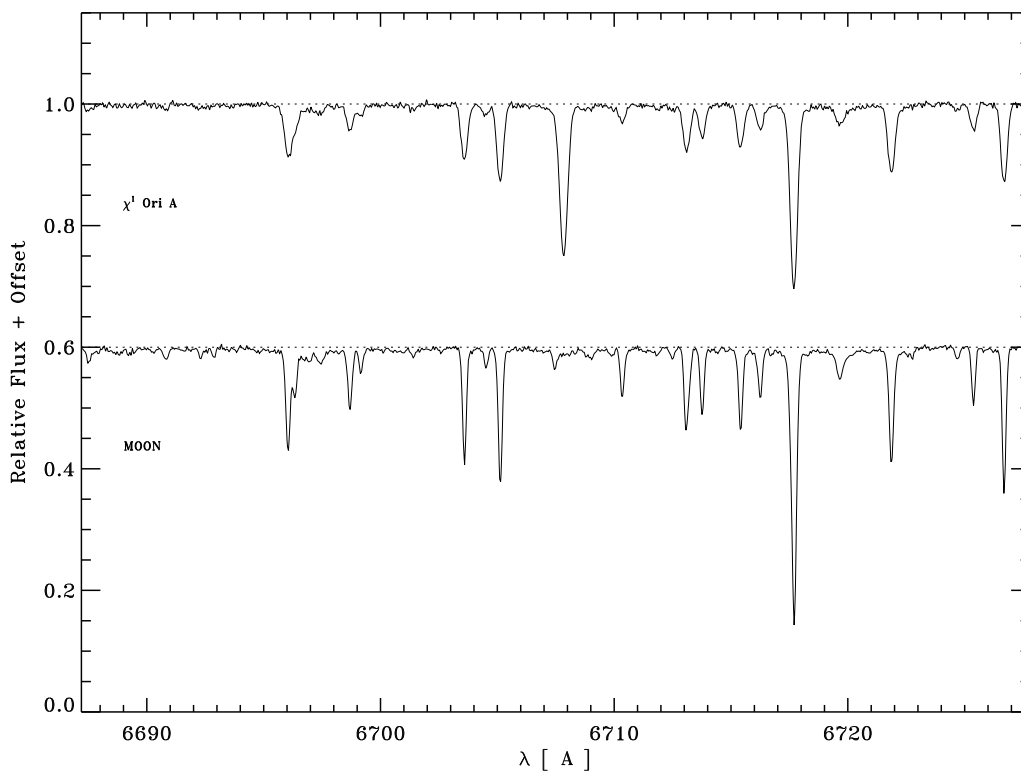


**Figure 4.5:** Same as Fig. 2, but for the range of lithium at 6707.8 Å and calcium at 6717.8 Å.

[Fe/H] as derived above, we find the mass to be M= 1.04 M$_\odot$ (implied from the tracks given in Fuhrmann et al., 1997), i.e. slightly above solar and with an uncertainty of about 0.05 M$_\odot$. The secondary, being more than five magnitudes (extrapolating the measured H-band magnitude) fainter in the visible, does not have an impact on our spectra.

## Results and Discussion

In the sequel, we want to test pre-main sequence models from different authors. The classical way to do this is to find a binary star with a solved orbit and almost equal masses. The conditions the tracks and isochrones have to fulfill is that for the given masses, both stars have to lie on the same isochrone. Of course in our case this is not possible because we already know by the fact that the primary star has $1.01 \pm 0.13$ M$_\odot$ and from the spectrum, that it

must lie on the main sequence. The tests performed will therefore be slightly different. We use the additional knowledge that the star is a member of the Ursa Major association. For this association the age could be derived by independent methods. We therefore change the way the tests are performed. For the tracks and isochrones which are available covering the mass range of the primary and the secondary, we want to check the position of the primary on the main sequence and on the right mass track. The secondary will be used to determine an age which will be in a final step compared to independent methods to derive an age for the Ursa Major association.
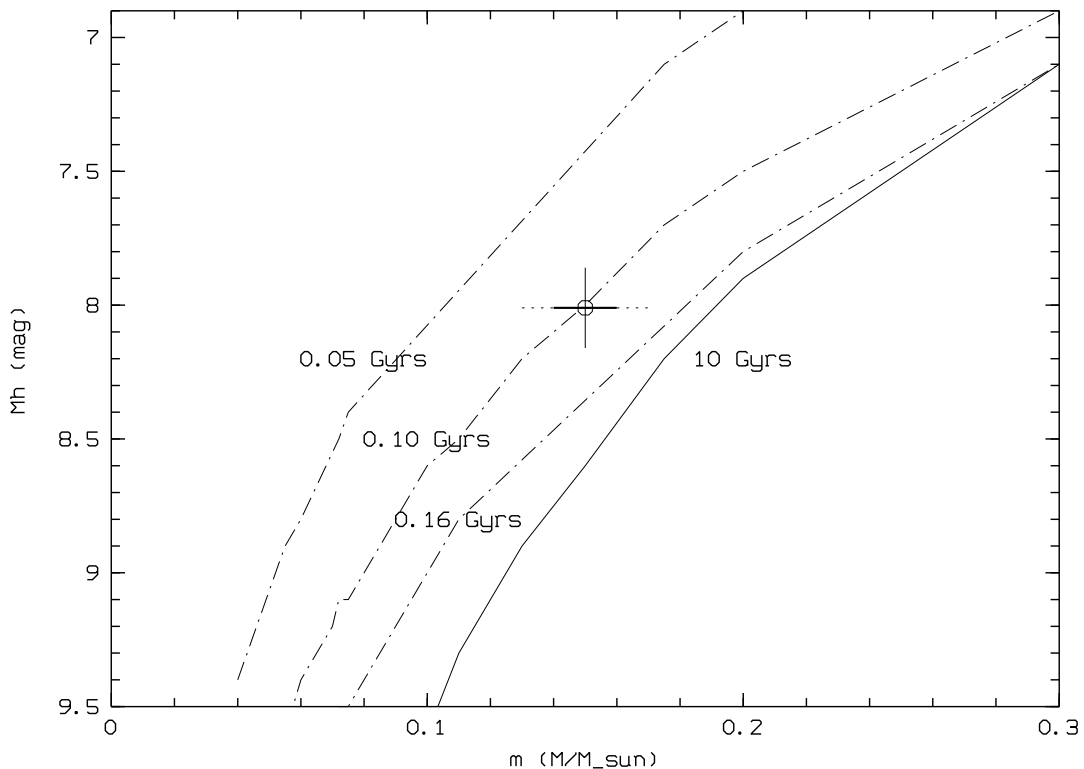


**Figure 4.6:** Baraffe et al. (1998) isochrones for solar metallicity in a mass-luminosity plot compared to the position of $\chi^1$ Ori B. The error bars for the mass are derived by the spectroscopy (solid) and for the dynamical mass (dots). The age for $\chi^1$ Ori B ranges from 70-130 Myrs using the dynamical mass.

**Baraffe et al. (1998) models:**   We now use the fact that the mass of the companion B of $\chi^1$ Ori A was determined precisely to be $(0.15 \pm 0.005) \cdot M_{\chi^1 \text{ OriA}}$ (Han & Gatewood, 2002). The main uncertainty is $M_{\chi^1 \text{ OriA}}$. This leads to a spectroscopic $(0.15 \pm 0.01 M_\odot)$ and dynamic mass $(0.15 \pm 0.02 M_\odot)$ of the companion, which are both in good agreement.

The position of the $\chi^1$ Ori B in the mass-luminosity plot (Fig. 4.6 and 4.7 a) compared to the isochrones provided by Baraffe et al. (1998) indicates that the star lies about $0.50 \pm 0.10$ mag above the main sequence.

Figure 4.7 b and c show Hertzsprung-Russell diagrams for the primary star including the tracks of Baraffe et al. (1998). Figure 4.7 b shows models for $[M/H] = 0$, $Y = 0.275$, and the mixing length of $L_{\text{mix}} = H_{\text{P}}$. Baraffe et al. (1998) acknowledge that these models do not reproduce the sun at present age. Those tracks and isochrones also do not reproduce $\chi^1$ Ori A as we have expected.
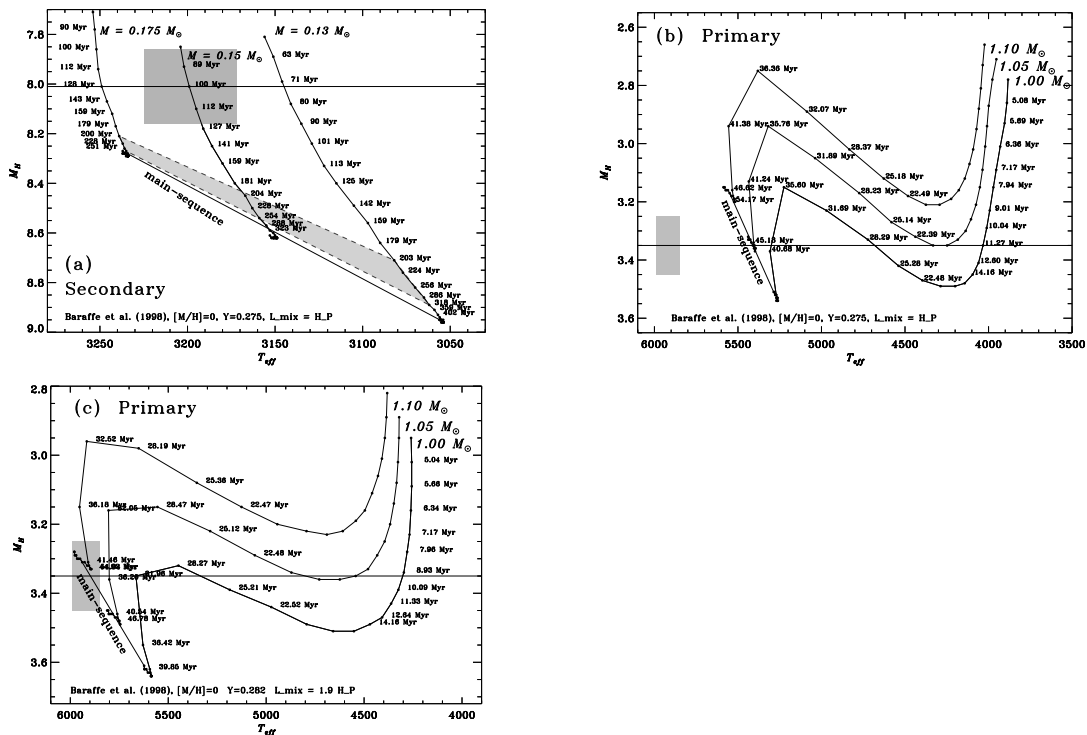
**Figure 4.7:** Baraffe et al. (1998) tracks for solar metallicity. The horizontal line in the first plot gives $M_H$ for the companion star with the top shaded area indicating the $1\sigma$ error for $M_H$ and the temperature range. In panel (a), the bottom shaded area is the age range determined for the Ursa Major cluster using different methods. With a mass of $0.15 M_\odot$ the companion appears younger compared to the age range of the Ursa Major cluster. In the other two panels the same tracks plotted are for the primary, indicating the position of the primary by the shaded area. In panels (a) and (b) the model parameters are [M/H]=0, Y=0.275 and $L_{mix} = H_P$. For (c) the parameters have been adjusted to fit the sun to [M/H]=0, Y=0.282 and $L_{mix}$=1.9 $H_P$.

Figure 4.7 c shows the same range of the Hertzsprung-Russell diagram as Fig. 4.7 b except that the parameters $[M/H] = 0$, $Y = 0.282$, and the mixing length of $L_{mix} = 1.9 H_P$ were adjusted to fit the sun. With these parameters the present sun could be reproduced. For $\chi^1$ Ori A they also seem to work. The $M_H$ predicted by Baraffe et al. (1998) is a bit lower than the measured $M_H$ value for $\chi^1$ Ori A. The reason for this could be because $\chi^1$ Ori A is slightly iron under-abundant ($[Fe/H] = -0.07 \pm 0.07$) compared to the sun and the tracks were calculated for solar abundance. No tracks for masses of 0.15 - 0.175 $M_\odot$ are available for the model with the parameter set to fit the sun.

**D'Antona & Mazzitelli (1997) models:** The D'Antona & Mazzitelli (1997) tracks and isochrones were updated by D'Antona & Mazzitelli (1998). In particular the treatment of deuterium burning which is dependent on the initial deuterium abundance for low mass stars and brown dwarfs was improved. We chose to compare the three different models to $\chi^1$ Ori B only because D'Antona & Mazzitelli (1997) do not provide model tracks and isochrones for the primary.

D'Antona & Mazzitelli (1997) calculate a model with a gray atmosphere. This results in a bolometric luminosity but not in color information. To derive absolute H-band magnitudes, we have to convert the luminosity to a color by applying bolometric corrections. As we can see
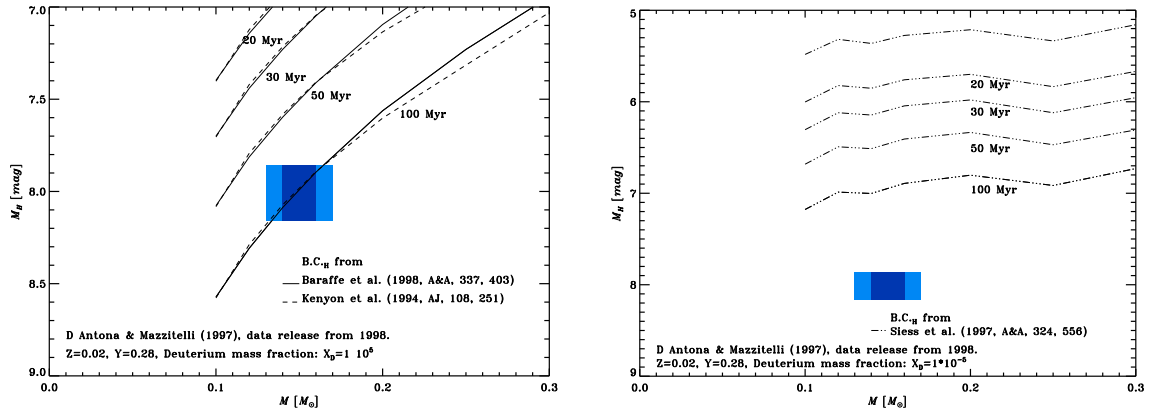
**Figure 4.8:** D'Antona & Mazzitelli (1997) isochrones. Plotted are the isochrones of the data released from 1998 (D'Antona & Mazzitelli, 1998). The reason for the different initial Deuterium abundances is given in (Censori & D'Antona, 1998). Both panels above are for the initial Deuterium mass fraction of $1 \cdot 10^{-5}$. In the left panel the bolometric corrections are taken from Baraffe et al. (1998) and from Kenyon et al. (1994). In the right panel the corrections are taken from Siess et al. (1997).
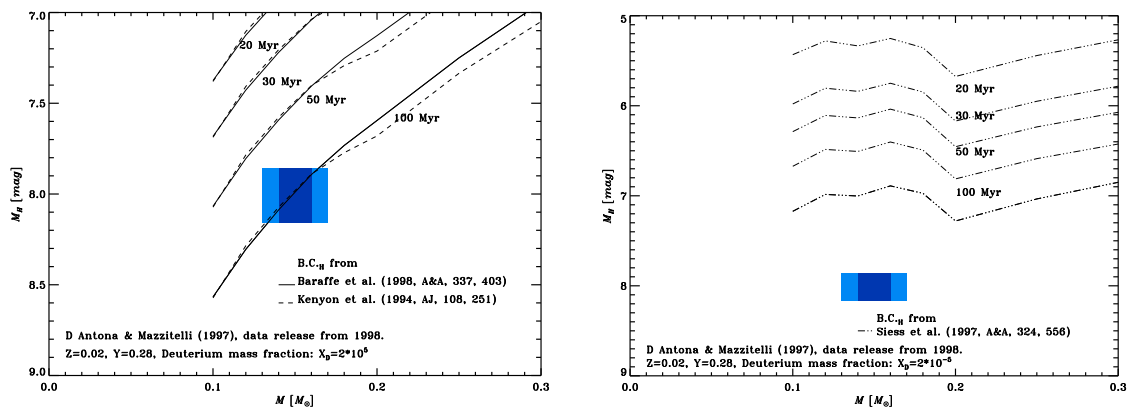


**Figure 4.9:** D'Antona & Mazzitelli (1997) isochrones. Plotted are the isochrones of the data release from 1998 (D'Antona & Mazzitelli, 1998). The reason for the different initial Deuterium abundances is given in Censori & D'Antona (1998). Both panels above are for the initial Deuterium mass fraction of $2 \cdot 10^{-5}$. In the left panel the bolometric corrections are taken from Baraffe et al. (1998) (line) and from Kenyon et al. (1994) (dashed line). In the right panel the corrections are taken from Siess et al. (1997).

in Fig. 4.14 different authors give different bolometric corrections. To be on the safe side we do not trust any of them a priori and plot the isochrones with several bolometric corrections.

The star is quite evolved and we do not expect the initial Deuterium abundance to play a major role in the age determination. As can be seen in the Fig. 4.8, 4.9, and 4.10 this is the case. The bolometric corrections used play a much more important role. The Siess et al. (1997) bolometric corrections at $0.15_\odot$ do not lead to tracks and isochrones which reproduce $\chi^1$ Ori B at the expected age and color.

**Siess et al. (2000) models:** In this section we perform the same test as with the D'Antona & Mazzitelli (1997) models. Yet, Siess et al. (1997) have computed a non-gray atmosphere model and provide therefore bolometric corrections to convert the given bolometric luminosity
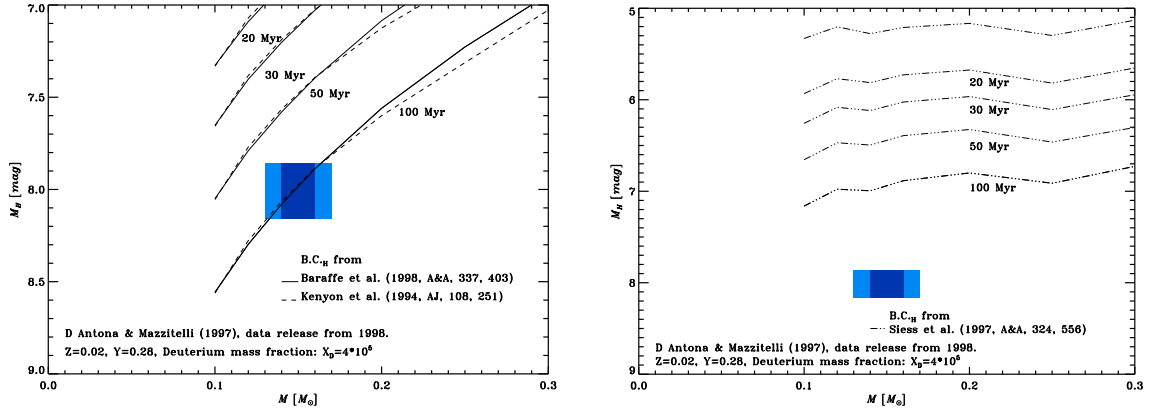
**Figure 4.10:** D'Antona & Mazzitelli (1997) isochrones. Plotted are the isochrones of the data release from 1998 (D'Antona & Mazzitelli, 1998). The reason for the different initial Deuterium abundances is given in Censori & D'Antona (1998). Both panels above are for the initial Deuterium mass fraction of $4 \cdot 10^{-5}$. In the left panel the bolometric corrections are taken from Baraffe et al. (1998) (line) and from Kenyon et al. (1994) (dashed line). In the right panel the corrections are taken from Siess et al. (1997).
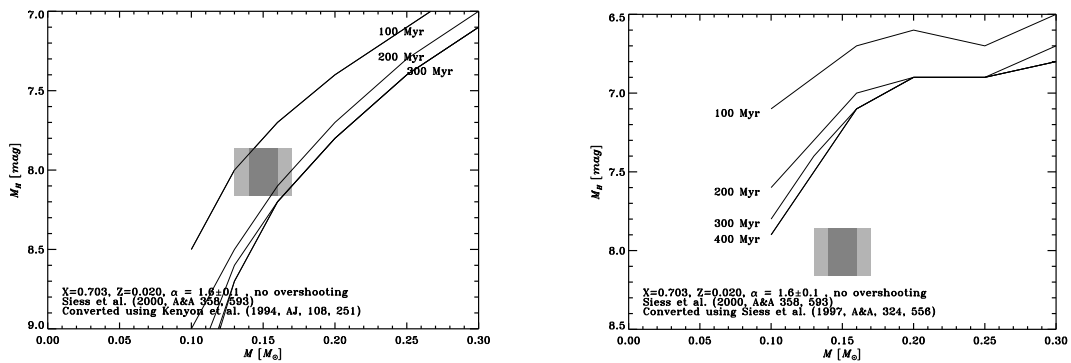


**Figure 4.11:** Siess et al. (2000) isochrones of the model without overshooting. In the left panel using bolometric corrections from Kenyon et al. (1994) and in the right panel Siess et al. (1997).

to an absolute H-band magnitude. As a first estimate we would expect these bolometric corrections to provide consistent results. But as we can see in these plots, they deviate substantially when compared to the observed bolometric corrections by Kenyon et al. (1994) (dashed line) and the computed ones by Baraffe et al. (1998) (line).

### Age determination of the Ursa Major Association

The age prediction by the pre-main sequence models can be directly compared to other age determinations for the Ursa Major association. While the canonical value for the age of the Ursa Major association is 300 Myrs (cf. e.g. Soderblom & Mayor, 1993, , and the references therein) derived by comparing the members of the Ursa Major association nucleus stars in a color magnitude diagram to theoretical isochrones computed by Vandenberg (1985) (see Fig.4.1.1). King et al. (2003) have revised the work and have redone the determination of the age using the A-stars of the Ursa Major association nucleus stars and derived an age of
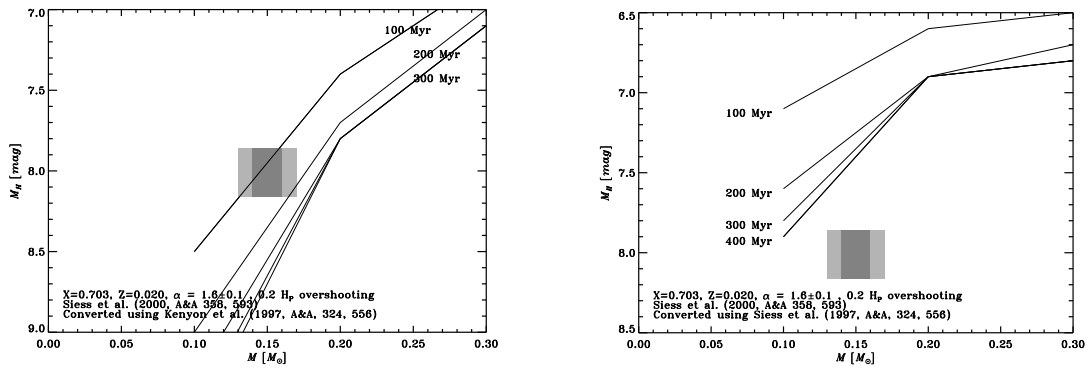
**Figure 4.12:** Siess et al. (2000) isochrones of the model with $0.2H_P$ overshooting. In the left panel using bolometric corrections from Kenyon et al. (1994) and in the right panel Siess et al. (1997).
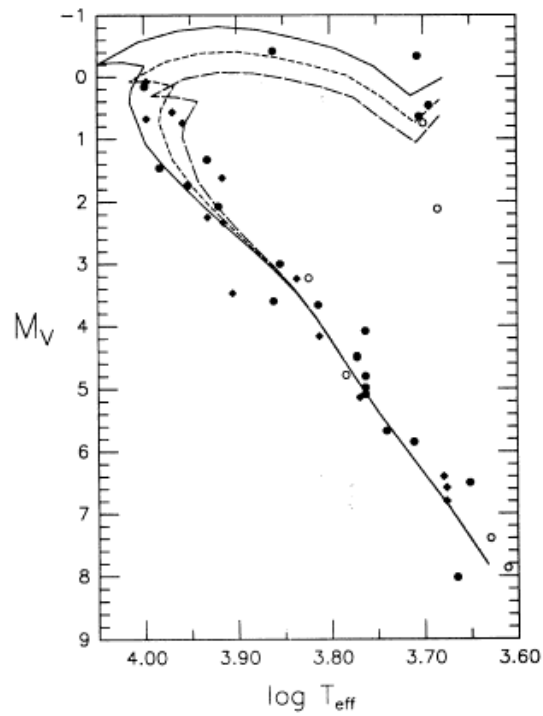


**Figure 4.13:** Soderblom & Mayor (1993) have determined the age of the Ursa Major cluster using post-main sequence tracks published by Vandenberg (1985). They placed all known and suspected members of the UMa into the Hertzsprung-Russell diagram and compared Vandenberg (1985) he position of especially the a stars to the theoretical isochrones. Using statistical methods, they claim the most likely age is 300 Myrs.

500 Myr.

It is known that Sirius is a confirmed member of the Ursa Major association. It has a well studied white dwarf companion with a dynamical mass and a known chemistry. More thorough observations of Sirius' white dwarf companion led Holberg et al. (1998) to suggest an age of 160 Myr for the white dwarf with reference to the cooling tracks of Wood (1992).

Since Sirius B is also well-known as a fairly massive degenerate white dwarf with a mass of M = $1.034 \pm 0.026$ $M_\odot$ (Holberg et al., 1998), the initial-final mass relation suggests a progenitor of about 6-7 $M_\odot$ which means that we can expect another $\sim$60-70 Myr for the pre-white dwarf evolution. Hence, this leads us to a total life time of the white dwarf of only somewhat above 200 Myrs and also an age of 200 Myr for the Ursa Major association. More recent white dwarf cooling models of Salaris et al. (2000) (models with a pure hydrogen atmosphere) suggest the age of the white dwarf of 111 Myrs derived from its V-magnitude and temperature published by Holberg et al. (1998). Assuming the lifetime of the progenitor of the white dwarf of 46 Myrs estimated by Salaris et al. (2000) leads us to an age of the white dwarf and of the Ursa Major association of 157 Myrs.

The comparison of the age using Baraffe et al. (1998) (70-130 Myrs) to the ages of the Ursa Major Cluster (160-500 Myrs) indicate that either: (i) the Ursa Major Cluster has a larger than expected age spread, (ii) there are problems with the models at a solar and/or at $\sim 0.15 M_\odot$ mass, (iii) the canonical age for the Ursa Major Cluster is too high (300 Myrs), or (iv) $\chi^1$ Ori is not a member of the Cluster. Considering possibility (i), we note that the age spread of 70-300 Myrs seems too large for a Cluster. As for the option (iv), $\chi^1$ Ori is a classical member of the Ursa Major Cluster, located near the cluster center. The spectrum of $\chi^1$ Ori A would support an age of 200 Myrs regarding the activity indicators, as would the cooling tracks for the Sirius B white dwarf.
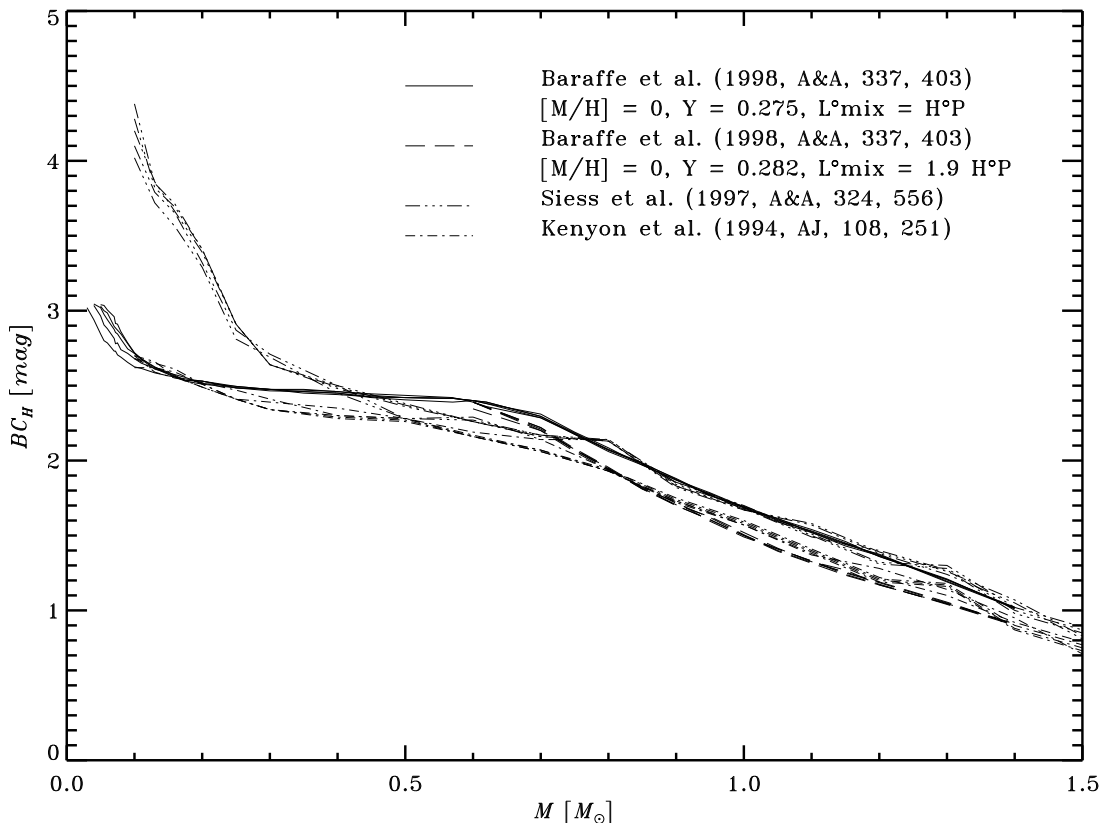


**Figure 4.14:** For a direct comparison we have plotted the bolometric corrections from Baraffe et al. (1998), Kenyon et al. (1994), and Siess et al. (1997). The large discrepancy between Siess et al. (2000) and the others for small masses is striking. But also the fact that the bolometric corrections at $1 M_\odot$ do not agree, alerts us to take care drawing conclusions.

Comparing D'Antona & Mazzitelli (1997) models in the data release version of 1998, we

have to convert stellar luminosities to absolute H-band magnitudes. To do this we must rely on bolometric corrections which were also computed using models. In the literature we find three sources of bolometric corrections from Baraffe et al. (1998), Kenyon et al. (1994), and from (Siess et al., 1997). These bolometric corrections are available for a mass range including the mass of $\chi^1$ Ori B and in some cases also $1 M_\odot$. The tracks and isochrones of D'Antona & Mazzitelli (1997) and of Siess et al. (2000) do not cover the regime of $\chi^1$ Ori A, so that a direct test of both mass regimes cannot be performed.

Yet, the estimate of the age for the secondary is possible and in the case of D'Antona & Mazzitelli (1997), we again get $100 \pm 30$ Myr as in the case of Baraffe et al. (1998), if we use the bolometric corrections from Kenyon et al. (1994) or from Baraffe et al. (1998). The tracks and isochrones of Siess et al. (2000) using the bolometric corrections from Kenyon et al. (1994) give us a somewhat older age of $150 \pm 70$ Myr.

In any case applying the bolometric corrections of Siess et al. (1997), we find that the theoretical tracks and isochrones lie away from the measured position of the star and would predict a rather old object. But as we have discussed above, $\chi^1$ Ori B is a member of the Ursa Major association and must therefore be in the age range derived for the association, either that or the age of association is overestimated.

### 4.1.2 [GKL 99] 104, HIP 18512 A, HD 24916 A

**Table 4.2:** Spectral parameters of HIP 18512 A

| $T_{\text{eff}}$ [K] | $\log g$ | [Fe/H] | $v \sin i$ [km/s] | $m_{\text{V}}$ [mag] | $M_{\text{bol}}$ [mag] | mass $M_\odot$ |
|---|---|---|---|---|---|---|
| $4600 \pm 100$ | $4.60 \pm 0.10$ | $-0.03 \pm 0.07$ | $2.1 \pm 1.0$ | $8.06$ | $6.53$ | $0.70$ |

King et al. (2003) have compiled space velocities of $U = 7.436 \pm 0.786$ km/s, $V = 0.342 \pm 0.196$ km/s, $W = -17.652 \pm 0.730$ km/s and list it not as a kinematic member of the Ursa Major association whereas Montes et al. (2001) list it as a member candidate. Favata et al. (1997) have derived a temperature of $4394$ K and have measured a lithium equivalent width of $4$ mÅ and an abundance of $\log N(\text{Li}) = -0.55$. They consider the star to be kinematically young. The spectral signatures are consistent with the star being an Ursa Major member.

The discrepancy between the Hipparcos parallax and the spectroscopic parallax is 1.2%. The lithium absorption line is not present in our spectrum. The space motion, and the iron abundance support the membership in the Ursa Major association.

### 4.1.3 [GKL 99] 109, HIP 19855, HD 26913

King et al. (2003) have compiled space velocities of $U = 13.512 \pm 0.333$ km/s, $V = -1.297 \pm 0.219$ km/s, $W = -8.735 \pm 0.380$ km/s. They are not conclusive about the membership in the Ursa Major association. The star has a common proper motion companion (HD 26923). The spectral age indicators as well as the metallicity suggest that the star is an Ursa Major association member. The radial velocity measurements by de Medeiros & Mayor (1999) result in a value of $RV = -7.37 \pm 0.119$ km/s with a variation of $\sigma(RV) = 0.46$ km/s. The projected rotational velocity is $v \sin i = 3.9 \pm 1.0$ km/s.

The discrepancy between the spectroscopic distance and the Hipparcos distance is only 5.6%. The iron abundance, the projected velocity of rotation, $v \sin i$, and the space motion support the membership in the Ursa Major association.

**Table 4.3:** Spectral parameters of HIP 26913

| $T_{\mathrm{eff}}$ [K] | $\log g$ | [Fe/H] | $v \sin i$ [km/s] | $d_{\mathrm{HIP}}$ [pc] | $d_{\mathrm{sp}}$ [pc] | disc. [%] |
|---|---|---|---|---|---|---|
| 5630±70 | 4.50±0.10 | -0.07±0.07 | 5.9±1.0 | 20.89±2.89 | 21.86±2.99 | 4.6 |

### 4.1.4 [GKL 99] 231, HIP 53985

This star was observed with the Tautenburg échelle spectrograph. The Hα-line is filled in and lithium is not measurable within the noise level. At the spectral type of M0V this is not unusual for UMa. We propose HIP 53985 as a bona-fide member because its space motion is also consistent with the UMa.

### 4.1.5 [GKL 99] 239 and [GKL 99] 240, or HIP 55454 A & B

The star is a visual binary with one component being a K4/5V, and the other being an M0V star. We have observed both stars with DFOSC and we find the Hα-line again filled in but we do not see significant lithium absorption above the noise level. The space motion for the A component is consistent with the star being a Ursa Major association member. The origin of the space motion for the B component is from the Catalog of nearby stars and is flagged as not well determined so the star could also be member of Ursa Major association. Our radial velocity measurement do not improve the space motion measurement because the precision is not high enough.

## 4.2 Local association

The local association was described by Eggen (1983b,a,c) as a coherent stream of young associations in the solar vicinity. In this association are embedded the Pleiades supercluster, the α Persei cluster, the IC 2602 cluster, and NGC 2516 cluster, the Scorpio-Centaurus moving cluster, as well as newly discovered associations like the TW Hydrae association, the β Pictoris moving group, the Horologium-Tucana association, and the Hercules-Lyra association. Montes et al. (2001) instead name this association the Pleiades moving group. The age range of the stars span 20 to 150 Myr. All stars show lithium absorption in their spectrum and consistent space motion (Montes et al., 2001). But we have seen that a more detailed view of the stars can disentangle this conglomerate of associations and clusters. Only a minor fraction of stars cannot be classified so they might remain as local association stars. Maybe this can be improved in the future.

The space motion of all these associations and clusters summed up as the local association is close to the motion of the local standard of rest (LSR) which means that it is not surprising to find many stars and also young stars with this space motion. It could be possible that the local association is not real but a matter of the incomplete knowledge of young associations in the solar vicinity or the space motion of individual stars. We will try not to use the term local association if we can identify the membership of a star to a certain association.

## 4.3 The region of TW Hydrae Association

In the TW Hydrae Association (TWA) we will discuss a new member candidate among the stars of the Gershberg et al. (1999) flare stars catalog. TWA is one of the closest known

associations of young stars at about 60 pc. Three supposedly young flare stars are located in the same region of the sky as TWA. One of them (HIP 57269) shows strong lithium absorption with spectral type K1/K2V and a high level of chromospheric and coronal activity. It also shows common proper motion, and rotational velocity with the known stars of the association and is located at a distance of 48.7±6.3 pc in common with the five TWA members observed with Hipparcos (46.7 to 103.9 pc). The close binary HIP 57268 A & B has a wide companion C which shows lithium at 6707 Å and which has common proper motion with HIP 57269, as well as a close companion resolved visually by Tycho. HIP 57269 A, B & C lie above the main sequence and are clearly pre-main sequence stars. The two other flare stars in the TWA sky region do not show lithium at all and are, hence, unrelated. The star TW Hya was first thought to be an isolated T Tauri star. Only later similar stars and member candidates were found by accident and by systematic searches among infrared and X-ray sources (Hoff et al., 1996; Kastner et al., 1997; Jensen et al., 1998; Sterzik et al., 1999; Webb et al., 1999; Zuckerman et al., 2001b). More kinematic member candidates can be found in Makarov & Fabricius (2001), Torres et al. (2000), and Tachihara et al. (2003). TWA was found to be a loose group without nearby cloud material. Today there are 19 known and confirmed member systems of the association, called TWA 1-19 (Webb et al., 1999; Zuckerman et al., 2001b). These stars have a common radial velocity and proper motion and comparable lithium abundance.
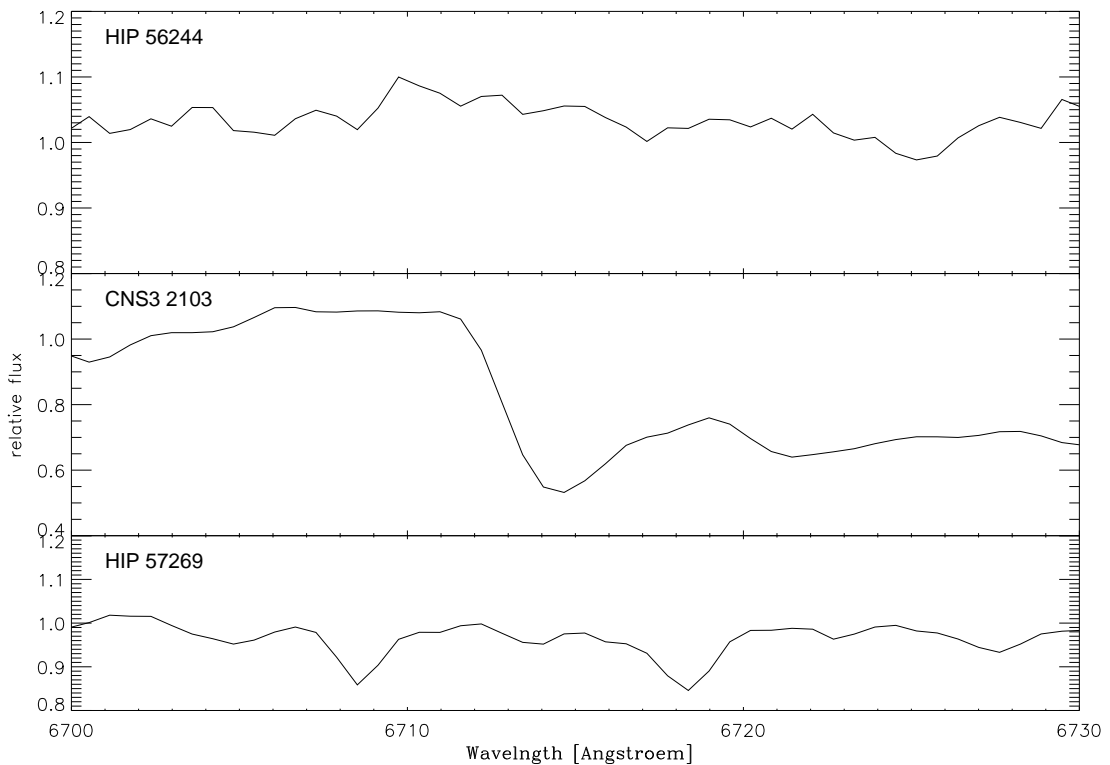


**Figure 4.15:** A section of the spectrum of HIP 57269 A & B showing lithium at 6708 Å and calcium at 6718 Å and HIP 56244 and GJ 3780 without lithium.

Hipparcos has observed five confirmed member stars of the association. This leads to a mean distance of 62.2±7.8 pc with a range of 46.7±7.2 pc to 103.9±17.5 pc. The newly proposed member candidate is the sixth member with a Hipparcos parallax.

The sample of stars were taken from Gershberg et al. (1999) and listed in Table 4.4, namely

the stars located in the region of Ra: 10 h to 13 h and Dec: -24° 30$^m$ to -50$^s$.

### 4.3.1   The sample in TWA

There are three flare stars in that region (see Table 4.4).

**Table 4.4:** Basic data of the flare stars located in the TWA sky region

| name | plx [mas] | V [mag] | SpT. | $T_{\rm eff}$ [K] | $v \sin i$ [km/s] |
|------|-----------|---------|------|-------------------|-------------------|
| HIP 57269 | 20.55±2.38[1] | 9.34[11] | K1/K2V[9] | 4990±100[12] | 20[7] |
| HIP 56244 | 95.46±2.59[1] | 11.5[4] | M3.5e [2] | 3420±100[12] | |
| GJ 3780 | 62.5±14.4[3] | 12.9[4] | M3.5[2] | 3420±100[12] | |
| TWA range[4,10] | 9.62 to 21.43 | 8 to 14 | A0 to M9 | | 5 to 58 |

| name | $\mu_\alpha$ [mas/yr] | $\mu_\delta$ [mas/yr] | Rad. Vel. [ km/s] | Remarks |
|------|-----------------------|-----------------------|-------------------|---------|
| HIP 57269 | -137.21±1.90[1] | -47.71±1.37[1] | 16[8], 19.0±3.0[13] | b |
| HIP 56244 | -715.75±1.38[1] | 170.75±1.38[1] | 6.0[6] | a |
| GJ 3780 | -556[5] | -249[5] | -0.3[6] | a |
| TWA range[4,10] | -122.2 to -30.0 | -38.0 to +16.3 | 5.73 to 14.0 | |

1: Hipparcos catalog 2: Gershberg et al. (1999) 3: Hawley et al. (1997) 4: SIMBAD 5: Bakos et al. (2002) 6: Gliese & Jahreiss (1995): Catalog of nearby stars (CNS4) 7: Pallavicini et al. (1992) 8: Anders et al. (1991) 9: Cutispoto (1998) 10: Torres et al. (2003) 11: Fabricius & Makarov (2000) 12: Adapted from spectral type using Kenyon & Hartmann (1995) 13: this work a: foreground b: member candidate

The two stars HIP 56244 and CNS3 2103 do not show lithium (see Fig 4.15). Their proper motion is not consistent with the mean proper motion of the TWA member stars ($\mu_\alpha = -80.9 \pm 5$ mas/a, $\mu_\delta = -26.4 \pm 5$ mas/a, Webb et al., 1999). HIP 56244 is a foreground object at a distance of 10.48±0.28 pc. Hawley et al. (1997) give a spectroscopic distance to CNS3 2103 of 16.0±4.8 pc, which also leads us to the conclusion that it is a foreground star.

**Table 4.5:** Spectroscopic data of HIP 57269

| $W_\lambda$(Li) [mÅ] | $W_\lambda$(Ca) [mÅ] | log N(Li) | $v \sin i$ [km/s] | rad. vel. [km/s] | ref. |
|----------------------|----------------------|-----------|-------------------|------------------|------|
| 196±5 | 200±3 | 2.7 | 20 | | P |
| | | 2.2 | 20 | | R |
| 205 | | 2.5 | 23 | 15.9 | A |
| 200±20 | 270±20 | 2.9 | | 19.0±3.0 | K |

P: Pallavicini et al. (1992), R: Randich et al. (1993), A: Anders et al. (1991), K: this work

Udalski & Geyer (1985) first classified HIP 57269 as a BY Dra type variable. The primary component HIP 57269 A is a star with spectral type K1/K2V which shows lithium absorption (see Fig. 4.15). The spectral type was published by Cutispoto (1998) and references therein after a thorough study of the stellar system, and was confirmed by our DFOSC spectrum.
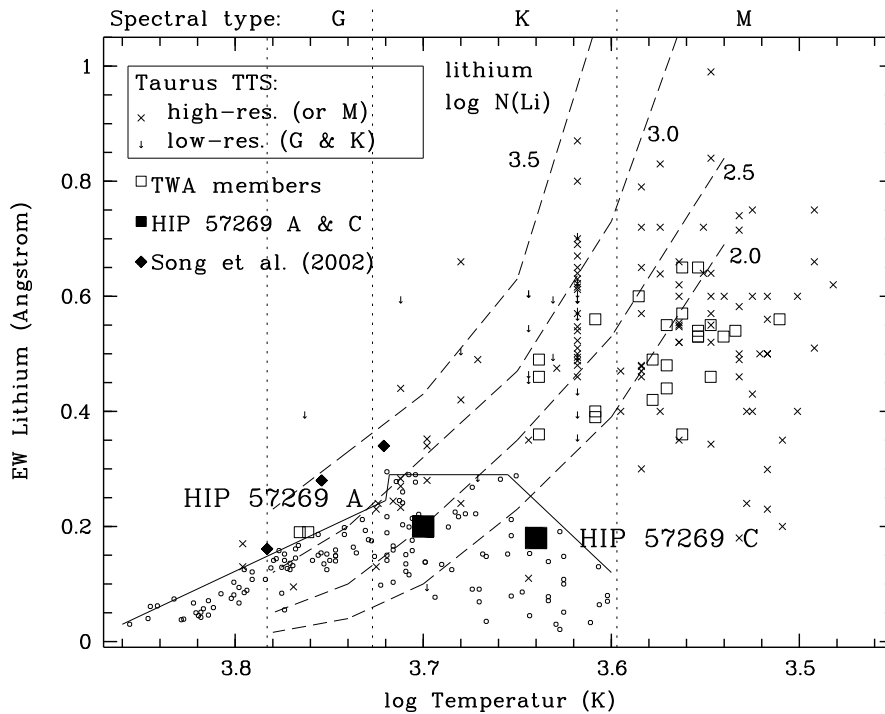
**Figure 4.16:** The lithium equivalent width versus temperature of the confirmed TWA member stars (open boxes) and HIP 57269 A and its companion C (filled box). The three member candidates from Song et al. (2002) are also shown (big dots) with temperatures adopted from Mamajek et al. (2002) for two stars and for one estimated from Kenyon & Hartmann (1995). Underlayed are T Tauri stars in Taurus (crosses and arrows (upper limits)) and Pleiades stars (open dots) for reference. Figure adapted for the T Tauri star and Pleiades stars from Neuhäuser (1997). The temperatures for the TWA members and member candidates were derived from published spectral types using the Kenyon & Hartmann (1995) temperature scale. lithium isoabundance lines are taken from Pavlenko & Magazzù (1996).

The equivalent width (EW) of the 6707 Å line is 0.20±0.01 Å while calcium at 6718 Å has 0.27±0.01 Å. This is very similar to the lithium equivalent width of the known TWA member TWA-19 with spectral type G 3-5, with 0.19 Å equivalent width (Webb et al., 1999; Sterzik et al., 1999; Zuckerman et al., 2001b), see Fig. 4.16. We wish to note here that Mamajek et al. (2002) have doubts and propose TWA-19 to be a Scorpius-Centaurus-Crux association member. This lithium equivalent width and spectral type leads to a lithium abundance of $\log(N(Li)) = 2.5$ for HIP 57269 following Pavlenko & Magazzù (1996) for dwarfs. This lithium abundance is near the upper envelope of the lithium abundance of the Pleiades member stars at the spectral type early K and similar as in G- and early K-type T Tauri star in Taurus (see Fig 4.16).

Pallavicini et al. (1992) and Randich et al. (1993) observed HIP 57269 with high resolving poser of $\Delta\lambda/\lambda = 50,000$ and analyzed it in their sample of chromospheric active stars and RS CVn stars. Randich et al. (1993) conclude that it is a young chromospheric active star and not an old RS CVn star, see Tab. 4.5.

Anders et al. (1991) have also analyzed high resolution spectra of this star deriving high lithium abundances. They also take into account the proper motion, the space motion and a distance of 42 pc, they conclude that the star is a Pleiades supercluster member. We note that

before 1997, when Pallavicini et al. (1992), Randich et al. (1993), and Anders et al. (1991) studied this star, TWA was not yet recognized as a young cluster and the proper motion of the Pleiades supercluster is quite similar to the proper motion of TWA.

## 4.3.2 Kinematics and multiplicity
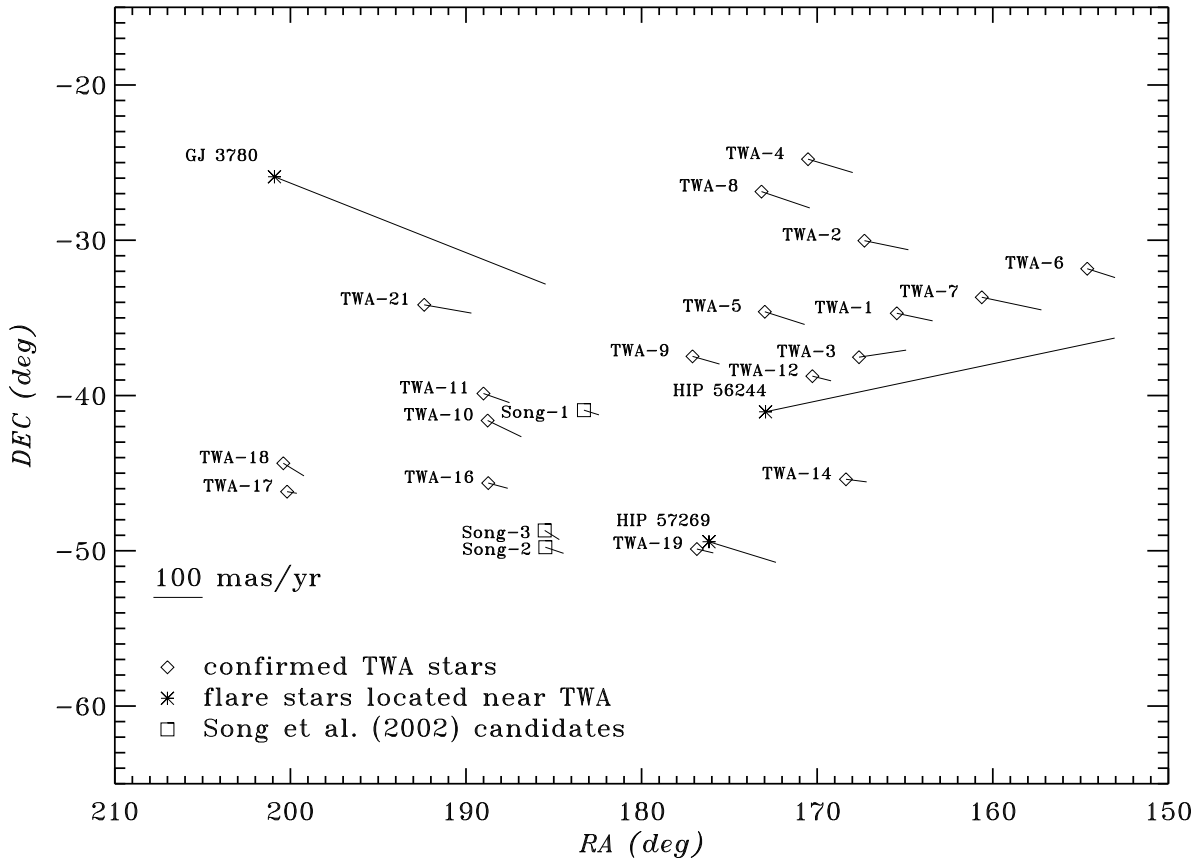


**Figure 4.17:** Proper motion of the known confirmed TWA members and the flare stars discussed in this paper: HIP 57269, GJ 3780 and HIP 56244. Proper motions were taken from Torres et al. (2003) for the TWA members and the Song et al. (2002) member candidates, for the flare stars from the Hipparcos catalog or from the SIMBAD database. The labels song-1 correspond to TYC 7760-0835-1, song-2 to TYC 8238-1462-1, and song-3 to TYC-8234-2856-1.

The proper motion of HIP 57269 (-137.21±1.0 mas/yr, -47.71±1.37 mas/yr) is consistent with the proper motion (see Fig. 4.17) of the other stars in TWA, so that Makarov & Fabricius (2001) list it as a kinematic member candidate. The radial velocity measured by us of 19.0±3.0 km/s and the space motion leads to a space velocity of $U$ =18.5 km/s, $V$ =-28.4 km/s and $W$ =-15.2 km/s which is quite different from the average space velocity of TWA ($U$ =10.8 km/s, $V$ =17.7 km/s, $W$ =-5.6 km/s, Torres et al., 2002) and is more consistent with the star being a Pleiades Super Cluster member (Chereul et al., 1999).

HIP 57269 (component A: V=9.34 mag) is a common proper motion triple star with the secondary (component B) being a V=10.48 mag companion at a position angle of 306° and 0.430″ separation (Fabricius & Makarov, 2000) and the third star (component C) with V=13.5 mag at a position angle of 349° and 9.6″ separation (Hipparcos catalog) (see also Fig. 4.19). The component C also shows lithium absorption at 6707 Å (Fig. 4.20). Multiplicity is typical for young stars.

## 4.3.3   Hertzsprung-Russell diagram
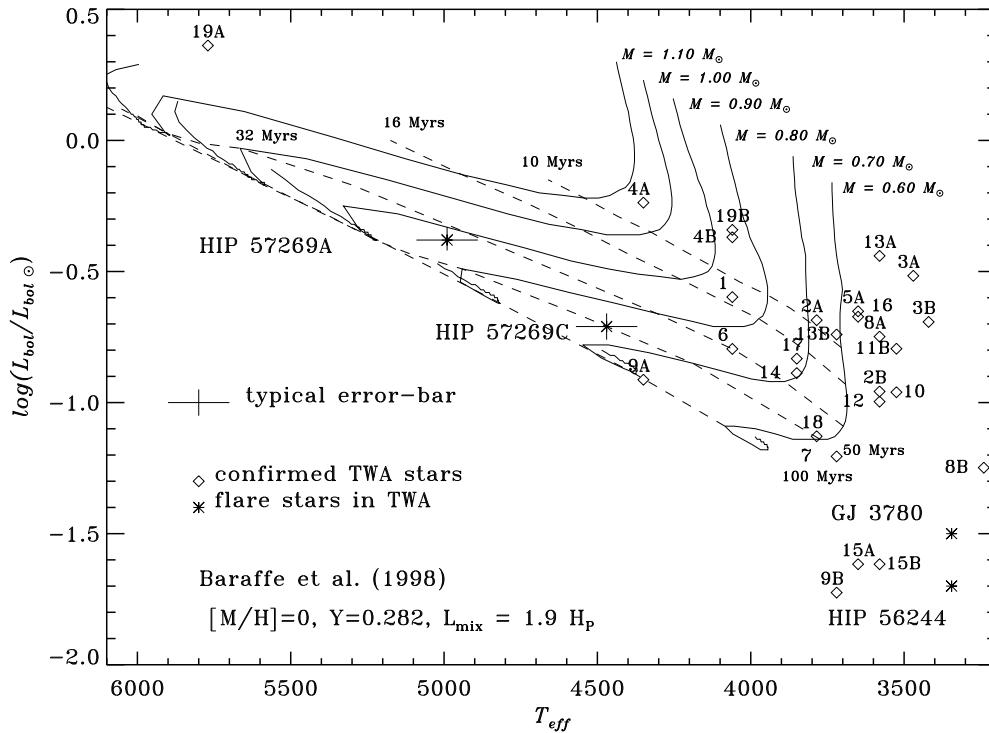


**Figure 4.18:** The three flare stars and HIP 57269 C (big asterix) together with the confirmed members of TWA (TWA-1 - 19) plotted in an Hertzsprung-Russell diagram using distances from Tab. 4.4. The luminosity for HIP 57269 A was computed using Tycho $V_T$- and $B_T$-magnitudes for the component A only. The V-magnitude for component C was taken from SIMBAD. For a comparison are overlayed the theoretical tracks and isochrones of Baraffe et al. (1998). It can be seen that both HIP 57269 A & C lie above the main sequence and on the same isochrone taking into account the errors in photometry and conversion to temperature from their spectral type. The temperature for all stars in the diagram were derived using Kenyon & Hartmann (1995). The photometry was taken from various sources (the references can be found in Torres et al., 2003) and the distance to the individual objects was taken from Hipparcos or from Frink (2001) when possible, for the other stars we use a mean distance of 61.5 pc. GJ 3780 and HIP 56244 are unrelated foreground stars. TWA-9 B and TWA-15 A & B are also located on the lower right below the main sequence, most certainly because the assumed mean distance of 61.5 pc to TWA may be different to the true distance of these stars.

We use the Tycho $V_T$- and $B_T$-magnitudes for component A which is resolved from the close companion B (Fabricius & Makarov, 2000) to convert to luminosity, and to place it into the Hertzsprung-Russell diagram at a temperature of 4990±100 K at a spectral type of K1/2V. In the Hertzsprung-Russell diagram (Fig. 4.18) HIP 57269 A lies above the main sequence, with an age of 40±10 Myrs and a mass of 0.88±0.05 M$_\odot$ compared to tracks and isochrones of (Baraffe et al., 1998). This age is comparable to the age of TWA-19A.

We also include the wide companion HIP 57269 C in the diagram. Assuming that the star is at the same distance as the component A, the star has an age of 50±10 Myrs, consistent with A and a mass of 0.75±0.05 M$_\odot$. This star is clearly younger than the confirmed member TWA-9A and it lies on the same isochrone as TWA-7 and TWA-18.

Song et al. (2002) argue that HIP 57269 not a member of TWA because the lithium

abundance is more consistent with a 30 Myrs star rather than a 10 Myrs, and that it lies on the main sequence on a specific set of the Siess et al. (2000) models.

Fabricius & Makarov (2000) give Tycho $B_T$ and $V_T$ for the components HIP 57269 A & B separately. Transforming those to a Johnson V-magnitude and calculating the absolute magnitude, we find that HIP 57269 A appears above the main sequence on the 30 Myrs isochrone using the Siess et al. (2000) model shown in the paper of Song et al. (2002). Given the error bars and using the combined photometry of the components A & B, we note that the star may also be consistent with an age of 10 Myrs in the Siess et al. (2000) models.

### 4.3.4 X-ray emission

The region of the TW Hydrae association was observed during the ROSAT all sky survey (RASS) using the Position Sensitive Proportional Counter (PSPC) in scanning mode. A total of 127 s X-ray data has been taken, making it possible to detect HIP 57269 clearly with a maximum likelihood (ML) of 268.7. The source has a count rate of 0.75±0.08 cts/sec. The count rate range for single or unresolved TWA members is 0.11 cts/s to 0.66 cts/s (Stelzer & Neuhäuser, 2000). The triple HIP 57269 appears to be the X-ray brightest TWA member (candidate), not surprising, because it is an unresolved multiple in the RASS, it has a relatively close distance, it shows activity (as a flare star), and it has one of the earliest spectral types in TWA. A high level of X-ray activity is a strong youth signature.

The PSPC provides some spectral information, allowing us to calculate hardness ratios:

$$HR1 = \frac{cr_{H1} + cr_{H2} - cr_S}{cr_{H1} + cr_{H2} + cr_S} \tag{4.5}$$

$$HR2 = \frac{cr_{H2} - cr_{H1}}{cr_{H1} + cr_{H2}} \tag{4.6}$$

where $cr_S, cr_{H1}, cr_{H2}$ denote the count rates in the three ROSAT-PSPC energy bands soft (0.1 - 0.4 keV), hard 1 (0.4 - 0.9 keV) and hard 2 (0.9 - 2.1 keV) respectively. See Tab. 4.6 for the ROSAT data. These hardness ratios for HIP 57269 are typical for TWA (HR1: -0.31 to 0.58 and HR2: -0.29 to 0.53, Stelzer & Neuhäuser, 2000).

The RASS observations of field rs932622 do not show flare activity for HIP 57269 because of the short exposure time. Follow-up XMM spectroscopy and variability monitoring as well as high angular resolution X-ray imaging by Chandra would be interesting.

**Table 4.6:** X-ray data of the FSs located in the sky region of TWA.

| name | RASS cts/s | ML | HR1 | HR2 |
|------|------|-----|------|------|
| RASS-fields rs932622, rs932233 and rs932425 | | | | |
| HIP 57269 | 0.75±0.08 | 268.7 | -0.27±0.10 | 0.04±0.18 |
| HIP 56244 | 0.79±0.06 | 600.0 | -0.35±0.07 | 0.27±0.27 |
| GJ 3780 | 0.15±0.02 | 71.6 | -0.28±0.16 | 0.05±0.27 |

### 4.3.5 Near-infrared imaging of HIP 57269

We imaged HIP 57269 in the near infra red H-band with the Son of Isaac (SofI[†] ) at the 3.5 m New Technology Telescope (NTT) of the European Southern Observatory (ESO) at

---

[†] see www.ls.eso.org/lasilla/Telescopes/NEWNTT/

La Silla, Chile, on 2001 Dec 8 from 08:38 h to 08:58 h UT with 500 times 1.2 s integrations. The SofI detector is an Hawaii HgCdTe 1024×1024 array with 18.5 μm pixel size. We used the small SofI field with its best pixel scale for better angular resolution and determined the pixel scale by comparing the separations between several stars on other images taken in the same night with 2MASS images of the same fields to be 0.150±0.002″ per pixel. Darks, flats, and standards were observed in the same nights with the same set up and data reduction was done with *eclipse*[†] version 3.8, a C-based software library. While *eclipse* is made for VLT data reduction, like e.g. the Infrared Imaging And Array Camera (ISAAC), and not guaranteed to work for SofI data, it does work for SofI imaging data reduction (dark, flat, shift+add); after all, SofI is the Son of Isaac. See Fig. 4.19 for the final coadded image of HIP 57269 and its surroundings. The FWHM in the final image is 0.9″.

The bright object 8.5″ SE of HIP 57269 AB is the known wide companion HIP 57269 C. We label the additional companion candidates cc 1 to cc 4 (cc for companion candidate) considering only of those candidates within (the somewhat arbitrary) 1,000 AU, i.e. 16.6″. The faint HST standard stars S361-D and S754-C (Persson et al., 1998) were used to obtain the H-band magnitudes of HIP 57269 AB and C as well as its companion candidates, see Tab. 4.7. Whether the companion candidates are truly bound companions to HIP 57269 can be decided on the bases of spectroscopy and/or proper motion follow up observations. 2MASS data of this field are not yet available.

**Table 4.7:** HIP 57269 and companion candidates

| Name | Separation [arcsec] | | | H | Spec |
|---|---|---|---|---|---|
| | $\Delta\alpha$ | $\Delta\delta$ | | [mag] | type |
| HIP 57269 A | primary | | | 7.1[⋆] | K1/2V |
| HIP 57269 C | 5.11 | -6.74 | SE | 9.6 | K4-6 |
| HIP 57269/cc 1 | 7.18 | 12.48 | NE | 10.7 | K5-7 |
| HIP 57269/cc 2 | -0.43 | 6.74 | NW | 12.8 | G-M |
| HIP 57269/cc 3 | -10.22 | -4.65 | NW | 15.3 | mid-K |
| HIP 57269/cc 4 | 10.15 | -8.68 | SE | 15.2 | ? |

⋆: Combined H-band magnitude of A & B

### 4.3.6 Spectroscopic follow up of companion candidates

To verify or reject the companion candidates as real companions or unrelated background objects, we have taken follow up spectra, both in the optical and in the infrared (for cc 1 through cc 3).

Optical spectra have been obtained with DFOSC at the 1.54 m Danish telescope located at ESO La Silla on 2002 January 24th for both HIP 57269 C and HIP 57269/cc 1 to determine their spectral type and to check for lithium absorption, a youth indicator, which should be present, if the objects were real companions, i.e. as young as the primary.

Figure 4.20 shows part of the spectrum taken with DFOSC and the same setup as for HIP 57269 A of the companion at the separation of 8.46″. In the spectrum, lithium and calcium are again clearly seen. With a lithium equivalent width of 0.18±0.20 Å at a spectral type of K5V quite similar to the component A. We have also taken an optical spectrum with DFOSC of cc 1 (see Fig. 4.20). The spectrum reveals that the object is a star with spectral

---

[†] see www.eso.org/projects/aot/eclipse/
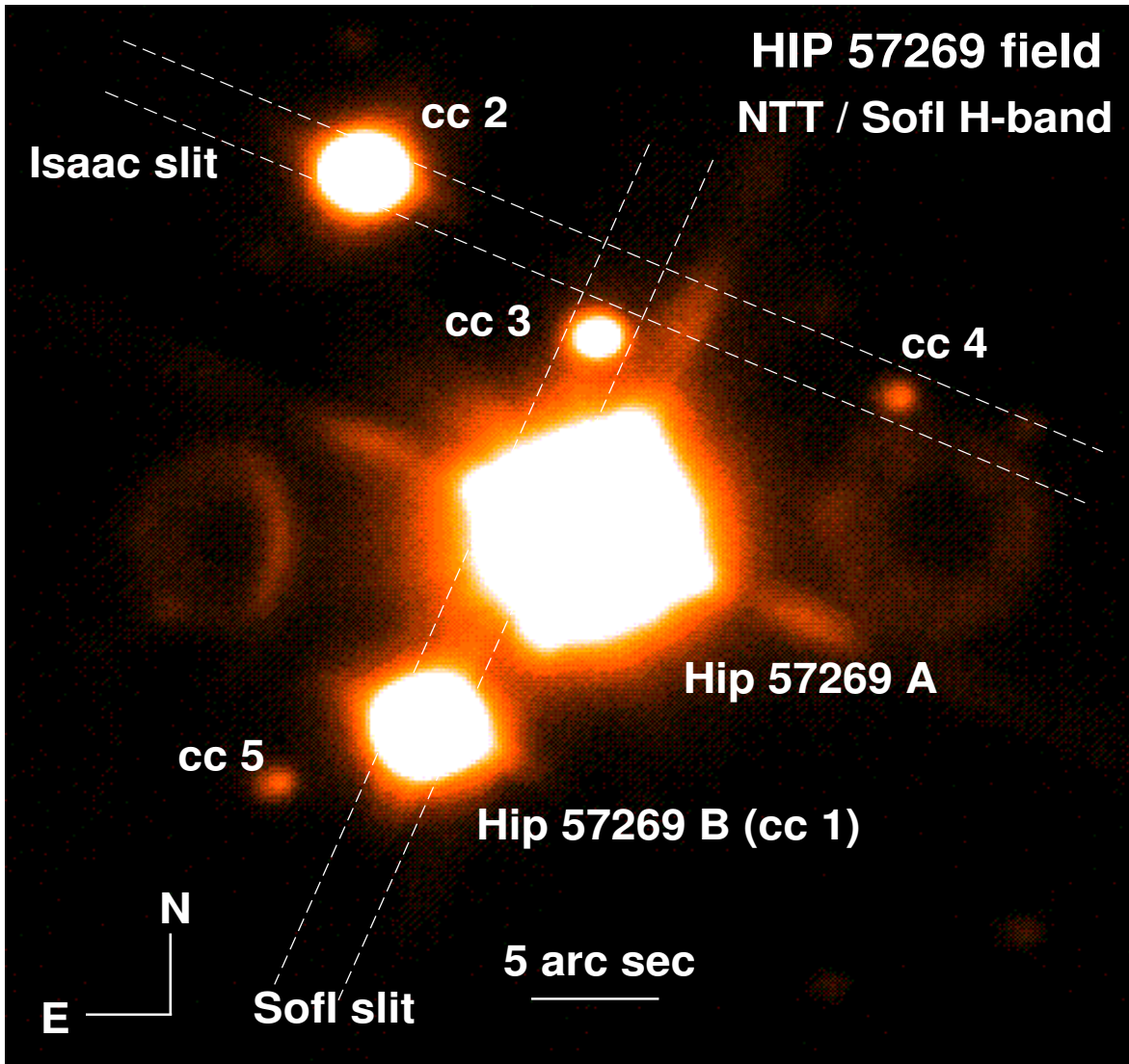
**Figure 4.19:** HIP 57269 A with companion C and a few more companion candidates labeled cc 1 to cc 4 detected in our SofI H-band image; superimposed are the slit orientations for follow up spectroscopy with the two instruments SofI and ISAAC. Slit widths are not to scale.

type K5-K7 not showing lithium at all. This leads to the conclusion, that it is not a member of the HIP 57269 system and also not of TWA.

Infrared spectra for HIP 57269 C and cc 2 on the slit (together with HIP 57269 A itself off the slit) have been obtained with SofI in the night 9 Dec 2001 between 08:35 h and 08:56 h UT. We took 40 spectra with 30 s exposure each through a $1''$ slit with a red grism including both the H- and K-band (1.53 to 2.52 $\mu$m) with a resolving power of $R \simeq 1,000$. Data reduction was done in the usual way using IRAF: Dark subtraction, normalization, flat fielding, sky subtraction, wavelength calibration, and co adding the spectra. The spectra were not flux calibrated. The final K-band spectra of HIP 57269 A, C, and cc 2 are shown in Fig. 4.21: HIP 57269 A is known to be a K1/K2-type dwarf star (see Fig. 4.20), and the spectral type of HIP 57269 C was just determined to be K5±1 by us (Fig. 4.20).

Our IR-spectra are consistent with those spectral types, we can see the typical Na, Mg, and Ca lines as well as weak CO-molecular bands, but no Br $\gamma$ lines which would be typical for earlier types. Unfortunately, the spectrum of cc 2 is very noisy, so that it is hard to determine
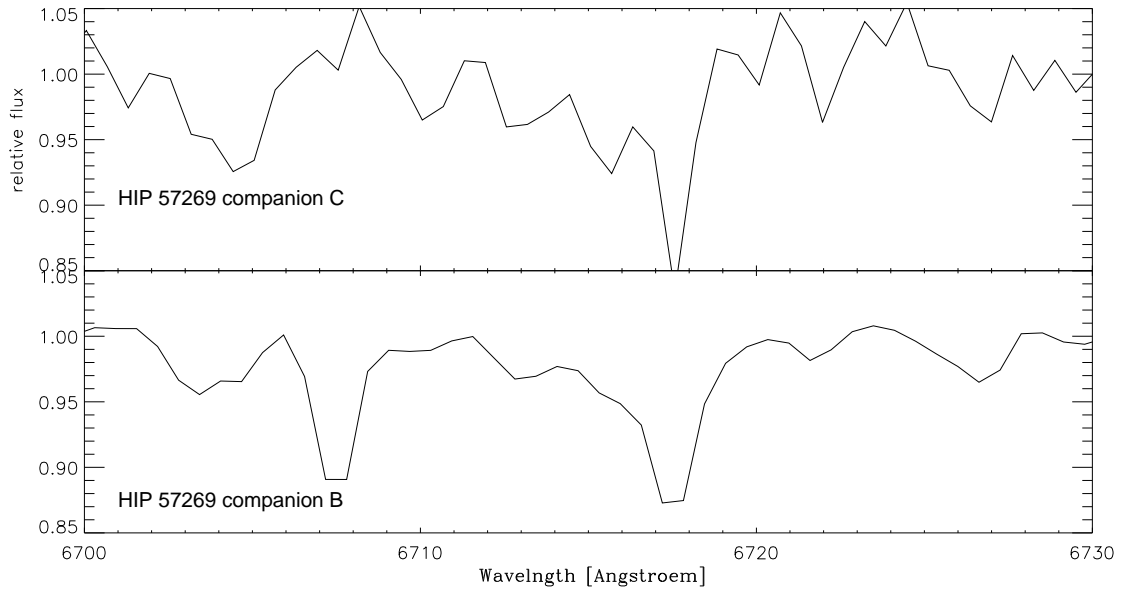
**Figure 4.20:** A section of the optical spectrum taken with DFOSC at La Silla of HIP 57269 C and cc 1. Lithium is detected in the HIP 57269 C.

the spectral type. Na and Br $\gamma$ are very weak or not present at all, CO-molecular bands are also weak, so that it is a dwarf star between early G and late M. It is definitely not an L- or T-type object. If cc 2 were a real companion, then given the difference in magnitude between primary and cc 2, the object should be below the substellar limit with an early L spectral type (at the same age and distance as the primary), which we can exclude from our spectrum. Hence, cc 2 is a background object.

Then, we took H-band spectra of cc 1 and 3 with the Infrared Spectrograph and Array Camera (ISAAC, 1024 by 1024 ESO-Hawaii chip) at the ESO 8.2 m telescope Antu, Unit Telescope No. 1 (UT1) of the Very Large Telescope (VLT) on Cerro Paranal on 19 March 2001 between 07:20 h and 08:16 h UT in service mode, 28 spectra with 60 s each through a 1″ slit. The slit was aligned such that both cc 1 and cc 3 were on the slit, but so that the bright primary HIP 57269 A was outside the slit. In the acquisition image and during the spectroscopy, the seeing was around 0.4″ to 0.5″. Darks, flats, arcs, and spectrophotometric standards were taken in the same night. Data reduction was done in the standard way: dark subtraction, normalization, flat fielding, sky subtraction, wavelength calibration, and coadding the spectra. Both objects are clearly detected in the final coadded spectrum, see Fig. 4.22.

Using the optical DFOSC spectrum, we showed the companion candidate HIP 57269/cc 1 to be K5-7 in Fig. 4.20 above. This is consistent with the infrared spectrum, where we can see the typical magnesium and silicium lines and the CO bands; and the peak emission is more in the blue than in, e.g., the young M1 dwarf TWA-5 A shown for comparison (taken from Neuhäuser et al., 2000), so that HIP 57269/cc 1 is a bit hotter than TWA-5 A. Because HIP 57269/cc 1 does not show lithium absorption (in its optical spectrum, Fig. 4.20), it is not a companion. HIP 57269/cc 3 is very similar to HIP 57269/cc 1, with the magnesium and silicium being slightly weaker, i.e. of spectral type mid-K. Since the spectral type (mid-K)
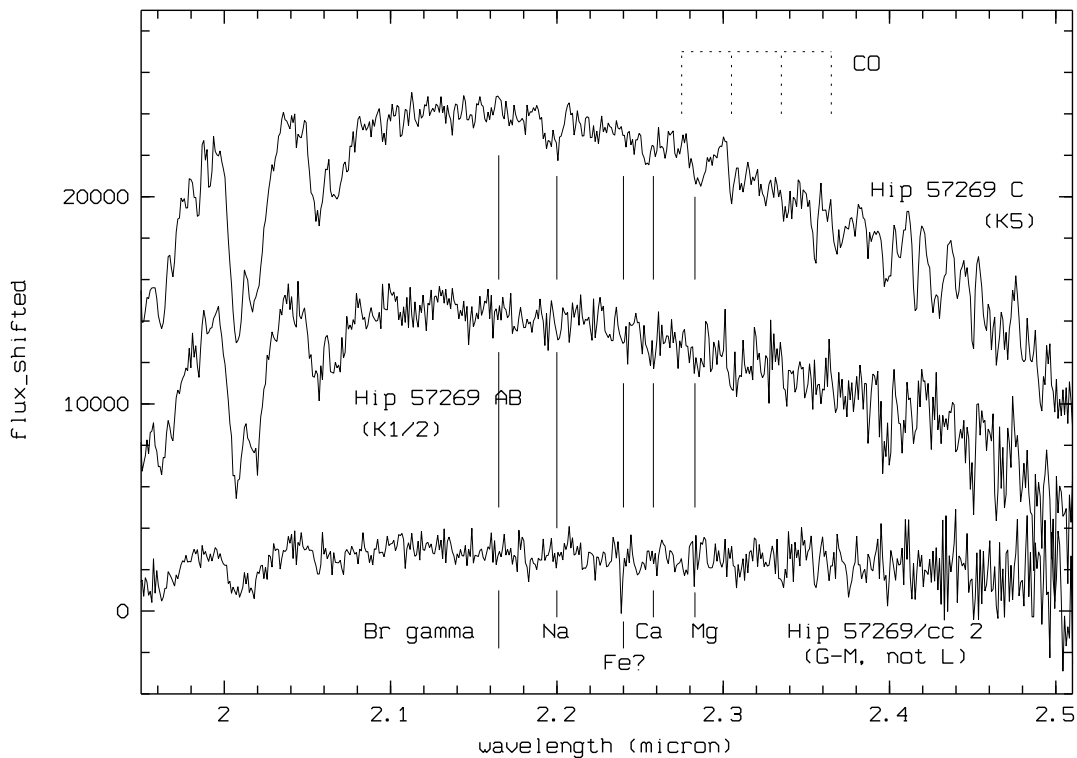
**Figure 4.21:** Infrared spectra taken with SofI. For alignment of the slit, see Fig. 4.19. We determine the spectral type of component C to K5±1, and of cc 2 to G-M, not L as the H-band magnitude suggests, if cc 2 would be a true companion.

and its faintness are in the infrared, HIP 57269/cc 3 cannot be a companion to HIP 57269 A; as a true companion, it would be a low mass brown dwarf with spectral type L (similar for cc 4, for which we have not yet obtained spectra). Hence, HIP 57269/cc 3 is an unrelated background K star. HIP 57269 is a hierarchical triple with a close pair A & B and a wide companion C.

### 4.3.7 Summary and Discussion

Is HIP 57269 a member of TWA? The distance (48.49±6.54 pc), the location in the sky and the spectral type, the position in the Hertzsprung-Russell diagram, the $v \sin i$ and X-ray emission are very similar to the other confirmed TWA-members. It is a visual binary with a known radial-velocity companion, in total a triple system, which is typical for young stars. But the space motion, as well as the lithium absorption suggest that it is more likely a young star belonging to the Pleiades Super cluster. It is clearly a pre-main sequence star. The other companion candidates cc 1 - cc 4 are likely not members of the HIP 57269 group nor of TWA.

In Fig. 4.17 we have plotted the proper motion of the members and member candidates of TWA. The stars GSC 07204-00998 N&S, CD-34 7390 N and HD 98764 show proper motions which are not in common with the other TW Hya member stars. Also for the stars GSC 07204-00998 N&S (0.05 Å and 0.055 Å) HD 98764 (0.120 Å) the lithium equivalent width is lower than that for the confirmed members of TWA. While the lithium equivalent width of CD-34 7390 N&S (0.650 Å and 0.590 Å) have more in common with the other TWA members, and also the proper motion.

The star PPM 28568 was observed in the sample of Sterzik et al. (1999). They conclude
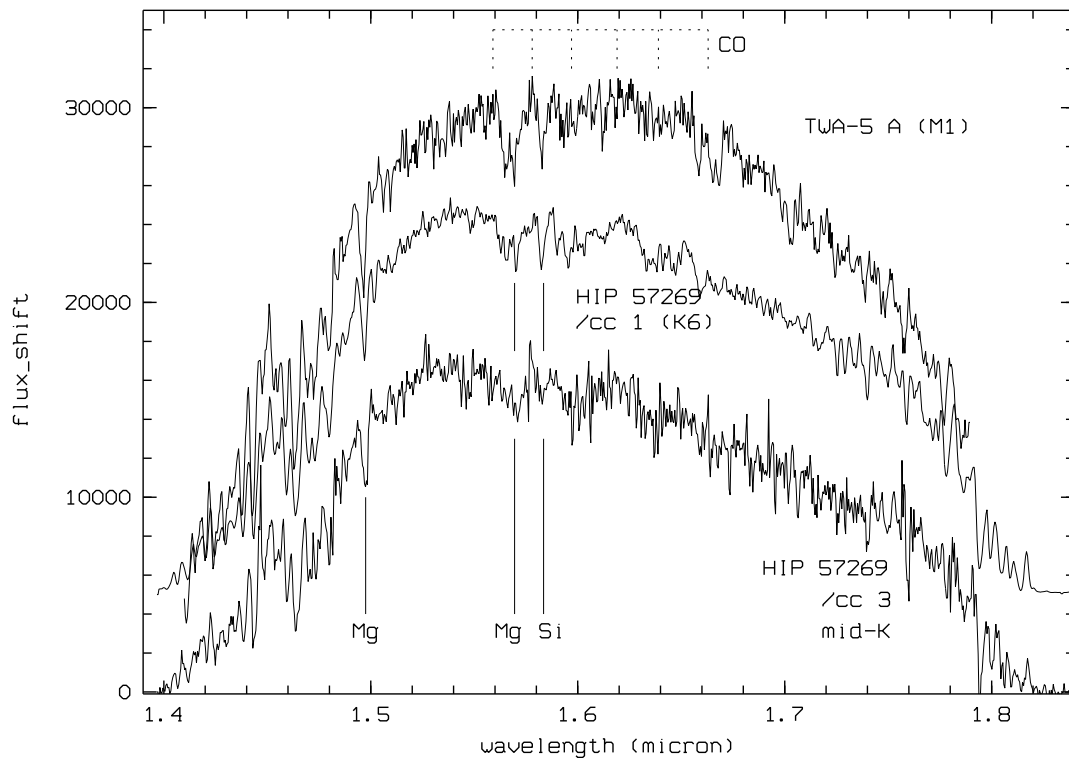
**Figure 4.22:** Spectra taken with ISAAC at the VLT in March 19th 2001. For the alignment of the slit see Fig. 4.19. We show a spectrum of TWA-5 A (M1) for comparison and we determine the spectral type of cc 1 to K6 and of cc 3 to mid-K.

PPM 28568 is a background star; however, its proper motion is consistent with the other members, but its lithium abundance (0.19 Å) is at the lower level. In the Hertzsprung-Russell diagram it appears below the main sequence.

Is HIP 57269 a member of TWA? The answer is no, but the stellar system is still pre-main sequence and it belongs to the Pleiades supercluster.

## 4.4    The flare stars in the region of Tuc and HorA

In the region of the Tucana and the Horologium associations, two very nearby ($\sim$45 pc) associations, a total of five flare stars are located. All of them, except one, seem to be foreground objects according to their spectrum (lithium absorption is not present), their proper motion, as well as their parallax ($<$40 pc).

We will consider the space region of Tucana (Ra: 19 h to 00 h 30 m, Dec: -47° to -70°) and Horologium (Ra: 01 h to 07 h, Dec: -46° to -70°) where young stars at about 45 pc were recently discovered.

## 4.5    The Tucana Association

The Tucana Association was discovered by Zuckerman et al. (2001b). Contrary to the tradition of correlating X-ray emission and space motion to preselected candidates for young associations, the Tucana Association was discovered by correlating IRAS 60 $\mu$m sources and space motion. Later detailed X-ray studies based on the ROSAT All Sky Survey (RASS)
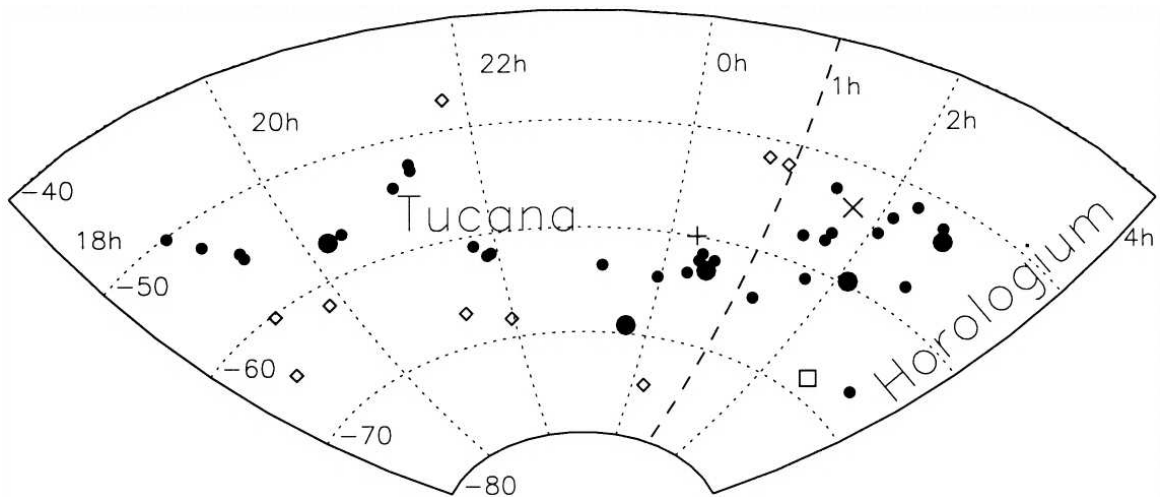
**Figure 4.23:** Space distribution of the member stars in the Tucana - Horologium Association. Small circles to the left of 1h R.A. are from Zuckerman et al. (2001b). Small circles to the right of 1h R.A. are members of Horologium but are modified as described above from the initial set of stars proposed by Torres et al. (2000). Diamonds are several stars from Zuckerman et al. (2001b) that we regard as likely members of the Tucana stream. The plus sign is HIP 1399, the cross is HD 10647, and the square is HIP 12394 (= HD 16978). Large circles indicate binaries or triples. The figure was taken from Zuckerman et al. (2001b).
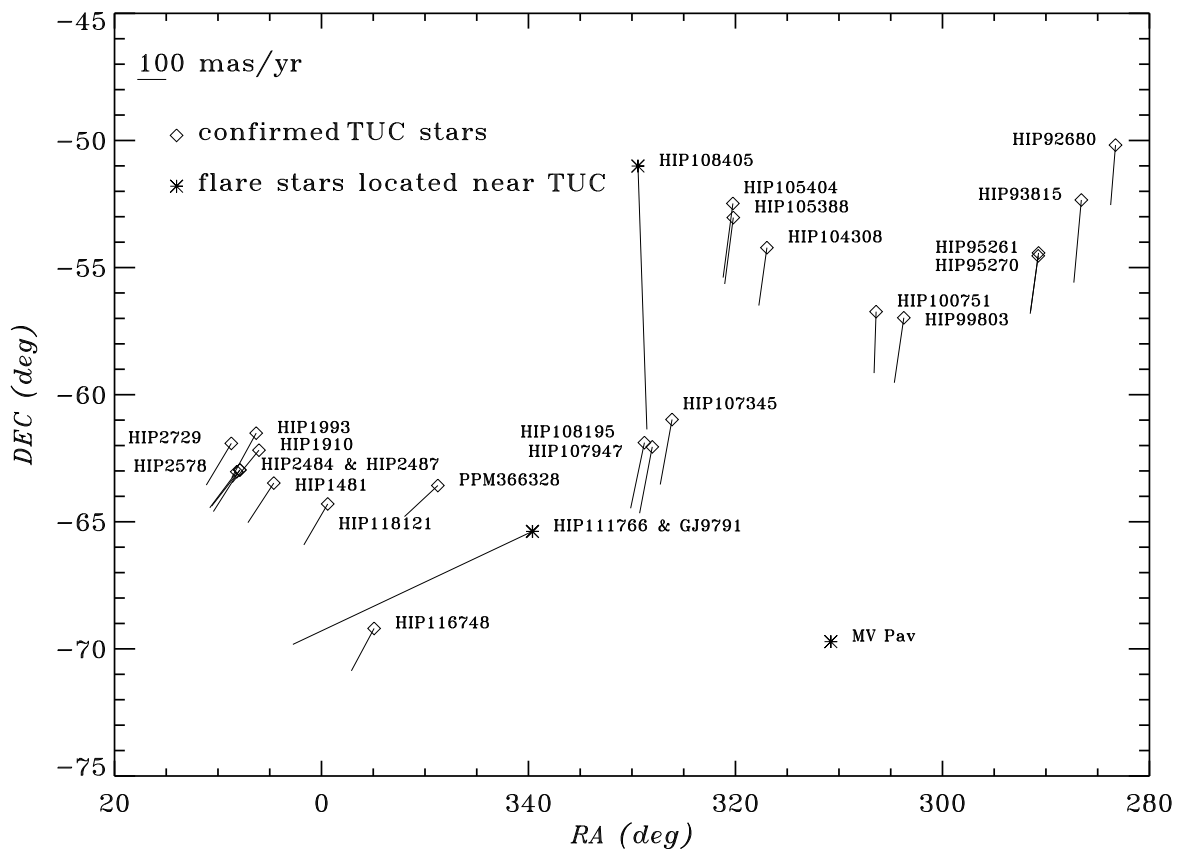


**Figure 4.24:** Proper motion of the known confirmed Tuc members and the flare stars discussed in this work: MV Pav, HIP 108405, HIP 111766 A & C, and GJ 9791

were carried out (Stelzer & Neuhäuser, 2000) for the known member stars. All of these stars show X-ray emission and X-ray variability as it is typical for young stars. And the emission is comparable to TWA members.

Spectroscopy of all the member "candidates" was performed (Zuckerman et al., 2001b; Zuckerman & Webb, 2000; Torres et al., 2000) and all these stars show signatures of youth, such as lithium absorption, H$\alpha$-core filling in or emission, and rapid rotation. Based on these criteria Zuckerman et al. (2001b) have derived an age range of 20 to 40 Myr, were they suggest 40 Myr as the most likely age. Stelzer & Neuhäuser (2000) have estimated an age of 30 Myr based on the X-ray emission.

The space motion of the Tuc ($U = -10.5 \pm 2.3$ km/s, $V = -20.8 \pm 2.4$ km/s, $W = +0.3 \pm 3.0$ km/s, Zuckerman et al., 2001b) is very similar to the space motion of the Local Association ($U = -11$ km/s, $V = -21$ km/s, $W = -11$ km/s, Eggen, 1998). The spectroscopic and color criteria for the membership must therefore be inspected with great care. In a manner similar to the Ursa Major Association, the Tucana stars were divided into the Tucana stream and nucleus.

## 4.6   The Horologium Association
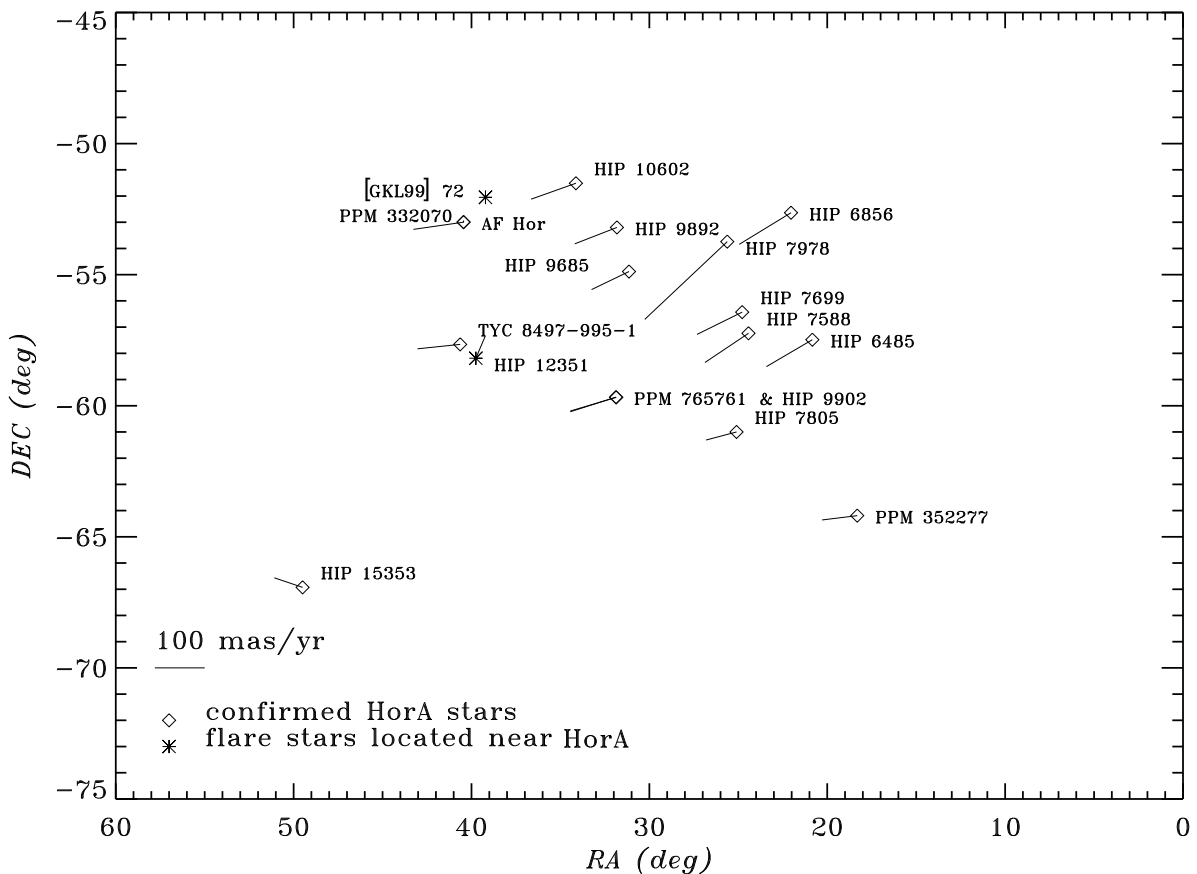


**Figure 4.25:** Proper motion of the known confirmed HorA members (diamonds) and the flare stars discussed in the section HIP 12351, and [GLK 99] 72 in this work (stars).

Shortly after the discovery of the Tucana Association, the Horologium Association was discovered by Torres et al. (2000) in the traditional way of correlating X-ray emitting stars with Hipparcos space motions and selecting candidates. They announced the association with

its center at about 60 pc. Zuckerman & Webb (2000) noted that the Horologium Association has similar space motion as the Tucana Association. For better consistency they revised the member list given by Torres et al. (2000) and removed distant member candidates where the membership is somewhat dubious. Instead they added new members which are closer to the sun but which showed common space motion and signatures of youth. By these changes the center of the Horologium Association was moved to ∼45 pc.

### 4.6.1 The Tucana - Horologium association

Based on these suggestions the Tucana and the Horologium Association could well be one wide spread association at a distance of ∼45 pc and with common membership criteria. In the sequel we will think of it as one single association.

In the Tuc association four flare stars are located: MV Pav, HIP 108405, HIP 111766 A & C, and GJ 9791. The two stars with Hipparcos measurements are at about 20 pc in front of the association with proper motions not consistent with the association. For the other two stars neither parallax nor proper motion measurements are available. The spectra of MV Pav taken the 4th of June 2001 is too noisy even after coadding two one hour exposures.

In the region of HorA two stars are located: HIP 12351, and [GLK 99] 72. The star [GLK 99] 72 was not observed in our survey because it was too faint to be observed with the available equipment.

### 4.6.2 [GKL 99] 428, HIP 111766
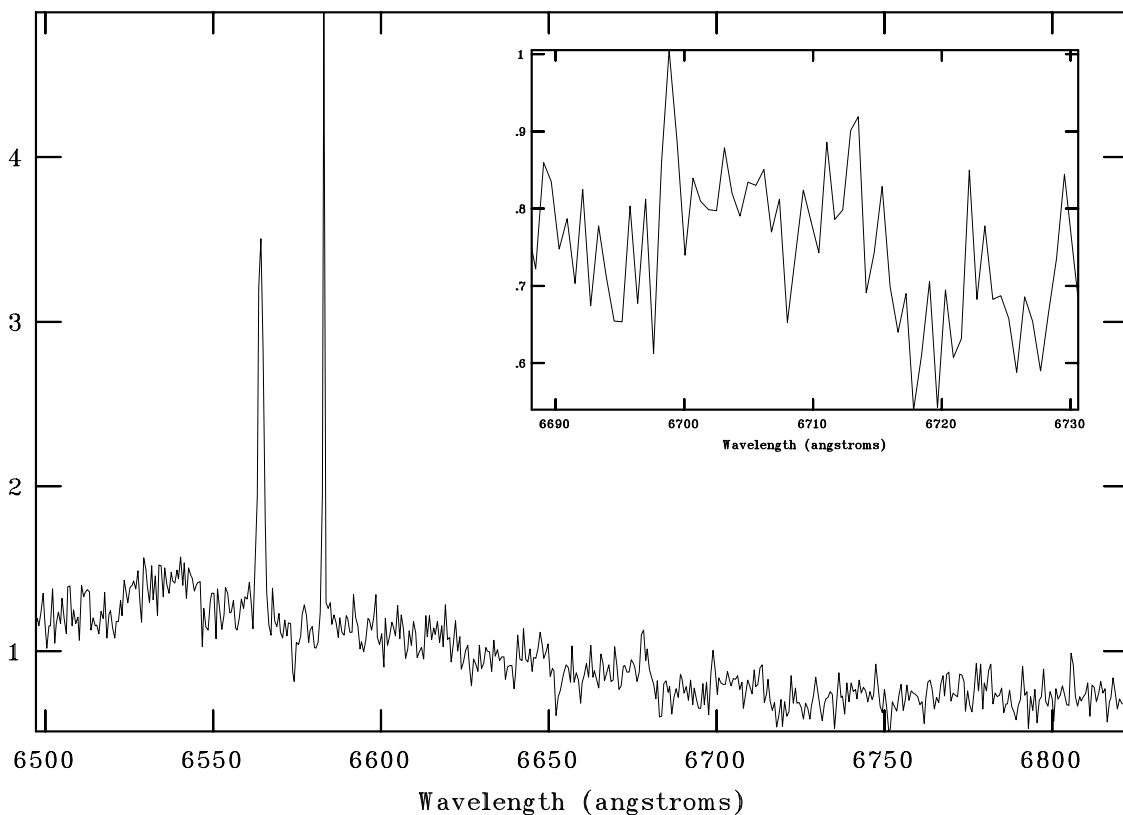


**Figure 4.26:** A section of the DFOSC spectrum taken during the night of 05. Oct. 2001 of HIP 111766. Hα can be seen in emission. In the small inserted spectrum the section of lithium and calcium is enlarged. The star shows a little lithium absorption.

In the SIMBAD data base the star is listed as a triple system. The resolution of the DFOSC spectrum does not allow us to see the binarity in the spectrum but the Hipparcos data suggests that the star is at a triple with the optical components A & C and the close companion C. The stellar spectrum reveals a star with spectral type late K to early M. Montes et al. (2001) list the star as single and a member candidate of the Hyades supercluster. Its space motion ($U = -55.4 \pm 10.8\,\mathrm{km/s}$, $V = -19.9 \pm 7.9\,\mathrm{km/s}$, $V = -14.5 \pm 13.3\,\mathrm{km/s}$) is consistent with the Hyades cluster and excludes it as a member of the Horologium-Tucana association. The X-ray emission in the RASS shows a count rate of $0.42\pm0.03\,\mathrm{cts/s}$ with a hardness ratio of $HR1 = -0.28\pm0.06$ and $HR2 = -0.20\pm0.12$. This hardness ratio is typical for stars of the Hyades cluster (Stelzer & Neuhäuser, 2001) and the spectral type of K0V to M0V. The source is extended by $23''$.

### 4.6.3   [GKL 99] 414, HIP 108405
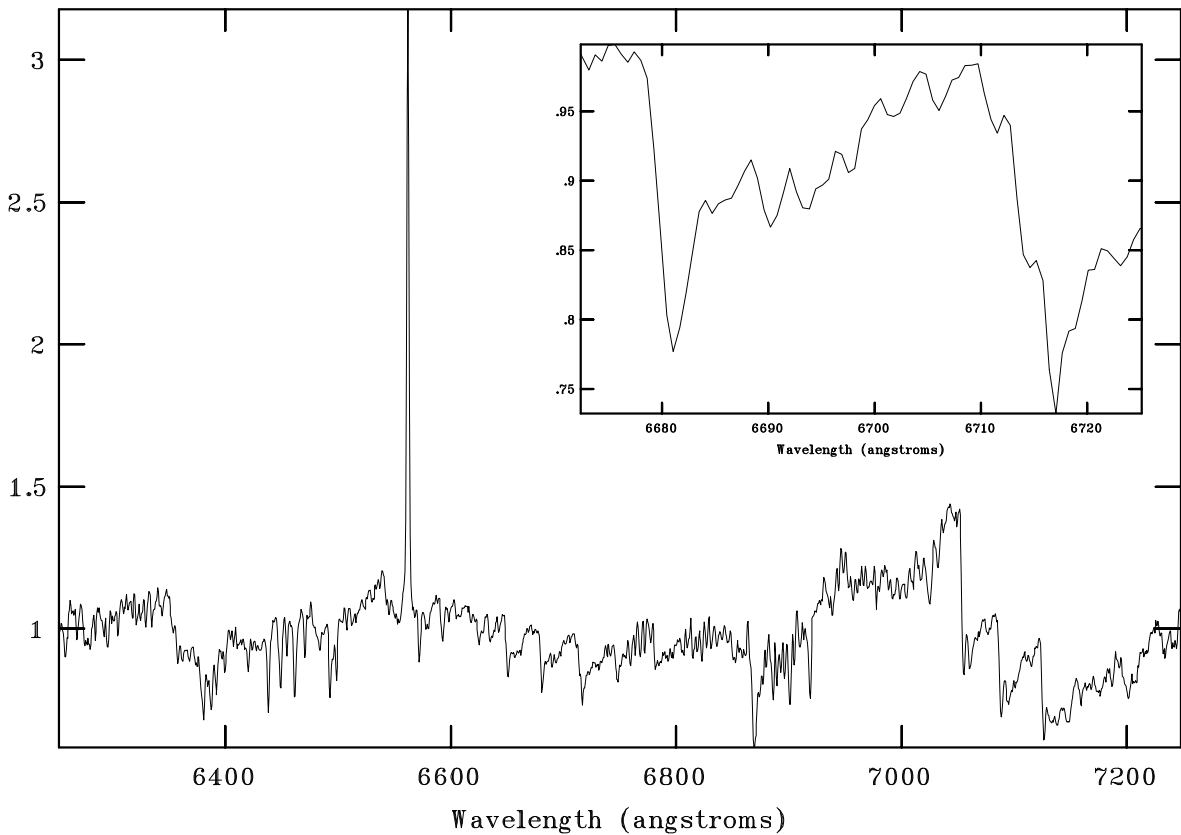


**Figure 4.27:** A section of the DFOSC spectrum of HIP 108405 observed in the night of 04. June 01 of HIP 108405. Hα can be seen in emission. In the small inserted spectrum the section of lithium and calcium is enlarged. The star shows only a weak not significant lithium absorption line.

From the literature not a lot is known about this star. It was detected in the RASS with a count rate of $1.08\pm0.8\,\mathrm{cts/s}$. Its two band hardness ratio HR1 = -0.18±0.07 and HR2 = -0.20±0.11. The star shows Hα in emission with a full width half maximum of 2.11 Å. The not very prominent lithium absorption line has an equivalent width of 0.04 Å which at a spectral type M2.5V is very small for a young star. Its space motion ($U/V/W$) = ($-2.3 \pm 4.6/ -26.5 \pm 1.7/13.0 \pm 5.7$) km/s is more consistent with the AnA but not totally.

The star seems to be young but not a member of Tuc or HorA. The star is located above the main sequence on the 10±10 Myr isochrone in the Baraffe et al. (1998) models. In the literature no measurement could be found which would prove that the star is a close unresolved binary. At a distance of 16.1 pc it is a close pre-main sequence star, closer to the sun than GJ 182.

### 4.6.4 [GKL 99] 72

In the publication of the discovery of the Horologium association, Torres et al. (2000) list the Gershberg flare star [GKL 99] 72 as a member candidate for the Horologium association. They have performed high resolution spectroscopy using the FEROS échelle spectrograph at the ESO 1.52 m telescope in La Silla. The instrument is quite similar to the échelle spectrograph FOCES we have used at Calar Alto, Spain.

They decided to observe the star because of the X-ray emission. Indeed the star shows signatures of youth: H$\alpha$ in emission with an full width half maximum of 5 Å and lithium absorption with an equivalent width of 0.400 mÅ. This converts to a lithium abundance of $N(\text{Li}) = 1.3$. At a spectral type of M3Ve which converts to a temperature of 3500±200 K, this is fairly high. We note here that the star rotates rapidly (37 km/s) and is known to exhibit flares. Lithium could also be produced in flares.

The star does not have proper motion measurements and parallax measurements so that the kinematics are unknown as yet.

## 4.7 Stars with space motion consistent with AnA

The AnA was recently discovered by Torres et al. (2003) by combining RASS sources with optical spectroscopy. All stars of the AnA show signatures of youth in their spectrum. The core of the association is located at a parallax of $\pi = 19.0$ mas.

### 4.7.1 [GKL 99] 423, HIP 110526

The star is a visual binary ($(U/V/W) = (-6.62\pm1.66/-30.94\pm/-13.86\pm4.05)$ km/s Montes et al., 2001) with consistent space motion of the AnA. Having a parallax of $\pi =$62.18±10.01 mas the star is located at a distance of 16.08±3.09 pc and in the northern hemisphere. We conclude that it is not a member of the AnA and it is also clearly not a member of the Local Association.

## 4.8 Stars in the Pleiades

The Pleiades are a young cluster which contains hundredth of stars distributed over a huge fraction of the sky. Its mean cluster parallax measured by the Hipparcos mission lies at 8.60±0.24 mas (Mermilliod et al., 1997), or 8.45±0.25 mas (van Leeuwen, 1999). This converts to a distance of $d = 116\pm3$ pc, or $d = 118\pm4$ pc, respectively. The mean distance of the cluster center depends strongly on which stars are assumed to be bona fide members. We also have to keep in mind that at a distance of ∼100 pc the Hipparcos mission began to reach its limits in precession and in crowded fields such as the Pleiades, problems with the measurements of the parallaxes occurred. We will use 120 pc as an estimate and if necessary the individual parallaxes of the stars.

The cluster depth was estimated to be 23 pc (Rosvick et al., 1992). Adams et al. (2001) have estimated the total cluster mass using a selection criterion for cluster members based on consistent proper motion. The total mass is measured using near infrared photometry and

they estimate the mass to be $M \sim 800 \, \mathrm{M_\odot}$. Brown dwarfs are abundant in the Pleiades but they are not numerous enough to contribute significantly to the cluster mass.

The age of the Pleiades supercluster was estimated to be $2 \cdot 10^6 - 5 \cdot 10^7$ yr (Eggen, 1995). He also claims that the Pleiades supercluster contains the $\alpha$ Persei cluster and the eponymus cluster. Maybe IC 2602 and NGC 2516 are also part of the Pleiades supercluster. Other authors do not share this opinion. Already Herbig (1962) noted that at an age of $7.5 \cdot 10^7$ yr the Pleiades cluster must still contain low mass stars which are contracting to the main sequence. Haro & Chavira (1973) have performed a search for flare stars in this region and have found about 100 flare stars. The ones with consistent proper motion were regarded as members. The typical relaxation time of open cluster is $10^8$ yr or less. This time is comparable with the typical crossing time for the cluster. Because of the age of this cluster we must be able to observe evolution effects such as mass segregation, the development of a halo, and tidal forces which cause the dispersal of escaping stars. All this can be observed in the Pleiades supercluster.

The metallicity of Pleiades stars was determined to be [Fe/H] = 0.0 by Boesgaard & Friel (1990) using high resolution spectra. Other estimates using Geneva photometry get values of -0.11 which is not confirmed by the photometry performed by Stello & Nissen (2001). Photometric distance estimates compared to the Hipparcos distance to the cluster center lead to the socalled Pleiades distance problem. This is thought to be solved by assuming an iron underabundance but even the measured underabundance by the Geneva photometry is not enough to explain this discrepancy. Another explanation for the distance problem could be that the Pleiades have remaining gas and dust which cause variable extinction throughout the cluster and which was not accounted for in the photometric measurements.

### 4.8.1 [GKL 99] 74, HIP 12351
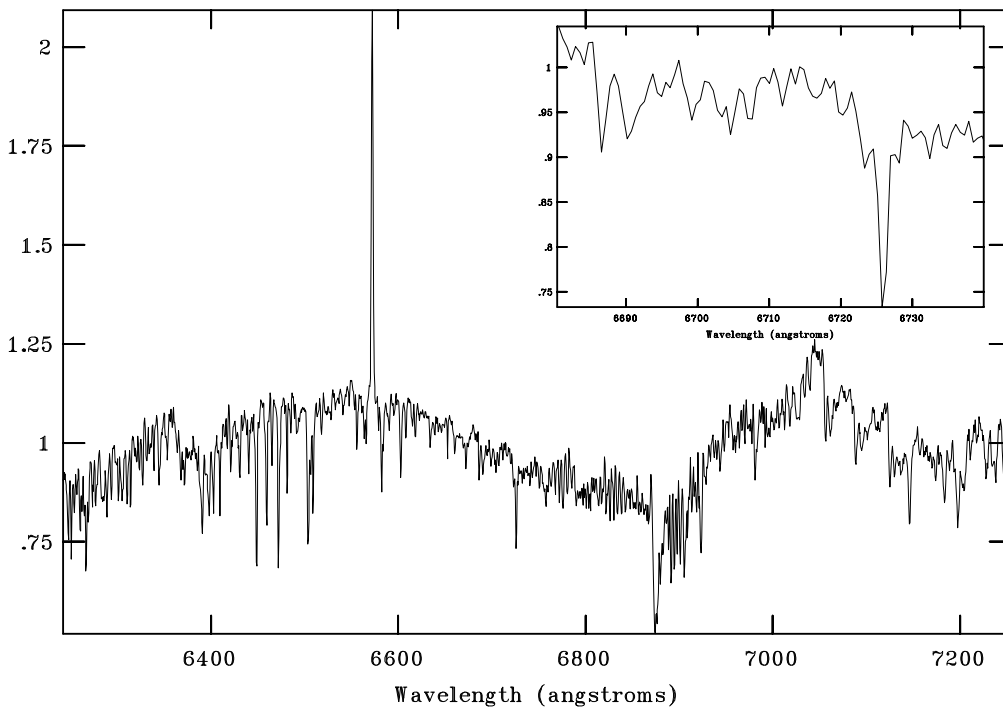


**Figure 4.28:** A section of the DFOSC spectrum of HIP 12351 taken in the night of 04. June 2001 of HIP 12351. H$\alpha$ is filled in. In the small inserted spectrum the section of lithium and calcium is enlarged. The star shows little lithium absorption.

The star HIP 12351 shows weak lithium absorption with an equivalent width of $W(\text{Li}) = 0.08\,\text{Å}$ which transforms into a lithium abundance of $N(\text{Li}) = 0.09$ at a spectral type of M0Ve/K7V. This is less lithium content than in confirmed Pleiades stars with the same spectral type. The spectrum shows filled in H$\alpha$. The space motion is consistent with the Pleiades supercluster. The star was also a candidate for the Horologium Association from Torres et al. (2000) which they rejected.

### 4.8.2 [GKL 99] 312, HIP 73555

Recent classification in the SIMBAD database list it as G8IIIa which would mean that it is a post-main sequence subgiant. Since the star was listed in the catalog, it was observed with high resolution spectroscopy using the FOCES instrument at Calar Alto in Feb. 13th 2001.
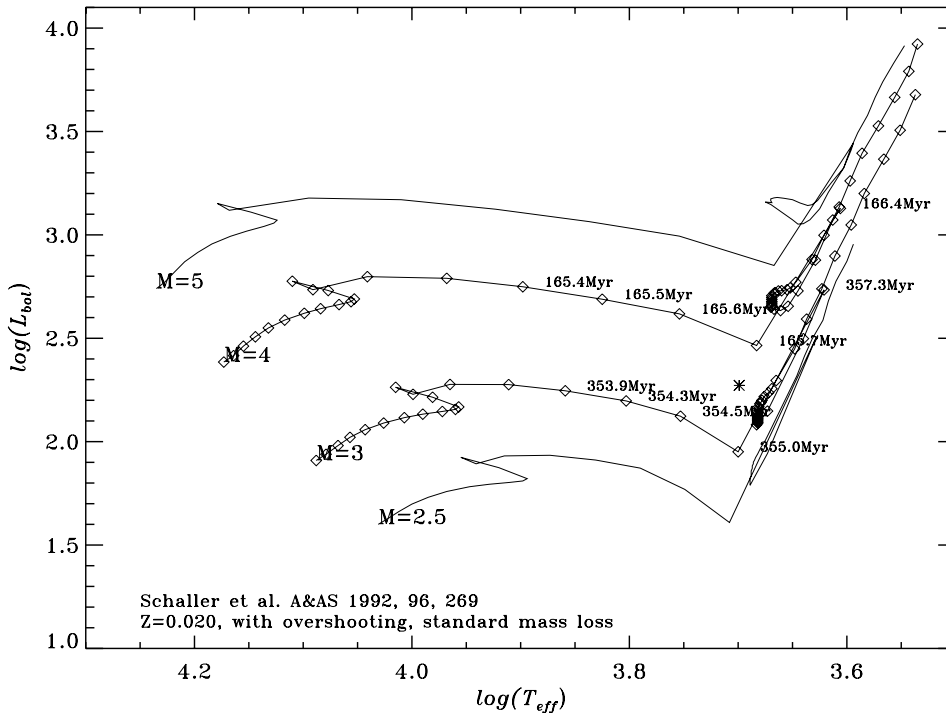


**Figure 4.29:** Schaller et al. (1992) post-main sequence tracks and age marks. The position of the star HIP 73555 is marked with an asterix.

The spectral synthesis analysis very soon reveal the nature of the star to be a subgiant or a giant given the estimated surface gravity ($\log g = 2.40 \pm 0.10$) using the Fe I/Fe II and Fe/Mg ionisation equilibrium. The projected velocity of rotation $v \sin i$ is $4.1 \pm 1.0\,\text{km/s}$.

Further detailed analysis lead to the following measured parameters:(see Tab: 4.8).

Placing the star into an Hertzsprung-Russell diagram and using post-main sequence tracks of Schaller et al. (1992), we estimate the mass to be $3.4 \pm 0.2\,\text{M}_\odot$ and the age to be 240 Myrs. This would imply that it is still a young star, but because of its high mass, the evolution time scales are smaller and yet it has reached the post-main sequence. Calculating a spectroscopic parallax and comparing it with the Hipparcos parallax, we find the difference to be 3.6%. The kinematics of this star reveal a spatial velocity of $U = 6.6\,\text{km/s}$, $V = -17.1\,\text{km/s}$, $W = -1.2\,\text{km/s}$. This is consistent with the Pleiades supercluster. The age estimated from the post-main sequence tracks of Schaller et al. (1992) cannot be confirmed or disproved by this finding.

For the subgiant HIP 73555, a radius measurement is available in Richichi & Percheron (2002) and references therein. The interferometric measurements listed therein obtain a di-

| $T_{\rm eff}$ [K] | log g | [Fe/H] [dex] | $M_V$ [mag] | $M_{\rm bol}$ [mag] | $d_{\rm HIP}$ [pc] | $d_{\rm spec}$ [pc] | diff. [%] | source |
|---|---|---|---|---|---|---|---|---|
| 4990±70 | 2.40±0.10 | 0.01±0.07 | 3.51 | -0.96 | 67.70 | 69.45 | 3.6 | K |
| 5000 | 2.00 | -0.07 | | -1.04 | | 110.77 | 65.2 | B |
| 5150 | 3.06 | -0.13±0.10 | | 0.47 | | 35.52 | 47.0 | McW |
| 4929 | 2.30 | 0.04 | | -1.24 | | 74.98 | 11.8 | B&G |

K: this work, B: Brown et al. (1989), McW: McWilliam (1990), B&G: Bell & Gustafsson (1989)

**Table 4.8:** Spectral parameters of HIP 73555 derived using the spectral synthesis analysis methods described before (first row of the table). The last three rows summarize the work of the other authors. The spectral parameters were used to calculate the spectroscopic distance and compare to the Hipparcos distance to investigate the accuracy of the analysis.
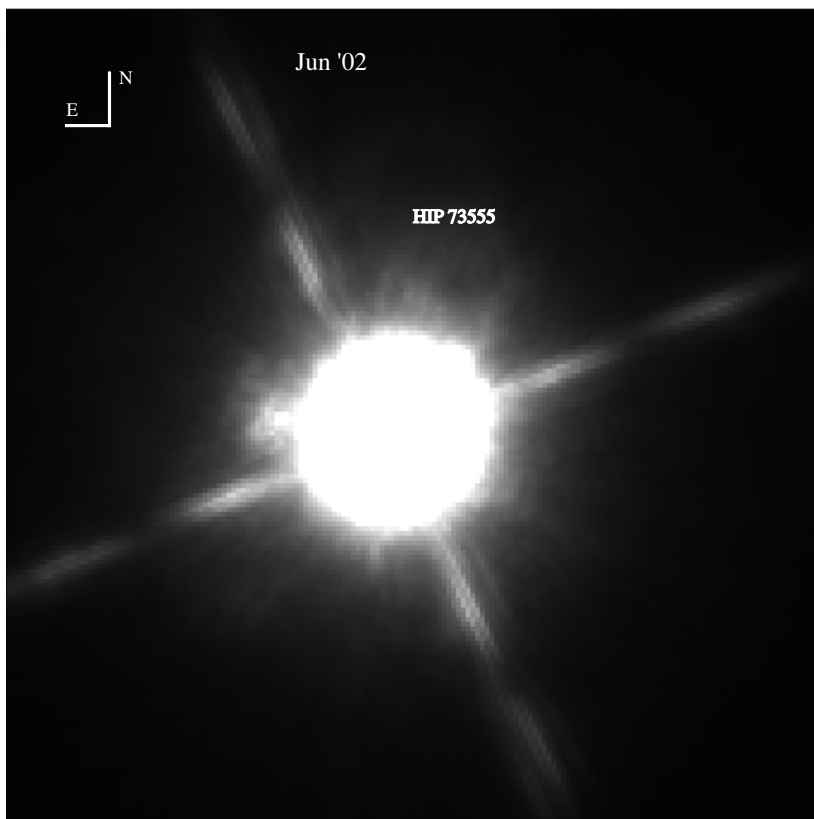


**Figure 4.30:** H-band images of the star HIP 73555 taken with the adaptive optics system ALFA at the 3.5 m telescope in Calar Alto, Spain. There is no evidence for a companion in this image.

ameter of 2.99±0.01 mas and a parallax of $\pi$ =14.91±0.57 mas for this star. This can be transformed into a diameter of $d$ =43.0±2.0 R$_\odot$ or a radius of $R$ =21.5±1.0 R$_\odot$ for the star. Comparing this value to the predicted radius of $R$ =19.0±1.0 R$_\odot$ using the model atmosphere we are confident that our temperature determination techniques is working well also for subgiants.

The stellar parameters for this star derived by Gray et al. (2002) are $T_{\rm eff}$ =5036 ± 16 K, and [Fe/H] = 0.025±0.054. Brown et al. (1989) measured stellar parameters of $T_{\rm eff}$ =5000 K,

$\log g = 2.0$, [Fe/H] = -0.07, and $\log N$(Li) = 1.2. Blackwell & Lynas-Gray (1994) measured a temperature of $T_{\text{eff}} = 5001\,\text{K}$ using the infrared flux method and give a diameter of 2.461 mas. The angular diameter converts to a physical diameter of $35.4\,\text{R}_\odot$ or a radius of $17.7\,\text{R}_\odot$. McWilliam (1990) obtained spectroscopic parameters for the stars: $T_{\text{eff}} = 5150\pm145\,\text{K}$ (4940 K), $\log g = 3.06$, [Fe/H] = -0.13±0.10. Bell & Gustafsson (1989) measured the spectral parameters by spectroscopy and temperature by infrared flux method: $T_{\text{eff}} = 4929\,\text{K}$, $\log g = 2.30$, [Fe/H] = 0.04.

The conclusion for this star is: it is a young post-main sequence star with an age of only 240 Myrs but due to its mass it has already evolved past the main sequence and thus does not belong to this sample. But since the star is relatively young, it might be interesting to search for planets in its vicinity anyway. The surface gravity is tested by the comparison of the spectroscopic to Hipparcos distance and the effective temperature by the comparison of the measured to predicted stellar radius. With the small discrepancies of our analysis from the measured values (surface gravity 3.6 % and effective temperature 11.6 %, or 7.3 % respectively), we are confident that the spectral synthesis method we use works well.

### 4.8.3 [GKL 99] 306, EK Dra, HIP 71631, HD 129333
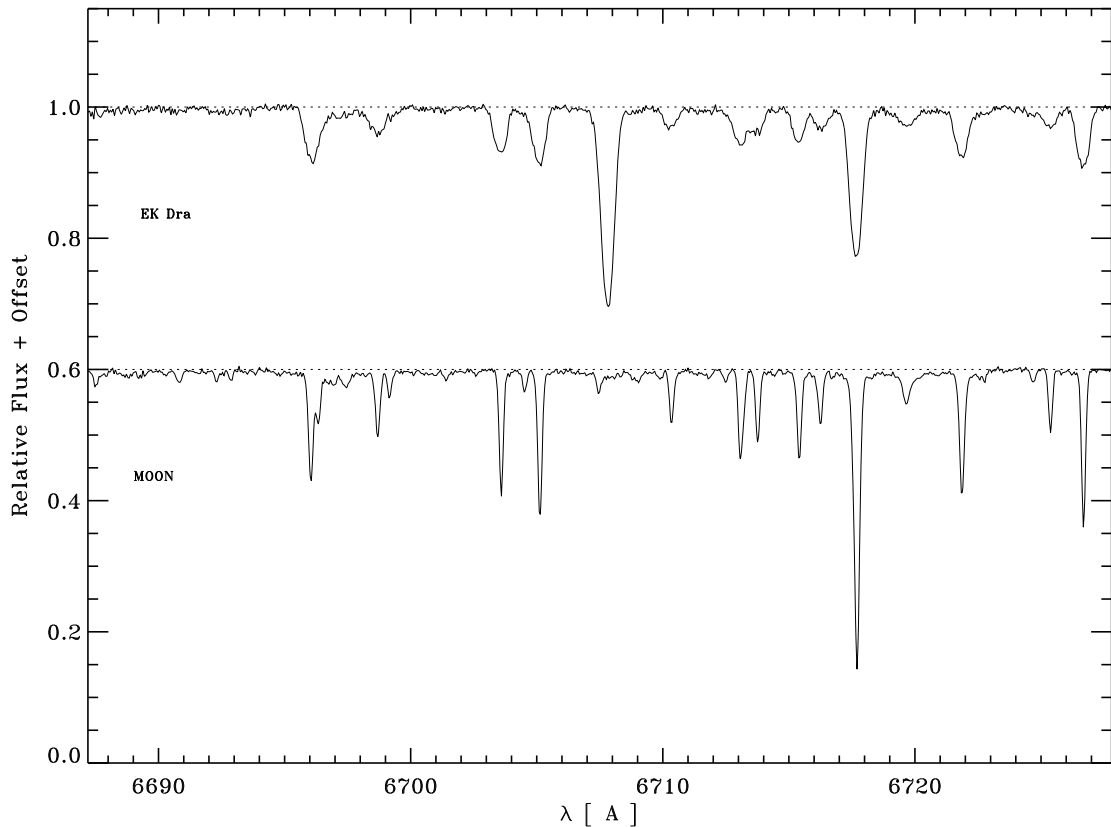


**Figure 4.31:** The lithium absorption line in the spectrum of EK Dra compared to reflected sunlight on the moon. Note the high $v \sin i$ of EK Dra.

EK Dra's space velocity of $U = 3\,\text{km/s}$, $V = -35\,\text{km/s}$ and $W = -12\,\text{km/s}$ (Eggen, 1998) indicates that the star could belong to the Pleiades supercluster. Photometric longterm

monitoring reveals a period of rotation of the star to be 2.605 days (Strassmeier & Rice, 1998). Doppler imaging of the stellar surface (Strassmeier & Rice, 1998) indicates large star spots at a latitude of +40° and at -60° and with a temperature difference $\Delta T$ between 1200 K to 400 K. A polar spot cannot be confirmed or excluded by their data. The measured inclination of the stellar axis of rotation is about 60°.

Duquennoy & Mayor (1991) measured radial velocity variations which indicate EK Dra to be a SB1 binary with a period of 4175 days (about 11.5 yrs). Assuming EK Dra has one solar mass and the inclination of the orbit of the companion is the same as for the star (60°), the companion then has a mass of $M_2 \geq 0.37 \, M_\odot$.

| $T_{\text{eff}}$ [K] | $\log g$ | [Fe/H] | $v \sin i$ [km/s] | $M_V$ [mag] | $M_{\text{bol}}$ [mag] | mass [$M_\odot$] |
|---|---|---|---|---|---|---|
| 5700±70 | 4.37±0.10 | -0.16±0.07 | 16.50±1.00 | 7.60 | 4.79 | 0.97 |

**Table 4.9:** Spectral parameters of EK Dra

The chromospheric activity, the variability, the presence of filling in of the H$\alpha$-line and a strong lithium absorption line at 6707 Å indicate that the star is indeed young. If we believe the star belongs to the Pleiades supercluster, we can assume an age of about 70 Myrs. But the activity level would also support the assumption that EK Dra could belong to the even younger cluster $\alpha$ Per with an even younger age of $\sim 40$ Myr.
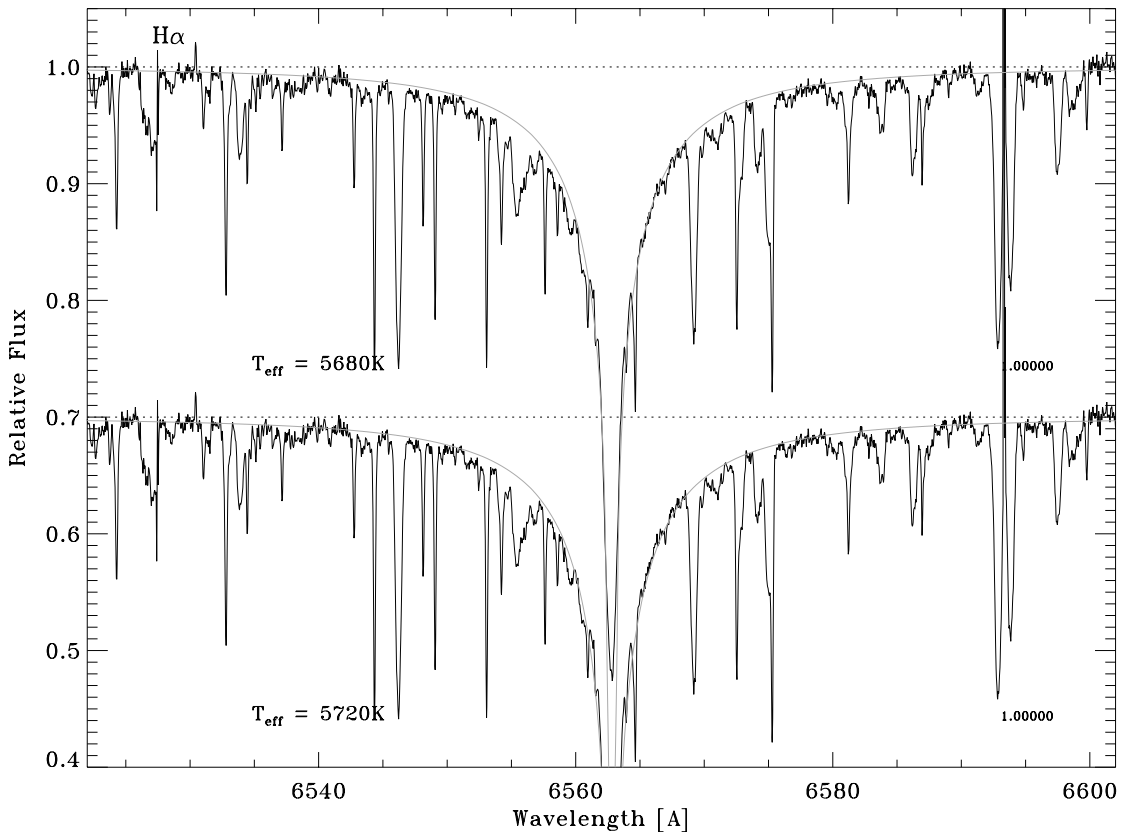


**Figure 4.32:** The H$\alpha$-line of EK Dra together with two theoretical H$\alpha$-line profiles to estimate the temperature. The real temperature lies between the plotted ones because both line profile fits are not optimal.

The spectral synthesis analysis we performed was complicated because it is known that

the star rotates fast ($\sim 16 - 17$ km/s) and it has large stellar spots which are much cooler that the surrounding surface and which can cover up to half of the visible surface. Depending on the position of the stellar spot, the star could appear cooler than it would actually be. On the other hand the H$\alpha$-line is filled in up to a level of 0.5. The H$\beta$-line is not that strongly affected. The temperature is measured using the H$\alpha$-temperature by comparing it the H$\beta$-temperature and then giving more weight to the H$\beta$-temperature. In case of the spectrum taken on Sep. 11, 2001, both temperatures were identical while in the spectrum taken at May 25, 2002, the H$\beta$-line leads to a 40 K hotter star. The spots influence the bisector of the spectral lines, they become asymmetric (see Chap. 5). The fit to the asymmetric line profiles are not as good as to symmetric ones. The high velocity of rotation, $v \sin i$, increases the number of blended lines. There are less iron lines which can be used for the spectral synthesis analysis.

Comparing the spectroscopic distance determined by us with the Hipparcos parallax, we have a 5.8% discrepancy. This makes us confident that the analysis we performed is reasonable. The discrepancy can be caused by the spots as well as by the companion.

Comparing our analysis with the results from Wyse & Gilmore (1995), we find that they measure a much lower metallicity abundance of -0.21 dex which was estimated by narrow-band Strömgen photometry. The temperature of EK Dra estimated by Dorren & Guinan (1994) of 5930 K is significantly higher than our measured temperature of 5700 K. But in our case the H$\alpha$ and H$\beta$ line-profiles would not support such a high temperature in our spectrum.

Eggen (1998) also estimated a metallicity of EK Dra using Strömgen photometry of -0.24 dex, which is lower than the metallicity measured by us of -0.16 dex. Using Strömgen photometry, one cannot account for the rotational broadening of the spectral lines and thus might underestimate the metal contents of the star.

### 4.8.4  [GKL 99] 210, GJ 3562

The star has a spectral type of M4V. The space motion is listed in the catalog of nearby stars with $(U/V/W) = (+11/ - 20/ - 15)$ km/s. We have observed this star with FOCES at high resolution. The star does not show any lithium, any chromospheric activity, or any other signature of youth in its spectrum. We conclude that it is an unrelated foreground object.

### 4.8.5  Summary

In the sample are Pleiades supercluster stars, like HIP 57269 which was formerly confused to be a TWA member candidate. The core of the Pleiades cluster lies at 120 pc but we find young stars which are members and which lie much closer to the sun. The Pleiades is a huge cluster and it is fairly evolved so that we are not surprised to find such stars that far off the cluster center.

## 4.9  Hercules-Lyra association

The Hercules-Lyra association consists of young stars in the solar neighborhood which form a distinct structure. First Gaidos (1998) named this group of stars Hercules kinematic group with a kinematic of $(U, V, W) = (-4.7, -11.1, -2.1)$ km/s or with respect to the local standard of rest: $(U, V, W)_{\text{LSR}} = (-13.7, -22.6, -9.1)$ km/s. Young et al. (1987) noticed a local group of stars with Pleiades like kinematics but with their mean distance within 25 pc. Soderblom & Clements (1987) called these local solar type stars "siblings of the Pleiades" and Jeffries & Jewell (1993) found evidence for a young group in the solar neighborhood which is kinematically coherent but not spatially. Fuhrmann (2004) also found this group of spatially coherent stars which show signatures of youth such as fairly rapid rotation, lithium absorption, and

filling in of the Balmer and the calcium H & K, as well as the magnesium I b lines. They first
gave the name Hercules-Lyra association. The $(U, V)_{\text{LSR}} = (-5, -23)$ km/s. The W-velocity
has a high scatter.

### 4.9.1   [GKL 99] 410, HN Peg, HIP 107350, HD 206860

HN Peg ([GKL 99] 410) was observed from Calar Alto using the FOCES spectrograph on
Nov. 29, 2001. What guides the eye in this spectrum is the strong lithium absorption
feature, the filling in of H$\alpha$ of about 10% and the line broadening due to the high projected
rotational velocity $v \sin i$. The activity level, namely the line filling in, would support an age
of 100-300 Myrs. The space motion indicates that the star belongs to the local Hercules-Lyra
association with $U - 14.6 \pm 0.3$ km/s, $V = -21.5 \pm 0.6$ km/s, and $W = -10.8 \pm 0.5$ km/s.
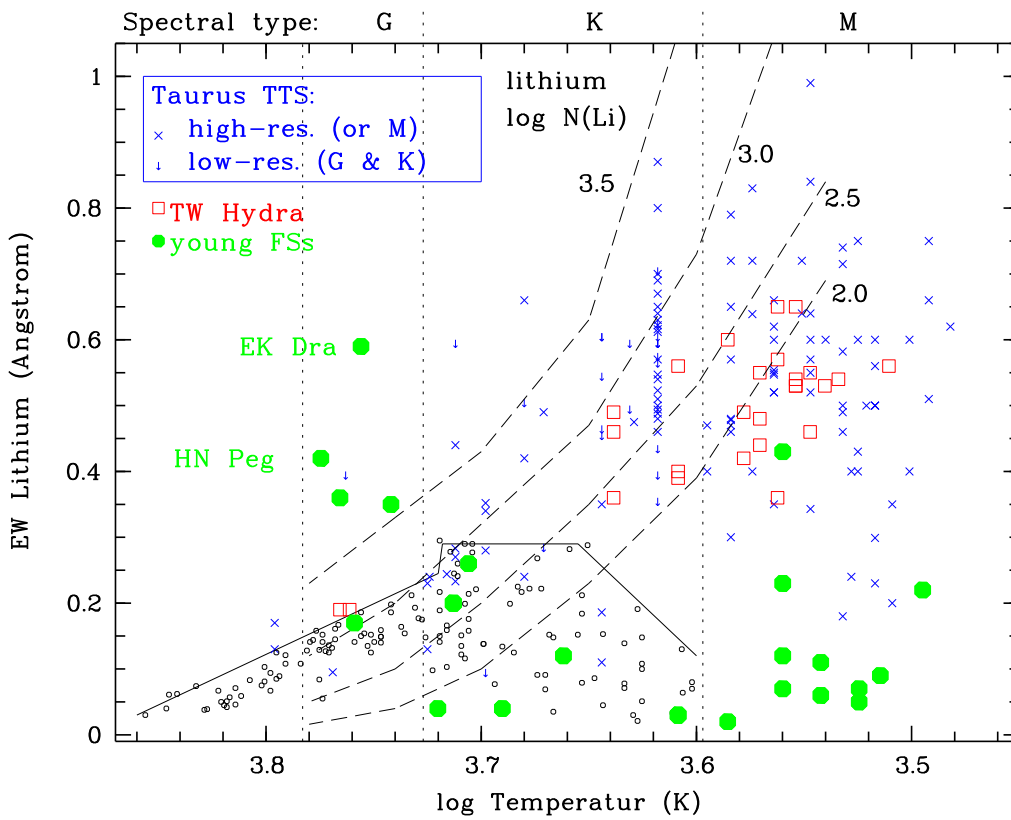


**Figure 4.33:** The figure shows the lithium equivalent width versus temperature. Note that
HN Peg and EK Dra are the G-stars with extremely high lithium abundance, which is even
higher than the mean initial abundance. It is clear that these stars must have a mechanism
to generate lithium in their atmosphere.

The spectral synthesis analysis reveals a star close to the main sequence on the zero-age
main sequence.

The measured lithium equivalent width in the observed spectrum is 108.1 mÅ. Modeling
the lithium line leads to a lithium abundance of $N(\text{Li}) = +2.90$.

In the Lick planet search (Cumming et al., 1999) HN Peg was observed with a precision
of $\sim 5$ m/s, but no significant radial velocity variations were detected.

| $T_{\rm eff}$ [K] | $\log g$ | [Fe/H] | $v \sin i$ [km/s] | $M_V$ [mag] | $M_{bol}$ [mag] | mass [$M_\odot$] |
|---|---|---|---|---|---|---|
| 5950±70 | 4.35±0.10 | -0.07±0.07 | 9.90±1.00 | 5.94 | 4.51 | 0.96 |

**Table 4.10:** Spectral synthesis analysis data for HN Peg.
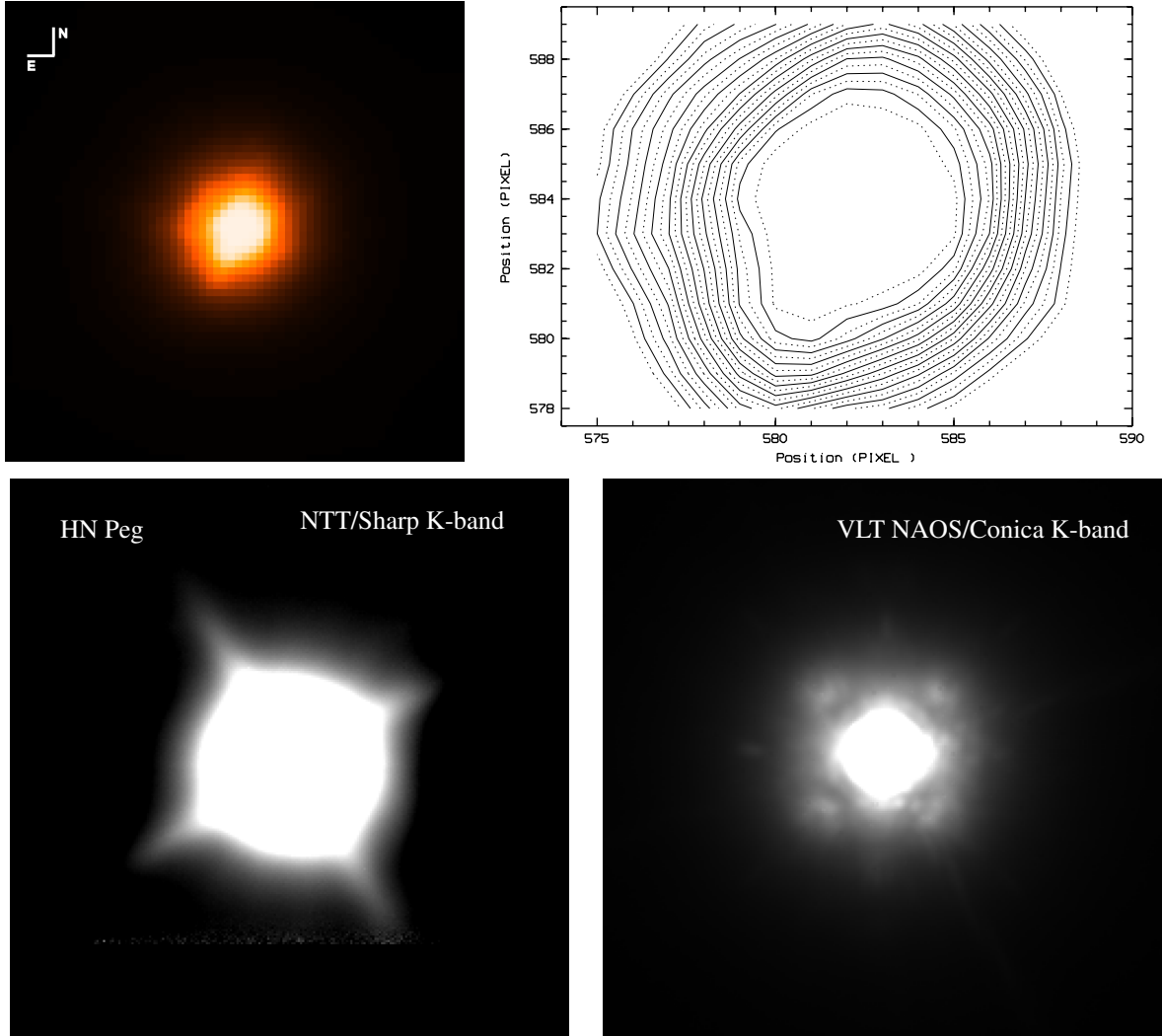


**Figure 4.34:** The upper two panels show the adaptive optics image of HN Peg taken with the AO system ALFA at Calar Alto and the contour plot of the same image. The two images in the lower panel show left the K-band images taken with the speckle camera Sharp at the NTT located at ESO La Silla and the lower right panel shows the NAOS/Conica K-band images taken at the VLT in Paranal, ESO. Note that in the two lower images the elongation of the star cannot be seen and is probably due to problems with the AO system. Note the diffraction rings in the NAOS/CONICA image.

We have performed near infrared adaptive optics imaging at Calar Alto using the AO system and $\Omega$ Cass in high resolution mode. The image shows a bump in the image contour plots which is in the image of HN Peg but not in other images. Therefore it is likely to be real

and not a residuum of the adaptive optics system. HN Peg was also observed in the K-band by speckle imaging using the 3.58 m NTT at ESO La Silla with the speckle camera Sharp and it was observed with the VLT and the NAOS/CONICA adaptive optics system. In those images the elongation of the star is not seen.

### 4.9.2   HIP 114385, and [GKL 99] 440, HIP 114379

The stars HIP 114385 and HIP 114379 A & B form a triple system where HIP 114385 and HIP 114379 form a visible binary system and HIP 114379 A & B is a spectroscopic and AO binary. HIP 114385 and HIP 114379 are located at the same distance at 34.06±2.31 mas and 39.56±7.67 mas respectively. They are comoving. Note the big error in the parallax measurement of Hipparcos. For HIP 114379 this clearly shows that the companion disturbed the precision of the parallax measurement. But also the stray light from HIP 114379 disturbed the parallax measurement of HIP 114385 which can be noticed by an error much greater than 1 in the Hipparcos measurement. The space motion $U = -14.0 \pm 3.2$ km/s, $V = -12.2 \pm 1.3$ km/s, and $W = -3.9 \pm 1.3$ km/s which makes the star consistent with the local association.

For HIP 114379 the following data is available from the catalog of nearby star metallicities (Zakhozhaj & Shaparenko, 1996) obtained from photometric UBV data. For the visual companion no data is available.

| Star | SpType | plx [arcsec] | [Fe/H] |
|------|--------|--------------|--------|
| HIP 114379 | G5 | 0.0287 | -0.30 |

**Table 4.11:** Data for the star HIP 114379 taken from Zakhozhaj & Shaparenko (1996) and measured by UBV photometry. This data was not corrected for the fact that the star is a binary.

This result must be regarded with care, because the HIP 114379 is a binary and the data has not been corrected for this. Our analysis of the comoving visual companion HIP 114385 reveal the following data: (see Tab. 4.12).

| $T_{\mathrm{eff}}$ [K] | $\log g$ | [Fe/H] | $v \sin i$ [km/s] | $m_{\mathrm{V}}$ [mag] | $M_{\mathrm{bol}}$ [mag] | mass $M_{\odot}$ |
|------|------|------|------|------|------|------|
| 5830±70 | 4.38±0.10 | 0.08±0.07 | 6.10±1.00 | 7.11 | 4.65 | 1.08 |

**Table 4.12:** Spectral synthesis data for the comoving visual companion HIP 114385 of the flare star HIP 114379.

Its lithium is already burned which makes the star older than the Pleiades, but its activity indicates an age similar to the Ursa Major cluster. Our analysis does not confirm the metallicity determined by photometry of Zakhozhaj & Shaparenko (1996).

The adaptive optics H-band images ware taken at the Calar Alto observatory in Spain In November 2001 and June 2002 using the AO system ALFA and the $\Omega$ Cass infrared camera. In the image one can see the visual binary. The star in the south-west is HIP 114379, a spectroscopic binary. With the north-east star it forms a hierarchical triple system with HIP 114385.

Since it is known that the two bright stars are comoving and they are at the same distance of about 30 pc, we can assume that the all have the same elemental abundances. Regarding
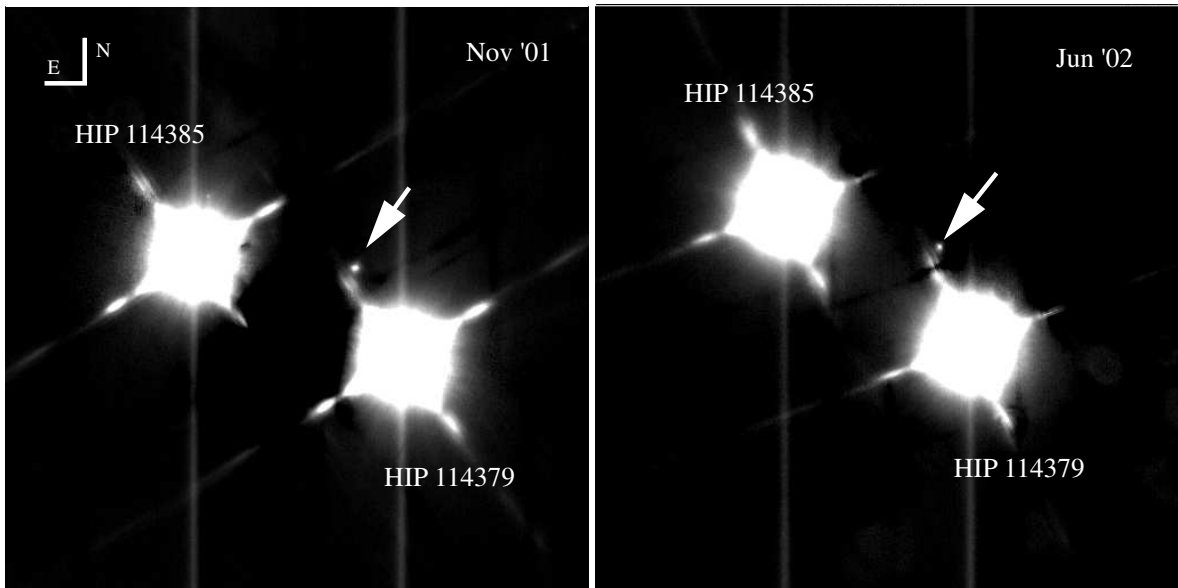
**Figure 4.35:** The adaptive optics H-band image of HIP 114379 and HIP 114385 taken with the AO system ALFA and the camera $\Omega$ Cass at Calar Alto, Spain. Note the circled star which could be a low-mass companion, but which is not yet confirmed. The estimated mass of the low-mass object assuming it is bound to the system is $0.05\,M_\odot$.

the high resolution ALFA adaptive optics image closely, one can see a faint object north-east of HIP 114379 which is marked with a circle. Assuming it is at the same distance, using the H-band photometry we estimate the mass to $0.05\,M_\odot$ (brown dwarf) at a separation of 207 AU. The object must be confirmed to be a low mass companion by proper motion measurements and spectroscopy. The proper motion measurement within this half year does not yet lead to a clear conclusion. Within the error the faint companion candidate could or could not be comoving.

The two bright objects have almost the same brightness and one object is a single star, we could perform a point spread function subtraction, which means, we scale the maximum count in the single star to the maximum count level of the binary star and then subtract the single star from the binary. It worked and only light from SB2 secondary is left over so that it was made visible.

## 4.10  $\beta$ Pictoris moving group

The star $\beta$ Pictoris was identified to be an isolated young star by Jura et al. (1993). Later Barrado y Navascués et al. (1999) found that the stars GJ 799 and GJ 803 are comoving with $\beta$ Pic. They estimated an age of $20 \pm 10$ Myr for the three stars.

Starformation scenarios agree that relative massive stars such as $\beta$ Pic form in clusters or associations with dozens of members. These associations dissociate in time but at the estimated age of $\sim 20$ Myr one expects still to find comoving members. And indeed Zuckerman et al. (2001a) identified 15 additional members. The average distance from the sun of these 18 stars is $\sim 35$ pc and its mean space motion is $U = -10.5\,\text{km/s}$, $V = -15.8\,\text{km/s}$, $V = -9.5\,\text{km/s}$. The stars are located in the range of Ra: 00h to 21h and Dec: -02° 20m to -72° 03m.

### 4.10.1   [GKL 99] 82, HIP 13402, HD 17925

The iron abundance of this star is [Fe/H]= $+0.083 \pm 0.038$ taken from Taylor (2003). Habing et al. (2001) give a $V = 6.05$ mag and a temperature of $T_{\text{eff}} = 5000$ K measured with Geneva photometry. They suggest an age of 80 Myr and it has a distance of $d = 10.4$ pc. Around the star is a disk. Wichmann et al. (2003) measured $W_{\text{Li}}^m = 215$ Å which they corrected for the nearby iron absorption to $W_{\text{Li}}^c = 194$ Å. The radial velocity is $v_{\text{rad}} = 18.2$ km/s with a $v \sin i < 10$ km/s. The space motion is $U = -5.4$ km/s, $V = -16.6$ km/s, and $W = -2.1$ km/s which makes it consistent with the $\beta$ Pictoris moving group or local association. Montes et al. (2001) list it as a member of the local association. Cayrel de Strobel & Cayrel (1989) suggest that the birth place of the star lies in the Scorpio-Centaurus-Complex.

### 4.10.2   [GKL 99] 145, HIP 26779

The space motion of this star ($U = -14.0 \pm 0.7$ km/s, $V = -23.0 \pm 0.4$ km/s, $W = -14.2 \pm 0.2$ km/s) is consistent with the $\beta$ Pictoris moving group or the local association.

Analyzing the FOCES spectra, we get very good agreement of the spectroscopic distance with the Hipparcos distance with a discrepancy of only 0.5%.

| $T_{\text{eff}}$ [K] | $\log g$ | [Fe/H] | $v \sin i$ [km/s] | $m_{\text{V}}$ [mag] | $M_{\text{bol}}$ [mag] | mass $M_{\odot}$ |
|---|---|---|---|---|---|---|
| 5260±70 | 4.50±0.10 | 0.09±0.07 | 3.10±1.00 | 6.12 | 5.43 | 0.90 |

**Table 4.13:** Spectral parameters of HIP 26779.

Comparing with the photometric metallicity abundance, Haywood (2001) measures a value of -0.01 dex, while Gaidos & Gonzalez (2002) measure 0.08±0.04 dex and an effective temperature of 5295±47 K in good agreement with our data.

### 4.10.3   [GKL 99] 132, HIP 23200

The space motion is $(U/V/W) = (-11.3 \pm 0.7/ -16.9 \pm 0.9/ -9.1 \pm 0.4)$ km/s. Its location in the northern hemisphere (Ra: 04 h 59 m 04.8 s, Dec: 01° $47^m$ $01^2$) could make it the most northern member of $\beta$ PicA but it has a fairly high lithium abundance of $\log N(\text{Li}) = 1.5$ at a spectral type M0V and its H$\alpha$ emission with an equivalent width of 1.9 Å shows that the star is fairly young, younger than the Pleiades given the lithium abundance. Christian & Mathioudakis (2002) also observed this star and they measure a lithium abundance of $\log N(\text{Li}) = 1.5$ and an H$\alpha$-emission line with an equivalent width of 1.4 Å. Its position in the Siess et al. (2000) models makes it consistent with the $\beta$ PicA member stars with 20±10 Myr. We propose this star to be a member candidate of the $\beta$ Pic association.

### 4.10.4   [GKL 99] 137 and [GKL 99] 136, or GJ 3331 A & B

The visual binary GJ 3331 A & B consists of two stars with M2V and M3V. It is located in the line of sight of the $\beta$ PicA. For these stars no distance measurement is available. We have observed them from La Silla, ESO using the DFOSC instrument. The A component shows H$\alpha$ in emission ($EW(\text{H}\alpha) = 1.8$ Å) and a lithium abundance comparable with the Pleiades ($EW(\text{Li}) = 0.06$ Å). The lithium abundance is too low for the star to be a member of $\beta$ PicA.

GJ 3331 B does not show any signatures of youth or chromospheric activity in its DFOSC-spectrum.

### 4.10.5  [GKL 99] 146, GJ 1083 A & B

The star was not observed during our survey because it was too faint. Its space motion is consistent with the $\beta$ PicA but it is located too far north to be a member candidate.

### 4.10.6  [GKL 99] 387 and [GKL 99] 388, or HIP 102141 A & B

AT Mic is one of the very well known flare stars. The space motion (A: $(U/V/W) = (-9.61 \pm 2.40/-16.88 \pm 0.94/-11.0 \pm 1.91)$ km/s, B: $(U/V/W) = (-8.81 \pm 2.40/-16.72 \pm 0.93/-9.60 \pm 1.90)$ km/s,  Montes et al., 2001) of the star is consistent with the $\beta$ PicA and it is located in the line of sight of the association but it is at a distance of $d = 10.22 \pm 0.51$ pc. Zuckerman et al. (2001a) list it as a bona-fide member. Both stars have a spectral type of M4.5Ve. We have observed both stars with DFOSC from La Silla but only the primary shows H$\alpha$ emission ($EW$(H$\alpha$) = 2.5) Å but none of them shows lithium in absorption. Barrado y Navascués et al. (1999) conclude that the star is a member of the $\beta$ PicA at an age of $20 \pm 10$ Myr.

### 4.10.7  [GKL 99] 394, HIP 102409

AU Mic is the second well studied flare star in this space region. It is listed in Zuckerman et al. (2001a) as a bona-fide member of $\beta$ PicA. In reality this star is a quadruple system. Its spectral type is listed as M1.5V. We have observed this star with DFOSC. It shows H$\alpha$ in emission with an equivalent width of 2.1 Å but it does not show lithium absorption in its spectrum.

## 4.11  The translucent cloud MBM 12

The translucent cloud MBM 12 with young stars in its vicinity was discovered by Hobbs et al. (1986) and they estimated a distance to the cloud of 50 to 100 pc. It is located in the sky at Ra: 02h 50m 00s to 03h 00m 00s and between Dec: $+19°$ 25m 00s to $+20°$ 45m 00s. More recently Hearty et al. (2000) have revised the distance estimate and derive 53 to 102 pc. The extinction in the line of sight is $A_V =$ 0 - 5 mag and can reach up to $A_V = 10$ mag.

Luhman (2001) used the knowledge of the extinction of the cloud and claimed that all stars Hearty et al. (2000) placed behind the cloud, are in fact in front of the cloud. This places the cloud at about 275 pc.

Using the X-ray properties of MBM 12 member star Hearty (2001) derived again a distance of 142 pc. This enforces the on-going discussion of deriving distances to stellar associations and especially MBM 12. Yet, none of our flare stars show properties consistent with MBM 12.

## 4.12  Stars belonging to the Hyades Cluster

The Hyades cluster has distinct space motion so that its stars cannot be confused with stars of the local association. It is one of the nearest clusters at a distance of 40-50 pc to its center and with about 300 members. The cluster mass is 300-400 $M_\odot$ and its space motion with respect to the local standard of rest is $(U, V, W)_{LSR} = (-32.7, -7.3, +5.9)$ km/s. The distance to its center of mass is 46.34±0.27 pc. The cluster stars are slightly iron overabundant with [Fe/H] = $0.14 \pm 0.05$ and Helium has an abundance of $Y = 0.26 \pm 0.02$. The age of the cluster is estimated to be 625±50 Myr (Perryman et al., 1998).

Eggen (1982) measured space velocities of all bona fide members $(U, V, W) = (40.5 \pm 2.3, -18.4 \pm 2.3, -4.9 \pm 6.0)$ km/s and of the brighter cluster members $(U, V, W) = (41.7 \pm 2.6, -18.4 \pm 1.3, -2.0 \pm 2, 9)$ km/s.

### 4.12.1   [GKL 99] 15, HIP 1803, HD 1835, HR 88

| $T_{\mathrm{eff}}$ [K] | $\log g$ [dex] | [Fe/H] [dex] | $m_V$ [mag] | $M_{\mathrm{bol}}$ [mag] | $d_{\mathrm{HIP}}$ [pc] | $d_{\mathrm{spec}}$ [pc] | diff. [%] | source |
|---|---|---|---|---|---|---|---|---|
| 5740±70 | 4.37±0.10 | 0.13±0.07 | 6.39 | 4.65 | 20.39 | 20.95 | 2.8 | K |
| 5771 | 4.44 | 0.15 | | 4.81 | | 19.50 | 4.4 | Katz |
| 5675±60 | 4.31±0.12 | 0.17±0.05 | | 4.56 | | 21.74 | 6.6 | G |
| 5860 | 4.4 | -0.09 | | 4.65 | | 21.06 | 3.3 | M, C |
| 5793 | 4.5 | 0.19 | | 4.95 | | 18.37 | 9.9 | M, C |
| 5860 | 4.4 | 0.28 | | 5.65 | | 21.24 | 4.2 | M, C |
| 5793 | 4.6 | 0.24 | | 5.20 | | 16.39 | 19.6 | M, C |
| 5793 | 4.5 | 0.2 | | 4.95 | | 18.38 | 9.9 | M, C |
| 5673 | 4.22 | -0.01 | | 4.34 | | 24.02 | 17.8 | M, C |
| 5781 | 4.40 | | | | | | | Glu |
| 5800 | 4.60 | 0.24 | | 4.69 | | 20.70 | 1.6 | A |

K: this work, Katz: Katz et al. (2003), G: Gaidos & Gonzalez (2002), M: Malagnini et al. (2000), C: Cayrel de Strobel et al. (1997) and references therein, Glu: Glushneva et al. (2000), A: Abia et al. (1988)

**Table 4.14:** Spectral parameters of HIP 1803 derived using the spectral synthesis analysis methods described before (first row of the table). The last ten rows summarize the work of the other authors, where most of the data was compiled by Cayrel de Strobel et al. (1997) from several sources. Malagnini et al. (2000) has listed the same stars in their work. The spectral parameters were used to calculate the spectroscopic distance and compare to the Hipparcos distance to investigate the accuracy of the analysis.

The star HIP 1803 in the spectral synthesis analysis gives a star of effective temperature of 5740±70 K with a surface gravity $\log g = 4.37 \pm 0.10$, and an iron abundance of [Fe/H] $= 0.13 \pm 0.07$. The star is quite similar to the sun but showing signatures of a young star, such as lithium absorption with an equivalent width of $W(\mathrm{Li}) = 74.5$ mÅ corrected for the iron blend. This translates into a lithium abundance of $\log N(\mathrm{Li}) = 2.35 \pm 0.10$. We measure a projected rotation velocity of $v \sin i = 6.4 \pm 1.0$ km/s. The space velocity of $U = -36$ km/s, $V = -15$ km/s, $W = -10$ km/s makes the star consistent with the Hyades Cluster.

Gaidos et al. (2000) have also measured a lithium equivalent width of $W_{6708}(\mathrm{Li}) = 76.1 \pm 4.1$ mÅ, and an abundance of $\log N(\mathrm{Li}) = 2.58 \pm 0.10$ at an effective temperature of $T_{\mathrm{eff}} = 5860$ K. The lithium abundance they derived deviates from our value due to the fact that they estimated the temperature to be about 80 K hotter than in our measurement.

## 4.13   Summary

We finally conclude that we have identified young stars in the solar vicinity which belong to different stellar associations. In some cases the membership was already known or they were at least proposed member candidates, in other cases the membership could be cleared up. Below we give a table of the youngest stars found in the survey.

As summarized in Table 4.16 we have identified young stars in an age range from 10 Myr to ZAMS. Generally, we conclude that if the flare stars were correctly classified, they are indeed young pre-main sequence stars. For the related objects with a spectral classification of K, or G we must conclude that they are mainly ZAMS stars which still have a high level

**Table 4.15:** A list of the youngest flare stars of this survey. We give the relevant spectroscopic data as well as the ages and masses derived from pre-main sequence models.

| [GKL 99] | designation | r [pc] | $M_V$ [mag] | $T_{eff}$ [K] | $\log(L_{bol}/L_\odot)$ | remark |
|---|---|---|---|---|---|---|
| 132 | HIP 23200* | 26.7±1.7 | 8.94 | 3850±200 | -0.33±0.30 | |
| 50 | HIP 9275 | 29.8± 4.1 | 10.70 | 3485±200 | -0.70±0.32 | |
| 93 | LP 772-73 | 34.2±10.3 | 11.70 | 3345±170 | -0.80±0.24 | binary, phot. dist. |
| 199 | HIP 45731 | 32.5± 2.4 | 9.27 | 3850±200 | -0.29±0.31 | binary |
| 321 | HIP 79796 | 20.7± 0.5 | 8.93 | 3705±200 | -0.47±0.34 | binary |
| 367 | HIP 94557 | 19.1± 0.9 | 10.73 | 3345±170 | -0.92±0.39 | |
| 406 | Wo 9652 | 45.9± 6.9 | 9.88 | 3630±200 | -0.12±0.27 | susp. binary |
| 436 | HIP 112909 | 14.2± 0.6 | 11.30 | 3415±200 | -1.60±0.10 | |
| 456 | HIP 117069 | 28.9± 1.6 | 9.03 | 3785±200 | -0.26±0.32 | susp. binary |
| 104 | HIP 18512 | 15.8± 0.5 | 7.05 | 4600±100 | -0.55±0.02 | |
| 109 | HIP 19855 | 20.9± 0.5 | 5.33 | 5630± 70 | -0.16±0.02 | |
| 231 | HIP 53985 | 11.7± 0.2 | 9.22 | 3850±200 | -1.25±0.36 | |
| 239 | HIP 55454 A | 13.2± 0.3 | 8.01 | 4590±230 | -1.47±0.36 | binary |
| 245 | HIP 57269 A | 48.7± 6.4 | 5.90 | 4990±100 | -0.30±0.02 | |
| | HIP 57269 B | 48.7± 6.4 | 7.04 | 4730±200 | -0.69±0.43 | SpT? |
| | HIP 57269 C | 48.7± 6.4 | 10.06 | 4470±100 | -1.84±0.05 | |
| 428 | HIP 111766 | 14.8± 1.3 | 10.63 | 3345±200 | -1.41±0.38 | |
| 414 | HIP 108405 | 16.2± 0.7 | 9.36 | 3485±200 | -0.94±0.36 | |
| 423 | HIP 110526 | 16.1± 2.2 | 9.71 | 3415±200 | -1.39±0.34 | |
| 74 | HIP 12351 | 16.5± 0.3 | 8.56 | 4060±200 | -0.82±0.33 | |
| 306 | EK Dra | 33.9± 0.7 | 4.89 | 5700± 70 | -0.02±0.01 | |
| 210 | GJ 3562 | 20.5± 5.9 | 12.47 | 3415±200 | -1.14±0.23 | |
| 410 | HN Peg | 18.4± 0.3 | 4.62 | 5950± 70 | +0.11±0.01 | |
| 440 | HIP 114379 | 25.3± 4.1 | 5.89 | 5250±300 | -0.34±0.13 | |
| 145 | HIP 26779 | 12.1± 0.1 | 5.81 | 5260± 70 | -0.26±0.01 | |
| 136 | GJ 3331 A | 11.8± 3.4 | 9.93 | 3680±200 | -1.46±0.24 | |
| 387 | HIP 102141 | 10.2± 0.5 | 10.24 | 3270±170 | -1.03±0.19 | |
| 394 | HIP 102409 | 9.9± 0.1 | 8.77 | 3850±200 | -1.12±0.25 | |
| 15 | HIP 1803 | 20.4± 0.4 | 4.84 | 5740± 70 | +0.04±0.01 | |

Notes: ∗ HIP 23200 is also called GJ 182. The star is one of the youngest and closest stars to the sun. Favata et al. (1998) determined the age of the star in the range of 20 to 50 Myr. As a member of the $\beta$ PicA it is probably 20±10 Myr old.

of activity. This can be seen in the spectrum by the filling in of the H$\alpha$-, the calcium H & K lines, and the magnesium-Ib lines. But we have also shown that the activity level is not too high so that we are able to perform spectral synthesis analysis with reasonable results (see Figure 4.36).

Compared to the star GJ 182 which is up to now the closest nearby pre-main sequence star (Favata et al., 1998) and which is a member of the $\beta$ Pictoris association. We have identified other young stars which are bona-fide members of the $\beta$ Pictoris association and which are located even closer to the sun and which have about the same age as GJ 182 (see Table 4.16).

**Table 4.16:** Ages and masses estimated by comparing to theoretical tracks and isochrones of Baraffe et al. (1998), and Siess et al. (2000) with conversion from Siess et al. (2000), and from Kenyon & Hartmann (1995).

| [GKL 99] | $M_{\mathrm{BCAH}}$ [M$_\odot$] | age$_{\mathrm{BCAH}}$ [Myr] | $M_{\mathrm{Siess}}$ [M$_\odot$] | age$_{\mathrm{Siess}}$ [Myr] | $M_{\mathrm{SK}}$ [M$_\odot$] | age$_{\mathrm{SK}}$ [Myr] |
|---|---|---|---|---|---|---|
| 132 | 0.70±0.10 | 20±10 | 0.60±0.10 | 3±10 | 0.60±0.10 | 4±10 |
| 50 | 0.40±0.20 | 20±15 | 0.25±0.10 | 7±10 | 0.30±0.10 | 4±10 |
| 367 | 0.30±0.20 | 20±20 | 0.21±0.10 | 5±10 | 0.25±0.10 | 5±10 |
| 436 | 0.30±0.20 | ZAMS | 0.21±0.10 | 60±10 | 0.23±0.10 | 50±10 |
| 104 | 0.75±0.10 | 50±10 | 0.75±0.10 | ZAMS | 0.80±0.10 | ZAMS |
| 109 | 1.00±0.10 | ZAMS | 1.10±0.10 | ZAMS | 1.10±0.10 | ZAMS |
| 231 | 0.55±0.10 | 75±10 | 0.55±0.10 | ZAMS | 0.55±0.10 | ZAMS |
| 245A | 0.87±0.05 | 40±10 | 0.90±0.10 | ZAMS | 0.90±0.10 | ZAMS |
| 245C | 0.75±0.05 | 50±10 | 0.75±0.10 | ZAMS | 0.75±0.10 | ZAMS |
| 428 | 0.20±0.10 | 50±20 | 0.20±0.10 | 10 ± 10 | 0.20±0.10 | 13±10 |
| 414 | 0.45±0.10 | 10±10 | 0.30±0.10 | 10 ± 10 | 0.30±0.10 | 5±10 |
| 423 | 0.40±0.10 | 40±10 | 0.20±0.10 | 10 ± 10 | 0.25±0.10 | 15±10 |
| 74 | 0.75±0.10 | 50±10 | 0.70±0.10 | 20 ± 20 | 0.70±0.10 | 30±20 |
| 306 | 1.00±0.10 | 32±10 | 1.10±0.10 | ZAMS | 1.10±0.10 | ZAMS |
| 210 | 0.40±0.10 | 30±10 | 0.25±0.10 | 9 ± 10 | 0.25±0.10 | 7±10 |
| 410 | 1.10±0.10 | ZAMS | 1.20±0.10 | ZAMS | 1.20±0.10 | ZAMS |
| 440 | 0.85±0.10 | ZAMS | 0.90±0.10 | ZAMS | 0.90±0.10 | ZAMS |
| 145 | 0.90±0.10 | 40±10 | 0.90±0.10 | ZAMS | 0.95±0.20 | ZAMS |
| 136 | 0.45±0.20 | ZAMS | 0.20±0.10 | 30 ± 20 | 0.20±0.10 | 30±10 |
| 387 | out of range | | 0.13±0.05 | 20 ± 10 | 0.13±0.05 | 10±10 |
| 394 | 0.65±0.10 | 50±10 | 0.50±0.10 | 25 ± 10 | 0.45±0.10 | 30±10 |
| 15 | 1.05±0.10 | ZAMS | 1.10±0.10 | ZAMS | 1.10±0.10 | ZAMS |

Finally, the direct imaging search was not fully satisfying because at this point we could not gather enough data. Especially it was not possible to obtain second epoch imaging or follow up spectroscopy for all the candidate companions. We have detected some (sub)stellar companion candidates which must be confirmed by proper motion or spectroscopy. In the case of HIP 57269 we could already perform the follow-up spectroscopy and reject some candidates. The status in case of the faint companion to HIP 114379 is yet unclear. The proper motion measurements with half a year time separation do not reveal the nature of the companion.

## 4.14   Discussion - Why not use Photometry?

The aim of this thesis is to identify and understand the nature of young stars in the solar vicinity. In recent years young associations have been identified and it leads to the question why is it so important to take spectra and model their atmosphere.

The first problem arises when using only photometry is that the colors are calibrated on main sequence stars. Young stars have emission lines, or filled in line cores which change the flux in the associated wavelength bands and thus the stellar parameters derived with these colors could lead to a misinterpretation.

### 4.14.1   The colors of a star

The complete flux $F$ of a star emitted can be described by the law of Stefan-Boltzmann, where the flux is dependent on the luminosity $L$ and the radius $R$ of the star.

$$F = \frac{L}{4\pi R^2} = \sigma T_{\text{eff}}^4 = f \cdot \left(\frac{d}{R}\right)^2 \tag{4.7}$$

$f$ is the total flux of the star measured on earth and $d$ the distance to the star. This equation holds only if there is no interstellar extinction. The flux of the star $F$ can be derived using model atmospheres. To be consistent with our work, we of course use the model atmosphere described in the following chapters.

One can transform this equation to the following:

$$\sigma T_{\text{eff}}^4 = f \frac{F(\lambda)}{f(\lambda)} \tag{4.8}$$

where $f$ and $f(\lambda)$ can be measured, and $f(\lambda)$ and $F(\lambda)$ denote the monochromatic flux on earth or on the surface of the star, respectively.

In principle measuring the flux of a star with different filters can lead to color information. The color and spectral type information was calibrated by several authors. For young stars this has been done by Luhman (1999) and Kenyon & Hartmann (1995).

Broad band photometry using filters such as the Johnson-Cousins filters (U, B, V, $R_C$, $I_C$, J, H, K) can be used to investigate the spectral type of an object. Originally Johnson used only the three filters U, B, and V (ultraviolet, blue and visible), but when the detectors became sensitive to the red light and the infrared wavelength regime, Johnson added the following filter (R, I, J, H, K). At about the same time Cousins also introduced a $R_C$ and $I_C$, which are now more commonly used. Usually one should carefully notice which filters were used since there is confusion over the different filter-systems which cover different wavelength regimes in the spectrum and therefore have to be handled differently. For a discussion of the subject see Bessell (1993).

Since absolute calibration of the flux in each filter is not in general possible, because the absolute distance to the star is not known, one can use color indices. These indices are for the Johnson-Cousins system B-U, B-V, $R_C$-B, etc. The color indices then give a measure if the star appears redder (cooler) or bluer (hotter). A calibration of these indices can give an idea which spectral type the star has. Some of the indices are more sensitive to temperature (B-V) in cool stars, while others are more sensitive to gravity, or to the stellar chemical composition (U-B). The stellar parameters measured this way might not be very accurate and must be used with care.

### 4.14.2   Narrow band photometry

Especially for classifying stars more accurately, Strömgen developed a narrow-band photometric system (u, b, v, y, $\beta_n$, $\beta_m$) where each filter does not cover more than 30 Å and the $\beta_n$, and $\beta_m$ filters are centered on the H$\beta$-line core and on the adjacent continuum. In hot stars the Balmer jump is in the middle of the u-band. This means (u-b) is sensitive to metallicity and the Balmer jump. The index $c_1 = (u - v) - (v - b)$ is a measurement for the effective temperature in hot stars and a luminosity indicator for cool stars. $(\beta_n - \beta_m)$ is a temperature indicator for cool stars and a luminosity indicator for hot stars. For cool stars the index $m_1 = (u - b) - (b - y)$ measures the amount of line-blanketing, meaning the dimming of the blue part of the spectrum because of millions of absorption lines of heavy elements.

Temperature estimated by narrow-band photometry by various authors can be compared to the temperature estimated by the Balmer lines using model atmospheres as described in Fuhrmann et al. (1998). To be consistent in this work, we only compared temperatures derived using the same model and method as in this thesis, e.g. Fuhrmann (1993). A not very systematic check of the temperature yields a difference up to $250\,\mathrm{K}$. For a systematic comparison of the stars of the sample investigated in this thesis see Fig. 4.36. This high discrepancy could lead to a wrong estimation of the metallicity and also the surface gravity.
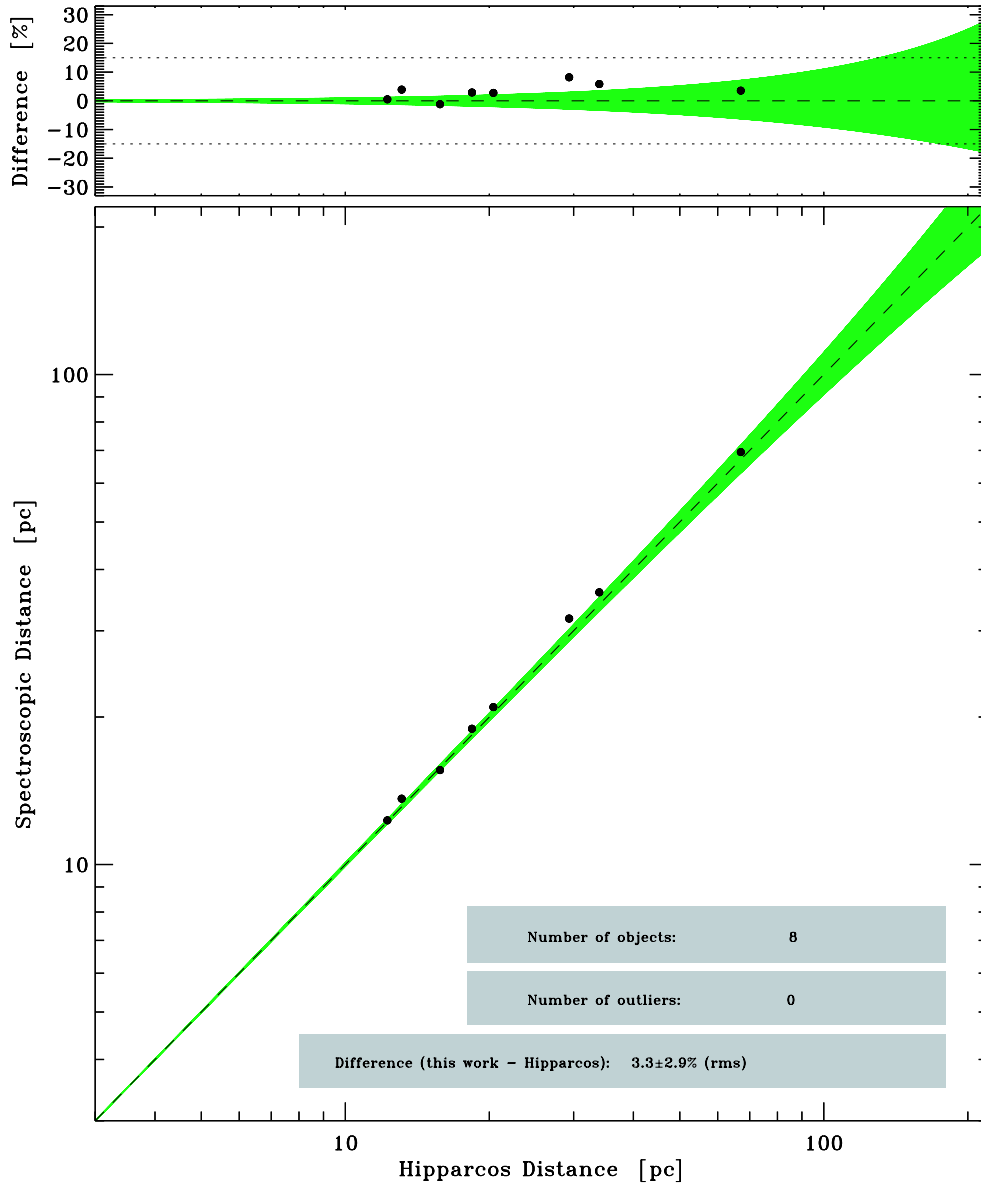


**Figure 4.36:** The stellar parameters derived by FOCES spectroscopy were converted to a spectroscopic distance using Eq. 4.7. Comparing these values to the trigonometric distance measured by the Hipparcos satellite, we can learn how good the stellar parameters are, especially the surface gravity. The upper panel in the figure shows the resulting distance discrepancy when subtracting the Hipparcos distance. The dashed line denotes a 15 % error. The shaded area in the lower and upper panel shows the average Hipparcos error bar.

As can be seen in Fig. 4.36 the photometric parameters do not predict the distance to the stars as well as the spectroscopic parameters. Since the sample is not very large (eight stars),

the comparison has to take place with a much larger sample to see systematic effects such as e.g. metallicity effects on the temperature or surface gravity. Fuhrmann (2004) has analyzed a sample of about 200 stars. The test of comparing spectroscopic to Hipparcos parallax can be seen in Fig. 4.37.
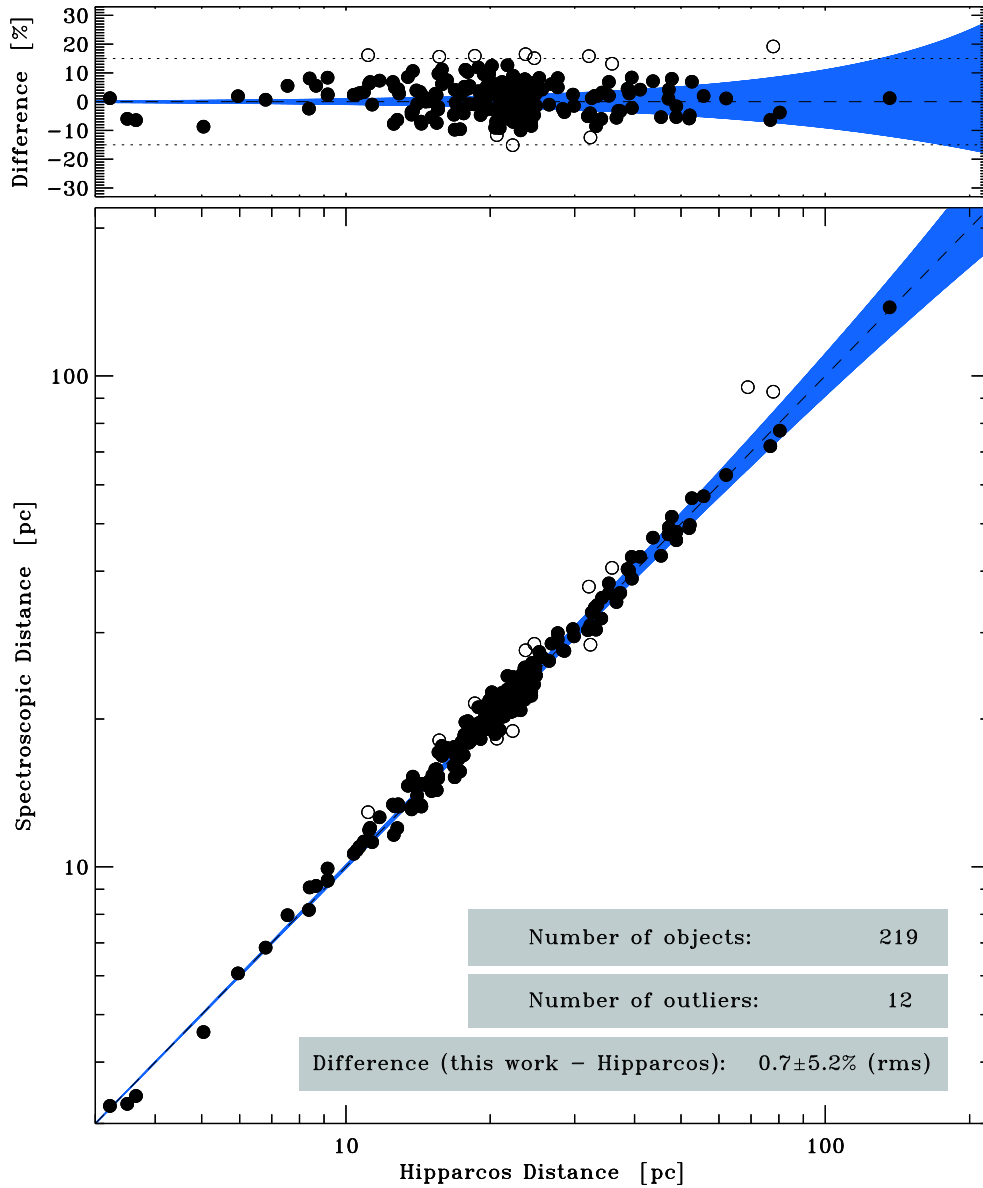


**Figure 4.37:** Figure taken from Fuhrmann (2004). Figure similar to Fig. 4.36. The open circles mark outliers which are in most cases known spectroscopic binaries.

Also a direct measurement of the angular diameter (radius) of the stars will help to validate the temperature measured using the following dependency:

$$\sigma T_{\mathrm{eff}}^4 = f\left(\frac{d}{R}\right)^2 = f\left(\frac{2}{\theta}\right)^2 \tag{4.9}$$

where $\theta$ is the angular diameter of the star.

This will lead to a much better calibration of the spectroscopic temperature as well as the

photometric temperature. The direct measurements of radii of stars will soon be possible as
the VLT interferometer has just seen first light and also the interferometer mounted on the
two Keck telescope is making progress.

### 4.14.3  Low resolution spectroscopy

The spectral classification system OBAFGKM with its subclasses was established using low
resolution spectroscopy with a resolution of 1.8 Å per resolution element. The resolution
of the spectrum is sufficient to resolve broad features but not detailed information, such as
metallicity. Given the resolution, high metallicity could mimic less overall emission which
would lead to an underestimation of the temperature and thus the spectral type. In the
recent years the two new classes L and T based on low resolution red spectra were added.

   The temperatures estimated by low resolution spectra, meaning by spectral type, can still
have errors as large as 200 K or larger. For low metallicity stars this could even be worse.

   As we have seen from our comparison of the low resolution spectra to the high resolution
spectra of the same objects, there are a lot of problems which cannot be easily overcome. E.g.
the instrument profile together with the noise level of the observed spectra does not allow a
measurement of the temperature. The iron abundance as well as the surface gravity cannot
be determined from the low resolution spectra accurately.

   To measure stellar parameters of stars without high resolution spectra cannot be performed
as accurately as one would like. In particular to determine the effective temperature, the
surface gravity, and the iron abundance is not possible. On the other hand an estimate of the
chromospheric activity regarding the filling in of sensitive lines is possible. Also the detection
of the youth indicator lithium at 6707.8 Å can be done without problems. But we have to
keep in mind that there are contributions to the measured abundance by weak iron line to
the measured lithium equivalent width.

# Chapter 5

# Radial velocity monitoring

The radial velocity (RV) search method for planets is very well established. Up to now about one hundred planet candidates were discovered. The method can only determine lower limits for the masses of the candidates since the measured value is $m \sin i$ and so depends on the usually unknown inclination $i$ of the system. By only measuring the RV the inclination is always the unknown parameter. Other methods such as astrometry and direct imaging have to be used to measure the inclination of the system.

The method is not limited to nearby stars, the only limitation is to obtain a spectrum with a signal-to-noise ratio of about 100 in a reasonable exposure time before the broadening of the spectral lines caused by the movement of the earth occurs. This effect is significantly visible at the resolving power of $\Delta\lambda/\lambda = 67,000$ and an exposure time longer than 45 min. The usual samples studied are G-type stars which are known to be inactive, like the sun. This sample was first chosen because of the similarities to our solar system and planet formation theories were developed to explain systems similar to ours because the general assumption was that our planetary system is typical. When the first extrasolar planet candidates were discovered, the community was surprised, because the candidate had half the Jupiter mass ($m \sin i$) on an orbit very close to the G-type star 51 Pegasus. The amplitude of the radial velocity variations was 59±15 m/s with a period of 4.2293±0.0011 days (Mayor et al., 1995). Theoreticians and also observers were in a dilemma. Theory would only predict planets such as Jupiter in a relatively wide orbit. New theories were developed allowing migration from the birth place of the planet in a wide orbit to the close-in orbit, or insitu formation directly in the close orbit.

The sample of inactive G-type stars was not sufficient in several respects. To study the timescales of planet formation, planets around younger stars must be found. But these younger stars are active, they exhibit spots and stellar flares which contribute a large noise level to the radial velocity signal. The strategy used to overcome this problem will be described in Section 5.3.

Young stars need to be studied to understand the timescales of planet formation. There are different theories for planet formation. The principle idea is that planet formation takes place in the disk material surrounding the star. This disk is formed as angular momentum is transferred outward while the star contracts. This means that very young stars are about to form planetesimals (progenitors of the planets) which gather gaseous material as they orbit the star in the disk. In the beginning these planetesimals are very small starting from dust grain size and then collecting material till they reach earth mass and even beyond. These planetesimals are believed to form the planets solid core and are collecting gaseous material to form for example Jupiter-like gaseous or rocky Earth-like planets.

From the observational point of view this means that very young stars should not have planets and the planetesimals are small and uniformly distributed. They therefore do not

cause a radial velocity signal. On the other hand around stars approaching the main sequence, planets at some point in the evolution should become observable. It should be possible to detect planets at the red dwarf state of the stars by means of spectroscopic radial velocity search because they should have formed. The reason why no major planet search programs for young stars based on radial velocity measurement have not been carried out yet is the difficulty that these stars usually show stellar spots and variability. For a review in radial velocity search programs and techniques, see Marcy & Butler (2000).

On the other hand young stars are well suited for direct imaging of planets since the planets are young and therefore still contracting which means they will radiate in the infrared and should be easier to detect by direct imaging than old planets.

At the Tautenburg observatory we are carrying out a radial velocity search for planets and on several telescopes around the world which are equipped with an adaptive optics system or a speckle camera we imaged some stars of the sample at the defraction limit of the telescope.

## 5.1   Observations

Two stars, or a star and a planet are orbiting each other and their spectra are therefore periodically red and blue shifted. In a doublelined spectroscopic binary we see the lines of both stars shift periodically relative to each other, while in a single lined spectroscopic binary or a star with a planet in orbit, we only see the spectral lines of the brighter star shift periodically, the spectral signatures of the secondary are not seen at all.

To detect the wobble of a normal star caused by a Jupitermass planet, we need to achieve high precision for the wavelength calibration in the order of a few meters per second. The equipment used in our case is the $2\,\mathrm{m}$ Tautenburg multipurpose Schmidt telescope with an échelle spectrograph of $\Delta\lambda/\lambda = 67,000$ resolving power in the Cassegrain focus. In the light path from the telescope to the spectrograph an iodine absorption cell can be mounted for a precise and stable wavelength reference recorded at exactly the same instrument conditions. The spectrograph is additionally equipped with a white light, flat field lamp and a thorium-argon reference lamp for wavelength reference. The following special calibrations, observation, and reduction steps are necessary:

### Climate and temperature stabilized spectrograph

In order to account for variations in the setup of the spectrograph from one night to the next, there have to be careful calibrations. To refill liquid Nitrogen into the dewar of the camera and to open the dust covers of the mirrors, gratings and prisms one has to enter the spectrograph room. This disturbs the temperature and climate conditions which have to be stable over several nights. Touching the spectrograph might move the optical components slightly. Therefore, after entering the room, the spectrograph has to stabilize for about one to two hours. The room should not be entered after the stabilizing phase. After that we take the usual calibration images (flat, thorium-argon, and bias) and in addition to that, we take images of the flat field lamp with the iodine absorption cell in the light path.

### Standard calibration:

First, the spectrograph has to be wavelength calibrated using the spectrum of a thorium argon lamp. For the flat fielding dedicated flat field images using the white light lamp in front of the entrance slit and nowadays also the white light dome flat lamp is available. These spectra are extracted, wavelength calibrated and divided by the flat-field using the astronomical software package IRAF. The procedure is described in Section 2.4.2.

**The iodine absorption cell**

The iodine absorption cell can be placed in the light path from the telescope to the spectrograph close to the entrance slit. The cell is heated to about 80°C and imposes iodine absorption lines in addition to the stellar spectrum. These lines cover a range of 1500 Å of the échelle spectrum and are always at laboratory wavelength.

The absorption lines of the iodine cell are used to compare to the spectrum of the same iodine cell but observed with the Fourier Transform Spectrograph (FTS) at the Kitt Peak National Observatory near Tucson, Arizona, U.S.A., with a resolving power of $\Delta\lambda/\lambda = 300,000$. We assume that this spectrograph does not have an instrument profile or at least the influence of the instrument profile is negligible.

Now the spectrum of the iodine cell taken in the observing night is unfolded using a Gauss profile until the $\Delta\lambda/\lambda = 300,000$ high resolving power iodine cell spectra is reproduced best. These parameters are the so called instrument profile: the depth and the width of the Gauss profile used, and the shift of the iodine lines.

**The stellar spectrum without iodine cell**

We need at least one template spectrum of the star at a resolving power of $\Delta\lambda/\lambda = 300,000$ and without the signatures of the instrument used. The would be best if the spectrum was observed with the FTS spectrograph. In practice this is not possible because the efficiency of the FTS spectrograph is too low. Observing a spectrum of the sun already takes 15 minutes. Extrapolating this to stars of magnitude eight, it would take several nights to obtain the spectrum.

The solution is to observe a template spectrum without the iodine cell in the light path and which has a signal-to-noise ratio of at least 100, better 200 or 300. This spectrum is now unfolded to a resolving power of $\Delta\lambda/\lambda = 300,000$ using the related instrument profile of the observing night determined by the spectrum of the iodine cell as described before. This spectrum serves as the stellar template in the radial velocity measurement. We only need to observe and unfold this spectrum once.

**The stellar spectrum with iodine cell**

During each observing night, we must observe the star with the iodine cell in the light path. A signal-to-noise ratio of about 100 is sufficient. For the active stars it could be shown that it is better to observe the star more often with shorter exposures than to have one well-exposed spectrum. The main error source in the radial velocity measurement is the stellar activity and not the signal-to-noise ratio of each spectrum.

## 5.2   Data analysis

The template spectrum of the star and the template spectrum of the iodine cell both with the same resolving power of $\Delta\lambda/\lambda = 300,000$ are shifted, coadded, and then folded with the instrument profile of the observing night until they reproduce the observed stellar spectrum with superimposed iodine absorption lines. Free parameters are the following: the instrument profile (3 parameters), the offset and the slope of the continuum (2 parameters), and the radial velocity shift of the spectral lines (1 parameter).

The iodine absorption lines cover a wavelength range of 1500 Å. The spectrum is divided in 300 chunks of 5 Å length each 100 pixels long. For each chunk the above described determination of the 6 parameters is done. This results in 300 independent and simultaneous measurements of the radial velocity. For the final radial velocity shift the mean value of

these 300 measurements is taken. The spread of the 300 independent measurements actually resembles the measurement accuracy. The accuracy for inactive stars with this method is $\sim 5\,\mathrm{km/s}$.

Depending on the activity level this value can decrease. A solution is to take a number of spectra with a long time baseline. The radial velocity signal will be stable if the star is indeed a binary. The activity will only be stable for a short time, e.g. flares decline after hours, spots could live longer but they also change on the surface as the star rotates. Some spots are known to have a life time of years but this is not the normal case. Any activity known up to now declines after some time. Spots can be excluded by studying the change of the bisector of the spectral lines.

## 5.3   Error sources

As already discussed above there are several sources of error in the radial velocity measurement. The effects of stellar activity on the radial velocity measurement will be described and a solution to achieve a reliable measurement in spite of these effects will be presented.

### 5.3.1   Stellar spots
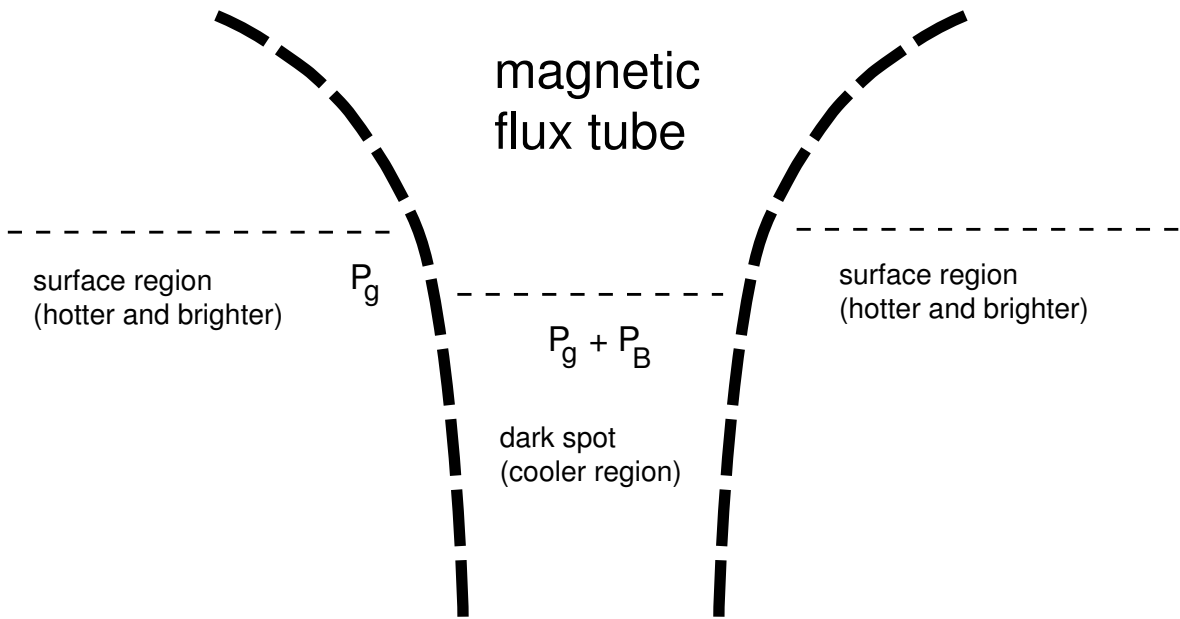


**Figure 5.1:** Stellar spots are cooler than the surrounding stellar surface and therefore appear dark. The stellar spots are the footpoints of the magnetic field lines which are emerging on the stellar surface. Often they are associated with bright regions and with the flare activity of the star.

Stellar spots are regions of the stars which are cooler than the rest of the surface. Temperature differences of several $100\,\mathrm{K}$ can occur. On the surface of the sun these spots can sometimes be seen by eye. For the sun an activity cycle of two times 11 years could be established. In fact the activity cycle is about 22 years which are needed to reconfigure the magnetic field of the sun to its initial value. By Doppler imaging methods, it could be shown that stars exhibit cool stellar spots. In some cases the spots are much bigger than the solar spots and could cover a large fraction of the surface.

As the star rotates around its axis, the spot rotates with it. The spot appears on one side of the star. The region of the spot is several hundred Kelvin cooler than the surrounding medium, so that the star emits less light in this region than in a region without a spot. The other brighter side of the star without a spot moves away from us. The spectrum appears to be red shifted. As the spot moves along the surface it approaches the other side and begins to disappear. On the other side of the star the brighter unspotted region now approaches us and the stellar spectrum seems to be blue shifted.

It is very unusual that only one spot is on the surface but even if this is the case, measurements spanning several months or even years could rule out this error source. If the possibility of observing a radial velocity signal due to stable spots should be ruled out, imaging of the star in several filter bands over several nights, best over at least spanning the time of one full rotation of the star could reveal the spots. Additionally, information of the rotation period of the star can be achieved in this way.

## 5.3.2 Plage regions

It is known that stellar spots as well as solar spots are associated with bright plage regions. On the sun during an activity period these plage regions can be observed. The main cause for this is the magnetic field of the star. For a review on sources for activity see Stix (2002).

The effect of these bright regions of the star acts opposite to the effect of a dark spot. As the bright region rotates with the star it appears at one side of the star and is blue shifted. As it disappears on the other side, it is red shifted.

**Convection**
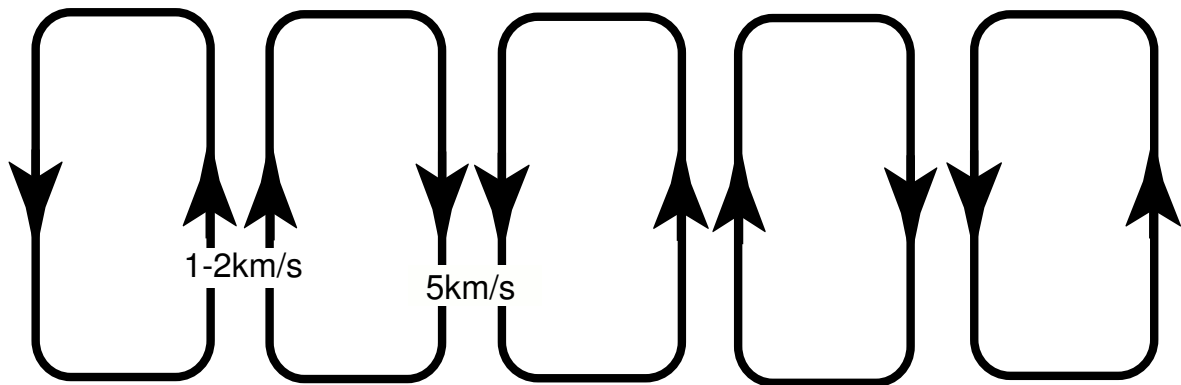


**Figure 5.2:** Convective motion on the star produces irregularities on the stellar surface the socalled convection cells. They can be seen in Fig. 5.3.1 outside the dark sun spots. If the convection cells are homogeneously spread over the complete surface of the star they will not add additional noise to the radial velocity signal. But together with a magnetic field convection can increase and cause variability.

All late type stars are known to have a convection layer on the surface. Convection transports hot material from the center of the star in flux tubes to the surface. The center of the convection cell is therefore hotter and brighter than it would be without convection. On the edges of the convection cell cooler gas is transported to the inside of the star. These regions of the surface appear darker. The speed for the upward flow is 1-2 km/s and for the downward flow 5 km/s observed on the sun. The bright regions therefore expand.
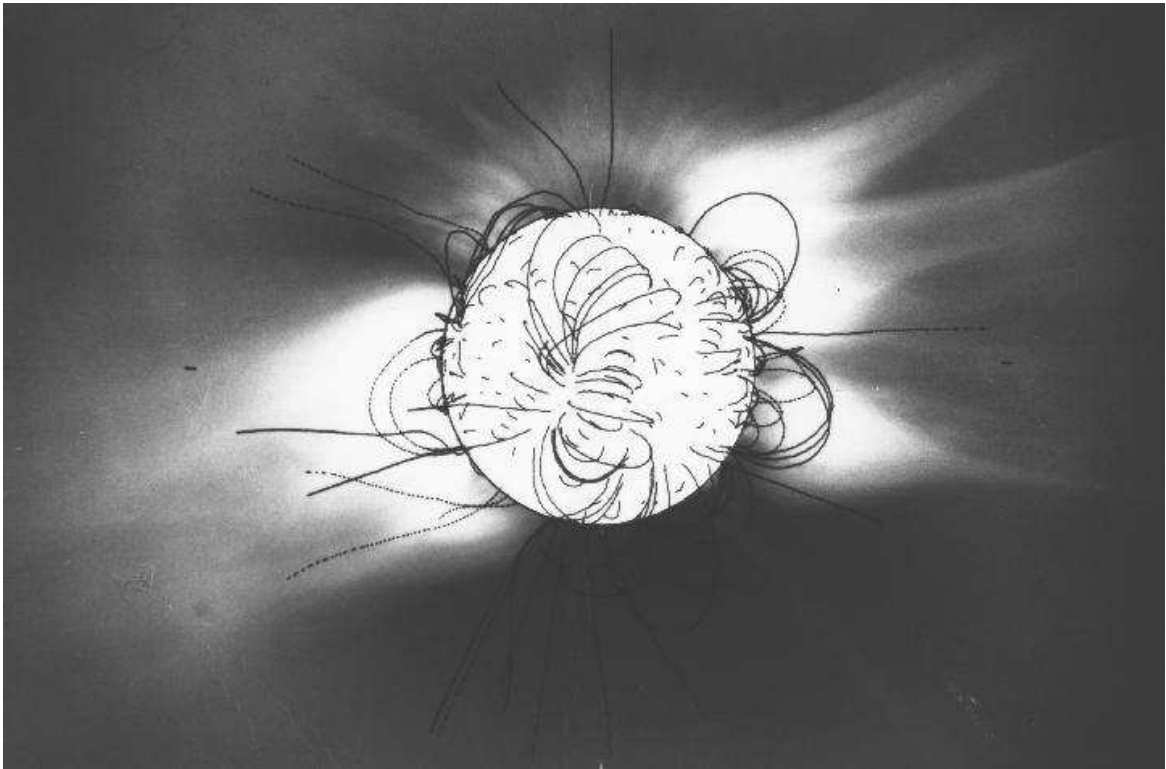
**Figure 5.3:** A schematic view of the principal magnetic field line configuration of the sun. Especially the magnetic loops are shown, underlayed is an image of the corona of the sun (wide extended filaments), a photograph of the eclipse of 30 June 1973 (Altschuler et al., 1977).

### Magnetic field

The existence of a magnetic field on the sun and on stars can be measured e.g. by Zeemann splitting of magnetically sensitive spectral lines. The magnetic field lines are frozen into the plasma and are drawn with the movement of the plasma. On the sun the surface rotates differentially meaning the equator region rotates faster than the poles. The magnetic field which is coupled to the plasma is therefore twisted up and as it becomes stronger it emerges at the surface. The characteristic plasma loops can be observed. In the footpoints of the magnetic field lines on the surface of the star, we observe the dark spots. These are cooler regions without convective motion.

In the cooler regions which are less dense the gas pressure and the magnetic pressure are both present compared with the region outside where only the gas pressure is valid. The gas density in the spots decreases and we see a region of greater optical depth.

### On the border of convection and dark spots

On the sun it can be observed that the field lines always move to the cooler downward motion regions in the convective cell. The downflow is established along the magnetic field lines because the plasma cannot cross the magnetic field lines. As the gas moves downward it is in contact with the even cooler dark spot. The downward moving gas is additionally cooled and it speeds up. It can reach speeds from 7 km/s to supersonic speed.

On the other hand the upward motion does not increase. This means that the cooler regions get smaller and the hotter regions expand. This effect can produce large hot regions which induce additional variability. This kind of variability is difficult to identify.
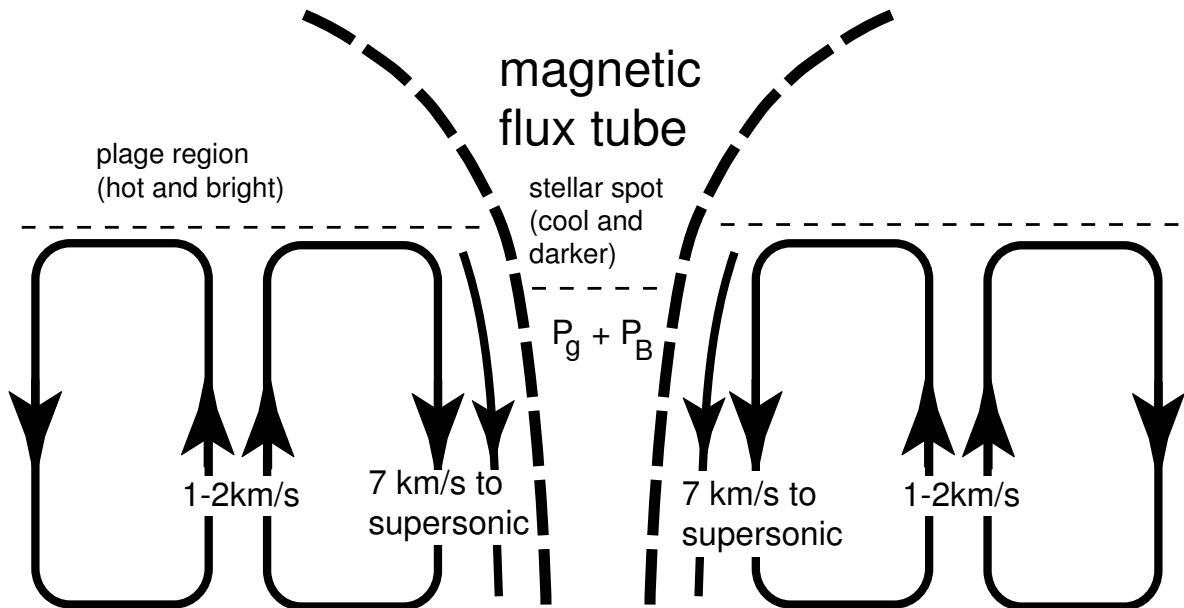
**Figure 5.4:** The schematic view shows the principal conditions how plage regions are associated with the magnetic field and the convective motion of the atmosphere of the star. As the magnetic field lines are forced to leave the surface, the footpoints on the surface soon move to cooler regions of the convection cells where the gas is transported to the inner part of the star. In the center of the dark spot the gas is even cooler than the gas moving downward by convective motion in the convection cell. It is not mixed because the magnetic field lines separate the different regions and plasma cannot move perpendicular to magnetic field lines. The downward moving gas is in contact with the cooler gas in the spot. That leads to additional cooling and the downward motion of the gas increases to speeds from $7\,\mathrm{km/s}$ to supersonic speeds. The upward motion by contrast stays the same with a speed of $1$-$2\,\mathrm{km/s}$. This means the bright regions expand and the cool regions shrink in size.

### $\alpha$-$\Omega$ Dynamo

The combined action of differential rotation and helical convection on the magnetic field in the convection zone of late type stars is called $\alpha$-$\Omega$-dynamo. Such a dynamo is believed to sustain a cyclic large scale magnetic field, like the Sun's 22 year magnetic cycle and it is also believed to be responsible for the flaring activity of these active stars such as T Tauri stars or flare stars.

### 5.3.3 Solution

Spectral lines are sensitive to plage regions and to stellar spots. The line profile of all spectral lines becomes asymmetric. As the star rotates, the asymmetry of the lines changes. Especially the calcium H & K lines are very sensitive. The bisector of all available absorption lines should be monitored for all observed spectra for this test.

A measurement with a long time baseline can also help to provide a reliable radial velocity curve. Most plage regions and stellar spots are only stable for some days or weeks. But one has to be careful. As Vogt et al. (1987) and Neuhäuser et al. (1998) have shown, there are stars which can have stable spots over several years. With Doppler imaging of e.g. P1724, such spots could be found. Measuring the radial velocity shift over more than one rotation period can help detect the periodic signal and distinguish it from the short time variations due to activity. With a long time baseline and the monitoring of the bisectors of the spectral
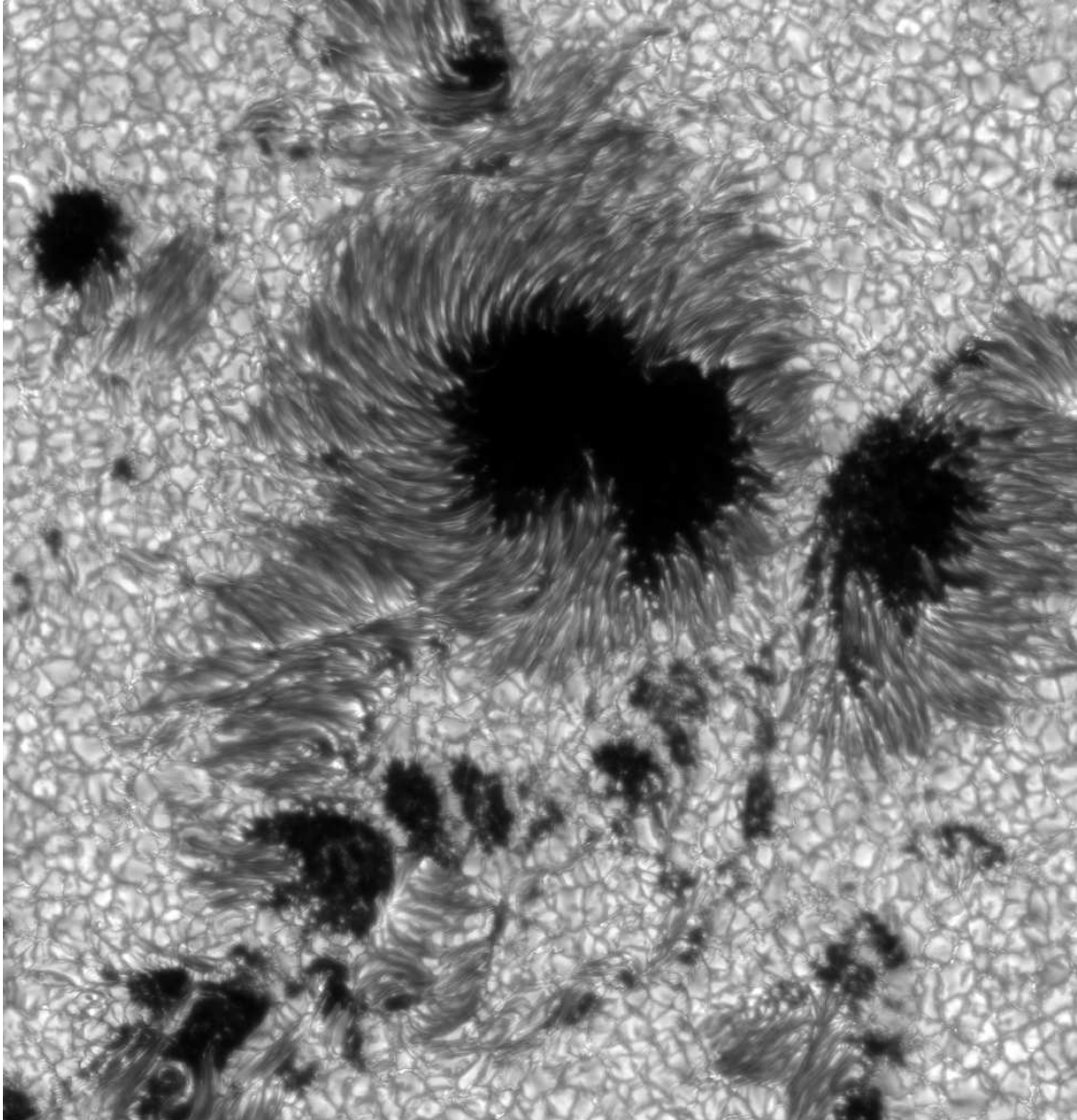
**Figure 5.5:** Large field of view image of sunspots in Active Region 10030 observed on 15 July 2002 observed with the new Swedish 1 m solar telescope at the Canary Islands on La Palma. In the image the dark spots and the convection cells can be seen. The view from top does not allow one to see the magnetic flux tubes and the plage regions would be located outside the image. Publication with credit to the Royal Swedish Academy of Sciences.

lines, one can be confident that the shortterm variations do not affect the mean 'real' radial velocity signal too strongly.

## 5.4   Results

During bright times the Tautenburg telescope is used for spectroscopic observations. Each month several nights of observation time are available. But as we all know the weather also plays an important role and in Germany it is not guaranteed that one can observe continuously due to the weather conditions. The radial velocity observations are now ongoing for over one year but we need to continue them for at least one more year.

| name | RA | DEC | Spec [mag] | V | points [m/s] | $\sigma(RV)$ |
|---|---|---|---|---|---|---|
| HD 17925 | 02 52 32.129 | -12 46 10.96 | K2 | 6.1 | 20 | 31.6 |
| V891 Tau | 04 15 25.787 | +06 11 58.76 | G8V | 6.9 | 14 | 18.9 |
| HIP 73555 | 15 01 56.762 | +40 23 26.04 | G8 | 3.5 | 24 | 9.6 |
| HIP 114379E | 23 09 57.362 | +47 57 30.14 | dK0e | 6.0 | 12 | 15.0 |

The selection criterion for the stars are the following for the observations in Tautenburg: Young flare stars which are brighter than 8 magnitude in the V-band located in the northern hemisphere ($\delta \geq -10°$). The youth of the star has to be confirmed by its location in the Hertzsprung-Russell diagram and by spectroscopic age indicators such as the lithium absorption line at 6707 Å. But we have to take care: It has been shown that lithium can be produced in stellar flares meaning that lithium in the spectrum could also be visible in the spectrum of an old active star.

With the first year of observations done, one can clearly detect nonvariability, meaning boring inactive single stars without companions. These stars have been found and examples will be shown. Two other stars are double lined spectroscopic binaries (SB2). For SB2 the radial velocity search method does not work well. The cross correlation technique with a template spectrum observed at a certain orbital phase of the double lined spectroscopic binary, will not match the spectrum at another orbital phase because the spectral lines of the binary are shifted relative to each other and in opposite directions. Therefore, a correlation with this template file would only produce a match when the stars are again at the same orbital phase as they were when the template was observed.

For the stars which show variations in some cases nonperiodic variability was found. Overlayed on this variability could be a periodic radial velocity signal but the results are at this moment still unclear.

In some other cases there is a clear periodic signal. In those cases the variability of the star itself causes a huge scatter of the data points and a good solution of the orbit will need at least one more year of observations.

**HD 17925, [GKL 99] 82, HIP 13402**
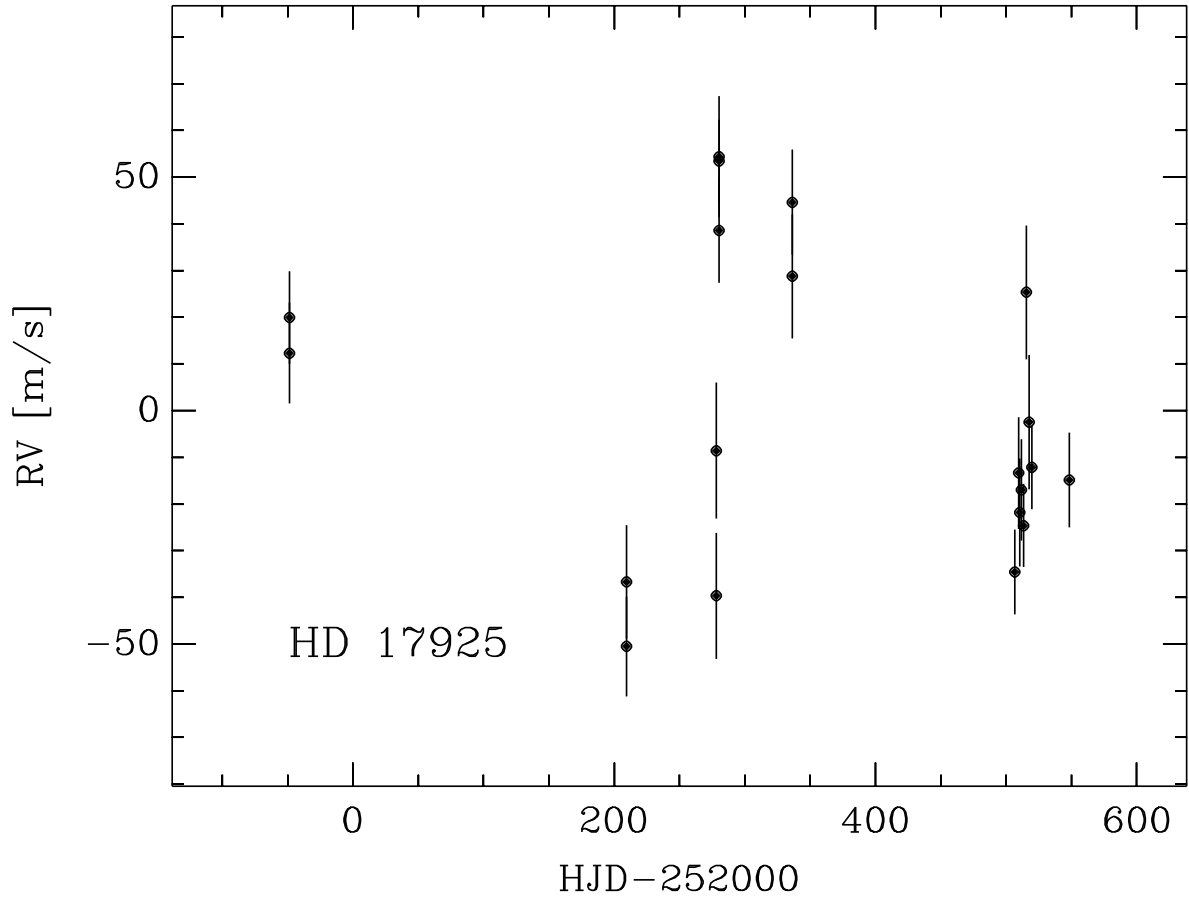


**Figure 5.6:** The radial velocity curve measured with the Tautenburg échelle spectrograph of HD 17825. The star is known to exhibit large spots and shows flares. As can be seen in the radial velocity curve the 'noise' of the signal is high compared to the nominal accuracy of about $5\,\text{m/s}$ which can be archived with the instrument.

Nidever et al. (2002) list the star with a constant radial velocity of $RV = 18068 \pm 3\,\text{m/s}$ whereas in our radial velocity measurements, the star indeed shows a variation of $\sigma(RV) = 31.6\,\text{m/s}$. This radial velocity variation level can be due to stellar activity.

**V891 Tau, [GKL 99] 109, HIP 19855**

V891 Tau shows radial velocity variation of $\sim 50\,\mathrm{m/s}$ measured from peak-to-peak. There is
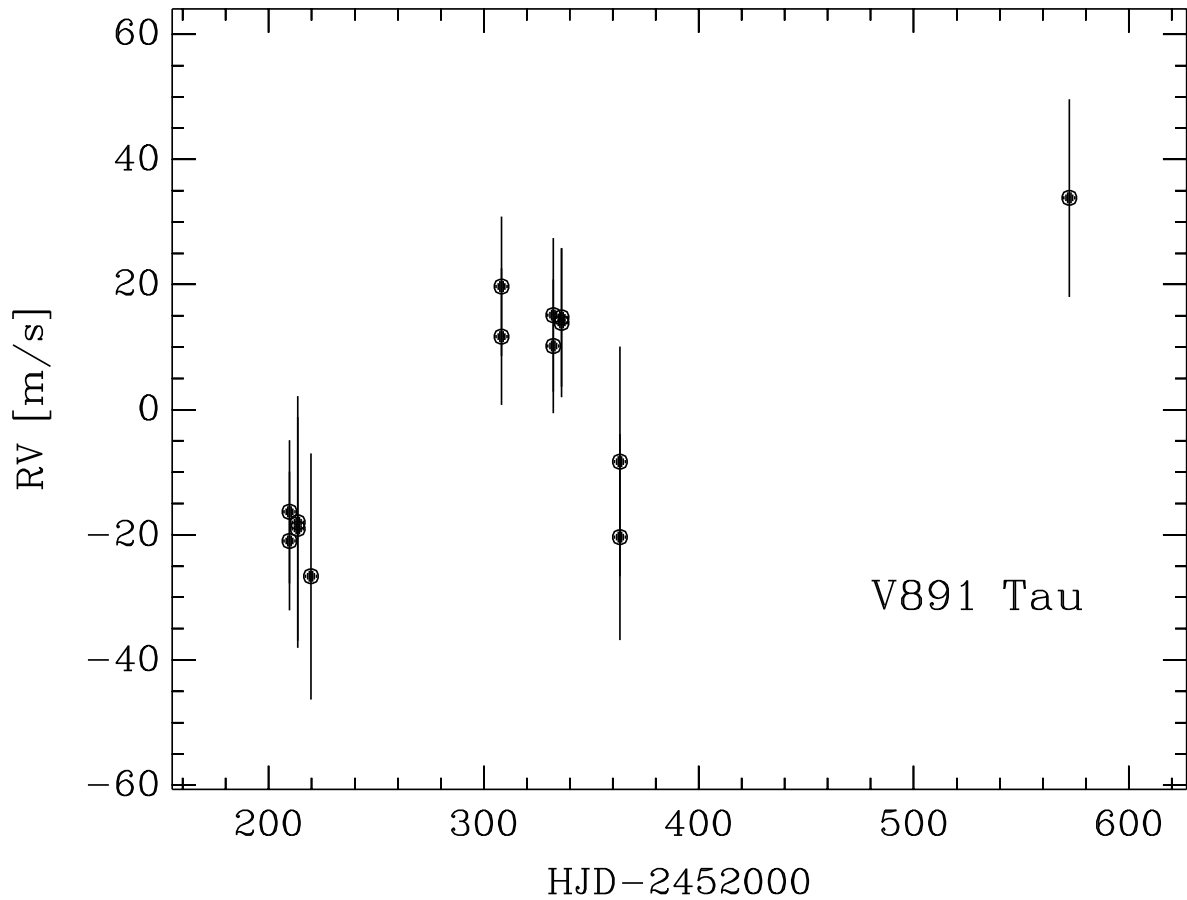


**Figure 5.7:** The radial velocity curve measured with the Tautenburg échelle spectrograph of V891 Tau. The star is known to exhibit large spots and shows flares. As can be seen in the radial velocity curve the 'noise' of the signal is high compared to the nominal accuracy of about $5\,\mathrm{m/s}$ which can be archived with the instrument.

no periodic signal visible in the data and the variation which can be seen is due to spots and plage regions on the surface.

**HN Peg**
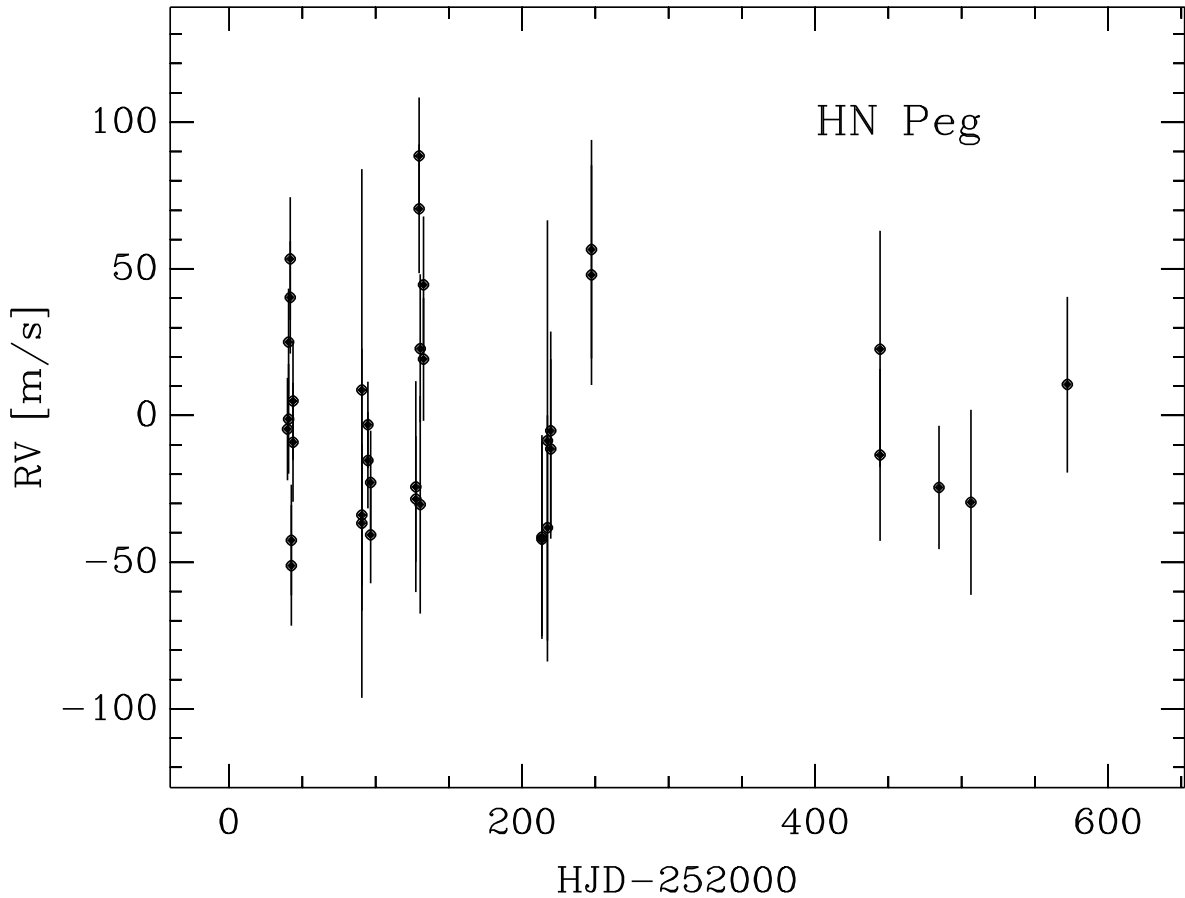


**Figure 5.8:** The radial velocity curve measured with the Tautenburg échelle spectrograph of HN Peg. The star is known to exhibit large spots and shows flares. As can be seen in the radial velocity curve the 'noise' of the signal is high compared to the nominal accuracy of about $5\,\mathrm{m/s}$ which can be archived with the instrument.

The high radial velocity variation of the signal gives the imression that this star could host a planet. HN Peg shows a $\sim 100\,\mathrm{m/s}$ peak-to-peak variation. This variation is coupled to the rotation period of the star which then leads to the natural explanation that the star shows huge spots and plage regions. The bisector of the spectral lines also changes periodic with the rotation period of the star which is another hint that the radial velocity variation is coupled with stellar activity.

**HIP 114385**
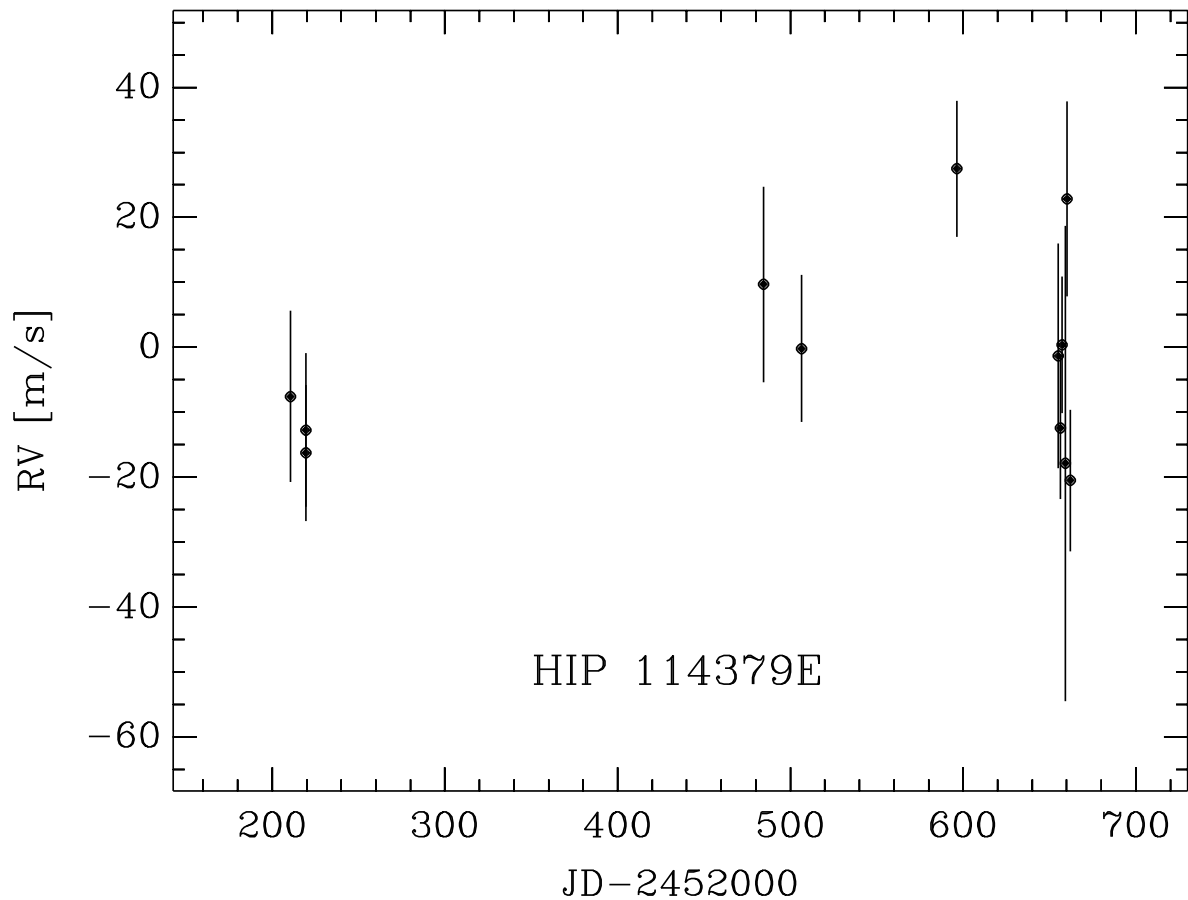


**Figure 5.9:** The radial velocity curve measured with the Tautenburg échelle spectrograph of HIP 114385 (First we gave it the designation HIP 114379 E because there were some confusions identifying the star). This is the visual comoving companion to the flare star HIP 114379 which is known to be a single star. As can be seen in the radial velocity curve the 'noise' of the signal is high compared to the nominal accuracy of about 5 m/s which can be archived with the instrument.

The radial velocity variations are of the order of 50 m/s which do not show any periodicity over the observing time span. They can easily be explaned by surface variability of the star.

**Radial velocity histogram**
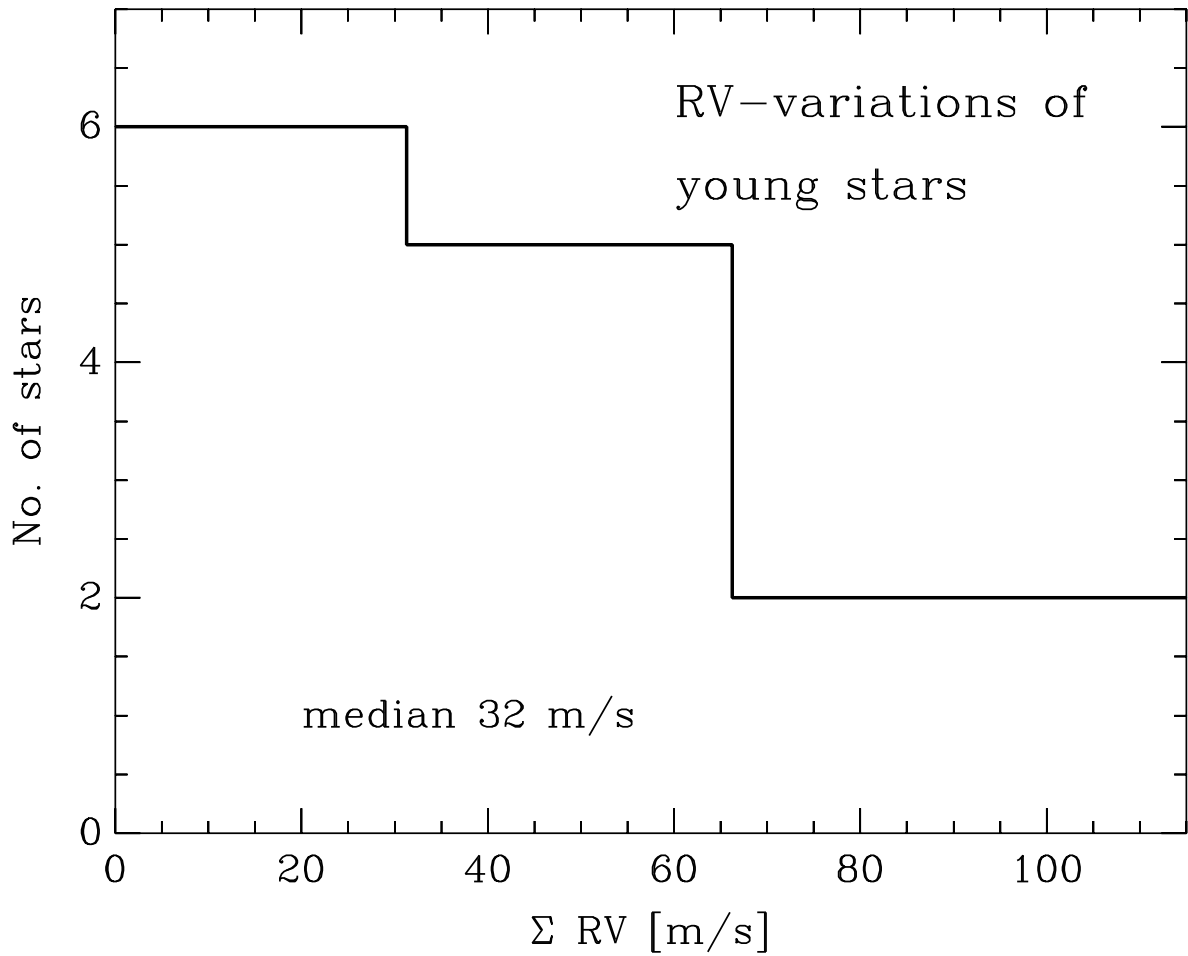


**Figure 5.10:** A histogram of the radial velocity variations of all young stars included in the radial velocity monitoring program. Radial velocity variations of 30 m/s can easily be explained by spots and plage regions on the star. The flare stars listed above are included in this sample.

All the young stars of our show small radial velocity variations which are in most cases coupled with the period of the star. These radial velocity measurements can be explained by spots on the stellar surface. As one can see in the histogram of all the young stars of our sample the variability of the flare stars is not unusual.

# Chapter 6

# Résumé

The aim of this PhD thesis was to find young nearby, stars within 100 pc, to review the understanding of local starformation, to understand young stars in an intermediate phase between the T Tauri phase and the main sequence phase, and to find targets for the direct imaging search for planets. The tools used therefore are high- and low resolution spectroscopy, where the high resolution spectra are used to perform a spectral synthesis analysis. The methods and reliability of such an analysis of the G- and early K-type stars of the sample has to be established. We have shown in this thesis that it is possible to analyze these active stars using spectral synthesis analyses with the same accuracy as it can be done for inactive main sequence stars.

As a byproduct, this search and analysis of young stars enables us to identify stars which are optimal in order to study planet formation directly. The idea for the direct imaging search was the following: Planets form in a disk surrounding the star and they need time to develop. After the dissipation of the disk material we should be able to immediately observe planets around those young stars. Around such a young star the planet is also young and still contracting. It emits infrared light and could therefore be much easier to detect by direct imaging methods than around a more evolved star. We started a program with the VLT and the adaptive optics system NAOS/CONICA of imaging possible (sub)stellar companions around the young stars of this sample. By now the first epoch images are taken and companion candidates are identified. Depending on the proper motion of the star, second epoch images must be taken in the next years.

The way to find stars in an intermediate evolutionary phase is not as easy as to identify very young objects, because in the spectrum of these stars prominent features such as H$\alpha$, calcium H & K -, magnesium Ib emission or a strong lithium absorption line at 6707 Å, together with infrared excess indicating surrounding disk material are missing. Though these stars might still be found in associations, e.g. the Ursa Major Association (maybe a little older than the stars we are looking for). A combination of lithium absorption as well as H$\alpha$, calcium, and magnesium Ib line filling in is used to identify these stars and estimate the age. Placing them into a Hertzsprung-Russell diagram and comparing their position with the theoretical tracks and isochrones gives a second method to estimate the ages.

## 6.1   The Sample

Gershberg et al. (1999) compiled a catalog of stars (Gershberg catalog) all of which show flares in different wavelength ranges. The catalog is supposed to contain only the socalled red dwarf flare stars. These flare stars are thought to be the missing link between the T Tauri phase and the main sequence phase of a star. The stars are in a quiescent phase similar to

normal main sequence stars but in flare phase they the show signatures of young stars, e.g. core emission in H$\alpha$, calcium, magnesium, X-ray emission, and infrared excess. Regarding these signatures, the stars are thought to be at least as young as the Pleiades, which means the F-, G- and K-type stars in the sample should still show the lithium absorption at 6707Å as a prominent feature. Though lithium is not a very reliable indicator, as it can be destroyed fast in close binaries, we can use it as one signature which is easy to identify. In case we find a strong lithium absorption line, we still have to be careful since lithium could be produced in stellar flares.

## 6.2   Evaluation of the sample

The Gershberg catalog is the base of the search, since it has a uniform criterion which is used to identify the stars. The criteria Gershberg used must be evaluated. Therefore, we took both spectra with high resolving power of $\Delta\lambda/\lambda = 60,000$ at Calar Alto, Spain using the FOCES spectrograph mounted on the 2.2 m telescope and the échelle spectrograph of the Thüringer Landessternwarte at Tautenburg with resolving power of $\Delta\lambda/\lambda = 67,000$, as well as spectra with low resolving power of $\Delta\lambda/\lambda = 5,000$ also from Calar Alto using the focal reductor instrument CAFOS at the 2.2 m telescope for the northern part of the sample. For the southern part we used DFOSC, a focal reductor instrument mounted on the Danish 1.5 m telescope located at ESO La Silla, Chile, with a resolving power of $\Delta\lambda/\lambda = 6,000$ when used in échelle mode.

The high resolution FOCES spectra of the F-, G-, and K-stars of the sample were used to perform a spectral synthesis analysis. A grid of model atmospheres was calculated using the model atmosphere code of the Gehren group developed at the Ludwig-Maximilian-Universität, Munich and called MAFAGS (Model Atmospheres for F- and G-stars). Temperatures of the stars were derived fitting models of the H$\alpha$- and H$\beta$-line to the wings of the observed spectra. After that the iron abundance as well as the surface gravity $\log g$ was measured using the ionisation equilibrium of iron I and iron II. The so derived surface gravity was compared with the surface gravity measured by the magnesium Ib lines after fixing the magnesium abundance. For all the stars at least two high resolution spectra were taken to revise the analysis. Although the cores of the Balmer lines are filled in, an estimate of the effective temperature is still possible with high accuracy. Compared with the measurements of other authors using e.g. the infrared flux method, narrow band photometry or high resolution spectroscopy, we could achieve reasonable results. In case of HIP 73555 the temperature estimate could even be double checked because an interferometric radius measurement was published. The radius we predict for the subgiant HIP 73555 compared with the measured radius were identical within the error bars. Surface gravity was estimated in two ways: First using the iron I/II ionisation equilibrium after fixing the iron abundance and the effective temperature and second using the wings of the gravity sensitive magnesium Ib lines. A double checking of the estimated surface gravity can easily be done by calculating the socalled spectroscopic distance which mainly depends on the surface gravity. In our analysis the discrepancy of the spectroscopic to the independent parallax measurement performed by the Hipparcos mission was for all stars below the 2$\sigma$-error level.

The low resolution spectra were observed mainly for the M-type stars (which are too faint for high resolution spectroscopy) and also in the south because there was no instrument with higher resolving power available. The spectra are used to search for prominent features such as the lithium absorption and the filling in of the H$\alpha$-, calcium H & K- and magnesium-lines, depending on the spectral range covered (north: 5500 - 6800 Å, south: complete optical range). The spectra were also used to determine the spectral type, since the spectral type listed in the Gershberg catalog was compiled from different sources, for some stars it was previously

derived using only the color information. To identify and measure the very small features in the low resolution spectra such as the Hα-line filling in, the true continuum must be known very precisely, also to compare the results with the high resolution spectra. Therefore, the spectra of some stars were taken from Calar Alto with FOCES and from La Silla with DFOSC to compare the results directly. The comparison was not successful because the resolution of the DFOSC spectra was too low and the noise level too high. The continuum was not well established for the DFOSC spectra because of the flat field procedure. Stellar parameters derived with the DFOSC and CAFOS spectra are comparable to narrow band photometry data.

Among the apparently younger stars observable from the north, a radial velocity search for planets is going on. The idea for that is simple, the time scales for planet formation are not completely clear: Planets around a star are supposed to be formed in a disk. So in principal the disk must be optically thin or have formed a planet. Since it is not easy to perform a radial velocity search on active stars (the younger the more active) because stellar spots and flares might mimic an orbiting object, long term measurements of several periods must be carried out, and the stars must be observed more frequently. Flares arise and decline on timescales of minutes to hours, so observations of the same star in short time intervals can help identify outliers due to flare activity. The equipment we use for these observations is the Tautenburg échelle spectrograph ($\Delta\lambda/\lambda = 67,000$). In the light path an iodine cell can be mounted to superimpose iodine absorption lines for precise wavelength calibration. The young stars of our sample show a high level of activity. The currently available data allows us to conclude that in principle we should be able to detect a significant radial velocity signal. For the stars where enough data points are available we conclude that the stars do not host a companion with short orbital period. For some other stars there might be a periodical signal but it is not yet confirmed. In addition to that, we also want to detect planets with a longer period. Therefore, we must continue this survey for the next years.

Around the stars within 100 pc and which show significant signs of youth, we also searched for planets by direct imaging techniques. The main reason to target young nearby stars is to achieve sufficient angular resolution at a high dynamical range. If the star is young, the planet(s) in orbit of the star is (are) still young. It is still contracting because its formation process has not come to a halt and it should therefore be bright in infrared light (Burrows et al., 2001). The search is ongoing and we have showed some images of companion candidates which still have to be confirmed by proper motion and/or spectroscopy. The star HIP 108405 A is the youngest star in our sample. It is located at a distance of about 16 pc closer to the sun than GJ 182 which is at about 27 pc. A planet around an M-type star such as HIP 108405 A and with a mass of $5\,\mathrm{M_{Jup}}$ and at a projected separation of 1" would be detectable with available adaptive optics systems on 8 to 10 m class telescopes such as VLT or Keck. The magnitude difference, $\Delta K$, is around 8 to 14 mag.

## 6.3 Results

As a general conclusion, the sample is very inhomogeneous, meaning e.g. that among the G-stars, one star was a young subgiant and not a pre-main sequence star as demanded by the definition of flare stars. For the G- and early K-type stars the detailed spectral synthesis analysis could help identify the true younger stars of the sample also by establishing a secondary age scale using spectroscopic signatures as the Hα-line filling in of the cores, as well as the magnesium Ib and calcium line filling in or for the even younger ones core emission, which is produced by surrounding material.

The spectral synthesis analysis of these stars has shown that it is possible to analyze flare stars and derive precise stellar parameters using the methods described by Fuhrmann et al.

(1998). Especially the core filling in of Hα and the magnesium Ib lines does not affect the wings of these lines. Before performing the analysis, we expected to measure too low $\log g$ values, because the iron II lines compared with the iron I lines could slightly be filling in and which would mimic too low $\log g$ values. But the spectroscopic distances derived with our measured stellar parameters ($\log g$, $T_{\text{eff}}$, [Fe/H]) compared with the parallax measurements of the Hipparcos satellite shows, that there is no such problem.

The ages of the M-stars when placing them into a Hertzsprung-Russell diagram reveal stars at very different stages of evolution. But the error bars for these stars are much larger since we derive the temperature by a spectral type temperature conversion and the distances to the stars might be more uncertain due to the lack of Hipparcos measurements for most of the stars. Additionally, some might be yet unknown close binaries. The M-stars are widely spread when placing them into an Hertzsprung-Russell diagram, from places which are occupied by classical T Tauri stars down to regions which are occupied by evolved (main sequence) M-stars. Some (but not all) of the apparently younger M-stars exhibit lithium absorption and Hα emission with equivalent width of around 0.1 to 0.3 Å, i.e. the stars we were searching for. The other M-stars which lie close to the main sequence are more evolved and therefore not members of the sample. Why they exhibit flares in different wavelength range could not be cleared up in this survey. To understand this we need to measure and understand the magnetic field configuration of these stars. But we lack magnetically sensitive lines in our spectrum, so this question cannot be addressed.

We have identified at least 17 young pre-main sequence stars in the flare star catalog. One of them is the youngest and closest star: HIP 108405 has an age of 10±10 Myr and is located at a distance of 16.1 pc. The next closest young star is GJ 182 located in 27 pc at an age of 20 Myr. For our sample, we can clearly say, except the stars that were confused like the white dwarfs and the subgiants, all other stars are at least zero-age main sequence stars.

Some of the flare stars of the Gershberg catalog are located in the line of sight to the TW Hydra, the Horologium-Tucana, the $\beta$ Pictoris, the Ursa Major, the Hercules-Lyra association, as well as to the Pleiades supercluster, and the Hyades cluster. In most cases the flare stars are foreground objects not related to the association, but one star is located in the TW Hydra Association, at the same distance, with spectroscopic indicators and space motion rejecting the membership in the TW Hydra Association but establishing the membership to the Pleiades supercluster. Further, the star is a multiple system typical for a young star (König et al., 2003). Some flare stars in the $\beta$ PicA, and the Hor-TucA were already proposed as bona-fide members, some others were proposed as member candidates. We can confirm the youth of these member (candidates) by our spectra. Most of the flare stars have an age consistent with the Pleiades or even older. The membership of these stars to the Hyades, or to the even older Ursa Major and Hercules-Lyra association is therefore reasonable.

During the imaging search, we have detected the companion of $\chi^1$ Orionis. With the published radial velocity and astrometric measurements by Han & Gatewood (2002), we are now able to calculate dynamical masses of the two components only using Kepler's law. These masses enable us to pose a new constraint on the age measurements of the Ursa Major Association or on the other hand to test low mass pre-main sequence evolutionary tracks and isochrones (see König et al., 2002). In the case of $\chi^1$ Orionis B, the test of the pre-main sequence isochrones gives a unique possibility: Because the star is a member of the Ursa Major association we have the possibility to derive ages and to calibrate the pre-main sequence models. The result of this test is that for a low mass star ($0.15\,\text{M}_\odot$) the predicted age is lower (100±30 Myr) than the predicted age of the Ursa Major association (300-500 Myr) or the cooling models of the white dwarf companion of Sirius (200±30 Myr). This kind of test has to be performed for all masses. Anyway, these tests show that the pre-main sequence models might in general underestimate the ages of the stars. The ongoing direct imaging search for

visual companions to other flare stars will soon produce results after we will have obtained the second epoch images. Without a confirmation we cannot conclude if the companion candidate is a real bound companion to the star.

We have carried out the first radial velocity measurements with a sample of young active stars. From the available data we can conclude that we are in principle able to detect a significant signal of a planet in orbit of such a star. The variations we have seen up to now are caused by the variability of the stars observed. Periodic variations could have been detected in one object but are not yet confirmed by a second epoch observation. Stars with a long orbital period ($> 1$ year) cannot be found with the available measurements because the search is now ongoing for only about one year.

# Bibliography

ABIA, C., REBOLO, R., BECKMAN, J. E. & CRIVELLARI, L., 1988. Abundances of light metals and NI in a sample of disc stars. *Astronomy and Astrophysics*, **206**, 100–107.

ADAMS, J. D., STAUFFER, J. R., MONET, D. G., SKRUTSKIE, M. F. & BEICHMAN, C. A., 2001. The Mass and Structure of the Pleiades Star Cluster from 2MASS. *Astronomical Journal*, **121**, 2053–2064.

ALLARD, F., HAUSCHILDT, P. H., ALEXANDER, D. R., TAMANAI, A. & SCHWEITZER, A., 2001. The Limiting Effects of Dust in Brown Dwarf Model Atmospheres. *ApJ*, **556**, 357–372.

ALTSCHULER, M. D., LEVINE, R. H., STIX, M. & HARVEY, J., 1977. High resolution mapping of the magnetic field of the solar corona. *Solar Physics*, **51**, 345–375.

AMBARTSUMIAN, V. A., 1954. Flare stars. *Comm. Byuarkan Obs.*, **13**, 3.

AMBARTSUMIAN, V. A., MIRZOYAN, L., PARSAMIAN, E. S., CHAVUSHIAN, O. S. & ERASTOVA, L. K., 1970. Flare stars in the Pleiades. *Astrofizika*, **6**, 7–30.

ANDERS, G. J., COATES, D. W., THOMPSON, K. & INNIS, J. L., 1991. Evidence that the active stars HD 102077 (V 838 Cen) and HD 139084 (V 343 Nor) are members of the Local Association. *MNRAS*, **252**, 408–413.

ANDRE, P. & MONTMERLE, T., 1994. From T Tauri stars to protostars: Circumstellar material and young stellar objects in the $\rho$ Ophiuchi cloud. *ApJ*, **420**, 837–862.

BAKOS, G. Á., SAHU, K. C. & NÉMETH, P., 2002. Revised Coordinates and Proper Motions of the Stars in the Luyten Half-Second Catalog. *ApJS*, **141**, 187–193.

BARAFFE, I., CHABRIER, G., ALLARD, F. & HAUSCHILDT, P. H., 1998. Evolutionary models for solar metallicity low-mass stars: mass-magnitude relationships and color-magnitude diagrams. *Astronomy and Astrophysics*, **337**, 403–412.

BARRADO Y NAVASCUÉS, D., STAUFFER, J. R., SONG, I. & CAILLAULT, J.-P., 1999. The Age of beta Pictoris. *ApJL*, **520**, L123–L126.

BELL, R. A. & GUSTAFSSON, B., 1989. The effective temperatures and colours of G and K stars. *MNRAS*, **236**, 653–707.

BERNKOPF, J., 2001. *Untersuchungen zur Altersbestimmung von hauptreihenahen kühlen Sternen*. Ph.D. thesis, Ludwig-Maximilians-Universität München, Fakultät für Physik.

BESSELL, M. S., 1993. Photometric Systems. In *IAU Colloq. 136: Stellar Photometry - Current Techniques and Future Developments*, 22.

BINNEY, J. & TREMAINE, S., 1987. *Galactic dynamics*. Princeton, NJ, Princeton University Press, 1987, 747 p.

BLACKWELL, D. E. & LYNAS-GRAY, A. E., 1994. Stellar effective temperatures and angular diameters determined by the infrared flux method (IRFM): Revisions using improved Kurucz LTE stellar atmospheres. *Astronomy and Astrophysics*, **282**, 899–910.

BOESGAARD, A. M. & FRIEL, E. D., 1990. Chemical composition of open clusters. I - Fe/H from high-resolution spectroscopy. II - C/H and C/Fe in F dwarfs from high-resolution spectroscopy. *ApJ*, **351**, 467–491.

BOK, B. J. & REILLY, E. F., 1947. Small Dark Nebulae. *ApJ*, **105**, 255–257.

BRANDEKER, A., LISEAU, R., ARTYMOWICZ, P. & JAYAWARDHANA, R., 2001. Discovery of a New Companion and Evidence of a Circumprimary Disk: Adaptive Optics Imaging of the Young Multiple System VW Chamaeleon. *ApJL*, **561**, L199–L202.

BROWN, J. A., SNEDEN, C., LAMBERT, D. L. & DUTCHOVER, E. J., 1989. A search for lithium-rich giant stars. *ApJS*, **71**, 293–322.

BURROWS, A., HUBBARD, W. B., LUNINE, J. I. & LIEBERT, J., 2001. The theory of brown dwarfs and extrasolar giant planets. *Reviews of Modern Physics*, **73**, 719–765.

CAYREL DE STROBEL, G. & CAYREL, R., 1989. Strong lithium in the very nearby K-dwarf HD 17925. *Astronomy and Astrophysics*, **218**, L9–L12.

CAYREL DE STROBEL, G., SOUBIRAN, C., FRIEL, E. D., RALITE, N. & FRANCOIS, P., 1997. A catalogue of [Fe/H] determinations: 1996 edition. *Astronomy and Astrophysics, Supplement*, **124**, 299–305.

CENSORI, C. & D'ANTONA, F., 1998. Brown Dwarfs and the Luminosity Functions of Young Stellar Populations. In *ASP Conf. Ser. 134: Brown Dwarfs and Extrasolar Planets*, 518–523.

CHEREUL, E., CRÉZÉ, M. & BIENAYMÉ, O., 1999. The distribution of nearby stars in phase space mapped by Hipparcos. Clustering and streaming among A-F type stars. *Astronomy and Astrophysics, Supplement*, **135**, 5–28.

CHRISTIAN, D. J. & MATHIOUDAKIS, M., 2002. High-Resolution Optical Observations of Extreme-Ultraviolet-selected Active Late-type Stars. *Astronomical Journal*, **123**, 2796–2805.

CLEMENS, D. P. & BARVAINIS, R., 1988. A catalog of small, optically selected molecular clouds - Optical, infrared, and millimeter properties. *ApJS*, **68**, 257–286.

CUMMING, A., MARCY, G. W. & BUTLER, R. P., 1999. The Lick Planet Search: Detectability and Mass Thresholds. *ApJ*, **526**, 890–915.

CUTISPOTO, G., 1998. Long-term monitoring of active stars. VIII. UBV(RI)_(c) photometry collected in February 1992. *Astronomy and Astrophysics, Supplement*, **131**, 321–344.

D'ANTONA, F. & MAZZITELLI, I., 1994. New pre-main-sequence tracks for M less than or equal to 2.5 solar mass as tests of opacities and convection model. *ApJS*, **90**, 467–500.

D'ANTONA, F. & MAZZITELLI, I., 1997. Evolution of low mass stars. *Memorie della Societa Astronomica Italiana*, **68**, 807–822.

D'Antona, F. & Mazzitelli, I., 1998. A Role for Superadiabatic Convection in Low Mass Structures? In *ASP Conf. Ser. 134: Brown Dwarfs and Extrasolar Planets*, 442–445.

de Medeiros, J. R. & Mayor, M., 1999. A catalog of rotational and radial velocities for evolved stars. *Astronomy and Astrophysics, Supplement*, **139**, 433–460.

Dehnen, W. & Binney, J. J., 1998. Local stellar kinematics from HIPPARCOS data. *MNRAS*, **298**, 387–394.

Dorren, J. D. & Guinan, E. F., 1994. HD 129333: The Sun in its infancy. *ApJ*, **428**, 805–818.

Duquennoy, A. & Mayor, M., 1991. Multiplicity among solar-type stars in the solar neighbourhood. II - Distribution of the orbital elements in an unbiased sample. *Astronomy and Astrophysics*, **248**, 485–524.

Eggen, O. J., 1982. The Hyades main sequence. *ApJS*, **50**, 221–239.

Eggen, O. J., 1983a. Concentrations in the Local Association - Part Two - the Northern Concentrations Including the Alpha-Persei Pleiades M34 and Delta-Lyrae Clusters. *MNRAS*, **204**, 391–403.

Eggen, O. J., 1983b. Concentrations in the local association. I - The southern concentrations NGC 2516, IC 2602, Centaurus-Lupus and upper Scorpius. *MNRAS*, **204**, 377–390.

Eggen, O. J., 1983c. Concentrations in the local association. III - Late-type bright giants, ages and abundances. *MNRAS*, **204**, 405–414.

Eggen, O. J., 1992. The kinematics of young disk population supercluster members. *Astronomical Journal*, **104**, 2141–2150.

Eggen, O. J., 1995. Pre-Main-Sequence Stars in the Pleiades Supercluster. *Astronomical Journal*, **110**, 1749–1761.

Eggen, O. J., 1998. Kinematics and Metallicity of Stars in the Solar Region. *Astronomical Journal*, **115**, 2397–2434.

Fabricius, C. & Makarov, V. V., 2000. Two-colour photometry for 9473 components of close Hipparcos double and multiple stars. *Astronomy and Astrophysics*, **356**, 141–145.

Favata, F., Micela, G. & Sciortino, S., 1997. The relationship between lithium and activity in disk population main sequence G and K stars. *Astronomy and Astrophysics*, **322**, 131–138.

Favata, F., Micela, G., Sciortino, S. & D'Antona, F., 1998. The evolutionary status of activity-selected solar-type stars and of T Tauri stars as derived from HIPPARCOS parallaxes: evidence for long-lived T Tauri disks? *Astronomy and Astrophysics*, **335**, 218–226.

Feigelson, E. D. & Montmerle, T., 1999. High-Energy Processes in Young Stellar Objects. *Ann. Rev. Ast. & Ast.*, **37**, 363–408.

Frink, S., 2001. Kinematic Distances to TW Hya Member stars via the Convergent Point. In R. Jayawardhana & T. P. Greene, eds., *Young Stars near Earth: Progress and Prospects*, vol. 244 of *A.S.P. Conf. Ser.*, 16–21.

FUHRMANN, K., 1993. *Temperatur und Elementhäufigkeiten von F- und G-Sternen.* Ph.D. thesis, Ludwig-Maximilians-Universität München, Fakultät für Physik.

FUHRMANN, K., 2004. Nearby stars of the Galactic disk and halo. III. *Astronomische Nachrichten*, **325**, 3–80.

FUHRMANN, K., PFEIFFER, M. J. & BERNKOPF, J., 1997. Solar-type stars with planetary companions: 51 Pegasi and 47 Ursae Majoris. *Astronomy and Astrophysics*, **326**, 1081–1089.

FUHRMANN, K., PFEIFFER, M. J. & BERNKOPF, J., 1998. F- and G-type stars with planetary companions: upsilon Andromedae, $\rho^1$ Cancri, $\tau$ Bootis, 16 Cygni and $\rho$ Coronae Borealis. *Astronomy and Astrophysics*, **336**, 942–952.

GAIDOS, E. J., 1998. Nearby Young Solar Analogs. I. Catalog and Stellar Characteristics. *Publications of the ASP*, **110**, 1259–1276.

GAIDOS, E. J. & GONZALEZ, G., 2002. Stellar atmospheres of nearby young solar analogs. *New Astronomy*, **7**, 211–226.

GAIDOS, E. J., HENRY, G. W. & HENRY, S. M., 2000. Spectroscopy and Photometry of Nearby Young Solar Analogs. *Astronomical Journal*, **120**, 1006–1013.

GATEWOOD, G., 1994. One milliarcsecond precision studies in the regions of Delta Equulei and $\chi^1$ Orionis. *Publications of the ASP*, **106**, 138–144.

GERSHBERG, R. E., KATSOVA, M. M., LOVKAYA, M. N., TEREBIZH, A. V. & SHAKHOVSKAYA, N. I., 1999. Catalogue and bibliography of the UV Cet-type flare stars and related objects in the solar vicinity. *Astronomy and Astrophysics, Supplement*, **139**, 555–558.

GHOSH, P. & LAMB, F. K., 1978. Disk accretion by magnetic neutron stars. *ApJL*, **223**, L83–L87.

GHOSH, P. & LAMB, F. K., 1979. Accretion by rotating magnetic neutron stars. III - Accretion torques and period changes in pulsating X-ray sources. *ApJ*, **234**, 296–316.

GLIESE, W. & JAHREISS, H., 1995. Nearby Stars, Preliminary 3rd Version (Gliese+ 1991). *VizieR Online Data Catalog*, **5070**, 0.

GLUSHNEVA, I. N., SHENAVRIN, V. I. & ROSHCHINA, I. A., 2000. Solar Analogs: Spectral Energy Distributions and Physical Parameters of Their Atmospheres. *Astronomy Reports*, **44**, 246–254.

GRAY, D. F., 1976. *The observation and analysis of stellar photospheres.* Research supported by the National Research Council of Canada. New York, Wiley-Interscience, 1976. 484 p.

GRAY, D. F., SCOTT, H. R. & POSTMA, J. E., 2002. Line Absorption as a Metallicity Index for Giant Stars. *Publications of the ASP*, **114**, 536–545.

HABING, H. J., DOMINIK, C., JOURDAIN DE MUIZON, M., LAUREIJS, R. J., KESSLER, M. F., LEECH, K., METCALFE, L., SALAMA, A., SIEBENMORGEN, R., TRAMS, N. & BOUCHET, P., 2001. Incidence and survival of remnant disks around main-sequence stars. *Astronomy and Astrophysics*, **365**, 545–561.

HAN, I. & GATEWOOD, G., 2002. A Precise Orbit Determination of $\chi^1$ Orionis from Astrometric and Radial Velocity Data. *Publications of the ASP*, **114**, 224–228.

HARO, G., 1957. The possible connexion between T Tauri stars and UV Ceti stars. In *IAU Symp. 3: Non-stable stars*, 26–30.

HARO, G. & CHAVIRA, E., 1973. New Flare Stars in the Pleiades Region (1972-1973). *Informational Bulletin on Variable Stars*, **788**, 1–2.

HARO, G. & MORGAN, W. W., 1953. Rapid Variables in the Orion Nebula. *ApJ*, **118**, 16–17.

HAWARDEN, T. G., LEGGETT, S. K., LETAWSKY, M. B., BALLANTYNE, D. R. & CASALI, M. M., 2001. JHK standard stars for large telescopes: the UKIRT Fundamental and Extended lists. *MNRAS*, **325**, 563–574.

HAWLEY, S. L., GIZIS, J. E. & REID, N. I., 1997. The Palomar/MSU Nearby Star Spectroscopic Survey.II. The Southern M Dwarfs and Investigation of Magnetic Activity. *Astronomical Journal*, **113**, 1458–1471.

HAYWOOD, M., 2001. A revision of the solar neighbourhood metallicity distribution. *MNRAS*, **325**, 1365–1382.

HEARTY, T. J., 2001. MBM 12: The Nearest Known Star-Forming Cloud. In *ASP Conf. Ser. 244: Young Stars Near Earth: Progress and Prospects*, 22–24.

HEARTY, T. J., FERNÁNDEZ, M., ALCALÁ, J. M., COVINO, E. & NEUHÄUSER, R., 2000. The distance to the nearest star-forming clouds: MBM12 and MBM20. *Astronomy and Astrophysics*, **357**, 681–685.

HENRY, T. J., FRANZ, O. G., WASSERMAN, L. H., BENEDICT, G. F., SHELUS, P. J., IANNA, P. A., KIRKPATRICK, J. D. & MCCARTHY, D. W., 1999. The Optical Mass-Luminosity Relation at the End of the Main Sequence (0.08-0.20 M_solar). *ApJ*, **512**, 864–873.

HERBIG, G. H., 1962. Spectral Classification of Faint Members of the Hyades and Pleiades and the Dating Problem in Galactic Clusters. *ApJ*, **135**, 736–747.

HOBBS, L. M., BLITZ, L. & MAGNANI, L., 1986. A molecular cloud in the local, hot interstellar medium. *ApJL*, **306**, L109–L113.

HOFF, W., ALCALÁ, J. M., PFAU, W. & STERZIK, M. F., 1996. New isolated T Tauri stars in the vicinity of TW Hydrae. In *Astronomische Gesellschaft Abstract Series*, 26.

HOLBERG, J. B., BARSTOW, M. A., BRUHWEILER, F. C., CRUISE, A. M. & PENNY, A. J., 1998. Sirius B: A New, More Accurate View. *ApJ*, **497**, 935–942.

HORNE, K., 1986. An optimal extraction algorithm for CCD spectroscopy. *Publications of the ASP*, **98**, 609–617.

HUÉLAMO, N., 2002. *The secret life of adolescent stars: Magnetic activity of Post-T Tauri stars in Lindroos systems*. Ph.D. thesis, Universidad Autónoma de Madrid, Facultad de Ciencias, Departamento de Física Teórica.

IRWIN, A. W., YANG, S. & WALKER, G. A. H., 1992. A precise radial-velocity determination of the orbit of $\chi^1$ Orionis. *Publications of the ASP*, **104**, 101–105.

JAYAWARDHANA, R. & GREENE, T., eds., 2001. *Young Stars Near Earth: Progress and Prospects*.

JAYAWARDHANA, R., HARTMANN, L., FAZIO, G., FISHER, R. S., TELESCO, C. M. & PIÑA, R. K., 1999. A Disk Census for the Nearest Group of Young Stars: Mid-Infrared Observations of the TW Hydrae Association. *ApJL*, **521**, L129–L132.

JAYAWARDHANA, R., LUHMAN, K. L., D'ALESSIO, P. & STAUFFER, J. R., 2002. Discovery of an Edge-On Disk in the MBM 12 Young Association. *ApJL*, **571**, L51–L54.

JAYAWARDHANA, R., WOLK, S. J., BARRADO Y NAVASCUÉS, D., TELESCO, C. M. & HEARTY, T. J., 2001. Protoplanetary Disks in the Nearest Star-Forming Cloud: Mid-Infrared Imaging and Optical Spectroscopy of MBM 12 Members. *ApJL*, **550**, L197–L200.

JEFFRIES, R. D. & JEWELL, S. J., 1993. The Kinematics of Active Late Type Stars Observed by the ROSAT Wide-Field Camera. *MNRAS*, **264**, 106–120.

JENSEN, E. L. N., COHEN, D. H. & NEUHÄUSER, R., 1998. ROSAT and HIPPARCOS Observations of Isolated Pre-Main-Sequence Stars near HD 98800. *Astronomical Journal*, **116**, 414–423.

JOY, A. H., 1945. T Tauri Variable Stars. *ApJ*, **102**, 168–195.

JOY, A. H. & VAN BIESBROECK, G., 1944. Five New Double Stars among Variables of the T Tauri Class. *Publications of the ASP*, **56**, 123–197.

JURA, M., ZUCKERMAN, B., BECKLIN, E. E. & SMITH, R. C., 1993. Constraints on the Evolution of Remnant Protostellar Dust Debris around HR 4796. *ApJL*, **418**, L37+.

KÖNIG, B., FUHRMANN, K., NEUHÄUSER, R., CHARBONNEAU, D. & JAYAWARDHANA, R., 2002. Direct detection of the companion of $\chi^1$ Orionis. *Astronomy and Astrophysics*, **394**, L43–L46.

KÖNIG, B., NEUHÄUSER, R., GUENTHER, E. W. & HAMBARYAN, V., 2003. Flare stars in the TW Hydrae association: the HIP 57269 system. *Astronomische Nachrichten*, **324**, 516–522.

KASTNER, J. H., ZUCKERMAN, B., WEINTRAUB, D. A. & FORVEILLE, T., 1997. X-ray and molecular emission from the nearest region of recent star formation. *Science*, **277**, 67–71.

KATZ, D., FAVATA, F., AIGRAIN, S. & MICELA, G., 2003. The photospheric abundances of active binaries. I. Detailed analysis of HD 113816 (IS Vir) and HD 119285 (V851 Cen). *Astronomy and Astrophysics*, **397**, 747–756.

KENYON, S. J., GOMEZ, M., MARZKE, R. O. & HARTMANN, L., 1994. New pre-main-sequence stars in the Taurus-Auriga molecular cloud. *Astronomical Journal*, **108**, 251–261.

KENYON, S. J. & HARTMANN, L., 1995. Pre-Main-Sequence Evolution in the Taurus-Auriga Molecular Cloud. *ApJS*, **101**, 117–171.

KING, J. R., VILLARREAL, A. R., SODERBLOM, D. R., GULLIVER, A. F. & ADELMAN, S. J., 2003. Stellar Kinematic Groups. II. A Reexamination of the Membership, Activity, and Age of the Ursa Major Group. *Astronomical Journal*, **125**, 1980–2017.

Korn, A. J., 2002. Rectifying échelle Spectra – A Comparison Between UVES, FEROS and FOCES. In *Scientific Drivers for ESO Future VLT/VLTI Instrumentation Proceedings of the ESO Workshop held in Garching, Germany, 11-15 June, 2001*, 199–203.

Kurucz, R. L., 1979. Model atmospheres for G, F, A, B, and O stars. *ApJS*, **40**, 1–340.

Lada, C. J., 1987. Star formation - From OB associations to protostars. In *IAU Symp. 115: Star Forming Regions*, 1–15.

Lippincott, S. L. & Worth, M. D., 1978. $\chi^1$ Orionis - A new solar-type astrometric binary. *Publications of the ASP*, **90**, 330–332.

Lowrance, P. J., McCarthy, C., Becklin, E. E., Zuckerman, B., Schneider, G., Webb, R. A., Hines, D. C., Kirkpatrick, J. D., Koerner, D. W., Low, F., Meier, R., Rieke, M., Smith, B. A., Terrile, R. J. & Thompson, R. I., 1999. A Candidate Substellar Companion to CD -33 deg7795 (TWA 5). *ApJL*, **512**, L69–L72.

Ludwig, H.-G., Allard, F. & Hauschildt, P. H., 2002. Numerical simulations of surface convection in a late M-dwarf. *Astronomy and Astrophysics*, **395**, 99–115.

Luhman, K. L., 1999. Young Low-Mass Stars and Brown Dwarfs in IC 348. *ApJ*, **525**, 466–481.

Luhman, K. L., 2001. On the MBM 12 Young Association. *ApJ*, **560**, 287–306.

Makarov, V. V. & Fabricius, C., 2001. Internal kinematics of the TW Hya association of young stars. *Astronomy and Astrophysics*, **368**, 866–872.

Malagnini, M. L., Morossi, C., Buzzoni, A. & Chavez, M., 2000. Observations and Atmospheric Parameters of Super-Metal-rich Candidates. *Publications of the ASP*, **112**, 1455–1466.

Mamajek, E. E., Meyer, M. R. & Liebert, J., 2002. Post-T Tauri Stars in the Nearest OB Association. *Astronomical Journal*, **124**, 1670–1694.

Marcy, G. W. & Butler, R. P., 1992. Precision radial velocities with an iodine absorption cell. *Publications of the ASP*, **104**, 270–277.

Marcy, G. W. & Butler, R. P., 1998. Detection of Extrasolar Giant Planets. *Ann. Rev. Ast. & Ast.*, **36**, 57–98.

Marcy, G. W. & Butler, R. P., 2000. Planets Orbiting Other Suns. *Publications of the ASP*, **112**, 137–140.

Marengo, M., Jayawardhana, R., Fazio, G. G., Hoffmann, W. F., Hora, J. L., Dayal, A. & Deutsch, L. K., 2000. Mid-Infrared Imaging of the Massive Young Star AFGL 2591: Probing the Circumstellar Environment of an Outflow Source. *ApJL*, **541**, L63–L66.

Mayor, M., Queloz, D., Marcy, G., Butler, P., Noyes, R., Korzennik, S., Krockenberger, M., Nisenson, P., Brown, T., Kennelly, T., Rowland, C., Horner, S., Burki, G., Burnet, M. & Kunzli, M., 1995. 51 Pegasi. *IAU Cirulars*, **6251**, 1.

McCabe, C., Duchêne, G. & Ghez, A. M., 2002. NICMOS Images of the GG Tauri Circumbinary Disk. *ApJ*, **575**, 974–988.

McCarthy, D. W., 1986. The search for substellar companions to nearby stars - Infrared imaging from the ground and from space. In *Astrophysics of Brown Dwarfs*, 9–19.

McWilliam, A., 1990. High-resolution spectroscopic survey of 671 GK giants. I - Stellar atmosphere parameters and abundances. *ApJS*, **74**, 1075–1128.

Mermilliod, J.-C., Turon, C., Robichon, N., Arenou, F. & Lebreton, Y., 1997. The Distance of the Pleiades and Nearby Clusters. In *ESA SP-402: Hipparcos - Venice '97*, 643–650.

Montes, D., López-Santiago, J., Gálvez, M. C., Fernández-Figueroa, M. J., De Castro, E. & Cornide, M., 2001. Late-type members of young stellar kinematic groups - I. Single stars. *MNRAS*, **328**, 45–63.

Neuhäuser, R., Brandner, W., Eckart, A., Guenther, E., Alves, J., Ott, T., Huélamo, N. & Fernández, M., 2000. On the possibility of ground-based direct imaging detection of extra-solar planets: the case of TWA-7. *Astronomy and Astrophysics*, **354**, L9–L12.

Neuhäuser, R., 1997. Low-mass pre-main sequence stars and their X-ray emission. *Science*, **276**, 1363–1370.

Neuhäuser, R., Guenther, E. W., Petr, M. G., Brandner, W., Huélamo, N. & Alves, J., 2000. Spectrum and proper motion of a brown dwarf companion of the T Tauri star CoD-33°7795. *Astronomy and Astrophysics*, **360**, L39–L42.

Neuhäuser, R., Wolk, S. J., Torres, G., Preibisch, T., Stout-Batalha, N. M., Hatzes, A. P., Frink, S., Wichmann, R., Covino, E., Alcalá, J. M., Brandner, W., Walter, F. M., Sterzik, M. F. & Koehler, R., 1998. Optical and X-ray monitoring, Doppler imaging, and space motion of the young star Par 1724 in Orion. *Astronomy and Astrophysics*, **334**, 873–894.

Nidever, D. L., Marcy, G. W., Butler, R. P., Fischer, D. A. & Vogt, S. S., 2002. Radial Velocities for 889 Late-Type Stars. *ApJS*, **141**, 503–522.

Pallavicini, R., Randich, S. & Giampapa, M. S., 1992. Lithium in RS CVn binaries and related chromospherically active stars. I - Observational results. *Astronomy and Astrophysics*, **253**, 185–198.

Pavlenko, Y. V. & Magazzù, A., 1996. Theoretical LTE and non-LTE curves of growth for LiI lines in G-M dwarfs and subgiants. *Astronomy and Astrophysics*, **311**, 961–967.

Perryman, M. A. C., Brown, A. G. A., Lebreton, Y., Gomez, A., Turon, C., de Strobel, G. C., Mermilliod, J. C., Robichon, N., Kovalevsky, J. & Crifo, F., 1998. The Hyades: distance, structure, dynamics, and age. *Astronomy and Astrophysics*, **331**, 81–120.

Persson, S. E., Murphy, D. C., Krzeminski, W., Roth, M. & Rieke, M. J., 1998. A New System of Faint Near-Infrared Standard Stars. *Astronomical Journal*, **116**, 2475–2488.

Pfeiffer, M. J., Frank, C., Baumüller, D., Fuhrmann, K. & Gehren, T., 1998. FOCES - a fibre optics Cassegrain Echelle spectrograph. *Astronomy and Astrophysics, Supplement*, **130**, 381–393.

RANDICH, S., GRATTON, R. & PALLAVICINI, R., 1993. Lithium in RS-Canum Binaries and Related Chromospherically Active Stars - Part Two - Spectrum Synthesis Analysis. *Astronomy and Astrophysics*, **273**, 194–211.

RICHICHI, A. & PERCHERON, I., 2002. CHARM: A Catalog of High Angular Resolution Measurements. *Astronomy and Astrophysics*, **386**, 492–503.

ROBICHON, N., ARENOU, F., MERMILLIOD, J.-C. & TURON, C., 1999. Open clusters with Hipparcos. I. Mean astrometric parameters. *Astronomy and Astrophysics*, **345**, 471–484.

ROSVICK, J. M., MERMILLIOD, J.-C. & MAYOR, M., 1992. Investigation of the Pleiades cluster. I - Radial velocities of corona stars. *Astronomy and Astrophysics*, **255**, 130–138.

RYAN, S. G., 1998. The importance of collision broadening of weak lines in stellar spectra. *Astronomy and Astrophysics*, **331**, 1051–1058.

SALARIS, M., GARCÍA-BERRO, E., HERNANZ, M., ISERN, J. & SAUMON, D., 2000. The Ages of Very Cool Hydrogen-rich White Dwarfs. *ApJ*, **544**, 1036–1043.

SCHALLER, G., SCHAERER, D., MEYNET, G. & MAEDER, A., 1992. New grids of stellar models from 0.8 to 120 solar masses at Z = 0.020 and Z = 0.001. *Astronomy and Astrophysics, Supplement*, **96**, 269–331.

SHU, F., NAJITA, J., OSTRIKER, E., WILKIN, F., RUDEN, S. & LIZANO, S., 1994. Magnetocentrifugally driven flows from young stars and disks. 1: A generalized model. *ApJ*, **429**, 781–796.

SHU, F. H., SHANG, H., GLASSGOLD, A. E. & LEE, T., 1997. X-rays and fluctuating X-winds from protostars. *Science*, **277**, 1475–1479.

SIESS, L., DUFOUR, E. & FORESTINI, M., 2000. An internet server for pre-main sequence tracks of low- and intermediate-mass stars. *Astronomy and Astrophysics*, **358**, 593–599.

SIESS, L., FORESTINI, M. & DOUGADOS, C., 1997. Synthetic Hertzsprung-Russell diagrams of open clusters. *Astronomy and Astrophysics*, **324**, 556–565.

SODERBLOM, D. R. & CLEMENTS, S. D., 1987. Chromospheric and transition-region emission from young solar-type stars in clusters, kinematic groups, and the field. *Astronomical Journal*, **93**, 920–937.

SODERBLOM, D. R. & MAYOR, M., 1993. Stellar kinematic groups. I - The Ursa Major group. *Astronomical Journal*, **105**, 226–249.

SONG, I., BESSELL, M. S. & ZUCKERMAN, B., 2002. Additional TWA members?. Spectroscopic verification of kinematically selected TWA candidates. *Astronomy and Astrophysics*, **385**, 862–866.

STELLO, D. & NISSEN, P. E., 2001. The problem of the Pleiades distance. Constraints from Strömgren photometry of nearby field stars. *Astronomy and Astrophysics*, **374**, 105–115.

STELZER, B. & NEUHÄUSER, R., 2000. X-ray emission from young stars in the Tucanae association. *Astronomy and Astrophysics*, **361**, 581–593.

STELZER, B. & NEUHÄUSER, R., 2001. X-ray emission from young stars in Taurus-Auriga-Perseus: Luminosity functions and the rotation - activity - age - relation. *Astronomy and Astrophysics*, **377**, 538–556.

Sterzik, M. F., Alcalá, J. M., Covino, E. & Petr, M. G., 1999. New T Tauri stars in the vicinity of TW Hydrae. *Astronomy and Astrophysics*, **346**, L41–L44.

Stix, M., 2002. *The sun: an introduction*. 2nd ed. /Michael Stix. Berlin: Springer, 2002. QB 521 .S75.

Strassmeier, K. G. & Rice, J. B., 1998. Doppler imaging of stellar surface structure. VI. HD 129333 = EK Draconis: a stellar analog of the active young Sun. *Astronomy and Astrophysics*, **330**, 685–695.

Tachihara, K., Neuhäuser, R., Frink, S. & Guenther, E., 2003. Proper motion and X-ray selected search for new members of the young TW Hya association. *Astronomische Nachrichten*, **324**, 543–551.

Taylor, B. J., 2003. Statistical cataloging of archival data for luminosity class IV-V stars. II. The epoch 2001 [Fe/H] catalog. *Astronomy and Astrophysics*, **398**, 731–738.

Telesco, C. M., Fisher, R. S., Piña, R. K., Knacke, R. F., Dermott, S. F., Wyatt, M. C., Grogan, K., Holmes, E. K., Ghez, A. M., Prato, L., Hartmann, L. W. & Jayawardhana, R., 2000. Deep 10 and 18 Micron Imaging of the HR 4796A Circumstellar Disk: Transient Dust Particles and Tentative Evidence for a Brightness Asymmetry. *ApJ*, **530**, 329–341.

Torres, C., Quast, G., de la Reza, R., da Silva, L. & Melo, C., 2002. SACY - Present Status. Astro-ph/0207078.

Torres, C. A. O., da Silva, L., Quast, G. R., de la Reza, R. & Jilinski, E., 2000. A New Association of Post-T Tauri Stars near the Sun. *Astronomical Journal*, **120**, 1410–1425.

Torres, G., Guenther, E. W., Marschall, L. A., Neuhäuser, R., Latham, D. W. & Stefanik, R. P., 2003. Radial Velocity Survey of Members and Candidate Members of the TW Hydrae Association. *Astronomical Journal*, **125**, 825–841.

Tsuboi, Y., Imanishi, K., Koyama, K., Grosso, N. & Montmerle, T., 2000. Quasi-periodic X-Ray Flares from the Protostar YLW 15. *ApJ*, **532**, 1089–1096.

Udalski, A. & Geyer, E. H., 1985. HD 102077 - a New by Draconis Star? *Informational Bulletin on Variable Stars*, **2691**, 1.

van Leeuwen, F., 1999. HIPPARCOS distance calibrations for 9 open clusters. *Astronomy and Astrophysics*, **341**, L71–L74.

Vandenberg, D. A., 1985. Evolution of 0.7-3.0 solar masses stars having Fe/H between -1.0 and 0.0. *ApJS*, **58**, 711–769.

Vogt, S. S., Penrod, G. D. & Hatzes, A. P., 1987. Doppler images of rotating stars using maximum entropy image reconstruction. *ApJ*, **321**, 496–515.

Wang, Y., Evans, N. J., Zhou, S. & Clemens, D. P., 1995. Collapse Candidates among the BOK Globules. *ApJ*, **454**, 217–232.

Warmels, R. H., 1992. The ESO–MIDAS System. In *ASP Conf. Ser. 25: Astronomical Data Analysis Software and Systems I*, 115–119.

Webb, R. A., Zuckerman, B., Platais, I., Patience, J., White, R. J., Schwartz, M. J. & McCarthy, C., 1999. Discovery of Seven T Tauri Stars and a Brown Dwarf Candidate in the Nearby TW Hydrae Association. *ApJL*, **512**, L63–L67.

Wichmann, R., Schmitt, J. H. M. M. & Hubrig, S., 2003. Nearby young stars. *Astronomy and Astrophysics*, **399**, 983–994.

Wielen, R., 1971. On the Lifetimes of Galactic Clusters. *Astrophysics and Space Science*, **13**, 300–308.

Wizinowich, P. L., Acton, D. S., Lai, O., Gathright, J., Lupton, W. & Stomski, P. J., 2000. Performance of the W.M. Keck Observatory Natural Guide Star Adaptive Optic Facility: the first year at the telescope. In *Proc. SPIE Vol. 4007, p. 2-13, Adaptive Optical Systems Technology, Peter L. Wizinowich; Ed.*, 2–13.

Wood, M. A., 1992. Constraints on the age and evolution of the Galaxy from the white dwarf luminosity function. *ApJ*, **386**, 539–561.

Wyse, R. F. G. & Gilmore, G., 1995. Chemistry and Kinematics in the Solar Neighborhood: Implications for Stellar Populations and for Galaxy Evolution. *Astronomical Journal*, **110**, 2771–2787.

Young, A., Sadjadi, S. & Harlan, E., 1987. The incidence of close binaries among stars of low mass Astrophysical binaries. *ApJ*, **314**, 272–282.

Yun, J. L. & Clemens, D. P., 1990. Star formation in small globules - Bart BOK was correct. *ApJL*, **365**, L73–L76.

Zakhozhaj, V. A. & Shaparenko, E. F., 1996. The catalogue of nearby stars metallicities. *Kinematika i Fizika Nebesnykh Tel*, **12**, 20–29.

Zinnecker, H. & Mathieu, R., eds., 2001. *The Formation of Binary Stars*.

Zuckerman, B., Song, I., Bessell, M. S. & Webb, R. A., 2001a. The $\beta$ Pictoris Moving Group. *ApJL*, **562**, L87–L90.

Zuckerman, B., Song, I. & Webb, R. A., 2001b. Tucana Association. *ApJ*, **559**, 388–394.

Zuckerman, B. & Webb, R. A., 2000. Identification of a Nearby Stellar Association in the Hipparcos Catalog: Implications for Recent, Local Star Formation. *ApJ*, **535**, 959–964.

# Revised data of the input catalog

**Table 1:** Names and basic input data of the Gershberg et al. (1999) flare star catalog, SpCl_1 is the original spectral class listed in Gershberg et al. (1999), SpCl_2 is the spectral class listed in Hawley et al. (1997), SpCl_3 is informtion that was available in the Hipparcos catalog and was different from the original data. The masses and ages were estimated using D'Antona & Mazzitelli (1994) by converting the spectral type to a temperature using Kenyon & Hartmann (1995) for the G- to early M-type stars and Luhman (1999) for the late M-type stars.

| GLK | designation | Ra [2000] | Dec [2000] | SpCl_1 | SpCl_2 | SpCl_3 | Mass [M$_\odot$] | age [Myr] |
|---|---|---|---|---|---|---|---|---|
| 1 | HIP 439 | 00 05 24.4 | -37 21 27 | M4V | M1.5 | M2V | | |
| 2 | HR Cep | 00 07 12.4 | 67 12 41 | | | | | |
| 3 | GJ 3010 | 00 08 53.9 | 20 50 26 | m | M4.5 | | 0.3 ± 0.5 | 7.5 ± 0.5 |
| 4 | GJ 3015 B | 00 13 45.1 | 80 39 18 | m | M5 | | 0.3 ± 0.5 | 7.5 ± 0.5 |
| 5 | EXO 0012.6-7307 | 00 15 00.8 | -72 50 32 | M2V | | | | |
| 6 | GJ 3017 | 00 15 36.4 | -29 45 59 | dM3.4 | M4.0 | | 0.3 ± 0.5 | 7.0 ± 0.5 |
| 7 | HIP 1295 A | 00 16 14.6 | 19 51 38 | M4 | M4 | M: | 0.3 ± 0.5 | 6.5 ± 0.2 |
| 8 | GJ 3022 | 00 16 56.6 | 20 03 54 | m | M3.5 | | 0.3 ± 0.5 | 6.7 ± 0.3 |
| 9 | HIP 1475 A | 00 18 22.9 | 44 01 23 | M2Ve | M1 | M1V | | |
| 10 | HIP 1475 B | 00 18 25.9 | 44 01 39 | M6Ve | M3.5 | | | |
| 11 | GJ 3027 | 00 18 58.4 | 27 48 31 | m | M4 | | 0.2 ± 0.5 | 6.7 ± 0.3 |
| 12 | HIP 1720 | 00 21 37.3 | -46 05 33 | M3: | M3.0 | M6 | 0.3 ± 0.5 | 6.8 ± 0.6 |
| 13 | GJ 3030 | 00 21 57.7 | 49 12 37 | m | M2.5 | | 0.3 ± 0.5 | 6.7 ± 0.3 |
| 14 | HIP 1771 | 00 22 25.2 | 06 40 03 | M1V | | M1Vvar | 0.5 ± 0.2 | 6.7 ± 0.3 |
| 15 | HIP 1803 | 00 22 51.8 | -12 12 34 | G2.V | | G3V | 0.8 ± 0.2 | 7.5 ± 0.2 |
| 16 | GJ 3033 | 00 24 34.5 | 30 02 28 | m | M4.5 | | 0.1 ± 0.5 | 7.0 ± 0.4 |
| 17 | GJ 2005 | 00 24 45.6 | -27 08 31 | M5.5 | M5.5 | | | |
| 18 | GJ 3036 | 00 28 53.6 | 50 22 32 | m | M4 | | 0.1 ± 0.5 | 7.1 ± 0.4 |
| 19 | HIP 2552 AC | 00 32 29.4 | 67 14 08 | dM2.5e | M2 | M2.5Ve | 0.1 ± 0.5 | 7.5 ± 0.3 |
| 20 | GJ 3039 | 00 32 34.7 | 07 29 26 | m | M4 | | 0.1 ± 0.5 | 7.4 ± 0.4 |
| 21 | HI And | 00 37 59.7 | 40 26 33 | | | | | |
| 22 | HW And | 00 41 11.3 | 43 33 21 | | | | | |
| 23 | HY And | 00 42 32.1 | 41 40 14 | | | | | |
| 24 | GS And | 00 42 42.5 | 40 08 27 | | | | | |
| 25 | HIP 3362 | 00 42 48.2 | 35 32 56 | dM1e | | M1Ve+... | 0.5 ± 0.2 | 6.5 ± 0.6 |
| 26 | BL Psc | 00 44 01.3 | 09 32 58 | K2.V | | | | |
| 27 | HIP 3493 B | 00 44 37.2 | -18 56 48 | m | M4.5 | M2 | 0.1 ± 0.5 | 6.5 ± 0.6 |
| 28 | GJ 3058 | 00 48 58.1 | 44 35 09 | m | M3 | | 0.2 ± 0.5 | 6.8 ± 0.4 |
| 29 | HIP 3937 A | 00 50 33.2 | 24 49 00 | m | M3.5 | | 0.1 ± 0.5 | 7.3 ± 0.5 |
| 30 | HIP 4022 B | 00 51 34.0 | -22 54 36 | m | M5.5 | K5V | | |
| 31 | HIP 4693 | 01 00 19.0 | -72 44 35 | dK0 | | G5 | 2.0 ± 0.3 | 6.5 ± 0.3 |
| 32 | HIP 4856 | 01 02 32.2 | 71 40 47 | dM3.5e | M3 | M3.5e | 0.1 ± 0.5 | 7.4 ± 0.5 |
| 33 | GJ 3069 | 01 01 58.4 | 54 11 12 | m | M5 | | | |
| 34 | GJ 51 | 01 03 19.8 | 62 21 56 | dM5e | M5 | | | |
| 35 | HIP 4927 B | 01 03 12.0 | 20 5 54 | M3.5 | | M | | |
| 36 | GJ 2021 | 01 09 19.9 | -24 30 30 | m | M4 | | 0.1 ± 0.5 | 6.7 ± 0.3 |
| 37 | GJ 3076 | 01 11 25.3 | 15 26 21 | m | M5 | | | |
| 38 | HIP 5643 | 01 12 30.6 | -16 59 56 | dM5e | M4.5 | M5.5Ve | | |
| 39 | GJ 1033 | 01 13 23.8 | -22 54 07 | | M4 | | 0.1 ± 0.5 | 7.0 ± 0.3 |
| 40 | | 01 17 24.3 | 65 26 08 | | | | | |
| 41 | CNS3 261 | 01 19 27.2 | -26 21 53 | m | M3 | | 0.2 ± 0.5 | 6.7 ± 0.3 |
| 42 | AO Scl | 01 19 56.7 | -33 25 32 | | | | | |
| 43 | CNS3 293 | 01 36 08.3 | -26 52 14 | m | M3 | | 0.2 ± 0.5 | 6.7 ± 0.3 |
| 44 | GJ 65 A | 01 39 01.4 | -17 57 03 | dM5.5e | M5.5 | | | |
| 45 | GJ 65 B | 01 39 01.5 | -17 57 04 | dM5.5e | M5.5 | | | |
| 46 | BO Psc A | 01 49 06.4 | 06 24 04 | dM1e | | | | |
| 47 | GJ 3119 | 01 51 03.6 | -06 07 02 | m | M4.5 | | | |
| 48 | HIP 8768 | 01 52 49.2 | -22 26 06 | M0V | K7 | K5/M0V | 0.6 ± 0.1 | 7.7 ± 0.3 |
| 49 | HIP 9291 | 01 59 23.4 | 58 31 16 | dM4e | M4 | M4Ve | 0.1 ± 0.5 | 7.0 ± 0.5 |
| 50 | HIP 9275 B | 01 59 12.4 | 03 31 09 | m | M2.5 | M1V: | 0.3 ± 0.5 | 6.3 ± 0.3 |
| 51 | GJ 3125 | 02 01 47.6 | 73 32 10 | m | M4.5 | | | |
| 52 | GJ 9066 | 02 00 15.2 | 13 03 40 | dM8e | M4.5 | | | |
| 53 | GJ 3127 | 02 00 47.4 | -10 21 17 | m | M3.5 | | 0.2 ± 0.5 | 6.6 ± 0.4 |
| 54 | GJ 3129 | 02 02 44.0 | 13 34 33 | dM5: | M4.5 | | 0.1 ± 0.5 | 7.3 ± 0.4 |
| 55 | GJ 3134 | 02 07 10.0 | 64 17 12 | m | M4 | | 0.2 ± 0.5 | 6.7 ± 0.4 |

Continued

| GLK | designation | Ra [2000] | Dec [2000] | SpCl_1 | SpCl_2 | SpCl_3 | Mass [M$_\odot$] | age [Myr] |
|---|---|---|---|---|---|---|---|---|
| 56 | WW Ari | 02 08 12.3 | 15 08 46 | | | | | |
| 57 | GJ 3136 | 02 08 53.4 | 49 26 58 | M5: | M3.5 | | 0.2 ± 0.5 | 7.2 ± 0.3 |
| 58 | GJ 3142 | 02 12 54.3 | 00 00 16 | m | M4 | | 0.1 ± 0.5 | 7.3 ± 0.3 |
| 59 | GJ 3143 | 02 15 34.3 | 33 57 43 | m | M3.5 | | 0.1 ± 0.5 | 7.0 ± 0.3 |
| 60 | GJ 3146 | 02 16 29.8 | 13 35 17 | m | M5.5 | | | |
| 61 | GJ 3147 | 02 17 08.2 | 35 26 18 | m+ | M5 | | | |
| 62 | HIP 10617 B | 02 16 34.0 | -30 58 13 | M4 | M3.5 | | 0.1 ± 0.5 | 7.4 ± 0.3 |
| 63 | HIP 10617 A | 02 16 41.2 | -30 59 18 | M4 | M3.0 | | 0.1 ± 0.5 | 7.3 ± 0.5 |
| 64 | GJ 3150 | 02 19 02.1 | 23 52 55 | m | M4 | | 0.1 ± 0.5 | 6.7 ± 0.3 |
| 65 | GJ 3153 | 02 20 46.1 | 02 58 39 | m | M4.5 | | 0.1 ± 0.5 | 7.0 ± 0.3 |
| 66 | GJ 3157 | 02 25 38.2 | 37 32 34 | m | M4 | | 0.1 ± 0.5 | 6.7 ± 0.3 |
| 67 | GJ 102 | 02 33 37.1 | 24 55 41 | M4 | M4 | | | |
| 68 | HIP 11964 | 02 34 22.6 | -43 47 47 | K7Ve | M0.0 | K7V comp SB | 0.6 ± 0.1 | 7.4 ± 0.5 |
| 69 | GJ 3166 | 02 35 22.6 | 23 34 31 | M3e | M3.5 | | 0.1 ± 0.5 | 6.7 ± 0.3 |
| 70 | GJ 3171 | 02 37 06.3 | 06 54 55 | M5e | M5 | | 0.1 ± 0.5 | 7.0 ± 0.3 |
| 71 | GJ 3172 | 02 37 29.9 | 00 21 26 | m | M4 | | 0.1 ± 0.5 | 6.9 ± 0.4 |
| 72 | EXO 0235.2-5216 | 02 36 51.5 | -52 03 04 | dM2e | M3Ve | | | |
| 73 | GJ 3174 | 02 39 17.0 | 07 28 17 | m | M4 | | 0.1 ± 0.5 | 6.7 ± 0.3 |
| 74 | HIP 12351 | 02 39 01.2 | -58 11 14 | M0Ve | K7.0 | M0Ve | 0.5 ± 0.1 | 7.4 ± 0.4 |
| 75 | HIP 12781 | 02 44 15.5 | 25 31 24 | dM3.5e | M3 | M3.5Ve | 0.1 ± 0.5 | 7.6 ± 0.6 |
| 76 | HIP 12886 B | 02 45 39.7 | 44 56 56 | m | M5 | K5V: | 0.1 ± 0.5 | 7.0 ± 0.5 |
| 77 | BY Cet | 02 47 26.9 | 00 12 22 | dG9e+dK4e | | | | |
| 78 | HIP 13081 C | 02 48 09.1 | 27 04 07 | m | M4.5 | K1V | 0.1 ± 0.5 | 7.0 ± 0.5 |
| 79 | HIP 13118 | 02 48 43.7 | 31 06 55 | G9e | | K0 | 1.7 ± 0.2 | 6.7 ± 0.3 |
| 80 | V483 Per | 02 51 34.2 | 37 50 14 | | | | | |
| 81 | GJ 3183 | 02 51 49.7 | 29 29 13 | m | M4 | | 0.1 ± 0.5 | 6.9 ± 0.3 |
| 82 | HIP 13402 | 02 52 32.1 | -12 46 11 | dK1e+dK2e | | K1V | 0.9 ± 0.1 | 7.5 ± 0.1 |
| 83 | HIP 14101 A | 03 01 51.4 | -16 35 36 | M3 | M3.5 | | 0.1 ± 0.5 | 7.5 ± 0.3 |
| 84 | HIP 14555 A | 03 07 55.7 | -28 13 11 | K7V | M0 | Se | 0.7 ± 0.2 | 7.0 ± 0.4 |
| 85 | HIP 14568 | 03 08 06.7 | -24 45 35 | m | K7 | K4 | 0.8 ± 0.2 | 6.5 ± 0.3 |
| 86 | QZ Per | 03 17 58.0 | 37 34 18 | | | | | |
| 87 | BP Cam | 03 22 23.5 | 61 37 47 | | | | | |
| 88 | GJ 3221 | 03 23 22.5 | 11 41 13 | m | M2.5 | | 0.3 ± 0.5 | 7.0 ± 0.4 |
| 89 | GJ 3224 | 03 25 42.3 | 05 51 52 | m+ | M4.5 | | 0.1 ± 0.5 | 7.5 ± 0.4 |
| 90 | GJ 3225 | 03 26 45.6 | 19 14 38 | m | M4.5 | | 0.1 ± 0.5 | 6.8 ± 0.4 |
| 91 | GJ 3227 | 03 28 49.4 | 26 29 13 | m | M3 | | 0.3 ± 0.5 | 6.7 ± 0.4 |
| 92 | GJ 3229 A | 03 28 40.3 | -15 37 20 | m | M3.5 | | 0.3 ± 0.5 | 6.7 ± 0.3 |
| 93 | GJ 3229 B | 03 28 40.6 | -15 37 34 | m | M3.5 | | 0.3 ± 0.5 | 6.2 ± 0.2 |
| 94 | GJ 1060 B | 03 28 47.9 | -27 19 06 | sdM3 | M3.5 | | 0.1 ± 0.5 | 7.0 ± 0.2 |
| 95 | GJ 3236 | 03 37 13.9 | 69 10 50 | m | M3.5 | | 0.2 ± 0.5 | 6.7 ± 0.3 |
| 96 | GJ 3237 | 03 36 40.7 | 03 29 19 | dM5: | M4.5 | | 0.1 ± 0.5 | 7.5 ± 0.3 |
| 97 | GJ 3240 B | 03 37 33.8 | 17 50 59 | g-k | M3 | | 0.3 ± 0.5 | 6.7 ± 0.3 |
| 98 | HIP 17032 | 03 39 04.5 | 09 39 10 | dG4e | | G | 1.0 ± 0.1 | 7.5 ± 0.1 |
| 99 | HIP 17102 B | 03 39 49.0 | 33 28 24 | | M3 | K5 | 0.3 ± 0.5 | 7.5 ± 1.0 |
| 100 | HIP 17609 | 03 46 20.1 | 26 12 56 | dK7 | M0 | K5 | 0.7 ± 0.2 | 7.0 ± 0.5 |
| 101 | II Tau | 03 49 43.2 | 24 19 05 | M3Ve-M5.Ve | | | | |
| 102 | GJ 3252 | 03 51 06.3 | 00 53 03 | m | M6 | | | |
| 103 | GJ 3253 | 03 52 41.4 | 17 01 09 | M4.5 | M4.5 | | 0.1 ± 0.5 | 7.3 ± 0.5 |
| 104 | HIP 18512 A | 03 57 28.7 | -01 09 34 | K4.V | | K4V | 0.7 ± 0.1 | 7.8 ± 0.3 |
| 105 | HIP 18512 B | 03 57 29.1 | -01 09 25 | dM3e | M2 | | | |
| 106 | GJ 3261 | 04 05 38.8 | 05 44 39 | dM5e | M3.5 | | 0.1 ± 0.5 | 7.3 ± 0.3 |
| 107 | GJ 3266 | 04 12 16.5 | 64 43 58 | m | M4 | | | |
| 108 | EXO 0408.4-7134 | 04 08 07.1 | -71 27 04 | dM0e | | | | |
| 109 | HIP 19855 | 04 15 25.8 | 06 11 59 | | | G5IV | 1.0 ± 0.1 | 7.7 ± 0.2 |
| 110 | 40 Eri C | 04 15 21.7 | -07 36 37 | dM4e | M4.5 | | | |
| 111 | GJ 3270 | 04 17 18.4 | 08 49 23 | dM4e | M4.5 | | 0.1 ± 0.5 | 7.4 ± 0.4 |
| 112 | EXO 0419.2+1908 | 04 22 08.4 | 19 15 22 | dM4.5e | M3 | | 0.2 ± 0.5 | 6.6 ± 0.3 |
| 113 | GJ 3283 A | 04 25 15.0 | 08 02 54 | m | M2.5 | | 0.3 ± 0.5 | 6.5 ± 0.3 |
| 114 | GJ 3283 B | 04 25 16.8 | 08 04 03 | m | M4 | | 0.2 ± 0.5 | 6.5 ± 0.3 |
| 115 | GJ 3286 | 04 24 56.3 | -40 02 36 | M3.5 | M3.0 | | 0.2 ± 0.5 | 7.4 ± 0.4 |
| 116 | GJ 3287 | 04 27 41.2 | 59 35 17 | m | M4 | | 0.1 ± 0.5 | 6.7 ± 0.3 |
| 117 | GJ 3289 | 04 26 27.0 | 03 36 11 | m | M6.5 | | | |
| 118 | HIP 20917 | 04 29 00.1 | 21 55 22 | K7.V | | K7V | 0.7 ± 0.2 | 7.6 ± 0.2 |
| 119 | GJ 107 | 04 30 25.3 | 39 51 01 | M4.5 | M4.5 | | | |
| 120 | GJ 3294 | 04 30 23.8 | 17 29 58 | k-m | M3.5 | | 0.1 ± 0.5 | 7.0 ± 0.3 |
| 121 | GJ 3296 | 04 33 33.6 | 20 44 48 | m | M4 | | 0.1 ± 0.5 | 7.0 ± 0.3 |
| 122 | HIP 21482 A | 04 36 48.3 | 27 07 56 | dK5ep | | K2 | 0.7 ± 0.1 | 7.3 ± 0.2 |
| 123 | HIP 21553 | 04 37 41.0 | 52 53 38 | K8Ve | K7 | K8V | 0.6 ± 0.1 | 7.8 ± 0.4 |
| 124 | GJ 3304 | 04 38 12.3 | 28 13 00 | m | M4 | | 0.1 ± 0.5 | 7.5 ± 0.3 |
| 125 | GJ 3305 | 04 37 37.0 | -02 29 29 | M1 | M0.5 | | 0.6 ± 0.1 | 7.2 ± 0.4 |
| 126 | HIP 21818 | 04 41 18.8 | 20 54 06 | K3.V | | K3V | 0.7 ± 0.1 | 7.8 ± 0.2 |
| 127 | HIP 21770 B | 04 40 33.7 | -41 51 50 | | M0.5 | F2V | 0.6 ± 0.1 | 7.0 ± 0.5 |
| 128 | HIP 22394 | 04 49 13.0 | 24 48 10 | K3V+K3.V | | K3V | 1.1 ± 0.2 | 7.1 ± 0.3 |
| 129 | HIP 22738 A | 04 53 31.2 | -55 51 37 | M2Ve | M2.0 | M2Ve | 0.1 ± 0.5 | 7.7 ± 0.3 |
| 130 | HIP 22738 B | 04 53 31.2 | -55 51 37 | | M3.5 | | | |
| 131 | HIP 22919 B | 04 55 55.9 | 04 40 14 | k | M1.5 | F8 | 0.5 ± 0.2 | 6.5 ± 0.5 |
| 132 | HIP 23200 | 04 59 04.8 | 01 47 01 | dM0.5e | M0 | M0.5Ve | 0.6 ± 0.1 | 6.3 ± 0.5 |
| 133 | HIP 23418 | 05 01 58.8 | 09 58 59 | dM3 | M4 | M3V: | 0.1 ± 0.5 | 6.4 ± 0.3 |
| 134 | GJ 3326 | 05 04 14.7 | 11 03 21 | m | M4 | | 0.1 ± 0.5 | 7.5 ± 0.5 |
| 135 | GJ 3327 | 05 05 11.8 | -12 00 26 | M4e | M3 | | 0.2 ± 0.5 | 6.7 ± 0.3 |
| 136 | GJ 3331 B | 05 06 49.6 | -21 35 06 | M3: | M3.5 | | 0.1 ± 0.5 | 7.3 ± 0.5 |
| 137 | GJ 3331 A | 05 06 49.6 | -21 35 06 | M2 | M1.5 | | | |
| 138 | GJ 3335 | 05 09 09.9 | 15 27 37 | M3 | M3 | | 0.1 ± 0.5 | 6.6 ± 0.3 |

Continued

| GLK | designation | Ra [2000] | Dec [2000] | SpCl_1 | SpCl_2 | SpCl_3 | Mass [M$_\odot$] | age [Myr] |
|---|---|---|---|---|---|---|---|---|
| 139 | UV Pic | 05 20 49.2 | -45 41 31 | dK5e | | | | |
| 140 | GJ 1078 | 05 23 49.2 | 22 32 40 | m | M4.5 | | 0.1 ± 0.5 | 7.2 ± 0.5 |
| 141 | GJ 3348 B | 05 28 56.4 | 12 31 54 | m | M4 | | 0.1 ± 0.5 | 6.5 ± 0.5 |
| 142 | HIP 25953 | 05 32 14.6 | 09 49 15 | dM4e | M3.5 | M4Ve | | |
| 143 | GJ 1081 | 05 33 19.1 | 44 49 00 | k-m | M3.5 | | 0.1 ± 0.5 | 6.8 ± 0.5 |
| 144 | HIP 26081 | 05 33 44.8 | 01 56 43 | dM2.5e | M2.5 | M2.5Ve | 0.2 ± 0.5 | 6.9 ± 0.5 |
| 145 | HIP 26779 | 05 41 20.3 | 53 28 52 | K1.Ve | | K1V | 0.9 ± 0.1 | 7.5 ± 0.1 |
| 146 | GJ 1083 AB | 05 40 25.6 | 24 48 08 | m | M5.5 | | | |
| 147 | GJ 3362 | 05 40 16.0 | 12 39 01 | M3 | M1 | | 0.5 ± 0.2 | 6.7 ± 0.3 |
| 148 | TZ Lep | 05 44 42.6 | -20 03 52 | | | | | |
| 149 | V962 Tau | 05 45 52.0 | 22 52 48 | | | | | |
| 150 | V910 Ori | 05 47 44.9 | 07 53 02 | | | | | |
| 151 | V1003 Ori | 05 49 57.5 | 06 46 59 | | | | | |
| 152 | GJ 3372 B | 05 59 55.7 | 58 34 16 | m | M4 | | 0.1 ± 0.5 | 7.5 ± 0.5 |
| 153 | TY Col | 05 57 50.8 | -38 04 04 | dG8e | | | | |
| 154 | GJ 3379 | 06 00 03.2 | 02 42 23 | M4 | M4 | | | |
| 155 | HIP 29295 | 06 10 34.6 | -21 51 53 | dM2.5e | M0.5 | M1/M2V | 0.3 ± 0.5 | 7.9 ± 0.5 |
| 156 | GJ 3391 | 06 21 12.9 | 44 14 31 | m | M2 | | 0.4 ± 0.2 | 6.7 ± 0.3 |
| 157 | HIP 30630 AB | 06 26 10.2 | 18 45 25 | dK3e-K2.Ve | | K0 | 1.0 ± 0.1 | 7.3 ± 0.2 |
| 158 | HIP 30920 A | 06 29 23.5 | -02 48 50 | dM4.5e | M4.5 | M4.5Ve | | |
| 159 | HIP 30920 B | 06 29 23.5 | -02 48 50 | | | | | |
| 160 | GJ 3395 | 06 31 01.3 | 50 02 49 | M0 | M0.5 | | 0.6 ± 0.2 | 6.7 ± 0.3 |
| 161 | GJ 3396 | 06 31 50.7 | 41 29 59 | m | M5 | | | |
| 162 | HM CMa | 06 45 20.0 | -16 48 36 | | | | | |
| 163 | HIP 32621 | 06 48 21.1 | 01 13 09 | dK2e | | K2Vevar | | |
| 164 | GJ 3417 | 06 57 56.7 | 62 19 23 | m | M4.5 | | | |
| 165 | GJ 3423 | 07 03 23.1 | 34 41 50 | m | M4 | | 0.1 ± 0.5 | 7.2 ± 0.3 |
| 166 | HIP 34603 | 07 10 01.8 | 38 31 46 | dM5e | M4.5 | M5Ve | 0.1 ± 0.5 | 7.5 ± 0.2 |
| 167 | GJ 1096 | 07 16 16.6 | 33 10 18 | m+ | M4 | | 0.1 ± 0.5 | 7.5 ± 0.2 |
| 168 | HIP 36626 B | 07 31 57.3 | 36 13 47 | dM4.5e | M3.5 | M4 | 0.1 ± 0.5 | 7.1 ± 0.4 |
| 169 | HIP 36626 A | 07 31 57.7 | 36 13 10 | dM3.5e | M2.5 | M3.5Ve | 0.3 ± 0.5 | 7.0 ± 0.4 |
| 170 | HD 60179 C | 07 34 37.4 | 31 52 09 | dM1e+dM1e | M0 | | | |
| 171 | GJ3454 | 07 36 25.0 | 07 04 44 | m | M5 | | | |
| 172 | HIP 37766 | 07 44 40.2 | 03 33 09 | dM4.5e | M4.5 | M4.5Ve | | |
| 173 | GJ 1101 | 07 55 55.5 | 83 23 08 | m | M3.5 | | 0.1 ± 0.5 | 7.5 ± 0.5 |
| 174 | GJ 3467 | 07 58 9.2 | 07 17 00 | m | M4 | | 0.1 ± 0.5 | 7.0 ± 0.5 |
| 175 | GJ 3469 B | 07 58 30.5 | 15 30 01 | m | M4.5 | | 0.1 ± 0.5 | 7.0 ± 0.5 |
| 176 | GJ 3468 A | 07 58 31.0 | 15 30 15 | m | M3.5 | | 0.1 ± 0.5 | 6.7 ± 0.5 |
| 177 | HIP 39826 B | 08 08 13.2 | 21 06 18 | m | M2.5 | M: | 0.1 ± 0.5 | 7.0 ± 0.5 |
| 178 | HIP 39896 B | 08 08 55.5 | 32 49 05 | dM3e | M3 | | 0.1 ± 0.5 | 6.8 ± 0.5 |
| 179 | HIP 39896 A | 08 08 56.4 | 32 49 11 | dM0.5e | K7 | M0.5V:e | 0.8 ± 0.1 | 6.7 ± 0.5 |
| 180 | CZ Cnc | 08 28 24.0 | 20 11 36 | | | | | |
| 181 | GJ 1111 | 08 29 49.5 | 26 49 24 | M6.5 | M6 | | | |
| 182 | BS Vel | 08 29 40.7 | -41 33 29 | | | | | |
| 183 | HIP 41824 B | 08 31 37.4 | 19 23 49 | | M4 | | 0.1 ± 0.5 | 7.5 ± 0.5 |
| 184 | HIP 41824 A | 08 31 37.6 | 19 23 39 | M5e | M3.5 | M5Ve | 0.1 ± 0.5 | 7.5 ± 0.5 |
| 185 | GJ 3504 | 08 32 30.7 | -01 34 45 | m | M6 | | | |
| 186 | G 051-019 | 08 37 22.8 | 26 12 22 | | | | | |
| 187 | DM Cnc | 08 38 32.1 | 18 27 54 | | | | | |
| 188 | GJ 3511 B | 08 39 48.2 | 08 56 16 | m+ | M3.5 | | 0.2 ± 0.5 | 6.4 ± 0.3 |
| 189 | GJ 3515 | 08 50 50.7 | 52 53 47 | m | M4.5 | | 0.1 ± 0.5 | 6.6 ± 0.3 |
| 190 | GJ 3517 | 08 53 41.3 | 03 06 40 | m | M9 | | | |
| 191 | GJ 3518 | 08 55 20.8 | -23 52 13 | m | M4 | | 0.1 ± 0.5 | 7.4 ± 0.3 |
| 192 | GJ 1116 A | 08 58 15.0 | 19 45 47 | m | M5.5 | | | |
| 193 | GJ 1116 B | 08 58 14.9 | 19 45 50 | m | M5.5 | | | |
| 194 | GJ 3522 | 08 58 56.1 | 08 28 28 | k | M3.5 | | | |
| 195 | GJ 1119 | 09 00 32.8 | 46 35 15 | m | M4.5 | | | |
| 196 | GJ 3537 | 09 09 39.2 | 06 42 08 | M4e | M3 | | 0.2 ± 0.5 | 6.6 ± 0.3 |
| 197 | HIP 45343 A | 09 14 22.8 | 52 41 12 | M0Ve | K7 | M0V | 0.5 ± 0.2 | 8.0 ± 0.7 |
| 198 | HIP 120005 B | 09 14 24.7 | 52 41 09 | M0Ve | K7 | | 0.5 ± 0.2 | 8.0 ± 0.7 |
| 199 | HIP 45731 | 09 19 22.9 | 62 03 17 | m | M0 | M: | 0.6 ± 0.1 | 6.1 ± 0.6 |
| 200 | GJ 3549 B | 09 18 49.7 | 26 45 27 | m | M5 | | 0.1 ± 0.5 | 7.5 ± 0.5 |
| 201 | GJ 1122 A | 09 19 19.1 | 38 31 18 | m | M4 | | 0.1 ± 0.5 | 7.0 ± 0.5 |
| 202 | GJ 1122 B | 09 19 19.1 | 38 31 23 | m | M4 | | 0.1 ± 0.5 | 7.0 ± 0.5 |
| 203 | GJ 3554 | 09 21 49.2 | 43 30 28 | m | M4 | | 0.1 ± 0.5 | 7.0 ± 0.5 |
| 204 | HIP 45963 | 09 22 25.9 | 40 12 04 | K2-K3.V | | K2V | 1.0 ± 0.1 | 7.3 ± 0.2 |
| 205 | HIP 46843 B | 09 32 43.8 | 26 59 19 | m | M5.5 | K0 | 0.1 ± 0.5 | 7.3 ± 0.2 |
| 206 | HIP 46816 | 09 32 25.6 | -11 11 05 | K0 | | K0 | 0.8 ± 0.2 | 7.8 ± 0.5 |
| 207 | HIP 47425 | 09 39 46.4 | -41 04 03 | M3 | M2.0 | M: | 0.2 ± 0.5 | 7.6 ± 0.5 |
| 208 | HIP 47650 | 09 42 51.7 | 70 02 22 | M3 | M3 | M4 | 0.2 ± 0.5 | 7.3 ± 0.6 |
| 209 | GJ 3571 | 09 53 55.4 | 20 56 42 | m | M4.5 | | | |
| 210 | GJ 3562 | 09 55 43.5 | 35 21 44 | M4 | M3 | | 0.3 ± 0.5 | 6.7 ± 0.3 |
| 211 | GJ 3577 A | 09 59 18.9 | 43 50 27 | m | M3.5 | | 0.3 ± 0.5 | 6.5 ± 0.3 |
| 212 | GJ 3578 B | 09 59 21.0 | 43 50 27 | m | M4 | | 0.3 ± 0.5 | 6.6 ± 0.3 |
| 213 | HIP 48904 | 09 58 34.3 | -46 25 30 | dM3.5e | M3.5 | M5 | 0.3 ± 0.5 | 6.7 ± 0.3 |
| 214 | HIP 49908 | 10 11 22.1 | 49 27 15 | K2Ve | K5 | K8V | | |
| 215 | HIP 50156 | 10 14 19.2 | 21 04 29 | dM0e | K7 | M0Ve | 0.8 ± 0.1 | 7.0 ± 0.5 |
| 216 | GJ 388 | 10 19 36.3 | 19 52 12 | dM4.5e | M3 | | | |
| 217 | GJ 9331 B | 10 31 30.7 | 57 05 16 | m | M4.5 | | 0.1 ± 0.5 | 7.1 ± 0.5 |
| 218 | GJ 3611 B | 10 34 30.4 | 46 18 09 | m+ | M4.5 | | 0.1 ± 0.5 | 7.1 ± 0.5 |
| 219 | GJ 398 | 10 36 01.2 | 05 07 12 | dM4e | M3.5 | | 0.1 ± 0.5 | 7.2 ± 0.5 |
| 220 | HIP 51884 | 10 36 02.2 | -11 54 48 | | | K0 | 0.9 ± 0.1 | 7.5 ± 0.1 |
| 221 | GJ 3613 | 10 38 27.4 | 48 32 05 | m | M3 | | 0.1 ± 0.5 | 6.6 ± 0.3 |

Continued

| GLK | designation | Ra [2000] | Dec [2000] | SpCl_1 | SpCl_2 | SpCl_3 | Mass [M$_\odot$] | age [Myr] |
|---|---|---|---|---|---|---|---|---|
| 222 | G 044-032 | 10 39 14.3 | 14 31 31 | | | | | |
| 223 | GJ 3622 | 10 48 12.6 | -11 20 10 | M6.5 | M6.5 | | | |
| 224 | GJ 3628 B | 10 50 38.3 | 51 45 01 | m | M3.5 | | 0.2 ± 0.5 | 6.5 ± 0.3 |
| 225 | GJ 3629 | 10 51 20.6 | 36 07 24 | m | M3 | | 0.2 ± 0.5 | 6.7 ± 0.3 |
| 226 | GJ 3630 | 10 52 03.5 | 00 32 38 | m | M4 | | 0.1 ± 0.5 | 7.3 ± 0.3 |
| 227 | GJ 3631 | 10 52 14.8 | 05 55 07 | m | M5 | | | |
| 228 | GJ 406 | 10 56 28.9 | 07 00 53 | dM6.5e | M5.5 | | | |
| 229 | GJ 3635 | 10 59 06.5 | 30 15 13 | m | M4.5 | | 0.1 ± 0.5 | 6.7 ± 0.4 |
| 230 | GJ 3636 | 11 00 51.3 | 12 04 30 | M5e | M5 | | 0.1 ± 0.5 | 7.0 ± 0.4 |
| 231 | HIP 53985 | 11 02 38.3 | 21 58 02 | dM2e | M0 | K | 0.6 ± 0.1 | 7.6 ± 0.4 |
| 232 | GJ 3639 | 11 03 10.0 | 36 39 07 | m | M3.5 | | 0.1 ± 0.5 | 6.7 ± 0.4 |
| 233 | HIP 54035 | 11 03 20.2 | 35 58 12 | M2Ve | M2V | | | |
| 234 | GJ 412 B | 11 05 30.4 | 43 31 17 | M6e | M6 | | | |
| 235 | CW UMa | 11 11 51.7 | 33 32 11 | dM4.5e | M3.5 | | 0.1 ± 0.5 | 7.1 ± 0.4 |
| 236 | DH Car | 11 14 52.4 | -61 45 38 | | | | | |
| 237 | GJ 3653 | 11 15 54.4 | 55 19 51 | M0 | M0.5 | | 0.6 ± 0.1 | 6.7 ± 0.3 |
| 238 | HIP 55360 | 11 20 04.8 | 65 50 47 | dM1.5 | M0 | M1Vvar | | |
| 239 | HIP 55454 A | 11 21 26.7 | -20 27 14 | dK4-5.J | | K4/K5V | 0.6 ± 0.2 | 8.0 ± 1.0 |
| 240 | HIP 55454 B | 11 21 26.6 | -20 27 18 | m | M1 | | | |
| 241 | BT UMa | 11 30 53.7 | 44 14 34 | | | | | |
| 242 | HIP 56244 | 11 31 46.5 | -41 02 47 | dM4.5e | M3.5 | M | 0.1 ± 0.5 | 7.3 ± 0.5 |
| 243 | HIP 56685 | 11 37 24.6 | 47 27 45 | M0.Ve | | K4V | 0.6 ± 0.1 | 7.2 ± 0.2 |
| 244 | GJ 3682 | 11 43 30.6 | 25 18 00 | m | M4 | | 0.1 ± 0.5 | 7.0 ± 0.4 |
| 245 | HIP 57269 | 11 44 38.5 | -49 25 03 | K1V/K2V | | K0/K1Vp | 0.9 ± 0.1 | 7.5 ± 0.1 |
| 246 | GJ 3684 | 11 46 49.6 | 70 01 56 | m | M4 | | 0.1 ± 0.5 | 7.0 ± 0.5 |
| 247 | GJ 3685 A | 11 47 45.8 | 00 15 33 | m | M4 | | 0.1 ± 0.5 | 7.3 ± 0.5 |
| 248 | HIP 57548 | 11 47 44.4 | 00 48 16 | dM4.5 | M4 | M4.5V | | |
| 249 | GJ 3693 | 11 47 49.6 | 00 15 18 | m | M5.5 | | | |
| 250 | HIP 57939 B | 11 52 58.8 | 37 43 07 | G8.VI | G8Vp | | | |
| 251 | GJ 3693 | 11 53 53.3 | 06 59 58 | M6: | M6 | | | |
| 252 | GJ 452.1 | 11 54 07.8 | 09 48 27 | M3.5 | M3.5 | | 0.1 ± 0.5 | 7.5 ± 0.5 |
| 253 | GJ 1154 AB | 12 14 17.1 | 00 37 26 | m | M5V | | | |
| 254 | GJ 459.1 | 12 15 44.1 | 52 31 02 | | DA | | | |
| 255 | GJ 3719 | 12 16 58.5 | 31 09 22 | dM4-5e | M3.5 | | 0.3 ± 0.5 | 6.7 ± 0.3 |
| 256 | GJ 1156 | 12 18 59.4 | 11 07 34 | MVe | M5 | | | |
| 257 | HIP 60178 | 12 20 25.5 | 00 35 00 | M0V | M0 | | 0.6 ± 0.1 | 7.2 ± 0.3 |
| 258 | EXO 121914+0213.2 | 12 21 48.0 | 01 56 36 | dM0e | M0Ve | | | |
| 259 | GJ 3726 C | 12 27 02.4 | 27 00 45 | dM5e | M4.5 | | 0.1 ± 0.5 | 6.7 ± 0.3 |
| 260 | GJ 3729 | 12 29 03.0 | 41 43 50 | m | M3.5 | | 0.1 ± 0.5 | 7.0 ± 0.3 |
| 261 | GJ 3720 | 12 29 27.2 | 22 59 46 | dM5 | M4 | | 0.1 ± 0.5 | 6.9 ± 0.3 |
| 262 | AS CVn | 12 30 01.0 | 31 55 16 | | | | | |
| 263 | GJ 3743 | 12 32 26.3 | 20 23 28 | dM3e | M3Ve | M2.5 | 0.3 ± 0.5 | 6.7 ± 0.3 |
| 264 | GJ 473 A | 12 33 17.4 | 09 01 15 | dM5.5e | M5 | | | |
| 265 | GJ 473 B | 12 33 17.4 | 09 01 15 | M7 | | | | |
| 266 | HIP 61722 | 12 39 04.7 | 47 02 23 | m | M2 | | 0.4 ± 0.1 | 6.7 ± 0.3 |
| 267 | GJ 3739 | 12 39 46.4 | 25 31 05 | m | M4.5 | | 0.1 ± 0.5 | 6.7 ± 0.3 |
| 268 | GJ 3745 | 12 45 47.2 | 52 55 17 | m | M3.5 | | 0.2 ± 0.5 | 6.7 ± 0.3 |
| 269 | HIP 62556 | 12 49 02.8 | 66 06 37 | dM4e | M3 | M4 | 0.1 ± 0.5 | 7.5 ± 0.5 |
| 270 | GJ 3751 | 12 49 34.4 | 09 28 30 | M3.5 | M3.5 | | 0.2 ± 0.5 | 6.7 ± 0.3 |
| 271 | GJ 488.2 B | 12 54 57.2 | -6 19 50 | m | M4 | | 0.1 ± 0.5 | 7.0 ± 0.4 |
| 272 | HIP 63253 B | 12 57 39.4 | 35 13 19 | dM4e | M4 | | 0.1 ± 0.5 | 6.7 ± 0.4 |
| 273 | HIP 63253 A | 12 57 40.3 | 35 13 30 | M0.5e | M0.5 | M0Vvar | 0.6 ± 0.1 | 6.8 ± 0.4 |
| 274 | GJ 493.1 | 13 00 33.5 | 05 41 08 | dM5e | M4.5 | | | |
| 275 | HIP 63510 | 13 00 46.6 | 12 22 33 | dM1.5e | M0.5 | M2 | 0.5 ± 0.1 | 7.5 ± 0.5 |
| 276 | EXO 1259.6+1238 | 13 02 06.5 | 12 22 27 | dM3e | | | | |
| 277 | GJ 1167 A | 13 09 35.1 | 28 59 07 | dM5 | M4 | | 0.1 ± 0.5 | 7.3 ± 0.5 |
| 278 | GJ 3780 | 13 23 38.6 | -25 54 40 | m | M3.5 | | 0.1 ± 0.5 | 7.0 ± 0.5 |
| 279 | GJ 3786 | 13 27 20.6 | -31 10 37 | M4 | M3.5 | | 0.1 ± 0.5 | 6.8 ± 0.5 |
| 280 | GJ 3789 | 13 31 46.7 | 29 16 36 | M4e | M4 | | | |
| 281 | VW Com A | 13 32 44.6 | 16 48 39 | dM3.5e | M2.5 | | 0.2 ± 0.5 | 7.4 ± 0.5 |
| 282 | VW Com B | 13 32 44.8 | 16 48 41 | dM4e | M3 | | | |
| 283 | HIP 66252 | 13 34 43.2 | -08 20 31 | dK5 | | K7V | 0.7 ± 0.1 | 8.0 ± 0.5 |
| 284 | GJ 520 C | 13 37 40.6 | 48 07 54 | m | M4 | | 0.1 ± 0.5 | 6.7 ± 0.5 |
| 285 | GJ 3800 | 13 42 10.0 | -16 00 21 | m | M4 | | 0.1 ± 0.5 | 7.0 ± 0.5 |
| 286 | HIP 67155 | 13 45 43.8 | 14 53 29 | M4Ve | M1.5 | M3V | 0.4 ± 0.1 | 7.5 ± 0.1 |
| 287 | GJ 3808 | 13 48 48.5 | 04 06 03 | m | M4 | | 0.1 ± 0.5 | 7.0 ± 0.1 |
| 288 | HIP 67422 A | 13 49 04.0 | 26 58 48 | K4.V | | K2 | 0.7 ± 0.1 | 8.0 ± 0.2 |
| 289 | HIP 67422 B | 13 49 04.0 | 26 58 44 | dK6 | | | | |
| 290 | GJ 3820 | 13 59 10.9 | -19 49 59 | K2: | M4 | | 0.1 ± 0.5 | 7.5 ± 0.5 |
| 291 | G 064-034 | 13 59 51.8 | -05 22 56 | | | | | |
| 292 | V760 Cen | 14 12 31.9 | -59 25 28 | | | | | |
| 293 | GJ 3828 B | 14 12 12.1 | 00 35 18 | m+ | M6.5 | | | |
| 294 | GJ 540.2 | 14 13 04.8 | -12 01 27 | dM5.5e | M4.5 | | 0.1 ± 0.5 | 7.5 ± 0.5 |
| 295 | HIP 69562 B | 14 14 17.0 | -15 21 09 | m | M3.5 | | 0.3 ± 0.5 | 6.4 ± 0.3 |
| 296 | HIP 69562 A | 14 14 21.4 | -15 21 22 | K4V | K7 | K4V | 0.8 ± 0.1 | 6.7 ± 0.4 |
| 297 | GJ 3839 | 14 17 03.2 | 31 42 47 | m | M4 | | | |
| 298 | GJ 3842 | 14 20 04.7 | 39 02 59 | M0:e | M2.5 | | 0.3 ± 0.5 | 6.8 ± 0.4 |
| 299 | GJ 1183 A | 14 27 56.2 | 00 22 31 | m | M4.5 | | | |
| 300 | GJ 1183 B | 14 27 56.5 | 00 22 19 | m | M4.5 | | | |
| 301 | HIP 70890 | 14 29 43.0 | -62 40 46 | dM5e | M5.5 | M5Ve | | |
| 302 | GJ 3849 | 14 28 43.3 | 33 10 34 | dM9 | M9 | | | |
| 303 | GJ 3855 | 14 30 35.0 | 59 43 08 | M6.5 | M5.5 | | | |
| 304 | GJ 3858 | 14 32 10.6 | 16 00 49 | m | M4 | | 0.1 ± 0.5 | 7.0 ± 0.4 |

Continues next page

Continued

| GLK | designation | Ra [2000] | Dec [2000] | SpCl_1 | SpCl_2 | SpCl_3 | Mass [M$_\odot$] | age [Myr] |
|---|---|---|---|---|---|---|---|---|
| 305 | GJ 3861 | 14 36 52.4 | 58 21 00 | m | M2.5 | | 0.2 ± 0.5 | 7.4 ± 0.4 |
| 306 | HIP 71631 | 14 39 00.2 | 64 17 30 | G0.Ve | | F8 | 1.1 ± 0.1 | 7.7 ± 0.4 |
| 307 | HIP 72659 A | 14 51 23.4 | 19 06 01 | dG8e | | G8V + K4V | 0.9 ± 0.1 | 7.6 ± 0.4 |
| 308 | HIP 72944 AB | 14 54 29.2 | 16 06 04 | dM2e | M2 | M2Ve | 0.3 ± 0.5 | 7.5 ± 0.4 |
| 309 | GJ 3875 | 14 54 55.0 | 41 08 46 | m | M4.5 | | 0.1 ± 0.5 | 6.7 ± 0.4 |
| 310 | GJ 3877 | 14 56 37.7 | -28 09 39 | dM8 | M7 | | | |
| 311 | GJ 1187 | 14 57 53.4 | 56 39 29 | m | M5.5 | | | |
| 312 | HIP 73555 | 15 01 56.8 | 40 23 26 | | | G8III | 4.0 ± 1.0 | 5.0 ± 0.3 |
| 313 | GJ 3898 | 15 12 38.4 | 45 43 43 | m | M4 | | 0.1 ± 0.5 | 7.0 ± 0.4 |
| 314 | HIP 75187 | 15 21 52.9 | 20 58 40 | dM0e | M1.5 | M9 | 0.4 ± 0.2 | 7.5 ± 0.4 |
| 315 | GJ 3910 | 15 31 54.4 | 28 51 08 | m | M4.5 | | 0.1 ± 0.5 | 7.2 ± 0.4 |
| 316 | HIP 76629 | 15 38 57.5 | -57 42 27 | | | K0V | 0.9 ± 0.1 | 7.5 ± 0.2 |
| 317 | GJ 3928 | 15 55 31.9 | 35 12 00 | m | M4.5 | | 0.1 ± 0.5 | 7.3 ± 0.5 |
| 318 | HIP 78259 | 15 58 43.9 | 25 34 11 | dK2+dK6 | | K2V | 0.9 ± 0.3 | 5.0 ± 0.3 |
| 319 | GJ 3936 B | 16 01 44.5 | 30 27 40 | m | M4.5 | | 0.1 ± 0.5 | 7.3 ± 0.5 |
| 320 | EXO 161538+0624.2 | 16 18 05.0 | 06 16 54 | dM3e | | | | |
| 321 | HIP 79796 | 16 17 05.4 | 55 16 09 | dM1.5e | M1 | M1.5Ve | 0.5 ± 0.2 | 6.3 ± 0.4 |
| 322 | GJ 3954 | 16 26 48.2 | -17 23 30 | m | M4.5 | | 0.1 ± 0.5 | 7.3 ± 0.5 |
| 323 | GJ 3959 | 16 31 18.8 | 40 51 48 | m+ | M5 | | | |
| 324 | GJ 630.1 A | 16 34 20.3 | 57 09 45 | dM4e | M4.5 | | | |
| 325 | GJ 3966 | 16 35 27.2 | 35 00 57 | m | M4 | | 0.1 ± 0.5 | 7.3 ± 0.5 |
| 326 | GJ 1204 | 16 36 05.8 | 08 48 49 | m | M4 | | 0.1 ± 0.5 | 7.3 ± 0.5 |
| 327 | HIP 81300 | 16 36 21.5 | -02 19 29 | K0.Ve | | K2V | 0.9 ± 0.1 | 7.5 ± 0.3 |
| 328 | V801 Ara | 16 40 54.9 | -53 45 34 | | | | | |
| 329 | GJ 3967 | 16 40 05.7 | 00 42 19 | m | M4 | | 0.1 ± 0.5 | 7.3 ± 0.5 |
| 330 | GJ 3971 | 16 40 19.1 | 67 35 34 | m | M5.5 | | | |
| 331 | GJ 3976 | 16 50 57.8 | 22 27 02 | m | M4.5 | | | |
| 332 | HIP 82588 | 16 52 58.8 | 00 01 35 | G8V | | | | |
| 333 | V781 Her | 16 54 43.1 | 46 54 24 | | | | | |
| 334 | HIP 82817 A | 16 55 28.8 | -08 20 11 | dM3.5e | M3 | M3Ve | 0.1 ± 0.5 | 7.7 ± 0.5 |
| 335 | HIP 82817 B | 16 55 28.8 | -08 20 11 | dM4.5e | | | | |
| 336 | HIP 82817 C | 16 55 35.2 | -08 23 35 | M7 | M7 | | | |
| 337 | GJ 1207 | 16 57 05.4 | -04 20 52 | dM3.5 | M3.5 | | 0.1 ± 0.5 | 7.7 ± 0.5 |
| 338 | HIP 82959 | 16 57 10.7 | 35 17 12 | K2 | K2 | | | |
| 339 | GJ 3981 | 16 58 25.4 | 13 58 09 | m | M4 | | 0.1 ± 0.5 | 7.3 ± 0.5 |
| 340 | V1802 Oph | 17 18 00.5 | -19 12 52 | | | | | |
| 341 | V1865 Oph | 17 19 30.3 | -19 26 26 | | | | | |
| 342 | HIP 84794 B | 17 19 53.0 | 26 30 02 | dM4.5e | M4.5 | | 0.1 ± 0.5 | 7.5 ± 0.5 |
| 343 | HIP 84794 A | 17 19 54.2 | 26 30 03 | dM4e | M3.5 | M4 | 0.1 ± 0.5 | 7.0 ± 0.5 |
| 344 | V475 Her | 17 19 59.6 | 24 12 06 | | | | | |
| 345 | V1932 Oph | 17 21 21.8 | -19 05 22 | | | | | |
| 346 | V2020 Oph | 17 23 49.5 | -21 53 28 | | | | | |
| 347 | HIP 86346 A | 17 38 39.6 | 61 14 16 | dK8 | K7 | M... | 0.8 ± 0.2 | 6.7 ± 0.3 |
| 348 | HIP 86346 B | 17 38 40.8 | 61 13 57 | | M4 | | 0.3 ± 0.5 | 6.4 ± 0.3 |
| 349 | GJ 1224 | 18 07 33.2 | -15 57 46 | m | M4.5 | | | |
| 350 | V2648 Sgr | 18 12 44.1 | -33 26 10 | | | | | |
| 351 | GJ 4044 | 18 13 06.3 | 26 01 51 | m | M4 | | 0.1 ± 0.5 | 6.9 ± 0.3 |
| 352 | AM Her | 18 16 13.4 | 49 52 04 | | | | | |
| 353 | V3127 Sgr | 18 21 46.1 | -36 37 04 | | | | | |
| 354 | GJ 4053 | 18 18 56.6 | 66 11 36 | m | M4.5 | | | |
| 355 | V2354 Sgr | 18 30 11.7 | -24 52 26 | M5 | | | | |
| 356 | V3497 Sgr | 18 31 27.4 | -31 25 29 | | | | | |
| 357 | HIP 90959 | 18 33 17.8 | 22 18 51 | K4.V | | K4V | 0.7 ± 0.1 | 8.0 ± 0.5 |
| 358 | HIP 91009 | 18 33 55.8 | 51 43 09 | dK6e | | K7Vvar | 0.8 ± 0.1 | 7.2 ± 0.3 |
| 359 | V3640 Sgr | 18 36 16.0 | -32 43 50 | | | | | |
| 360 | GJ 1230 A | 18 41 09.3 | 24 47 14 | k-m | M4.5 | | | |
| 361 | GJ 4068 | 18 35 51.8 | 80 05 37 | M4e | M3.5 | | 0.2 ± 0.5 | 7.0 ± 0.3 |
| 362 | GJ 4069 | 18 41 37.5 | 39 42 13 | m | M4 | | 0.1 ± 0.5 | 7.0 ± 0.3 |
| 363 | GJ 4071 | 18 42 45.0 | 13 54 16 | m | M4 | | 0.1 ± 0.5 | 7.5 ± 0.3 |
| 364 | GJ 4073 | 18 43 22.6 | 40 39 55 | m | M5.5 | | | |
| 365 | HIP 92403 | 18 49 49.4 | -23 50 10 | dM4.5e | M3.5 | M3.5Ve | | |
| 366 | HIP 92871 | 18 55 27.4 | 08 24 09 | dM3e | M3 | M2Ve | 0.2 ± 0.5 | 6.7 ± 0.5 |
| 367 | HIP 94557 A | 19 14 39.2 | 19 19 04 | M3 | M3.5 | M: | 0.2 ± 0.5 | 6.3 ± 0.5 |
| 368 | V1348 Aql | 19 16 17.3 | -09 27 13 | | | | | |
| 369 | HIP 94761 A | 19 16 55.2 | 05 10 08 | M3.5Ve | M2.5 | M3.5V | 0.2 ± 0.5 | 7.8 ± 0.5 |
| 370 | HIP 94761 B | 19 16 57.2 | 05 09 00 | dM5e | M8 | | | |
| 371 | V1335 Aql | 19 18 17.2 | -05 06 05 | | | | | |
| 372 | GJ 4110 | 19 26 49.3 | 16 43 03 | m | M3 | | 0.2 ± 0.5 | 6.7 ± 0.5 |
| 373 | G 125-012 | 19 31 15.4 | 31 21 53 | | | | | |
| 374 | FV Vul | 19 38 40.8 | 27 35 56 | dMe | | | | |
| 375 | V1406 Aql B | 19 45 57.4 | 04 14 55 | | | | | |
| 376 | GJ 1243 | 19 51 09.1 | 46 28 57 | m | M4 | | 0.1 ± 0.5 | 7.4 ± 0.6 |
| 377 | HIP 97944 | 19 54 17.8 | -23 56 28 | dK2-3e | | K3/K4V | 1.0 ± 0.1 | 7.4 ± 0.2 |
| 378 | GJ 1245 A | 19 53 54.5 | 44 24 50 | M5.5Ve | M5.5 | | | |
| 379 | GJ 1245 B | 19 53 55.2 | 44 24 48 | | M5.5 | | | |
| 380 | KO Vul | 19 57 16.4 | 29 06 21 | | | | | |
| 381 | HIP 98698 | 20 02 47.1 | 03 19 34 | K4.V | | K4V | 0.8 ± 0.1 | 7.7 ± 0.3 |
| 382 | HIP 98906 | 20 05 02.2 | 54 26 3 | dM3e | M0 | M3 | 0.5 ± 0.2 | 7.7 ± 0.3 |
| 383 | HIP 99150 B | 20 07 45.0 | -31 45 14 | M3.5 | M3.0 | M | 0.2 ± 0.5 | 7.3 ± 0.3 |
| 384 | GJ 1250 | 20 08 21.5 | 33 17 35 | m | M4.5 | | 0.1 ± 0.5 | 7.0 ± 0.4 |
| 385 | G 024-016 | 20 29 48.4 | 09 41 20 | dM6e | M4.5 | | | |
| 386 | G 144-016 | 20 37 20.8 | 21 56 54 | M2 | M0 | | 0.7 ± 0.2 | 6.9 ± 0.3 |
| 387 | HIP 102141 A | 20 41 51.2 | -32 26 08 | dM4.5eJ | M4.5 | Mpe | 0.1 ± 0.5 | 6.8 ± 0.5 |

Continued

| GLK | designation | Ra [2000] | Dec [2000] | SpCl_1 | SpCl_2 | SpCl_3 | Mass [M⊙] | age [Myr] |
|-----|-------------|-----------|------------|--------|--------|--------|-----------|-----------|
| 388 | HIP 102141 B | 20 41 51.1 | -32 26 13 | dM4.5e | M4.0 | | | |
| 389 | HIP 102119 | 20 41 42.2 | -22 19 20 | K5V | K5 | K5V | $1.0 \pm 0.2$ | $7.0 \pm 0.5$ |
| 390 | MV Pav | 20 43 10.4 | -69 42 44 | dM5.: | | | | |
| 391 | V1589 Cyg | 20 42 49.0 | 41 23 01 | | | | | |
| 392 | EXO 204152-3129.3 | 20 44 57.0 | -31 18 24 | dM3e | | | | |
| 393 | GJ 802 | 20 43 18.4 | 55 20 39 | dM5e | M5 | | $0.1 \pm 0.5$ | $7.4 \pm 0.5$ |
| 394 | HIP 102409 | 20 45 09.6 | -31 20 28 | dM2.5e | M0.0 | M1Ve | $0.6 \pm 0.1$ | $7.5 \pm 0.2$ |
| 395 | HIP 103393 A | 20 56 48.5 | -04 50 50 | dM4e | M4 | | $0.2 \pm 0.5$ | $6.5 \pm 0.4$ |
| 396 | HIP 103655 A | 21 00 05.3 | 40 04 13 | dM3eJ | M1.5 | M3Ve | $0.5 \pm 0.1$ | $7.0 \pm 0.5$ |
| 397 | HIP 103655 B | 21 00 05.4 | 40 04 13 | | | | | |
| 398 | HIP 104214 A | 21 06 53.8 | 38 44 58 | K5.Ve | | | | |
| 399 | HIP 104217 B | 21 06 55.3 | 38 44 32 | K7Ve | K5 | | | |
| 400 | HIP 104383 B | 21 08 44.8 | -04 25 17 | | M3 | | $0.2 \pm 0.5$ | $6.7 \pm 0.5$ |
| 401 | AK Mik | 21 09 52.3 | -39 50 15 | | | | | |
| 402 | GJ 4186 B | 21 16 03.6 | 29 51 45 | m | M3.5 | | $0.1 \pm 0.5$ | $7.0 \pm 0.5$ |
| 403 | GJ 4185 A | 21 16 05.6 | 29 51 50 | m | M3.5 | | $0.1 \pm 0.5$ | $7.5 \pm 0.5$ |
| 404 | HIP 105090 | 21 17 15.2 | -38 52 03 | M0Ve | K7.0 | M1/M2V | | |
| 405 | GJ 4187 A | 21 17 36.1 | -08 54 10 | M1 | M2.5 | | $0.3 \pm 0.5$ | $6.7 \pm 0.5$ |
| 406 | LHS 510 | 21 30 45.1 | -40 41 52 | M3 | M1.5 | | $0.4 \pm 0.1$ | $5.6 \pm 0.5$ |
| 407 | HIP 106231 | 21 31 01.7 | 23 20 07 | dK8 | | K8 | $0.7 \pm 0.2$ | $7.0 \pm 0.1$ |
| 408 | GJ 4201 | 21 32 21.8 | 24 33 41 | m | M3.5 | | $0.1 \pm 0.5$ | $7.4 \pm 0.5$ |
| 409 | G 026-013 | 21 33 48.8 | -06 51 06 | M3.5 | M4 | | $0.1 \pm 0.5$ | $7.3 \pm 0.5$ |
| 410 | HIP 107350 | 21 44 31.3 | 14 46 19 | G0.Ve | | G0V | $1.2 \pm 0.1$ | $7.5 \pm 0.2$ |
| 411 | GJ 4281 | 21 45 44.8 | 20 46 56 | m | M3.5 | | $0.1 \pm 0.5$ | $6.7 \pm 0.5$ |
| 412 | HIP 107705 | 21 49 5.9 | -72 06 09 | dM2e | M0.5 | M2Ve | $0.5 \pm 0.2$ | $7.2 \pm 0.5$ |
| 413 | HIP 107948 | 21 52 10.4 | 05 37 36 | dM2 | M3 | M1V: | $0.2 \pm 0.5$ | $6.4 \pm 0.4$ |
| 414 | HIP 108405 A | 21 57 41.2 | -51 00 22 | M2.5 | M2.5 | M0 | $0.3 \pm 0.5$ | $6.7 \pm 0.4$ |
| 415 | HIP 108706 | 22 01 13.1 | 28 18 25 | m+ | M4 | | $0.1 \pm 0.5$ | $7.5 \pm 0.4$ |
| 416 | EXO 220543-47255 | 22 08 51.0 | -47 10 48 | dK4e | | | | |
| 417 | G 188-046 | 22 11 33.4 | 31 33 40 | dM0e | | | | |
| 418 | GJ 4264 | 22 13 35.5 | 25 58 10 | m | M3.5 | | $0.1 \pm 0.5$ | $6.8 \pm 0.4$ |
| 419 | GJ4269 B | 22 16 01.0 | 54 39 59 | m | M4 | | $0.1 \pm 0.5$ | $6.7 \pm 0.4$ |
| 420 | GJ 852 A | 22 17 19.0 | -08 48 13 | dM4.5e | M4 | | | |
| 421 | GJ 852 B | 22 17 18.8 | -08 48 19 | dM5e | M5 | | | |
| 422 | GJ 4274 | 22 23 06.7 | -17 36 19 | M4 | M4.5 | | | |
| 423 | HIP 110526 A | 22 23 29.1 | 32 27 34 | dM0eJ | M3 | M0... | $0.2 \pm 0.5$ | $7.0 \pm 0.4$ |
| 424 | HIP 110526 B | 22 26 16.0 | 03 00 21 | m | M5 | | $0.1 \pm 0.5$ | $7.0 \pm 0.4$ |
| 425 | HIP 110893 B | 22 27 59.8 | 57 41 44 | dM4.5e | M4 | M2V | | |
| 426 | GJ 4281 | 22 28 53.9 | -13 25 31 | M6.5 | M6.5 | | | |
| 427 | GJ 4282 | 22 33 22.4 | -09 36 54 | M3 | M3 | | $0.2 \pm 0.5$ | $7.0 \pm 0.5$ |
| 428 | HIP 111766 | 22 38 29.8 | -65 22 43 | k-m | M3.5 | | $0.2 \pm 0.5$ | $7.0 \pm 0.6$ |
| 429 | GJ 9791 | 22 38 26.9 | -65 23 05 | | M3.5 | | $0.2 \pm 0.5$ | $6.7 \pm 0.5$ |
| 430 | G 156-031 AB | 22 38 33.7 | -15 18 02 | dM5.5e | M5.5 | | | |
| 431 | HD 214479 B | 22 38 45.3 | -20 36 52 | dM4e | M3.5 | | $0.1 \pm 0.5$ | $7.5 \pm 0.5$ |
| 432 | HD 214479 A | 22 38 45.6 | -20 37 16 | dM2e | M1.5 | | $0.4 \pm 0.2$ | $7.5 \pm 0.5$ |
| 433 | G 127-050 | 22 43 22.9 | 22 08 17 | m | M4.5 | | $0.1 \pm 0.5$ | $7.3 \pm 0.5$ |
| 434 | GJ 871 B | 22 45 00.0 | -33 15 25 | dM4e | | | | |
| 435 | HIP 112460 | 22 46 49.7 | 44 20 03 | dM4.5e | M3.5 | M4.5Ve | | |
| 436 | HIP 112914 | 22 51 59.6 | 31 43 42 | dM3.5e | M3 | K5 | $0.3 \pm 0.5$ | $6.0 \pm 1.0$ |
| 437 | HIP 113283 | 22 56 24.1 | -31 33 56 | K5.Ve | | K4Vp | $0.8 \pm 0.1$ | $7.5 \pm 0.3$ |
| 438 | HIP 114066 | 23 06 04.8 | 63 55 34 | dM0 | M0 | M0 | $0.7 \pm 0.2$ | $6.6 \pm 0.6$ |
| 439 | BD -16 621 | 23 08 34.5 | -15 24 35 | dM2.5e | M0 | | | |
| 440 | HIP 114379 | 23 09 57.4 | 47 57 30 | dK0e | | K0Ve | $0.9 \pm 0.1$ | $7.7 \pm 0.4$ |
| 441 | HIP 114622 | 23 13 17.0 | 57 10 06 | K3.Ve | | K3Vvar | $0.8 \pm 0.1$ | $7.5 \pm 0.3$ |
| 442 | G 068-005 | 23 17 27.8 | 19 36 47 | M4 | M3.5 | | $0.1 \pm 0.5$ | $7.3 \pm 0.3$ |
| 443 | FZ And | 23 25 34.9 | 53 07 51 | m | M4.5 | | | |
| 444 | G 190-027 B | 23 29 22.3 | 41 27 51 | M3: | M4 | | $0.1 \pm 0.5$ | $6.8 \pm 0.5$ |
| 445 | G 190-028 A | 23 29 23.2 | 41 28 6 | M2 | M3.5 | | $0.1 \pm 0.5$ | $6.8 \pm 0.5$ |
| 446 | HIP116003 | 23 30 13.4 | -20 23 28 | M2Ve | M3 | M2Ve | $0.1 \pm 0.5$ | $7.2 \pm 0.5$ |
| 447 | GJ 1285 | 23 31 44.9 | -02 44 40 | dM4e | | | | |
| 448 | HIP 116132 A | 23 31 52.2 | 19 56 14 | dM4e | M3.5 | M6Ve | $0.1 \pm 0.5$ | $7.6 \pm 0.5$ |
| 449 | HIP 116132 B | 23 31 52.5 | 19 56 13 | dM5e | M4.5 | | | |
| 450 | HIP 116191 A | 23 32 46.8 | -16 45 8 | M3.5J | M2 | | | |
| 451 | HIP 116317 | 23 34 03.3 | 00 10 46 | dM4 | M2.5 | M3 | $0.2 \pm 0.5$ | $7.0 \pm 0.5$ |
| 452 | GJ 4345 | 23 35 41.8 | 06 11 21 | m | M5 | | $0.1 \pm 0.5$ | $7.0 \pm 0.5$ |
| 453 | G 068-034 A | 23 38 58.6 | 21 01 23 | m | M3.5 | | $0.1 \pm 0.5$ | $6.7 \pm 0.5$ |
| 454 | G 190-042 | 23 41 55.0 | 44 10 39 | dM6e | M5 | | | |
| 455 | GJ 1288 | 23 42 50.0 | 30 49 08 | m | M4.5 | | $0.1 \pm 0.5$ | $7.2 \pm 0.5$ |
| 456 | HIP 117069 | 23 43 59.5 | 64 44 29 | M1.5 | M0.5 | M1 | $0.5 \pm 0.1$ | $6.0 \pm 0.3$ |
| 457 | GJ 1290 | 23 44 20.6 | 21 36 03 | m | M3.5 | | $0.1 \pm 0.5$ | $6.7 \pm 0.3$ |
| 458 | G 273-130 | 23 45 31.5 | -16 10 19 | m | M5 | | | |
| 459 | G 275-106 | 23 48 36.3 | -27 39 37 | M3.5: | M2.5 | | $0.2 \pm 0.5$ | $6.8 \pm 0.3$ |
| 460 | HIP 117473 | 23 49 12.6 | 02 24 06 | M2Ve | M1 | M2V | | |
| 461 | G 030-018 | 23 49 15.0 | 10 5 41 | dM4: | M4 | | $0.1 \pm 0.5$ | $6.8 \pm 0.3$ |
| 462 | G 273-185 B | 23 57 19.1 | -12 58 40 | M4 | M4 | | $0.1 \pm 0.5$ | $7.2 \pm 0.3$ |
| 463 | GJ 4381 | 23 57 49.9 | 38 37 46 | m | M3 | | $0.3 \pm 0.5$ | $6.8 \pm 0.3$ |

# Space velocity of the flare stars

**Table 2:** Space velocities of the Gershberg et al. (1999) flare stars. The data was taken from the Hipparcos catalog and the catalog of nearby stars version 4.

| GLK | designation | U | V | W | eU | eV | eW |
|---|---|---|---|---|---|---|---|
| 1 | HIP 439 | -75.2 | -98.1 | -33.9 | 0.4 | 0.5 | 0.7 |
| 3 | GJ 3010 | +16 | -27 | +13 | | | |
| 4 | GJ 3015 B | +7.8 | -2.2 | -17.6 | 0.1 | 0.5 | 0.5 |
| 7 | HIP 1295 A | -24.9 | -84.0 | -49.3 | 14.0 | 33.5 | 29.0 |
| 8 | GJ 3022 | -29 | +8 | -19 | | | |
| 9 | HIP 1475 A | -49.2 | -12.2 | -3.0 | 0.4 | 0.6 | 0.2 |
| 10 | HIP 1475 B | -49 | -12 | -3 | | | |
| 11 | GJ 3027 | -27 | -18 | -13 | | | |
| 12 | HIP 1720 | +51.7 | -25.6 | -32.6 | 5.4 | 4.2 | 17.0 |
| 13 | GJ 3030 | -20 | -9 | -6 | | | |
| 14 | HIP 1771 | +043 | -25 | -35 | | | |
| 15 | HIP 1803 | -35.7 | -14.9 | 0.4 | 0.7 | 0.3 | 0.7 |
| 16 | GJ 3033 | -48 | -24 | -8 | | | |
| 17 | GJ 2005 | -12 | +18 | +37 | | | |
| 18 | GJ 3036 | -21 | -19 | +7 | | | |
| 19 | HIP 2552 AC | -69.8 | -44.2 | -16.3 | 2.6 | 2.1 | 0.6 |
| 20 | GJ 3039 | -7 | -7 | -4 | | | |
| 25 | HIP 3362 | -27.2 | -13.2 | 7.0 | 2.2 | 2.9 | 1.7 |
| 27 | HIP 3493 B | -54.0 | 4.8 | -23.1 | 3.9 | 0.3 | 0.8 |
| 29 | HIP 3937 A | -12.7 | -1.3 | -7.4 | 7.9 | 11.9 | 11.0 |
| 30 | HIP 4022 B | -26.8 | -39.8 | -16.6 | 0.6 | 0.9 | 0.7 |
| 32 | HIP 4856 | -58.7 | -34.7 | -10.6 | 1.1 | 1.5 | 0.3 |
| 33 | GJ 3069 | +18 | +9 | -8 | | | |
| 34 | GJ 51 | -32 | -16 | +6 | | | |
| 35 | HIP 4927 B | -42.2 | -29.8 | 8.0 | 8.9 | 10.8 | 12.1 |
| 36 | GJ 2021 | -5 | -21 | -1 | | | |
| 37 | GJ 3076 | -8 | -3 | -9 | | | |
| 38 | HIP 5643 | -28.7 | -0.5 | -23.6 | 0.7 | 0.2 | 1.7 |
| 39 | GJ 1033 | -6 | -4 | -2 | | | |
| 44 | GJ 65 A | -44 | -20 | -19 | | | |
| 48 | HIP 8768 | -36.4 | -29.2 | -3.5 | 0.7 | 0.5 | 1.7 |
| 49 | HIP 9291 | -9.3 | -20.5 | -5.4 | 0.8 | 0.8 | 0.3 |
| 50 | HIP 9275 B | -26.7 | -21.3 | 14.1 | 10.4 | 5.6 | 14.8 |
| 51 | GJ 3125 | -36 | +23 | +8 | | | |
| 52 | GJ 9066 | +12 | -50 | +1 | | | |
| 53 | GJ 3127 | +44 | -5 | -47 | | | |
| 54 | GJ 3129 | -12 | -36 | +18 | | | |
| 55 | GJ 3134 | -25 | -9 | -8 | | | |
| 56 | WW Ari | -21 | -4 | -3 | | | |
| 57 | GJ 3136 | +9 | -41 | -5 | | | |
| 58 | GJ 3142 | -41 | -18 | -13 | | | |
| 59 | GJ 3143 | -20 | -16 | -32 | | | |
| 60 | GJ 3146 | -12 | -23 | -7 | | | |
| 61 | GJ 3147 | -20 | -21 | -4 | | | |
| 62 | HIP 10617 B | -42 | -22 | -22 | | | |
| 63 | HIP 10617 A | -49.5 | -24.8 | -11.5 | 4.3 | 4.6 | 17.0 |
| 64 | GJ 3150 | -24 | -22 | -2 | | | |
| 65 | GJ 3153 | -18 | -15 | -35 | | | |
| 66 | GJ 3157 | -21 | -16 | +1 | | | |
| 67 | GJ 102 | +5 | -21 | -23 | | | |
| 68 | HIP 11964 | +6.2 | -30.3 | -32.7 | 0.1 | 0.3 | 0.7 |
| 71 | GJ 3172 | -49 | -51 | -10 | | | |
| 73 | GJ 3174 | -45 | -30 | -14 | | | |
| 74 | HIP 12351 | +1.4 | -13.2 | -22.7 | 1.6 | 10.5 | 14.5 |
| 75 | HIP 12781 | -40.3 | -17.1 | -11.9 | 0.7 | 0.6 | 0.4 |
| 76 | HIP 12886 B | -51.2 | -20.8 | 1.2 | 14.2 | 10.6 | 4.0 |
| 78 | HIP 13081 C | -21.7 | -23.8 | -2.0 | 0.7 | 0.8 | 0.4 |
| 79 | HIP 13118 | -21.3 | -52.7 | -8.0 | 1.1 | 2.0 | 0.5 |
| 81 | GJ 3183 | +15 | -9 | -7 | | | |
| 82 | HIP 13402 | -15.5 | -22.0 | -9.2 | 0.4 | 0.2 | 0.6 |
| 83 | HIP 14101 A | +6.2 | -4.3 | -36.6 | 12.5 | 4.0 | 16.1 |
| 84 | HIP 14555 A | +5.2 | -4.8 | -61.4 | 7.2 | 6.4 | 15.6 |

Continues next page

Continued

| GLK | designation | U | V | W | eU | eV | eW |
|---|---|---|---|---|---|---|---|
| 85 | HIP 14568 | -53.2 | -29.1 | -7.2 | 7.8 | 5.6 | 15.5 |
| 89 | GJ 3224 | +17 | +0 | -15 | | | |
| 90 | GJ 3225 | +30 | -18 | +6 | | | |
| 91 | GJ 3227 | +5 | -22 | +10 | | | |
| 92 | GJ 3229 A | +10 | -2 | +45 | | | |
| 93 | GJ 3229 B | +5 | -5 | +38 | | | |
| 94 | GJ 1060 B | -82 | -41 | +18 | | | |
| 95 | GJ 3236 | -20 | -11 | +3 | | | |
| 97 | GJ 3240 B | -42 | -9 | -10 | | | |
| 99 | HIP 17102 B | -2.4 | 7.9 | -8.8 | 3.3 | 1.5 | 1.4 |
| 100 | HIP 17609 | -42.0 | -19.1 | -5.9 | 0.7 | 0.7 | 0.3 |
| 102 | GJ 3252 | +30 | -27 | -4 | | | |
| 103 | GJ 3253 | -63 | -43 | -43 | | | |
| 104 | HIP 18512 A | +7.1 | 0.5 | -16.2 | 0.7 | 0.2 | 0.6 |
| 107 | GJ 3266 | -43 | -12 | +7 | | | |
| 109 | HIP 19855 | +14.6 | -1.2 | -8.7 | 0.7 | 0.1 | 0.5 |
| 110 | 40 Eri C | +97 | -12 | -38 | | | |
| 115 | GJ 3286 | +46 | -30 | -11 | | | |
| 116 | GJ 3287 | -13 | -17 | -6 | | | |
| 117 | GJ 3289 | +93 | -47 | -16 | | | |
| 118 | HIP 20917 | 32.9 | 7.2 | 13.8 | 0.7 | 0.1 | 0.2 |
| 119 | GJ 107 | -34 | -18 | -12 | | | |
| 120 | GJ 3294 | -32 | -9 | -6 | | | |
| 121 | GJ 3296 | +6 | -42 | +13 | | | |
| 122 | HIP 21482 A | -38.3 | -17.6 | -1.0 | 0.7 | 0.5 | 0.2 |
| 123 | HIP 21553 | -42.9 | -8.8 | -1.6 | 0.7 | 0.4 | 0.1 |
| 124 | GJ 3304 | -44 | -7 | +2 | | | |
| 126 | HIP 21818 | 1.4 | -3.5 | -22.3 | 0.7 | 0.1 | 0.4 |
| 127 | HIP 21770 B | 9.9 | 5.9 | -10.0 | 0.3 | 0.5 | 0.5 |
| 129 | HIP 22738 A | -8.4 | -35.2 | -20.1 | 1.5 | 14.0 | 11.2 |
| 130 | HIP 22738 B | -11 | -77 | -56 | | | |
| 132 | HIP 23200 | -11.3 | -16.9 | -9.1 | 0.7 | 0.9 | 0.4 |
| 133 | HIP 23418 | -13.9 | -14.7 | -10.3 | 16.8 | 4.6 | 5.9 |
| 134 | GJ 3326 | +10 | +14 | +7 | | | |
| 135 | GJ 3327 | +3 | +5 | -14 | | | |
| 137 | GJ 3331 A | -12 | -14 | -9 | | | |
| 138 | GJ 3335 | +21 | -57 | -20 | | | |
| 140 | GJ 1078 | -65 | -41 | -5 | | | |
| 141 | GJ 3348 B | -49 | -43 | -15 | | | |
| 142 | HIP 25953 | -6.4 | -7.8 | -18.2 | 3.5 | 1.0 | 1.0 |
| 143 | GJ 1081 | -64 | -8 | -5 | | | |
| 144 | HIP 26081 | -13.4 | -7.1 | -28.0 | 0.8 | 0.4 | 1.5 |
| 145 | HIP 26779 | -14.0 | -23.0 | -14.2 | 0.7 | 0.4 | 0.2 |
| 146 | GJ 1083 AB | -9 | -18 | -7 | | | |
| 147 | GJ 3362 | -104 | -52 | -41 | | | |
| 154 | GJ 3379 | -2 | -6 | +3 | | | |
| 155 | HIP 29295 | 11.8 | -11.6 | -12.0 | 0.5 | 0.5 | 0.2 |
| 156 | GJ 3391 | +14 | -36 | +1 | | | |
| 157 | HIP 30630 AB | 8.8 | -4.3 | -13.2 | 0.7 | 0.2 | 0.2 |
| 158 | HIP 30920 A | -6.4 | -24.5 | 4.7 | 1.5 | 1.0 | 0.2 |
| 160 | GJ 3395 | +67 | -103 | +35 | | | |
| 161 | GJ 3396 | -9 | +11 | +1 | | | |
| 164 | GJ 3417 | -28 | -14 | +23 | | | |
| 165 | GJ 3423 | -22 | +0 | -12 | | | |
| 166 | HIP 34603 | -40.7 | -22.1 | -8.3 | 0.7 | 0.5 | 0.5 |
| 167 | GJ 1096 | -27 | -26 | -10 | | | |
| 168 | HIP 36626 B | -7.0 | -9.4 | -15.9 | 0.8 | 0.5 | 1.0 |
| 169 | HIP 36626 A | -7.5 | -7.8 | -12.9 | 0.7 | 0.4 | 0.7 |
| 171 | GJ3454 | -6 | -21 | +6 | | | |
| 172 | HIP 37766 | -19.7 | -22.9 | -7.6 | 0.6 | 0.4 | 0.3 |
| 173 | GJ 1101 | -26 | -26 | -13 | | | |
| 174 | GJ 3467 | +10 | +16 | -26 | | | |
| 177 | HIP 39826 B | -72.7 | -48.5 | 5.8 | 15.0 | 6.1 | 8.1 |
| 178 | HIP 39896 B | -4 | -1 | +2 | | | |
| 179 | HIP 39896 A | -10.6 | -21.8 | -1.5 | 0.7 | 1.4 | 0.7 |
| 181 | GJ 1111 | -13 | -8 | -16 | | | |
| 183 | HIP 41824 B | +10 | +4 | -19 | | | |
| 184 | HIP 41824 A | 4.3 | 2.1 | -20.3 | 13.9 | 6.7 | 9.3 |
| 185 | GJ 3504 | +32 | -33 | -9 | | | |
| 188 | GJ 3511 B | -31 | +18 | -2 | | | |
| 189 | GJ 3515 | -12 | -10 | -24 | | | |
| 190 | GJ 3517 | -8 | -2 | -22 | | | |
| 191 | GJ 3518 | -34 | -20 | -20 | | | |
| 192 | GJ 1116 A | +5 | +10 | -33 | | | |
| 193 | GJ 1116 B | -25 | -6 | -7 | | | |
| 194 | GJ 3522 | +27 | +5 | -10 | | | |
| 195 | GJ 1119 | -33 | -23 | -3 | | | |
| 197 | HIP 45343 A | -41.7 | -14.6 | -21.9 | 1.2 | 0.6 | 1.1 |
| 198 | HIP 120005 B | -43.0 | -17.5 | -22.2 | 1.6 | 0.9 | 1.4 |
| 199 | HIP 45731 | -80.7 | -37.9 | 19.9 | 12.5 | 7.7 | 12.0 |
| 200 | GJ 3549 B | -40 | -45 | +13 | | | |
| 201 | GJ 1122 A | -22 | +0 | -12 | | | |
| 202 | GJ 1122 B | -32 | -1 | -2 | | | |

<div align="right">Continues next page</div>

Continued

| GLK | designation | U | V | W | eU | eV | eW |
|-----|-------------|------|-------|------|------|------|------|
| 203 | GJ 3554 | -5 | -9 | -24 | | | |
| 204 | HIP 45963 | 3.6 | -41.4 | -58.1 | 5.2 | 1.1 | 5.4 |
| 205 | HIP 46843 B | -10.0 | -22.9 | -5.2 | 0.5 | 0.4 | 0.6 |
| 206 | HIP 46816 | -20.9 | -6.6 | -8.5 | 0.4 | 0.6 | 0.4 |
| 207 | HIP 47425 | -28.6 | -10.9 | -1.9 | 0.5 | 7.3 | 1.1 |
| 208 | HIP 47650 | -35.0 | -13.2 | -13.6 | 0.9 | 0.6 | 0.7 |
| 209 | GJ 3571 | -22 | +14 | -1 | | | |
| 210 | GJ 3562 | +11 | -20 | -15 | | | |
| 211 | GJ 3577 A | -18 | -23 | +16 | | | |
| 212 | GJ 3578 B | -15 | -23 | +11 | | | |
| 213 | HIP 48904 | 54.3 | -38.0 | -2.2 | 1.6 | 7.3 | 0.9 |
| 214 | HIP 49908 | -9.7 | -20.6 | -35.4 | 0.4 | 0.1 | 0.6 |
| 215 | HIP 50156 | -11.2 | -19.7 | -2.3 | 0.4 | 0.6 | 0.7 |
| 216 | GJ 388 | -15 | -8 | +3 | | | |
| 217 | GJ 9331 B | -24 | +20 | +6 | | | |
| 218 | GJ 3611 B | -21 | -21 | -36 | | | |
| 219 | GJ 398 | -46 | -17 | -3 | | | |
| 220 | HIP 51884 | 40.8 | -20.4 | -13.3 | 1.3 | 0.8 | 0.6 |
| 221 | GJ 3613 | -33 | -9 | +18 | | | |
| 223 | GJ 3622 | +28 | -15 | -15 | | | |
| 224 | GJ 3628 B | -35 | +0 | +11 | | | |
| 225 | GJ 3629 | -31 | -9 | +18 | | | |
| 226 | GJ 3630 | -24 | -19 | +8 | | | |
| 227 | GJ 3631 | -45 | -32 | -19 | | | |
| 228 | GJ 406 | -27 | -45 | -17 | | | |
| 229 | GJ 3635 | -47 | -53 | -1 | | | |
| 231 | HIP 53985 | 12.3 | 3.6 | -9.9 | 0.3 | 0.2 | 0.7 |
| 232 | GJ 3639 | -19 | -3 | -2 | | | |
| 233 | HIP 54035 | 45.8 | -53.6 | -74.8 | 0.3 | 0.1 | 0.7 |
| 234 | GJ 412 B | -126 | -6 | +15 | | | |
| 235 | CW UMa | -16 | +2 | +2 | | | |
| 238 | HIP 55360 | -139.9 | -12.3 | -2.1 | 1.2 | 0.5 | 0.7 |
| 239 | HIP 55454 A | 13.3 | -0.4 | -0.9 | 0.3 | 0.6 | 0.5 |
| 240 | HIP 55454 B | +15 | -6 | +4 | | | |
| 242 | HIP 56244 | -32.7 | -17.4 | -.8 | 5.2 | 16.2 | 5.9 |
| 243 | HIP 56685 | 28.4 | -2.5 | -24.9 | 2.6 | 0.9 | 1.9 |
| 244 | GJ 3682 | -12 | -10 | -10 | | | |
| 245 | HIP 57269 | -18.5 | -28.5 | -15.2 | | | |
| 246 | GJ 3684 | -29 | -8 | +4 | | | |
| 247 | GJ 3685 A | -15 | -20 | +4 | | | |
| 248 | HIP 57548 | 17.3 | 5.4 | -33.4 | 0.1 | 0.4 | 0.6 |
| 249 | GJ 3693 | -15 | -20 | +4 | | | |
| 250 | HIP 57939 B | 280.8 | -156.7 | -16.7 | 1.8 | 1.1 | 0.9 |
| 251 | GJ 3693 | +50 | -18 | -62 | | | |
| 252 | GJ 452.1 | +22 | -32 | -6 | | | |
| 253 | GJ 1154 AB | -27 | -25 | -13 | | | |
| 254 | GJ 459.1 | +24 | -45 | -63 | | | |
| 256 | GJ 1156 | -37 | -21 | +18 | | | |
| 257 | HIP 60178 | +8 | +3 | +5 | | | |
| 259 | GJ 3726 C | +23 | -17 | -14 | | | |
| 260 | GJ 3729 | -3 | -19 | -1 | | | |
| 261 | GJ 3720 | -12 | -8 | -27 | | | |
| 264 | GJ 473 A | -35 | -15 | -3 | | | |
| 267 | GJ 3739 | -5 | -23 | -8 | | | |
| 269 | HIP 62556 | -14.4 | -16.5 | 0.7 | 0.4 | 0.5 | 0.6 |
| 270 | GJ 3751 | -33 | -20 | +11 | | | |
| 271 | GJ 488.2 B | -27 | -44 | -19 | | | |
| 272 | HIP 63253 B | -13 | -22 | -1 | | | |
| 273 | HIP 63253 A | -9.9 | -26.1 | -5.1 | 0.6 | 1.4 | 0.8 |
| 274 | GJ 493.1 | -44 | -2 | -32 | | | |
| 275 | HIP 63510 | -29.3 | -17.4 | -9.8 | 0.5 | 0.4 | 0.7 |
| 277 | GJ 1167 A | -10 | -21 | -26 | | | |
| 278 | GJ 3780 | -28 | -31 | -7 | | | |
| 279 | GJ 3786 | -36 | -31 | -5 | | | |
| 280 | GJ 3789 | -6 | -13 | -33 | | | |
| 281 | VW Com A | +25 | +0 | -8 | | | |
| 282 | VW Com B | +25 | +0 | -8 | | | |
| 283 | HIP 66252 | -28.1 | -13.9 | -18.3 | 0.9 | 0.8 | 1.4 |
| 285 | GJ 3800 | -51 | +3 | -30 | | | |
| 286 | HIP 67155 | 61.1 | -1.4 | -3.4 | 0.5 | 0.0 | 0.7 |
| 287 | GJ 3808 | +5 | -9 | -8 | | | |
| 288 | HIP 67422 A | -20.8 | -24.5 | -13.9 | 0.3 | 0.4 | 0.7 |
| 289 | HIP 67422 B | -19 | -22 | -16 | | | |
| 290 | GJ 3820 | -37 | -5 | -22 | | | |
| 293 | GJ 3828 B | -98 | -34 | +22 | | | |
| 294 | GJ 540.2 | +14 | -58 | +34 | | | |
| 295 | HIP 69562 B | -18 | -23 | -27 | | | |
| 296 | HIP 69562 A | 30.6 | -53.2 | 36.4 | 11.9 | 9.0 | 12.2 |
| 297 | GJ 3839 | -29 | -43 | -8 | | | |
| 299 | GJ 1183 A | -14 | -17 | +29 | | | |
| 300 | GJ 1183 B | +0 | -20 | +48 | | | |
| 301 | HIP 70890 | -27.9 | 0.4 | 13.9 | 1.2 | 1.3 | 0.1 |
| 302 | GJ 3849 | +12 | -41 | -3 | | | |

Continued

| GLK | designation | U | V | W | eU | eV | eW |
|---|---|---|---|---|---|---|---|
| 303 | GJ 3855 | -32 | -12 | +22 | | | |
| 304 | GJ 3858 | +16 | +7 | +3 | | | |
| 305 | GJ 3861 | +67 | -18 | -31 | | | |
| 306 | HIP 71631 | -8.6 | -30.1 | -7.3 | 0.3 | 0.6 | 0.6 |
| 307 | HIP 72659 A | 4.8 | 1.8 | -1.7 | 0.3 | 0.1 | 0.6 |
| 308 | HIP 72944 AB | 7.6 | 3.2 | -13.4 | 0.4 | 0.2 | 0.6 |
| 309 | GJ 3875 | -28 | -9 | +8 | | | |
| 310 | GJ 3877 | -12 | -23 | -16 | | | |
| 311 | GJ 1187 | +36 | -16 | -8 | | | |
| 313 | GJ 3898 | -34 | -9 | +4 | | | |
| 314 | HIP 75187 | 0.5 | 9.6 | 4.4 | 0.4 | 0.3 | 0.6 |
| 315 | GJ 3910 | -21 | -24 | +31 | | | |
| 317 | GJ 3928 | -15 | -9 | -1 | | | |
| 318 | HIP 78259 | 23.8 | -53.8 | 10.5 | 2.2 | 4.4 | 1.3 |
| 319 | GJ 3936 B | -21 | -5 | +5 | | | |
| 321 | HIP 79796 | 41.5 | -29.7 | -20.0 | 1.1 | 0.6 | 0.5 |
| 322 | GJ 3954 | -51 | -29 | -20 | | | |
| 323 | GJ 3959 | -20 | -8 | -2 | | | |
| 324 | GJ 630.1 A | -102 | -121 | -34 | | | |
| 325 | GJ 3966 | +10 | +2 | -6 | | | |
| 326 | GJ 1204 | -8 | -34 | +21 | | | |
| 327 | HIP 81300 | 0.9 | -0.3 | -28.4 | 0.6 | 0.2 | 0.4 |
| 329 | GJ 3967 | +52 | +13 | +17 | | | |
| 330 | GJ 3971 | -15 | -82 | -50 | | | |
| 331 | GJ 3976 | -22 | +6 | -3 | | | |
| 332 | HIP 82588 | 85.2 | -110.2 | 8.8 | 0.9 | 1.8 | 0.4 |
| 334 | HIP 82817 A | 17.8 | -29.5 | 10.4 | 0.7 | 0.7 | 0.3 |
| 336 | HIP 82817 C | +23 | -32 | +12 | | | |
| 337 | GJ 1207 | +9 | +0 | -27 | | | |
| 339 | GJ 3981 | -3 | -12 | +18 | | | |
| 342 | HIP 84794 B | -36 | -19 | -4 | | | |
| 343 | HIP 84794 A | -36.4 | -18.9 | -1.4 | 1.4 | 0.6 | 1.2 |
| 347 | HIP 86346 A | -7.1 | 28.6 | 22.2 | 2.6 | 15.3 | 9.7 |
| 348 | HIP 86346 B | +0 | -8 | -5 | | | |
| 349 | GJ 1224 | +0 | -21 | +11 | | | |
| 351 | GJ 4044 | +8 | +15 | -8 | | | |
| 354 | GJ 4053 | +11 | +17 | -11 | | | |
| 357 | HIP 90959 | 67.7 | -4.8 | 5.2 | 1.4 | 1.2 | 0.2 |
| 358 | HIP 91009 | 18.0 | -17.4 | -28.7 | 0.3 | 0.7 | 0.4 |
| 360 | GJ 1230 A | -15 | -4 | -20 | | | |
| 361 | GJ 4068 | -18 | +9 | -2 | | | |
| 362 | GJ 4069 | +9 | -27 | +6 | | | |
| 363 | GJ 4071 | -36 | -17 | +4 | | | |
| 364 | GJ 4073 | -39 | -4 | +17 | | | |
| 365 | HIP 92403 | -8.6 | -0.4 | -7.8 | 1.7 | 0.4 | 0.3 |
| 366 | HIP 92871 | -9.2 | -9.5 | -6.8 | 0.6 | 0.5 | 0.2 |
| 367 | HIP 94557 A | -34.7 | -31.7 | 65.1 | 10.8 | 14.4 | 3.7 |
| 369 | HIP 94761 A | 53.2 | -7.3 | -5.5 | 0.6 | 0.5 | 0.1 |
| 370 | HIP 94761 B | +53 | -7 | -5 | | | |
| 372 | GJ 4110 | -16 | -40 | -13 | | | |
| 5 373 | G 125-012 | | | | | | |
| 376 | GJ 1243 | -15 | +7 | +0 | | | |
| 377 | HIP 97944 | 3.5 | -29.1 | 0.3 | 0.6 | 0.4 | 0.3 |
| 378 | GJ 1245 A | +14 | +41 | -8 | | | |
| 379 | GJ 1245 B | +20 | +72 | -4 | | | |
| 381 | HIP 98698 | -21.6 | -16.2 | 16.0 | 0.5 | 0.5 | 0.2 |
| 382 | HIP 98906 | 9.8 | -147.7 | 10.5 | 10.5 | 17.6 | 5.5 |
| 383 | HIP 99150 B | 15.3 | -42.8 | -42.7 | 15.4 | 4.5 | 9.2 |
| 384 | GJ 1250 | -58 | -16 | -6 | | | |
| 385 | G 024-016 | -35 | -14 | -12 | | | |
| 386 | G 144-016 | +17 | -31 | -10 | | | |
| 387 | HIP 102141 A | -9.6 | -16.9 | -10.9 | 2.9 | 1.0 | 2.3 |
| 388 | HIP 102141 B | -7 | -13 | -9 | | | |
| 389 | HIP 102119 | -77.5 | -68.8 | -38.2 | 3.0 | 2.1 | 3.2 |
| 393 | GJ 802 | -140 | -54 | +19 | | | |
| 394 | HIP 102409 | -9.2 | -16.3 | -11.1 | 1.4 | 0.4 | 1.1 |
| 395 | HIP 103393 A | -58 | -37 | -28 | | | |
| 396 | HIP 103655 A | -20.4 | -34.5 | -42.1 | 0.6 | 0.7 | 1.7 |
| 398 | HIP 104214 A | -093 | -54 | -9 | | | |
| 399 | HIP 104217 B | -92.2 | -54.1 | -8.1 | 0.2 | 0.7 | 0.1 |
| 402 | GJ 4186 B | -15 | -9 | -6 | | | |
| 403 | GJ 4185 A | -15 | -12 | -5 | | | |
| 404 | HIP 105090 | 61.1 | -18.9 | 25.7 | 0.6 | 0.1 | 0.6 |
| 406 | LHS 510 | -66 | -102 | -27 | | | |
| 407 | HIP 106231 | -5.1 | -23.9 | -15.9 | 0.2 | 0.7 | 0.7 |
| 409 | G 026-013 | -13 | -58 | +6 | | | |
| 410 | HIP 107350 | -14.6 | -21.5 | -10.8 | 0.3 | 0.6 | 0.5 |
| 411 | GJ 4281 | -16 | +2 | -21 | | | |
| 412 | HIP 107705 | -25.9 | -19.3 | -1.4 | 10.6 | 9.2 | 11.4 |
| 413 | HIP 107948 | -9.0 | -32.8 | -11.0 | 6.5 | 13.4 | 11.2 |
| 414 | HIP 108405 A | -2.3 | -26.5 | 13.0 | 4.6 | 1.7 | 5.7 |
| 415 | HIP 108706 | -15.6 | -21.5 | -0.5 | 1.8 | 16.7 | 6.5 |
| 417 | G 188-046 | 103.8 | 2.6 | -29.4 | 6.4 | 3.6 | 2.0 |

<div align="right">Continues next page</div>

| GLK | designation | U | V | W | eU | eV | eW |
|-----|-------------|-----|-----|-----|-----|-----|-----|
| Continued | | | | | | | |
| 418 | GJ 4264 | -6 | -36 | -10 | | | |
| 419 | GJ4269 B | -24 | +0 | -9 | | | |
| 420 | GJ 852 A | +45 | +21 | -33 | | | |
| 421 | GJ 852 B | +37 | +11 | -19 | | | |
| 422 | GJ 4274 | -5 | -30 | +0 | | | |
| 423 | HIP 110526 A | -6.6 | -31.0 | -13.8 | 1.5 | 3.7 | 4.0 |
| 424 | HIP 110526 B | +80 | -15 | -6 | | | |
| 425 | HIP 110893 B | 26.7 | -27.1 | 0.7 | 0.3 | 0.7 | 0.1 |
| 426 | GJ 4281 | +28 | -53 | +9 | | | |
| 428 | HIP 111766 | -55.4 | -19.9 | -14.5 | 10.8 | 7.9 | 13.3 |
| 430 | G 156-031 AB | -69 | -1 | +40 | | | |
| 431 | HD 214479 B | -26 | -15 | +16 | | | |
| 432 | HD 214479 A | -17.8 | -10.4 | -1.9 | 0.7 | 0.6 | 1.5 |
| 433 | G 127-050 | -27 | -30 | -3 | | | |
| 434 | GJ 871 B | +6 | -40 | +3 | | | |
| 435 | HIP 112460 | 19.7 | 3.9 | -2.0 | 0.2 | 0.7 | 0.2 |
| 436 | HIP 112914 | 85.2 | -2.8 | -30.7 | 5.3 | 1.6 | 2.0 |
| 437 | HIP 113283 | -5.3 | -8.1 | -11.9 | 0.3 | 0.1 | 0.7 |
| 438 | HIP 114066 | -6.4 | -26.9 | -15.6 | 0.9 | 1.7 | 0.6 |
| 439 | HIP 114252 | -7.2 | -4.4 | -7.6 | 0.6 | 0.5 | 0.7 |
| 440 | HIP 114379 | -14.0 | -12.2 | -3.9 | 3.2 | 1.3 | 1.3 |
| 441 | HIP 114622 | -52.6 | -39.9 | -13.6 | 0.4 | 0.7 | 0.1 |
| 442 | G 068-005 | -10 | -11 | -5 | | | |
| 444 | G 190-027 B | -22 | -19 | -8 | | | |
| 445 | G 190-028 A | -24 | -11 | -11 | | | |
| 446 | HIP116003 | -23.0 | -34.2 | 31.6 | 3.9 | 4.7 | 17.0 |
| 447 | GJ 1285 | -10 | -22 | +9 | | | |
| 448 | HIP 116132 A | 13.6 | -6.8 | -6.5 | 0.3 | 0.6 | 0.5 |
| 449 | HIP 116132 B | -15 | -6 | -6 | | | |
| 450 | HIP 116191 A | -16 | -24 | -9 | | | |
| 451 | HIP 116317 | 88.3 | -10.4 | -25.0 | 5.9 | 9.9 | 15.1 |
| 452 | GJ 4345 | -72 | +10 | -17 | | | |
| 453 | G 068-034 A | -34 | -10 | +11 | | | |
| 454 | G 190-042 | +33 | -74 | +0 | | | |
| 455 | GJ 1288 | +30 | -18 | +4 | | | |
| 456 | HIP 117069 | -80.3 | -6.9 | -4.9 | 8.8 | 16.2 | 1.0 |
| 457 | GJ 1290 | -41 | -20 | +1 | | | |
| 458 | G 273-130 | +22 | -21 | +24 | | | |
| 459 | G 275-106 | +51 | -1 | +12 | | | |
| 460 | HIP 117473 | -8.2 | -70.5 | 39.5 | 0.1 | 0.5 | 0.6 |
| 461 | G 030-018 | +9 | -7 | -41 | | | |
| 462 | G 273-185 B | -13 | -1 | -14 | | | |
| 463 | GJ 4381 | +16 | +6 | -11 | | | |

# Observation logfile

**Table 3:** Stars observed during the survey when marked with the instrument (CAFOS, DFOSC for low resolution spectroscopy, FOCES and Tauten. for high resolution spectroscopy). No stands for the fact that the stars are not observable with the available equippement: The stars are either too faint or companions to rather bright stars so that they could not be found on the aquisition image.

| GLK | Instrument | Obs.-date | $H_\alpha$ | Li | Remark |
|---|---|---|---|---|---|
| 1 | DFOSC | 05.10.01 | abs. | 0.05 | * |
| 2 | No | * | | | * |
| 5 | No | * | | | * |
| 6 | DFOSC | 05.10.01 | em. fwhm=1.91 | - | * |
| 8 | CAFOS | 31.07.01 | em. fwhm=5.83 | 0.08 | * |
| 9 | DFOSC | 05.10.01 | em. fwhm=1.70 | 0.057 | * |
| 12 | DFOSC | 05.10.01 | | | * |
| 15 | DFOSC/FOCES | 04.10.01/01.12.01 | abs./ | 0.13/ | * |
| 17 | DFOSC | 05.10.01 | | | * |
| 19 | FOCES | 02.12.01 | | | * |
| 21 | No | * | | | * |
| 22 | No | * | | | * |
| 23 | No | * | | | * |
| 24 | No | * | | | * |
| 25 | CAFOS/FOCES | 31.07.01/29.11.01 | em. fwhm=5.69/ | -/ | * |
| 26 | FOCES | Service | | | * |
| 29 | FOCES | 02.12.01 | | | * |
| 30 | DFOSC | 04.10.01 | abs. | - | * |
| 31 | DFOSC | 04.10.01 | abs. | - | * |
| 32 | FOCES | 01.12.01 | | | * |
| 33 | No | * | | | * |
| 42 | DFOSC | 05.10.01 | em. fwhm=1.68 | - | * |
| 43 | DFOSC | 04.10.01 | em. fwhm=1.57 | - | * |
| 46 | No | * | | | * |
| 48 | DFOSC | 04.10.01 | filled | 0.04 | * |
| 50 | FOCES | 02.12.01 | | | * |
| 53 | DFOSC | 22.01.02 | | | * |
| 56 | No | * | | | * |
| 60 | No | * | | | * |
| 61 | No | * | | | * |
| 62 | DFOSC | 05.10.01 | em. fwhm=1.65 | - | * |
| 63 | DFOSC | 06.10.01 | | | * |
| 68 | DFOSC | 04.10.01 | | | * |
| 71 | No | * | | | * |
| 72 | No | * | | | * |
| 74 | DFOSC | 04.10.01 | | | * |
| 77 | No | * | | | * |
| 79 | FOCES | Service | | | * |
| 80 | No | * | | | * |
| 82 | DFOSC | 04.10.01 | abs. | 0.21 | * |
| 83 | DFOSC | ?/06.10.01 | em. fwhm=2.03/abs. | -/- | A |
| 83 | DFOSC | 23.01.02 | em. fwhm=1.39 | - | B |
| 84 | DFOSC | 04.10.01 | | | A |
| 84 | DFOSC | 24.01.02 | abs. | - | B |
| 85 | DFOSC | 04.10.01 | filled | 0.06 | * |
| 87 | No | * | | | * |
| 92 | DFOSC | 23.01.02 | em. fwhm=1.74 | 0.08 | * |
| 93 | DFOSC | 23.01.02 | em. fwhm=1.68 | 0.14 | * |
| 94 | DFOSC | 24.01.02 | abs. | - | A, WD? |
| 98 | FOCES | 30.11.01 | | | * |
| 100 | FOCES | 01.12.01 | | | * |
| 101 | No | * | | | * |
| 102 | No | * | | | * |
| 104 | DFOSC/FOCES | 04.10.01/01.12.01 | abs./ | -/ | * |
| 105 | DFOSC | 04.10.01 | em. fwhm=1.55 | - | * |
| 108 | DFOSC | 24.01.02 | em. fwhm=1.89 | - | * |
| 109 | DFOSC/FOCES | 06.10.01/01.12.01 | | | * |

Continues next page

Continued

| GLK | Instrument | Obs.-date | H$_\alpha$-EW | Li-EW | Remark |
|-----|------------|-----------|---------------|-------|--------|
| 115 | DFOSC | 24.01.02 | em. fwhm=1.79 | 0.08 | * |
| 116 | No | * | | | * |
| 117 | No | * | | | * |
| 118 | FOCES | 02.12.01 | | | * |
| 122 | FOCES | 01.12.01 | | | * |
| 123 | FOCES | 02.12.01 | | | * |
| 125 | DFOSC | 04.10.01 | em. fwhm=1.91 | - | * |
| 126 | FOCES | 02.12.01 | | | * |
| 128 | FOCES | 02.12.01 | | | * |
| 132 | DFOSC | 24.01.02 | em. fwhm=1.91 | 0.26 | * |
| 135 | DFOSC | 22.01.02 | | | * |
| 136 | DFOSC | 24.01.02 | | | * |
| 137 | DFOSC | 24.01.02 | em. fwhm=1.81 | 0.06 | A |
| 137 | DFOSC | 24.01.02 | em. fwhm=1.79 | - | A |
| 139 | DFOSC | 23.01.02 | em. fwhm=2.76 | 0.28 | * |
| 142 | FOCES | 02.12.01 | | | * |
| 144 | DFOSC | 24.01.02 | em. fwhm=1.85 | 0.07 | * |
| 145 | FOCES | 30.11.01 | | | * |
| 146 | No | * | | | * |
| 148 | No | * | | | * |
| 149 | No | * | | | * |
| 150 | No | * | | | * |
| 151 | No | * | | | * |
| 154 | DFOSC | 24.01.02 | em. fwhm=1.73 | 0.04 | * |
| 155 | DFOSC | 22.01.02 | | | * |
| 158 | FOCES/DFOSC | 30.11.01/23.01.02 | /em. fwhm=2.23 | /- | * |
| 159 | DFOSC | 23.01.02 | | | * |
| 160 | FOCES | 02.12.01 | | | * |
| 161 | No | * | | | * |
| 162 | No | * | | | * |
| 163 | FOCES | 29.11.01 | | | * |
| 166 | FOCES | 02.12.01 | | | * |
| 172 | DFOSC | 24.01.02 | em. fwhm=1.54 | - | * |
| 174 | DFOSC | 24.01.02 | em. fwhm=1.69 | ? | * |
| 177 | FOCES | 30.11.01 | | | A&B |
| 180 | No | * | | | * |
| 181 | No | * | | | * |
| 182 | DFOSC | 25.01.02 | em. fwhm= ? | - | * H$_\alpha$ 2 peaks |
| 186 | No | * | | | * |
| 187 | No | * | | | * |
| 190 | No | * | | | * |
| 191 | DFOSC | 23.01.02 | | | * |
| 192 | No | * | | | * |
| 193 | No | * | | | * |
| 194 | DFOSC | 25.01.02 | em. fwhm=1.94 | - | * |
| 196 | FOCES | 20.02.01 | | | * |
| 197 | FOCES | 22.02.01 | | | * |
| 198 | FOCES | 22.02.01 | | | * |
| 199 | FOCES | 20.02.01 | | | * |
| 204 | FOCES | 13.02.01 | | | * |
| 206 | DFOSC | 22.01.02 | filled | 0.25 | * |
| 207 | DFOSC | 22.01.02 | | | * |
| 208 | Tauten. | 31.05.02 | em. | noise | SB2? |
| 210 | FOCES | 13.02.01 | | | * |
| 213 | DFOSC | 22.01.02 | | | * |
| 214 | FOCES | 01.12.01 | | | * |
| 215 | FOCES | 22.02.01 | | | * |
| 216 | Tauten. | 03.06.02 | em. fwhm=1.30 | noise | H$_\alpha$ double peak |
| 219 | DFOSC | 23.01.02 | em. fwhm=1.50 | - | * |
| 220 | FOCES | 02.12.01 | | | * |
| 221 | FOCES | 21.02.01 | | | * |
| 222 | No | * | | | * |
| 225 | FOCES | 21.02.01 | | | * |
| 226 | DFOSC | 23.01.02 | em. fwhm=2.62 | 0.07 | H$_\alpha$ em. 2 peaks |
| 231 | Tauten. | 31.05.02 | filled | noise | * |
| 233 | FOCES/Tauten. | 13.02.01/31.05.02 | /filling 0.50 | /noise | * |
| 235 | Tauten. | 31.05.02 | em. fwhm=1.25 | noise | * |
| 236 | DFOSC | 24.01.02 | em. fwhm=1.67 | 0.19 | * |
| 237 | No | * | | | * |
| 238 | FOCES/Tauten. | 20.02.01/31.05.02 | filling in 0.40 | /noise | * |
| 239 | DFOSC | 03.06.01 | filled in 0.88 | - | * |
| 240 | DFOSC | 03.06.01 | | | * |
| 242 | DFOSC | 01.06.01 | em. fwhm=2.07 | 0.06 | * |
| 243 | Tauten. | 03.06.02 | em. two peaks | - | SB2? |
| 244 | Tauten. | 31.05.02 | abs. | 0.09 | rad. vel. shift |
| 245 | DFOSC | 01.06.01/25.01.02 | filled/filled | 0.19/0.21 | A |
| 245 | DFOSC | 23.01.02 | abs. | - | B |
| 245 | DFOSC | 24.01.02 | filled | 0.17 | C |
| 248 | DFOSC | 03.06.01/23.01.02 | /filled | - | * |
| 249 | DFOSC | 03.06.01/23.01.02 | | | * |
| 255 | FOCES | 22.02.01 | | | * |
| 256 | DFOSC | 25.01.02 | em. fwhm = 1.78 | - | * |
| 257 | FOCES | 20.02.01 | | | * |

Continues next page

Continued

| GLK | Instrument | Obs.-date | $H_\alpha$-EW | Li-EW | Remark |
|---|---|---|---|---|---|
| 260 | Tauten. | 03.06.02 | em. fwhm = 1.42 | noise | * |
| 263 | FOCES | 21.02.01 | | | * |
| 264 | No | * | | | * |
| 265 | No | * | | | * |
| 266 | Tauten. | 31.05.02 | em. fwhm=1.29 | noise | * |
| 268 | FOCES | 20.02.01 | | | * |
| 269 | Tauten. | 03.06.02 | filled | noise | * |
| 270 | FOCES | 22.02.01 | | | * |
| 271 | DFOSC | 01.06.01 | abs. | - | A |
| 271 | DFOSC | 02.06.01 | | | B |
| 273 | FOCES | 19.02.01 | | | * |
| 274 | DFOSC | 23.01.02 | em. fwhm=1.64 | - | * |
| 275 | Tauten. | 31.05.02 | em. fwhm=1.32 | noise | * |
| 278 | DFOSC | 01.06.01 | em. fwhm=1.88 | noise | * |
| 279 | DFOSC | 03.06.01 | | | * |
| 280 | Tauten. | 03.06.02 | em. fwhm = 3.23 | noise | * |
| 282 | Tauten. | 31.05.02 | filled | noise | * |
| 283 | DFOSC | 25.01.02 | em. fwhm=1.99 | - | * |
| 286 | FOCES | 19.02.01 | | | * |
| 288 | FOCES | 19.02.01 | | | * |
| 289 | FOCES | 19.02.01 | | | * |
| 290 | DFOSC | 31.05.01 | em. fwhm= 1.93 | - | * |
| 292 | No | * | | | * |
| 294 | DFOSC | 03.06.01 | em. fwhm=3.03 | - | * |
| 295 | DFOSC | 02.06.01 | | | * |
| 296 | DFOSC | 01.06.01 | em. fwhm=4.49 | - | A |
| 296 | DFOSC | 02.06.01 | | | * |
| 299 | FOCES | 13.02.01 | | | * |
| 301 | No | * | | | * |
| 304 | Tauten. | 03.06.02 | em. fwhm=1.35 | noise | * |
| 305 | Tauten. | 31.05.02 | em. fwhm=1.45 | noise | double peak |
| 306 | FOCES/Tauten. | 13.02.01/02.08.01 | /filling 0.50 | /0.20 | * |
| 307 | CAFOS/Tauten. | 02.08.01 | /abs. | /0.11 | FOCES |
| 308 | CAFOS/Tauten. | 01.08.01/03.06.02 | em. fwhm=1.29 | noise | AB |
| 309 | FOCES | 20.02.01 | | | * |
| 310 | No | * | | | * |
| 311 | No | * | | | * |
| 314 | FOCES | 22.02.01 | | | * |
| 315 | CAFOS | 01.08.01 | | | * |
| 317 | CAFOS | 01.08.01 | | | * |
| 318 | CAFOS/Tauten. | 31.07.01/31.05.02 | filled/filled | 0.22/0.03 | high $v \sin i$ |
| 319 | CAFOS | 31.07.01 | | | * |
| 321 | FOCES | 13./19.02.01 | | | * |
| 322 | DFOSC | 02.06.01 | | | * |
| 323 | CAFOS | 31.07.01 | | | * |
| 324 | Tauten. | 31.05.02 | em. fwhm=1.297, 1.268 | noise | SB2 two $H_\alpha$, $H_\beta$ em. lines |
| 325 | CAFOS/Tauten. | 01.08.01/31.05.02 | /em. fwhm=1.28 | /noise | * |
| 326 | CAFOS/Tauten. | 01.08.01/31.05.02 | /filled | /noise | * |
| 327 | CAFOS/Tauten. | 31.07.01 | /abs. | /0.01 | * |
| 328 | No | * | | | * |
| 329 | DFOSC | 02.06.01 | | | * |
| 330 | No | * | | | * |
| 331 | Tauten. | 03.06.02 | em. fwhm = 1.09 | noise | * |
| 332 | CAFOS | 31.07.01 | | | * |
| 334 | DFOSC | 31.05.01 | em. fwhm = 3.26 | 0.11 | UL |
| 335 | DFOSC | 31.05.01 | | | * |
| 336 | DFOSC | 31.05.01 | | | * |
| 337 | DFOSC | 03.06.01 | em. fwhm=1.92 | ? | * |
| 338 | FOCES | 21.02.01 | | | * |
| 339 | Tauten. | 31.05.02 | small em. | noise | * |
| 340 | No | * | | | * |
| 341 | No | * | | | * |
| 342 | Tauten. | 03.06.02 | em. fwhm=1.28 | noise | B |
| 343 | Tauten. | 31.05.02 | em. fwhm=1.26 | noise | A |
| 344 | No | * | | | * |
| 345 | No | * | | | * |
| 346 | No | * | | | * |
| 347 | CAFOS/Tauten. | 2000/31.05.02 | /em. fwhm=1.62 | - | * |
| 348 | CAFOS | 31.07.01 | em. fwhm=5.44 | - | A |
| 348 | Tauten. | 03.06.02 | em. fwhm=1.40 | noise | B |
| 349 | DFOSC | 01.06.01 | em. fwhm=2.02 | - | * |
| 350 | No | * | | | * |
| 351 | Tauten. | 03.06.02 | em. fwhm=1.08 | - | * |
| 352 | No | * | | | * |
| 353 | No | * | | | * |
| 354 | No | * | | | * |
| 355 | No | * | | | * |
| 356 | No | * | | | * |
| 357 | CAFOS/Tauten. | 31.07.01/31.05.02 | /abs. | /- | * |
| 358 | CAFOS | 31.07.01 | | | * |
| 359 | No | * | | | * |
| 360 | No | * | | | * |
| 361 | CAFOS/Tauten. | 31.07.01/03.06.02 | em. fwhm=1.33 | noise | * |

<div align="center">Continues next page</div>

Continued

| GLK | Instrument | Obs.-date | $H_\alpha$-EW | Li-EW | Remark |
|---|---|---|---|---|---|
| 363 | DFOSC | 03.06.01 | em. fwhm=2.08 | 0.05 | Li UL |
| 364 | No | * | | | * |
| 365 | DFOSC | 31.05.01/05.10.01 | em. fwhm = 2.03/1.64 | ?/0.19 | |
| 366 | DFOSC | 01.06.01 | em. fwhm=2.03 | 0.04 | Li UL |
| 367 | CAFOS/Tauten. | 31.07.01/31.05.02 | filled-in 0.40 | - | * |
| 368 | No | * | | | * |
| 369 | DFOSC | 06.10.01 | abs. | 0.09 | A |
| 370 | No | * | | | * |
| 371 | No | * | | | * |
| 372 | CAFOS | 31.07.01 | | | * |
| 373 | No | * | | | * |
| 374 | No | * | | | * |
| 375 | No | * | | | * |
| 376 | No | * | | | * |
| 377 | DFOSC | 01.06.01/04.10.01 | abs./abs. | 0.03/- | Li UL |
| 380 | No | * | | | * |
| 381 | DFOSC | 01.06.01 | abs. | 0.09 | Li UL |
| 382 | Tauten. | 03.06.02 | em. fwhm=1.38 | - | * |
| 383 | DFOSC | 31.05.01 | em. fwhm=4.67 | 0.99 | B1 |
| 383 | DFOSC | 31.05.01 | filled | 0.04 | B2 |
| 384 | No | * | | | * |
| 386 | CAFOS | 01.08.01 | | | * |
| 387 | DFOSC | 01.06.01 | em. fwhm=2.50 | - | A |
| 388 | DFOSC | 02.06.01 | | | * |
| 389 | DFOSC | 03.06.01 | em. fwhm=2.07 | - | * |
| 390 | DFOSC | 05.10.01 | | | * |
| 391 | No | * | | | * |
| 392 | No | * | | | * |
| 393 | No | * | | | * |
| 394 | DFOSC | 03.06.01 | em. fwhm=2.06 | - | * |
| 395 | DFOSC | 03.06.01 | | | * |
| 396 | CAFOS | 31.07.01 | | | * |
| 397 | CAFOS | 31.07.01 | | | * |
| 398 | CAFOS | 31.07.01 | | | FOCES A&B |
| 400 | DFOSC | 04.06.01 | em. fwhm=2.05 | 0.06 | * |
| 401 | DFOSC | 04.10.01 | abs. | - | * |
| 402 | CAFOS | 01.08.01 | | | * |
| 403 | CAFOS | 01.08.01 | | | * |
| 404 | DFOSC | 04.06.01 | | | * |
| 405 | DFOSC | 04.06.01 | em. fwhm=2.35 | 0.065 | * |
| 406 | DFOSC | 03.06.01/04.10.01 | filled/filled | -/0.06109 | * |
| 407 | CAFOS/Tauten. | 31.07.01 | /em. | /0.05 | high rot., FOCES |
| 408 | FOCES | 01.12.01 | | | * |
| 409 | DFOSC | 04.10.01 | e. fwhm=0.86 | - | $H_\alpha$ 2 peaks |
| 410 | FOCES/DFOSC/Tauten. | 29.11.01/04.10.01 | abs. 0.48/abs. | 0.10/0.10/0.10 | $H_\alpha$ 10% filled in |
| 412 | DFOSC | 04.06.01 | em. fwhm=2.32 | - | * |
| 413 | CAFOS | 31.07.01 | em. fwhm=5.69 | UL | * |
| 414 | DFOSC | 04.06.01 | em. fwhm=2.11 | 0.04 | * |
| 415 | FOCES | 01.12.01 | | | * |
| 416 | No | * | | | * |
| 417 | No | * | | | * |
| 420 | DFOSC | 04.10.01 | em. fwhm=1.56 | 0.17 | * |
| 421 | DFOSC | 04.10.01 | em. fwhm=1.50 | 0.16 | * |
| 422 | DFOSC | 06.10.01 | em. fwhm=1.57 | - | * |
| 423 | FOCES | 02.12.01 | | | * |
| 426 | No | * | | | * |
| 427 | FOCES | 31.05.01 | | | * |
| 428 | DFOSC | 05.10.01 | em. fwhm=1.82 | 0.18 | * |
| 429 | DFOSC | 05.10.01 | abs. | - | * |
| 430 | No | * | | | * |
| 431 | DFOSC | 06.10.01 | em. fwhm=1.75 | - | * |
| 432 | DFOSC | 06.10.01 | em. fwhm=1.90 | - | * |
| 434 | DFOSC | 05.10.01 | em. fwhm=1.85 | - | * |
| 435 | FOCES | 02.12.01 | | | * |
| 436 | CAFOS/FOCES | 31.07.01/01.12.01 | abs. filled in 0.85/ | 0.20 | * |
| 437 | DFOSC | 04.10.01 | abs. | - | * |
| 438 | FOCES | 30.11.01 | | | * |
| 439 | No | * | | | * |
| 440 | CAFOS/Tauten. | 31.07.01 | /abs | /0.11 | E |
| 440 | CAFOS/Tauten. | 31.07.01 | | | W |
| 441 | CAFOS/Tauten. | 31.07.01 | /abs | /0.02 | |
| 442 | FOCES | 02.12.01 | | | * |
| 451 | FOCES | 02.12.01 | | | * |
| 455 | No | * | | | * |
| 456 | FOCES | 02.12.01 | | | * |
| 457 | CAFOS | 31.07.01 | e. fwhm=5.36 | - | * |
| 460 | FOCES | 02.12.01 | | | * |
| 5463 | * | * | | | * |

# Danksagung

An dieser Stelle ist es Zeit all den Personen zu Danken, die zu dem Gelingen dieser Doktorarbeit beigetragen haben.

Zunächst ist natürlich Herr Prof. Dr. Gregor E. Morfill zu nennen, der diese Arbeit in der Theoriegruppe des MPEs möglich gemacht hat. Jederzeit fand er ein offenes Ohr, um mit mir wissenschaftliche Ideen zu diskutieren, aber auch mit Unterstützung bei alltäglichen Problemen konnte ich immer rechnen. Besonderen Dank gebührt ihm auch, daß ich internationale Konferenzen besuchen konnte, um dort meine Ergebnisse zu präsentieren und Kontakte zu Wissenschaftlern aus allen Teilen der Welt zu knüpfen.

Bei der täglichen Arbeit begleitete mich Prof. Dr. Ralph Neuhäuser. Ich möchte ihm für die häufigen Diskussionen danken und für die Vorschläge und Anregungen, die natürlich den Verlauf dieser Dissertation stark beeinflußt haben. Er begeisterte mich in dem interessanten und sich schnell entwickelnden Arbeitsgebiet Sternentstehung zu arbeiten.

Mein Dank geht natürlich auch an Dr. Klaus Fuhrmann, der mir die nötigen Grundlagen der Spektroskopie geduldig erklärte, bei der Suche nach Fehlern in Programmen half und auch immer eine Lösung hatte, wenn das Programm mal nicht compilierte. Für die viele Diskussionen über den Aufbau der Milchstraße möchte ich ihm speziell danken.

Für ein nettes Arbeitsumfeld möchte ich der Sternentstehungsgruppe danken. Einige haben das Institut bereits verlassen und trotzdem den Verlauf der Arbeit geprägt. Mein Dank geht an Matthias Ammler, Christorpher Broeg, Dr. Mathilde Fernández, Dr. Valeri Hambaryan, Dr. Thom Hearty, Dr. Nuria Huélamo, Dr. Viki Joergens, Bojan Pečnik, Dr. Beate Stelzer und Dr. Günter Wuchterl.

Ohne die schnelle und kompetente Hilfe unserer Systemadministratoren Harald Baumgartner, Achim Bonnet und Joachim Paul wäre die Arbeit nicht möglich gewesen. Ich möchte ihnen hier an dieser Stelle meinen besonderen Dank aussprechen.

Außerhalb des Instituts konnte ich besonders mit Dr. João Alves, Dr. David Charbonneau, Dr. Greg Doppmann, Alex Fiedler, Dr. Eike Guenther, Prof. Dr. Artie Hatzes, Prof. Dr. Dan Jaffe, Prof. Dr. Ray Jayawhardana und Dr. Russel White zusammenarbeiten. Diese Zusammenarbeiten bereicherten natürlich die Arbeit. Vielen Dank.

Vielen Dank an Dr. Gerardo Avila und Dr. Carlos Guirao, die die beiden Spektrographen FIASCO und LECHES entwickelt haben. Ich habe viel über Spektrographen gelernt in der Zeit, in der ich mit Euch arbeiten durfte. Mein Espanglisch ist natürlich auch besser geworden.

Ich danke Dr. Niv Drory, der mich wärend meiner Doktorarbeit begleitet hat, mit dem ich viel diskutiert habe und der mir unermüdlich meine Fragen zur Galaxienentstehung erklärt hat. Außerdem möchte ich Dr. Artur Erbe und Dr. Florian Dufey, sowie Niv für die netten Abende in der Physikertherapierunde danken.

Jetzt ist es an der Zeit Herrn Prof. Dr. Ron B. Guenther zu danken, der die Arbeit Korrektur gelesen hat. Dank seines schnellen und anspronenden Einsatzes wurde die Arbeit rechtzeitig fertig und natürlich auch viel besser lesbar.

Zum Schluß danke ich meinen Eltern und meiner Schwester. Auch wenn meinem Vater manchmal die Art und Weise, wie physikalische Forschung betrieben wird, aus der Sicht eines Mathematikers komisch vorkam, haben sie mich jederzeit unterstützt und den Fortschritt dieser Arbeit begleitet.

# Lebenslauf

## Persönliche Informationen

Geburtstag: 5. Dezember 1972
Geburtsort: Starnberg
Staatsangehörigkeit: deutsch
Vater: Dr. rer. nat. Dr. rer. nat. habil. Manfred König
Mutter: Hildegard König geb. Potrick
Familienstand: ledig

## Ausbildung

| | |
|---|---|
| 1979-1983 | Grundschule |
| 1983-1992 | Gymnasium Icking, Deutschland |
| 1992 | Abitur, Gymnasium Icking, Deutschland |
| 1992-1998 | Mathematik- und Physikstudium (Lehramt), Ludwig-Maximilians-Universität, München |
| 1994 ZP | Mathematik |
| 1995 ZP | Physik |
| 1998-2000 | Physikstudium (Diplom), Ludwig-Maximilians-Universität, München |
| 1998 Vordiplom | Physik, Ludwig-Maximilians-Universität, München |
| WS 1998/1999 | Übungsleitung der Vorlesung Lineare Algebra I |
| SoSe 1999 | Übungsleitung der Vorlesung Lineare Algebra II |
| 2000 Diplom | Physik, Ludwig-Maximilians-Universität, München |
| seit 2000 | Promotion in Astronomie am Max-Planck Institut für extraterrestrische Physik, Garching |

## Sprachen

Deutsch (Muttersprache)
Englisch, Französisch (in Wort und Schrift)
Russisch, Spanisch (Grundkenntnisse)